

**CATALYSTS AND ADVANCED MATERIALS FROM WASTE:
DIVERSIFYING BIOCHAR APPLICATIONS TOWARDS THE IMPLEMENTATION OF
A CIRCULAR AND BIO-BASED ECONOMY**

by

© Juliana Ladeira Vidal

A thesis submitted to the School of Graduate Studies
in partial fulfillment of the requirements for the degree of

Doctor of Philosophy

Department of Chemistry
Memorial University of Newfoundland

August 2021

St. John's

Newfoundland and Labrador

ABSTRACT

Biochar is a bio-sourced and carbon-based material produced from the thermochemical processing of wood residues. Besides presenting remarkable chemical and physical properties, biochar is a tool for carbon dioxide (CO₂) sequestration. Unfortunately, it has been mainly employed in low value-added fields in pollutant removal and soil amendment. The diversification of biochar applications is aligned with the Principles of Green Chemistry and could help to tackle our society's current environmental challenges through the achievement of the United Nations Sustainable Development Goals. The use of a material obtained from waste with recognized carbon sink potential for the further production of energy and chemicals can reduce the impacts of consumption, contribute to our good health and well-being, and also mitigate devastating climate change consequences.

A true sustainable future can only be achieved if interdisciplinary and collaborative approaches are considered. In this thesis, strategies in the areas of CO₂ transformation, layered materials exfoliation, polymer composites reinforcement, catalysis, and their respective applications in biochar research are discussed. Biochar after functionalization could be applied as catalyst for the synthesis of cyclic carbonates from epoxides using CO₂ as a feedstock. Besides presenting good efficiency (i.e. conversions higher than 78.5%) and having a wide substrate scope, the catalytic system proposed could be re-used at least five times without any loss in its activity. The same material could be applied in liquid-phase exfoliation processes to produce biochar nanostructures with improved chemical

and physical properties. Although greener environments for the exfoliation of biochar were obtained and studied through extensive solvent screening, the functionalization of this carbon-based material was able to further increase the yield of nanostructures obtained in benign solvents to human health and the environment. Using different catalysts, the functionalized biochar produced could then be applied as a polymer additive for the production of biodegradable poly(ϵ -caprolactone) composites with increased stiffness, crystallinity and conversions. Preliminary degradation studies also showed a positive effect of the exfoliated functionalized material in the degradation of poly(ϵ -caprolactone) under different conditions. Functionalized biochar also showed good activity (i.e. 75.2% conversion) as the first carbon-based catalyst used for the synthesis of cyclic ethers via ring-closing C-O/C-O metathesis of their aliphatic counterparts, and as an efficient alternative system for the synthesis of terpene esters from terpene alcohols and acetic anhydrides (i.e. conversions higher than 84.3%) under mild conditions.

ACKNOWLEDGEMENTS

I read once on Twitter a post about doctoral studies, which really spoke to my heart. It had something to do with the fact that your Ph.D. makes you fall, so you become the person you are meant to be when you stand up. Throughout these years, I was fortunate enough to have some amazing people helping me to get back up, move forward, and become a better person. “Thank you” will never be enough to express my feelings for everything they have done.

Firstly, I would like to acknowledge the importance that my superperson, supermother, and supervisor Dr. Francesca Kerton has had on this journey. Since day one, Fran has believed in me and pushed me out of my comfort zone so I could achieve my full potential by embracing the person I am. Her support as a mentor, a role-model, and as a friend made the whole difference in this adventure. From chemistry to smoothies, I will never forget the wonderful moments we shared and all the amazing things she has taught me. Thank you, Francesca, for your patience, love, comfort, and encouragement. I could had never asked for a more incredible person to share this journey with! (Bananas!)

Even from a distance, my co-supervisor Dr. Stephanie MacQuarrie has always been right next to me. Through virtual meetings, long e-mail chains, different applications or prompt messages on social media, Steph has always supported me in every single step of the way. She made herself present “in person” during the most difficult stages of my doctorate, and I am sure she would be here every day if she could! I am beyond grateful for having Steph as my mentor during this entire process, and I would like to thank her

from all of my heart for her trust, guidance, advice, and friendship!

Dr. Chris Kozak did not have to do everything he did for me, but he did it anyways. Giving me wonderful advice as my committee member, scaring me to death as Baba Yaga, or making me weak from laughing when the days are not the best, Chris has become my second father and someone I constantly look up to. Besides science, interesting glassware, fun memes, and the complete details of an event that happened in 1768 in the imaginary city of Humplestocks where a green man decided to dye himself purple after losing the battle of Pkispulska (and make it sound cool), Chris has taught me how to live life lighter and reminded me why I decided to do chemistry in the first place. I am forever grateful for having the chance to learn so much from Chris! Ekstra!

Although research can be very difficult sometimes, things can be easier when the environment helps. At Memorial University, I had the luck to be surrounded daily by people who I admire. I would like to thank the whole University, faculty and staff of the School of Graduate Studies and the Chemistry Department especially Ros, Mary, Melissa, Ann Marie, Randy, Dave Murphy, Nick Ryan, Natalie, Aimée, Mike, Erika and Heather for all the incentive and help during these years. A special thanks to Debbie for her friendship (and chocolates!) I will miss all of you. The Beyond Benign and NESSE team also made a whole difference in this process, and I feel extremely grateful for working with such a team with incredible people, working hard to make a difference in our future. A huge and special thanks to my wonderful friend and one of my favorite people in this world, Dr. Natalie O'Neil.

In this journey, I definitely got by with a little help from my friends! I am so proud and so happy for meeting every single one of you! Luke, Mikhailey, Olivia, Sachel, Cyler, Claire, Cloe, Kori, Nigel, Tim, Keegan, Hart, April, Kenson, Craig, Stephanie, and Silvana, I hope you know how amazing you are, and how much you inspired me by just being yourselves! I will take you and the moments we shared forever with me! I would also like to acknowledge Evan Connors, Douglas Richards, Vinny Andrea, Judy MacInnis, Dr. Ben Yavitt, Dr. Savvas Hatzikiriakos, Jennifer Kolwich, Lindsay Donovan, and Dr. Clarissa Sit for all the help during the work performed in my Ph.D. I would also like to acknowledge the Natural Sciences and Engineering Research Council (NSERC), the Canada Foundation for Innovation (CFI), the provincial government of Newfoundland and Labrador, and Dr. Liqin Chen Graduate Excellence Award, the Core Research Equipment and Instrument Training (CREAIT), and the Centre for Chemical Analysis, Research, and Training (C-CART).

Mom, Dad, Tati, and Nick, thank you! Thank you for understanding my journey to pursue my dreams, and thank you for allowing it to happen. Thank you for understanding my absence and all the missed birthdays, Christmas, New Year's Eves, and dates we would spend together. Thank you for the unconditional love, support, and for learning how to use WhatsApp so we could talk to each other! Regardless of where I am, I am always thinking of you, and I hope I could always make you proud.

The very last paragraph is dedicated to the beings who abdicated their own paths so I could chase mine. Not knowing what was waiting for them in St. John's, Arthur and

Cigano jumped (not that my dog had a choice, but anyways) with me in this adventure. A different language, different culture, different food, and... snow? Amongst tears, smiles, laughter, and barks, we overcame every difficult, happy, or overwhelming moment that crossed our way. We cried together, got anxious together, played in the mud together, swam together, studied together, and made new friends (even Freda!) and a new family together. We shared the same (small or big) successes, and I consider myself the luckiest person in the world for having you two by my side. Although Arthur is only aware that I work with “biochar” and Cigano prefers “not-burned-trees-in-the-form-of-sticks”, this thesis is also yours.

We are not lost; we are on our way.

TABLE OF CONTENTS

Abstract	i
Acknowledgements	iii
List of Figures	xii
List of Tables	xviii
List of Schemes	xx
List of Abbreviations and Symbols	xxi
CHAPTER 1: Introduction	1
1.1 Green Chemistry	1
1.2 United Nations Sustainable Development Goals.....	4
1.3 Biochar	6
1.3.1 Pyrolysis and Biochar for Climate Change Mitigation.....	7
1.3.2 Effects of Biomass Feedstock and Pyrolysis Conditions on Biochar.....	12
1.3.3 Functionalization of Biochar	15
1.3.4 Biochar Applications in Catalysis.....	18
1.3.5 Biochar Applications in Building Materials.....	24
1.3.6 Biochar, its Definition, and Other Carbon Materials Derived from Biomass.....	25
1.4 Implementation of a Circular and Bio-Based Economy.....	28
1.5 The Good and the Bad of CO ₂	29
1.5.1 Cycloaddition Reaction Between CO ₂ and Epoxides	31
1.6 Exfoliation of Layered Materials.....	33
1.6.1 Ultrasound	34
1.6.2 Liquid-Phase Exfoliation.....	36
1.7 Ocean Plastics Pollution	39
1.7.1 Polymer Composites	39
1.7.2 Poly(ϵ -caprolactone).....	43
1.8 Objectives	44
1.9 References.....	48

CHAPTER 2: Oxidized Biochar as a Renewable, Sustainable Catalyst for the Production of Cyclic Carbonates from Carbon Dioxide and Epoxides.....	67
2.1 Introduction	67
2.2 Results and Discussion.....	71
2.2.1 Preparation of Functionalized Biochars.....	71
2.2.2 Characterization of Functionalized Biochar	72
2.2.3 Cycloaddition of CO ₂ and Propylene Oxide.....	74
2.2.4 Cycloaddition of CO ₂ and Other Epoxides.....	79
2.2.5 Mechanism of the Cycloaddition Reaction.....	80
2.2.6 Recycling and Kinetic Studies.....	82
2.2.7 Oxidized Biochar as a Catalytic Material	84
2.2.8 Biochar and Other Carbon-Based Catalysts.....	89
2.3 Conclusions	92
2.4 Experimental	92
2.4.1 General Materials	92
2.4.2 Instrumentation.....	93
2.4.3 Preparation of Pristine Biochars (bc)	94
2.4.4 Preparation of Oxidized Biochars (oxbc).....	94
2.4.5 Preparation of APTES modified biochar (APTES-bc _{hw}).....	95
2.4.6 Synthesis of Cyclic Carbonates	95
2.4.7 Recycling Studies.....	96
2.5 References.....	97
CHAPTER 3: Green Solvents for the Liquid-Phase Exfoliation of Biochar	102
3.1 Introduction	102
3.2 Results and Discussion.....	106
3.2.1 Preparation of Exfoliated Biochars	106
3.2.2 Effects of Solvent Parameters in Biochar Exfoliation	106
3.2.3 Biomass Feedstock Interference in Liquid-Phase Exfoliation	109

3.2.4 Characterization of Exfoliated Biochars.....	110
3.2.5 Greener Solvents for Biochar Exfoliation.....	118
3.2.6 Effect of Sonication Time in Biochar Exfoliation	130
3.3 Conclusions	132
3.4 Experimental	133
3.4.1 General Materials	133
3.4.2 Instrumentation.....	133
3.4.3 Preparation of Exfoliated Biochars	135
3.5 References	144
CHAPTER 4: Biochar as a Sustainable and Renewable Additive for the Production of Poly(caprolactone) Composites	154
4.1 Introduction	154
4.2 Results and Discussion.....	155
4.2.1 Preparation of PCL/biochar Composites (PCL/Eoxbc)	155
4.2.2 Catalytic Screening for the Production of PCL/Eoxbc Composites.....	156
4.2.3 Characterization of PCL/Biochar Composites	160
4.2.4 Rheological Analysis of PCL/biochar Composites	168
4.2.5 Preliminary Enzymatic Degradation Studies	173
4.3 Conclusions	177
4.4 Experimental	178
4.4.1 General Materials	178
4.4.2 Instrumentation.....	179
4.4.3 Exfoliation of Biochar and Preparation of PCL/Biochar Grafted Composites ...	181
4.4.4 Rheological Analysis.....	182
4.4.5 Enzymatic Degradation Studies	183
4.5 References	184

CHAPTER 5: Green Ring-Closing Metathesis of Aliphatic Ethers and Esterification of Terpene Alcohols Catalyzed by Biochar Catalysts.....	190
5.1 Introduction	190
5.2 Results and Discussion.....	192
5.2.1 Ring-Closing Metathesis of 1,5-dimethoxypentane	192
5.2.2 Ring-Closing Metathesis of Other Aliphatic Ethers	196
5.2.3 Mechanism for the Ring-Closing Metathesis	197
5.3 Esterification of Cinnamyl Alcohol.....	198
5.3.4 Esterification of Other Terpene Alcohols	199
5.4 Conclusions	201
5.5 Experimental.....	201
5.5.1 General Materials	201
5.5.2 Instrumentation.....	202
5.5.3 Preparation of Sulfonated Biochars (sbc).....	202
5.5.4 Synthesis of <i>O</i> -heterocycles.....	202
5.5.5 Synthesis of Terpene Esters.....	203
5.5.6 Recycling Studies.....	203
5.6 References.....	205
CHAPTER 6: Future Work and Conclusions.....	207
6.1 Ideas for Future Work	207
6.2 Conclusions	212
6.3 References.....	217
APPENDIX A: Information for Chapter 2	222
APPENDIX B: Information for Chapter 3.....	230
APPENDIX C: Information for Chapter 4	232
APPENDIX D: Information for Chapter 5	235

LIST OF FIGURES

Figure 1.1. Risk of accident and damage is a function of hazard and exposure. The most effective way of minimizing risk is reducing hazard by applying Green Chemistry in the design of products and processes.	2
Figure 1.2. The 12 Principles of Green Chemistry created by John Warner and Paul Anastas in 1998. ⁴	3
Figure 1.3. The Sustainable Development Goals (SDGs). Used with permission from the United Nations. ¹²	5
Figure 1.4. An image of biochar and a representative fragment of its structure, with some important chemical and physical properties of this carbon-based material highlighted, such as high porosity, functionality, and surface area.	6
Figure 1.5. Illustrative representation of the sustainable biochar concept. Plants absorb CO ₂ during photosynthesis, which is released back to the atmosphere during respiration and decomposition. If waste biomass is treated via pyrolysis, climate change effects can be mitigated due to the production of biochar, a carrier for long-term carbon storage. Moreover, bio-oil and syngas are co-produced during the process and can be further used as renewable energy sources to feed and power the pyrolysis reactor.	8
Figure 1.6. Most important monomers of cellulose, hemicellulose, and lignin.	13
Figure 1.7. Characteristics and typical cellulose, hemicellulose, and lignin compositions of the two main groups of forestry biomass feedstocks: Hardwood and softwood trees.	14
Figure 1.8. General representation of the most common employed methods of biochar surface and carbon framework functionalization: Oxidation, amination, sulfonation, and doping.	17
Figure 1.9. Comparison between the linear and circular chemical sectors.	28
Figure 1.10. Share of total energy demand by fuel in 2019. Constructed with the data from the International Energy Agency (IEA) Global Energy Review for 2019. ¹⁵⁰	30
Figure 1.11. Cycloaddition reaction between CO ₂ and epoxides to synthesize cyclic carbonates, with their respective applications.....	32

Figure 1.12. Illustrative representation of the formation, growth, and implosion of bubbles created during the cavitation phenomenon.....	35
Figure 1.13. Illustrative representation of the LPE of layered materials. Ultrasound waves and further cavitation phenomenon overcome interactions between layers of the bulk material to produce single or a small number (< 10) of stacked nanosheets with superior applications.	37
Figure 1.14. Repeating unit of different polymer composites produced using biochar.	42
Figure 1.15. ROP of ϵ -CL to synthesize PCL and its current applications.....	44
Figure 2.1. Number of records per publication year on methods for CO ₂ capture, storage and transformation. Source: Web of Science (May 22 nd , 2020). Topic = CO ₂ AND fixation OR CO ₂ AND modification OR CO ₂ AND capture OR CO ₂ AND storage or CO ₂ AND transformation.	68
Figure 2.2. Schematic representation of the advantages in using oxbc as a catalyst for the production of cyclic carbonates using CO ₂ and epoxides.....	70
Figure 2.3. FT-IR spectra of bc_{hw} (top, purple), APTES-bc_{hw} (pink, middle), and oxbc_{hw} (blue, bottom).	73
Figure 2.4. TGA plots of bc_{hw} (purple), APTES-bc_{hw} (pink), and oxbc_{hw} (blue).....	74
Figure 2.5. Chemical structures of the co-catalysts screened during the investigation of oxbc as a catalyst for cycloaddition reaction between CO ₂ and epoxides.....	78
Figure 2.6. Recycling studies for the cycloaddition reaction between CO ₂ and epoxides using oxbc as a catalyst. Conditions: Epoxide (PO, 34 mmol), co-catalyst (TBAB, 0.34 mmol), catalyst (oxbc_{hw} , 100 mg), CO ₂ (10 bar), 110 °C, 6 h (bars represent SD).	82
Figure 2.7. 3D stack plot obtained by in situ FT-IR spectroscopy during the cycloaddition reaction between CO ₂ and PO using oxbc as a catalyst. Conditions: Epoxide (PO, 34 mmol), co-catalyst (TBAB, 0.34 mmol), catalyst (oxbc_{hw} , 100 mg), CO ₂ (10 bar), 110 °C, 6 h.	83
Figure 2.8. Absorbance of the PC C=O peak (1809 cm ⁻¹) in function of time for the cycloaddition reaction between CO ₂ and epoxides catalyzed by oxbc . Conditions:	

Epoxide (PO, 34 mmol), co-catalyst (TBAB, 0.34 mmol), catalyst (oxbc_{hw} , 100 mg), CO ₂ (10 bar), 110 °C, 6 h.....	84
Figure 2.9. Particle distribution and size analyses of (A) oxbc_{hw} and (B) oxbc_{sw}	85
Figure 2.10. SEM images of biochars after oxidation. (A), (B), and (C) images show the presence of pores on the surface of oxbc_{sw} . The presence of pores on the surface of oxbc_{hw} is seen in (D) and (E), whilst the presence of round particles on the surface of oxbc_{hw} is observed in image (F).....	86
Figure 2.11. Particles of (A) oxbc_{hw} and (B) oxbc_{sw} analyzed via SEM-EDX.....	87
Figure 2.12. Comparison between the FT-IR spectra of oxbc_{hw} (top, blue) and oxbc_{sw} (bottom, orange).	88
Figure 2.13. A model of porous oxbc as a catalyst for the cycloaddition reaction between CO ₂ and PO.....	89
Figure 2.14. Visual difference between oxbc_{hw} catalyst in diethyl ether (A) before and (B) after five cycles of the required treatment for its reutilization in another cycloaddition.....	96
Figure 3.1. Schematic diagram describing the LPE process for biochar. Efficient and preferred solvents minimize the energy requirement of the process and stabilize the produced nanosheets.....	105
Figure 3.2. Absorbance at 660 nm divided by cell length (A/l) as a function of biochar dispersion with an absorption coefficient of $\alpha_{660} = 422 \text{ L/m.g}$	107
Figure 3.3. Visual comparison of biochar dispersions from different feedstocks, in a range of solvents.	109
Figure 3.4. Raman spectra of bc_{hw} before and after exfoliation. The G and D bands are related to the crystallinity and deformities of the material produced, and can be used to estimate the effect of exfoliation on its chemical structure.	111
Figure 3.5. AFM characterization of exfoliated biochar samples. Figures (A-D) show the AFM images of exfoliated bc_{hw} samples used to calculate the number of nanostructures containing different heights. The correlation between frequency and exfoliated material thickness can be observed in Figure (E).	114

Figure 3.6. TEM micrographs of bc_{hw} samples. Figure (A) show the layered structure of bc_{hw} before exfoliation, whereas aromatic clusters (i.e. black dots), nanocrystalline stripes, and atomic arrangements are observed after LPE in Figure (B). Atomic arrangements observed at the edges of the exfoliated material are further highlighted in Figure (C).	115
Figure 3.7. Typical TEM micrographs of oxbc_{hw} , oxbc_{sw} and bc_{sw} samples before and after LPE.....	116
Figure 3.8. MALDI-TOF mass spectra of (A) exfoliated bc_{hw} , (B) exfoliated oxbc_{hw} , and (C) non-exfoliated oxbc_{hw} samples in positive-ion mode using DBH as a matrix.	117
Figure 3.9. Proposed interactions between bc and solvents with high polarizability, described by the Kamlet-Taft parameter π^*	123
Figure 3.10. Proposed interactions between oxbc and solvents with high hydrogen-bonding acceptance ability, described by the Kamlet-Taft parameter β	124
Figure 3.11. Influence of surface tension and Kamlet-Taft solvatochromic parameters in the exfoliation of (A) bc_{sw} and (B) oxbc_{sw} samples. To build this correlation, H ₂ O and C ₆ F ₆ have not been included in data analysis due to their exceptional values of γ and ρ , respectively.	125
Figure 3.12. Dispersions of exfoliated (A) bc and (B) oxbc samples in traditional and greener environments investigated for LPE.	129
Figure 3.13. Dispersions of exfoliated bc_{hw} as a function of exfoliation time, showing a linear behavior following the equation $y = 0.0011 x + 0.1323$ (bars represent SD).....	130
Figure 3.14. I _G /I _D ratios of exfoliated bc_{hw} as a function of processing time in EtOAc (bars represent SD).	131
Figure 3.15. Schematic representation of the sonication setup used to exfoliate bc and oxbc samples. The transducer converts the electrical signal supplied by the generator to mechanical vibrations, which are then transmitted by the probe. The cooling bath is used to avoid heating of samples, and the sound enclosure reduces sound levels.....	135
Figure 4.1. Schematic representation of PCL/Eoxbc composites production via ROP of ϵ -CL using Eoxbc as a support.	156

Figure 4.2. Visual comparison between PCL/Eoxbc composites containing different Eoxbc loadings (0.1, 0.5, 1.0, and 5.0 wt%).....	160
Figure 4.3. FT-IR spectra of oxbc (top, pink), neat PCL (middle, green), and the PCL/Eoxbc-5.0 composite (bottom, yellow).....	161
Figure 4.4. TGA analyses of neat PCL and PCL/Eoxbc composites with different Eoxbc loadings at a scanning rate of 10 °C/min under N ₂	162
Figure 4.5. DSC third heating (A) and third cooling (B) scans of neat PCL and its composites with different Eoxbc loadings at a scanning rate of 10 °C/min.....	164
Figure 4.6. SEM images for surfaces of (A) neat PCL, (B) PCL/Eoxbc-0.1 , (C) PCL/Eoxbc-0.5 , (D) PCL/Eoxbc-1.0 , (E) PCL/Eoxbc-5.0 , and (F) expansion of agglomerates in PCL/Eoxbc-5.0	167
Figure 4.7. TEM micrographs for the PCL/Eoxbc-0.1 composite, where the presence of Eoxbc nanostructures with approximate lengths of 9 nm embedded in the PCL matrix is shown.....	168
Figure 4.8. (A) Rheological analysis and correlation of the melt state shear viscosity for neat PCL and PCL/biochar composites containing M _n ~ 10,000 g/mol and (B) the solid state modulus (G', open symbols) and loss modulus (G'', closed symbols) over a range of oscillatory frequencies (ω). (C) Enhanced view of G' at 1 Hz (ω = 6.28 rad/s).....	170
Figure 4.9. Rheological measurements for neat PCL and PCL/biochar composites with M _n ~ 10,000 g/mol and correlation between angular frequency (ω) with (A) complex viscosity (η*) in the melt state, (B) complex viscosity (η*) in the solid state, and (C) storage modulus (G') and loss modulus (G'') in the melt state.....	172
Figure 4.10. Representative SEM images for the surfaces of PCL/Eoxbc-0.1 (A, B) stored in air, baseline samples, and after degradation studies in (C, D) deionized water, and (E, F) synthetic seawater.....	174
Figure 4.11. Representative SEM images for the surfaces of neat PCL after degradation studies in (A, B) air (control), (C, D) deionized water, and (E, F) synthetic seawater..	175

Figure 5.1. A comparison between the previous catalytic systems studied for the ring-closing C-O/C-O metathesis of aliphatic ethers and the catalytic system proposed herein using sbc	192
Figure 5.2. Effect of sbc loadings in the ring-closing C-O/C-O metathesis of 1,5-dimethoxypentane. Reactions conditions used: 1,5-dimethoxypentane (1, 2 mmol), 140 °C, 24 h.....	195
Figure 5.3. Effect of temperature in the ring-closing C-O/C-O metathesis of 1,5-dimethoxypentane. Reaction conditions used: 1,5-dimethoxypentane (1, 2 mmol), sbc (20 wt%), 24 h.....	195
Figure 6.1. Schematic representation of future work idea involving a systems thinking approach for the use of functionalized biochar as a catalyst for the synthesis of both O-heterocycles and cyclic carbonates.....	208
Figure 6.2. Schematic representation of future work idea involving the use of IL-grafted biochar as a bi-functional catalyst for (A) the cycloaddition reaction between CO ₂ and epoxides, and (B) the ring-closing C-O/C-O metathesis of aliphatic ethers.....	210
Figure 6.3. Schematic representation of future work idea involving the use of oxbc as a catalyst for the direct C-C cross-coupling of xanthenes with arenes.....	211

LIST OF TABLES

Table 1.1. Typical compositions and physical properties of oils obtained from biomass and fossil fuel feedstocks. ^a	9
Table 1.2. Typical yields of products obtained during slow and fast pyrolysis. ^a	12
Table 1.3. A comparison between biochar and other amorphous carbon materials.	26
Table 2.1. Optimization of the cycloaddition reaction between epoxides and CO ₂ using PO as a model substrate and different types of biochar as catalysts. ^a	75
Table 2.2. Cycloaddition of CO ₂ and different epoxides to yield cyclic carbonates using oxbc as a catalyst. ^a	79
Table 2.3. Minerals present on the surface of oxbc samples.	87
Table 2.4. Surface area and average pore size of oxbc_{hw} and oxbc_{sw} samples, obtained via BET analysis.	89
Table 2.5. Comparison of several carbon-based catalysts used for the production of cyclic carbonates from CO ₂ and epoxides.....	91
Table 3.1. Exfoliation effects in the molecular structure of biochars from different biomass sources, determined by Raman spectroscopy.....	112
Table 3.2. Exfoliation effects in the estimation of crystallite size (L_a), distance between defects (L_D), and number of defects (n_D) of biochars from different biomass sources, determined by Raman spectroscopy.....	113
Table 3.3. Achieved dispersions and solvent parameters (i.e. density, surface tension, and Kamlet-Taft solvatochromic parameters) for the LPE of bc samples.	119
Table 3.4. Achieved dispersions and solvent parameters (i.e. density, surface tension, and Kamlet-Taft solvatochromic parameters) for the LPE of oxbc samples.....	120
Table 3.5. Selected environmental, health, and safety information on some of the solvents investigated herein and their green credentials obtained from different solvent selection guides. ^a	127

Table 3.6. Chemical structures and health, safety, and environmental impacts for all solvents investigated during the LPE of biochar and green credentials from solvent guides where available.....	138
Table 3.7. Achieved dispersions and solvent parameters (i.e. HSP and viscosities) for the LPE of bc samples.	142
Table 3.8. Achieved dispersions and solvent parameters (i.e. HSP and viscosities) for the LPE of oxbc samples.....	143
Table 4.1. Catalyst screening for the ROP of ϵ -CL using biochar as a support. ^a	157
Table 4.2. Effect of Eoxbc loading in the production of PCL/Eoxbc composites using Sn(oct) ₂ as a catalyst. ^a	159
Table 4.3. TGA data from heating thermograms of neat PCL and PCL/Eoxbc composites with different Eoxbc loadings.....	163
Table 4.4. DSC data from third cooling and heating thermograms of neat PCL and its composites with different Eoxbc loadings at a scanning rate of 10 °C/min.	165
Table 4.5. Average molecular weights for the neat PCL and PCL/biochar composite samples produced for rheological measurements.	169
Table 4.6. Viscosity (η) and storage modulus values (G') obtained during rheological experiments in melt and solid states for neat PCL and PCL/biochar composites.	171
Table 4.7. Analysis of the degradability of neat PCL.....	176
Table 4.8. Analysis of the degradability of the PCL/Eoxbc-0.1 composite.....	176
Table 5.1. Optimization of the ring-closing C-O/C-O metathesis of aliphatic ethers using the conversion of 1,5-dimethoxypentane 1 to tetrahydropyran 2 as a model reaction system, and different types of biochar as catalysts. ^a	193
Table 5.2. Optimization of the esterification of terpene alcohols using the conversion of cinnamyl alcohol 4 to cinnamyl acetate 6 as a model reaction system and different types of biochar as catalysts. ^a	199
Table 5.3. Esterification of different terpene alcohols using sbc as a catalyst. ^a	200

LIST OF SCHEMES

Scheme 1.1. Generic form of the Fischer-Tropsch process, where n is typically between 10-20 and can be adjusted with the reaction conditions.....	11
Scheme 1.2. Representation of some products produced using biochar catalysts studied to date.....	20
Scheme 2.1. Preparation of functionalized biochar catalysts (oxbc , APTES-bc). Materials are represented as simplified fragments of the extended structures of biochar.	71
Scheme 2.2. Proposed mechanism for the cycloaddition reaction between CO ₂ and epoxides using oxbc as a catalyst.	81
Scheme 5.1. Proposed mechanism for the ring-closing C-O/C-O metathesis of 1,5-dimethoxypentane 1 to tetrahydropyran 2 using sbc as a catalyst.....	197

LIST OF ABBREVIATIONS AND SYMBOLS

°C:	degrees Celsius
1,2-DCB:	1,2-dichlorobenzene
2D:	two dimensional
3D:	three dimensional
ε-CL:	ε-caprolactone
η*:	complex viscosity
X _c :	degree of crystallinity
ρ:	density
<i>D</i> :	dispersity
δ _D :	energy from dispersion forces (Hansen solubility parameter)
δ _H :	energy from hydrogen bonds (Hansen solubility parameter)
δ _P :	energy from intermolecular forces (Hansen solubility parameter)
ΔH _m :	enthalpy of melting
ΔH _c :	enthalpy of crystallization
α:	hydrogen-bond donation ability (Kamlet-Taft parameter)
β:	hydrogen-bond acceptor ability (Kamlet-Taft parameter)
μm:	micrometer (s)
π*:	polarizability (Kamlet-Taft parameter)
λ _i :	Raman laser wavelength
γ̇:	shear rate

γ :	surface tension
η :	shear viscosity
ω :	oscillatory frequency
Å:	Ångstrom (10^{-10} m)
acetone- d_6 :	deuterated acetone
AFM:	atomic force microscopy
APTES:	3-aminopropyltriethoxysilane
APTES- bc_{hw} :	3-aminopropyltriethoxysilane hardwood biochar
APTMS-GO:	3-aminopropyltrimethoxysilane graphene oxide
atm:	atmosphere (s)
ATR:	attenuated total reflectance
a.u.:	absorbance unit (s)
bc:	pristine biochar
bc_{hw} :	pristine hardwood biochar
bc_{sw} :	pristine softwood biochar
BET:	brunauer-emmet-teller
BTL:	biomass-to-liquids
CALB:	<i>candida antarctica</i> lipase B
$CDCl_3$:	deuterated chloroform
C_6F_6 :	hexafluorobenzene
$CHCl_3$:	chloroform

CH ₂ Cl ₂ :	dichloromethane
ChCl:	choline chloride
cm:	centimeter (s)
Co.	company
CO:	carbon monoxide
CO ₂ :	carbon dioxide
Conv.:	conversion
CP:	cone-and-plate geometry
Da:	dalton (s)
DABCO:	1,4-diazabicyclo(2.2.2)octane
DBU:	diazabicycloundecene
DHB:	2,5-dihydroxybenzoic acid
DMA:	dynamic mechanical analysis
DMC:	dimethyl carbonate
DMF:	dimethyl formamide
DMSO:	dimethylsulfoxide
dn/dc:	refractive index increment
DSC:	differential scanning calorimetry
EDX:	energy dispersive X-ray
EG:	ethylene glycol
ETD:	everhart-thornley detector

EtOAc:	ethyl acetate
Eoxbc:	exfoliated oxidized biochar
FEG:	field emission gun
FL:	florida
FT-ICR:	fourier-tranform ion cyclotron resonance
FT-IR:	fourier transform infrared
g:	gram (s)
G':	storage modulus
G'':	loss modulus
GC:	gas chromatography
GF:	glycerol formal
GO:	graphene oxide
GPC:	gel permeation chromatography
h:	hour (s)
HHV:	higher heating value
HNO ₃ :	nitric acid
H ₂ O:	deionized water
HSP:	hansen solubility parameters
H ₂ SO ₄ :	sulfuric acid
HTC:	hydrothermal carbonization
Hz:	hertz

IEA:	international energy agency
IL:	ionic liquid (s)
Inc.:	incorporated
IUPAC:	international union of pure and applied chemistry
IPCC:	intergovernmental panel on climate change
H ₂ :	hydrogen gas
K:	kelvin
kg:	kilogram (s)
kHz:	kilohertz
kJ:	kilojoule (s)
kt:	kiloton (s)
kV:	kilovolt (s)
l:	cell length
L:	liter (s)
L _a :	crystallite size
L _D :	distance between defects
LPE:	liquid-phase exfoliation
M:	mol/L
m:	meter (s)
mg:	milligram (s)
mm:	millimetre (s)

MALDI:	matrix-assisted laser desorption/ionization
MHz:	megahertz
min:	minute (s)
mN:	millinewton
M_n :	number average molecular weight
mL:	milliliter (s)
MLA:	mineral liberation analyzer
MPa:	megapascal
MS:	mass spectrometry
m/z :	mass to charge ratio
N_2 :	nitrogen gas
N435:	Novozyme® 435
N51032	Novozyme® 51032
n_{CSF} :	number of carbon surface functional groups
n_D :	defect density
nm:	nanometer (s)
NMP:	<i>N</i> -methyl-pyrrolidone
NMR:	nuclear magnetic resonance
oxbc:	oxidized biochar
oxbc _{hw} :	oxidized hardwood biochar
oxbc _{sw} :	oxidized softwood biochar

Pa:	pascal
PC:	propylene carbonate
PCL:	poly(ϵ -caprolactone)
PE:	polyethylene
PEG:	polyethylene glycol
PhCN:	benzonitrile
PLA:	poly(lactic acid)
PO:	propylene oxide
PP:	polypropylene
ppm:	parts per million
PPNCl:	bis(triphenylphosphine)iminium chloride
PPNN ₃ :	bis(triphenylphosphine)iminium azide
PTT:	poly(trimethylene terephthalate)
ROP:	ring-opening polymerization
rpm:	revolutions per minute
rt:	room temperature
s:	second (s)
sbc:	sulfonated biochar
SD:	standard deviation
SDGs:	sustainable development goals
SEM:	scanning electron microscopy

Sn(oct) ₂ :	tin octoate
TBAB:	tetrabutylammonium bromide
TBAC:	tetrabutylammonium chloride
TBAI:	tetrabutylammonium iodide
T _c :	crystallization temperature
TGA:	thermal gravimetric analysis
THF:	tetrahydrofuran
T _m :	melting temperature
TOF:	time of flight
US:	ultrasound
USD:	united states dollar
UV-Vis:	ultraviolet-visible
W:	watt (s)
wt%:	weight percent

CHAPTER 1: INTRODUCTION

1.1 Green Chemistry

Our society has received significant benefits from the study of matter and the changes it can undergo. From pharmaceutical products to paints, chemistry has completely changed and improved the way we live. However, due to a lack of knowledge about those benefits and improvements, together with the occurrence of several well-publicized environmental disasters, chemistry is often viewed negatively by the general public. One important example is the Bhopal disaster, which happened in India in 1984. Union Carbide, a company producing pesticides, accidentally released thousands of kilograms of toxic methyl isocyanate into the air, leading to the immediate death of at least 3,000 people.¹ Another more recent example is the Sandy Pond, which has been transformed into a tailings pond for mining waste in Newfoundland, thus exterminating the entire the aquatic life of a pristine body of water for private purposes in 2008.² Other general examples of chemical pollution include the hole in atmospheric ozone layer, the eutrophication of lakes and rivers, and the presence of persistent organic pollutants.³ Although some accidents might be related to industry's stress to meet production targets and reduce costs, others can be associated with the unknown longer-term effects of the chemicals released into the environment.

In the late '80s and early '90s, concerns about human health and the environment, climate change, resource depletion, and chemical pollution increased significantly. The Kyoto protocol was signed, sustainable development was defined, and Green Chemistry

was created.³ Green Chemistry targets the design or modification of chemical processes and products to minimize, or ideally eliminate, the use and generation of hazardous substances.⁴

The hazard of a chemical consists of its ability to cause adverse consequences to human health and the environment, and it is considered an important parameter in the control of risk of accident and damage. Risk, as observed in **Figure 1.1**, can be defined as the probability that harm will occur and can be expressed as a function of exposure and hazard.⁴ The exposure can be minimized by using safety precautions such as personal protective equipment, whereas the hazard can be reduced through the design of safer chemical and processes. By employing Green Chemistry and minimizing intrinsic hazard, the risk of damage remains very low even in cases where exposure controls fail (e.g. spills, accidents, leakages).⁴

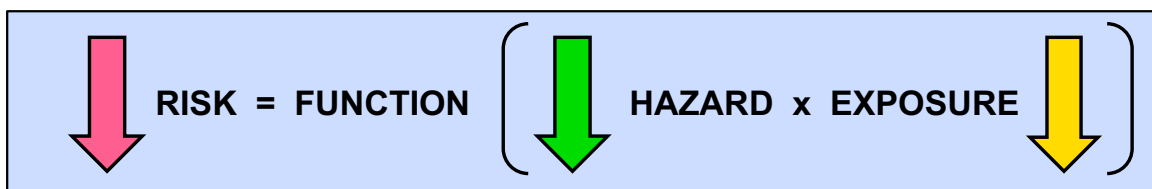


Figure 1.1. Risk of accident and damage is a function of hazard and exposure. The most effective way of minimizing risk is reducing hazard by applying Green Chemistry in the design of products and processes.

Green Chemistry is also economically profitable, especially from the perspective of environmental regulations around industry, because the reduction of hazards in the molecular design produces less unwanted materials and avoids expenses related to waste treatment and disposal. Each year, more and more important industries and start-ups are

incorporating Green Chemistry in the development of their products and processes, and the green chemicals market size is expected to grow by 50.38 billion USD during 2019-2023.⁵ Over the years, Green Chemistry has not only become a profitable approach for achieving sustainability and preserving the future of the planet, but a cultural tool for changing the negative mindset of the general public regarding the remarkable science that chemistry is.

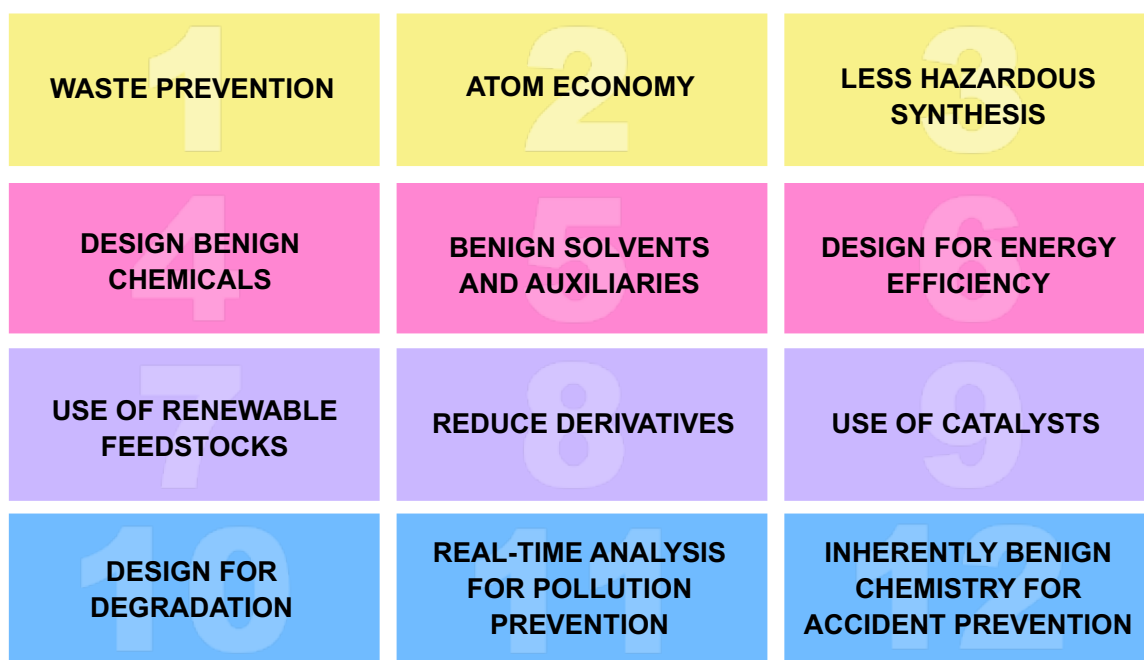


Figure 1.2. The 12 Principles of Green Chemistry created by John Warner and Paul Anastas in 1998.⁴

To facilitate the development of more efficient, more economically viable, and more benign to human health and the environment (i.e. greener) processes and products that are successful in the marketplace, John Warner and Paul Anastas created in 1998 the 12 Principles of Green Chemistry (**Figure 1.2**).⁴ Although some of these principles such as

Waste Prevention, Use of Renewable Feedstocks, Use of Catalysts, and Benign Solvents and Auxiliaries have served as a driving force for the research to be discussed in this thesis, it is worth mentioning that the 12 Principles of Green Chemistry should not be looked at separately or individually. They should be approached holistically as a guiding framework for chemistry to provide benefits to our society without harming human health and the environment. For John Warner and Paul Anastas, the ultimate goal for Green Chemistry is for the term to disappear, thus becoming the day-to-day way that chemists study, research, and practice chemistry.⁶

1.2 United Nations Sustainable Development Goals

The Sustainable Development Goals (SDGs) were created in 2015 by the United Nations as a universal call for action to protect our planet, end poverty, and promote peace by 2030.⁷ This framework with 17 goals recognizes that prosperity can be only achieved with the implementation of strategies that not only stimulate economic growth, but also address social needs and tackle environmental problems (**Figure 1.3**). The SDGs are being adopted worldwide by many organizations.^{7,8}

Chemistry has an important supportive role in the achievement of a sustainable development due its capability of broadly reaching and interconnecting different aspects of our society, such as economy, technology, human health, and the environment.^{9,10} The implementation of Green Chemistry in the design of processes and products has a direct and significant impact in the achievement of the Good Health and Well-Being (SDG

number 3). By minimizing or eliminating the presence of hazardous chemicals in our water, food, and environment, Green Chemistry enables humans to live healthier and longer lives.^{8, 11} Green Chemistry also contributes towards Quality Education (SDG number 4) and Industry, Innovation, and Infrastructure (SDG number 9). Through the advancement of Green Chemistry Education, knowledge and skills necessary for the achievement of sustainable development are shared and disseminated. Green Chemistry can also upgrade and transform our current industries processes and products to make them more sustainable.⁸



Figure 1.3. The Sustainable Development Goals (SDGs). Used with permission from the United Nations.¹²

Two more important SDGs discussed and addressed throughout this thesis are Responsible Consumption and Production (SDG number 12) and the Climate Action (SDG number 13). An increase in biochar use could help to promote economic growth

while reducing impacts of consumption through the use of a waste, bio-based, and alternative feedstock. Moreover, the production of biochar is a method of carbon dioxide (CO₂) sequestration, and if implemented on a large-scale, this material can help to mitigate the devastating consequences of climate change.¹³

1.3 Biochar

Biochar is a black solid material, and its history dates from over 2,500 years ago. Archaeological studies show the use of this material in traditional agricultural practices in the Brazilian Amazon rainforest. For the indigenous, biochar was known as *Terra Preta de Índio*, which translates to “Indigenous’ Black Earth”, and it was used to increase the amount of nutrients in the jungle soils, improving their quality and productivity.¹⁴

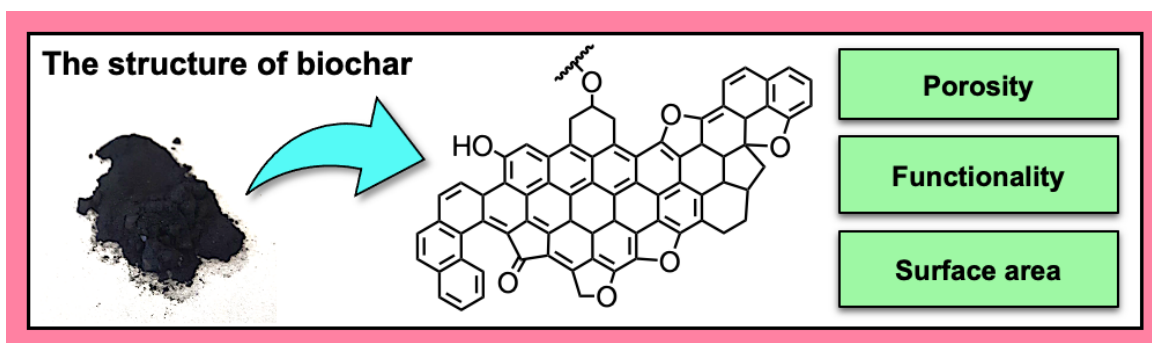


Figure 1.4. An image of biochar and a representative fragment of its structure, with some important chemical and physical properties of this carbon-based material highlighted, such as high porosity, functionality, and surface area.

From a structural point of view, biochar presents an inherently amorphous carbon-rich framework, consisting of sp³ carbons in an extended network with some crystalline areas of highly conjugated aromatic sheets containing sp² carbons cross-linked randomly.

Biochar has significant porosity, surface area, and surface functionality, exhibiting a rich and varied surface chemistry (**Figure 1.4**).¹³ These irregular but potentially highly tunable properties and characteristics of biochar confer this material great potential. It could be applied towards the production of various functional materials in different high-value fields (e.g. catalysis, energy, and medicine).

Compared to other crystalline and amorphous carbon materials, the utilization of biochar represents a more environmentally friendly and cost-effective alternative. Methods for the production of carbon nanotubes, carbon nanofibers, graphene, activated carbon, or even carbon black materials generally include drawbacks that limit their large-scale application and commercialization in lower value fields. These might involve the use of harsh processing conditions and complicated apparatus, as well as the reliance on metal catalysts, toxic organic solvents, and expensive precursors based on fossil fuels.^{13, 15} As a result, costs associated with the production of those carbon materials are extremely high, reaching about 200 USD per gram for graphene.¹⁶ Biochar is, however, produced sustainably and inexpensively from a wide range of waste biomass feedstocks through a thermal processing treatment under moderate temperatures (< 700 °C) known as pyrolysis.¹³

1.3.1 Pyrolysis and Biochar for Climate Change Mitigation

Sawmill, pulp, and paper mills produce materials that can be largely applied in different areas, from building products to consumer goods. During the manufacture of

these materials, large amounts of wood residues such as sludge, bark, and sawdust are generated and transported to landfills or abandoned on the harvested sites. For example, a report published by Memorial University of Newfoundland estimates the generation of more than 40 kt of forestry biomass residues in 2012 only in the province of Newfoundland and Labrador.¹⁷ Left aside, this waste decomposes, liberating greenhouse gases to our atmosphere. Through pyrolysis, the environmental problems generated by the decay of wood residues can be mitigated while producing energy in the form of bio-oil and syngas from renewable feedstocks.^{18, 19}

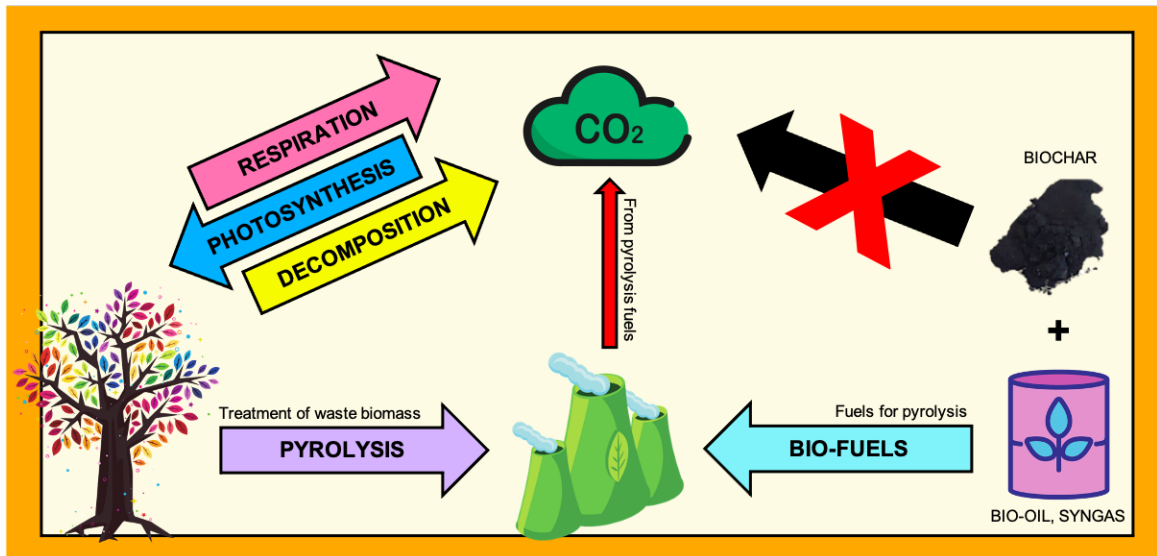


Figure 1.5. Illustrative representation of the sustainable biochar concept. Plants absorb CO₂ during photosynthesis, which is released back to the atmosphere during respiration and decomposition. If waste biomass is treated via pyrolysis, climate change effects can be mitigated due to the production of biochar, a carrier for long-term carbon storage. Moreover, bio-oil and syngas are co-produced during the process and can be further used as renewable energy sources to feed and power the pyrolysis reactor.

The photosynthesis of plants is a natural method of CO₂ sequestration. During this process, plants remove CO₂ from the atmosphere to produce energy for their development and growth (e.g. cellulose, pigments). However, when plant biomass is left aside to decompose, the CO₂ previously fixed during photosynthesis is now released back to the atmosphere via microbial degradation. The thermal treatment of waste biomass under low oxygen concentrations and moderate temperatures (i.e. pyrolysis) transforms these residues into biochar, which decomposes much more slowly than wood or other forms of the parent biomass.²⁰

Table 1.1. Typical compositions and physical properties of oils obtained from biomass and fossil fuel feedstocks.^a

Property/Composition	Bio-oil	Fuel oil
Oxygen (wt%)	36-52	0.1-1.0
Water (wt%)	17-30	0.02-0.10
Density (kg/m ³)	1.10-1.30	0.9-1.0
pH	2-3	Neutral

^aTable adapted from the work of Zacher and collaborators,²¹ and Wang and collaborators.²²

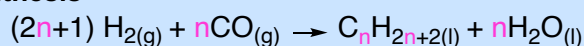
Decay rates are highly dependent on the feedstock and conditions of disposal, storage, and utilization, but estimated half-lives are between 1-3 years for plant biomass, and between hundreds to thousands of years for biochar.^{18, 23} Therefore, pyrolysis of waste biomass has the potential to mitigate anthropogenic CO₂ emissions and climate change consequences by rerouting carbon from the more rapid biological cycle into a much

slower cycle promoted by the production of biochar (**Figure 1.5**).²⁴ The potential of biochar as an important carbon sink has been recognized by the Intergovernmental Panel on Climate Change (IPCC) in their last assessment report.²⁵

Besides biochar, bio-oil and syngas are also co-produced during pyrolysis of waste biomass and represent important Biomass-to-Liquids (BTL) approaches to reduce our society's current dependency on non-renewable fossil fuel precursors. Bio-oil is a dark, viscous, and complex liquid mixture produced by the rapid cooling and condensation of the vapors generated during pyrolysis, containing a large number (> 300) of oxygenated compounds, including water, acids, aldehydes, alcohols, esters, ketones, and several heterocyclic compounds.²¹ It can be directly used as a low-grade fuel and combusted in boilers, engines, furnaces, and turbines to generate power and heat. However, as shown in **Table 1.1**, its high oxygen content gives bio-oil some undesirable chemical and physical properties that limit the applications of this sustainable fuel obtained from renewable sources. Some of those characteristics include high viscosity, corrosiveness, poor stability, low volatility and low heating value.²² In order for bio-oil to be ideally used as an alternative transportation fuel and as an important chemical building block, an additional step involving its upgrading (i.e. oxygen removal) into light hydrocarbons and aromatics is necessary. The most common methods for bio-oil conversion into fossil fuel replacements include hydrotreatment, zeolite upgrading, fermentation, and aqueous-phase processing.²⁶

Syngas is a gas mixture of hydrogen (H₂) and carbon monoxide (CO). It can be produced from various methods using different precursors, including fossil fuels and biomass.²⁷ In the latter case, syngas is also called biosyngas to emphasize the greener feedstock origin. Regardless of the starting material used for its manufacture, this gas mixture can be used directly in boilers, turbines, and furnaces, or as an important platform chemical for the synthesis of valuable chemicals and energy.²⁸ Probably the most significant example of syngas conversion is the Fischer-Tropsch Synthesis. This process allows the synthesis of liquid hydrocarbons from syngas (**Scheme 1.1**), thus readily producing a petroleum substitute for the production of fuels such as diesel and gasoline, as well as different chemical building blocks, including olefins and alcohols.^{28, 29} Methanol and ammonia are also other examples of important chemicals that can be produced using different approaches and syngas as a precursor.²⁹

Fischer-Tropsch Synthesis



Scheme 1.1. Generic form of the Fischer-Tropsch process, where **n** is typically between 10-20 and can be adjusted with the reaction conditions.

The yields of biochar, bio-oil and syngas produced during pyrolysis are dependent on the nature of the biomass feedstock and on the type of processing implemented.^{20, 29} Based on the conditions applied, pyrolysis may be classified into slow or fast. Although this classification is widely utilized, many processes have been performed in conditions ranging between the extremes of slow and fast pyrolysis.³⁰ Generally, slow pyrolysis is

performed over a wide temperature range (e.g. 300-800 °C), low heating rates (e.g. 5-7 °C/min) and long vapor residence times (e.g. > 1 h), and it favors the production of biochar as the main product.¹³ For fast pyrolysis, temperature ranges are narrower (e.g. 400-600 °C), heating rates are very high (e.g. > 300 °C/min), and vapor residence times are shorter (e.g. 0.5-10 s).¹³ In this case, bio-oil is produced primarily. A comparison between yields of biochar, bio-oil, and syngas typically produced during these two types of pyrolysis is shown in **Table 1.2**.

Table 1.2. Typical yields of products obtained during slow and fast pyrolysis.^a

Pyrolysis	Biochar Yield (wt%)	Bio-oil Yield (wt%)	Syngas Yield (wt%)
Slow	35-50	30-35	30-35
Fast	15-35	60-75	15-20

^aTable constructed with the data from Yu and collaborators,¹³ Lehmann and Joseph,²⁰ and Basu.²⁷

1.3.2 Effects of Biomass Feedstock and Pyrolysis Conditions on Biochar

The nature of the waste biomass feedstock and the conditions applied during pyrolysis not only have a significant influence on the yields of biochar obtained (**Section 1.3.1**), but also on the chemical and physical properties of the material produced.²⁰ The term “biomass” refers to any renewable organic material derived from plants, animals, and micro-organisms.²⁹ Throughout this thesis, the focus will remain on residues obtained from lignocellulosic biomass, which includes waste derived from wood, plants, leaves, crops, and vegetables. Those second-generation feedstocks are inedible plant materials and therefore, their use to produce chemicals and energy does not threaten or

compete with the food supply.²⁷

The major constituents of lignocellulosic biomass are cellulose, hemicellulose, and lignin. Cellulose is a crystalline, linear, long-chain polymer, with thousands of D-glucose units linked together.²⁹ Hemicellulose presents a more amorphous structure composed of different sugars (e.g. D-glucose D-xylose, D-galactose, and others), whereas lignin consists of a complex branched phenolic polymer.²⁹ The most important constituent monomers of cellulose, hemicellulose, and lignin are highlighted in **Figure 1.6**. The rates of and degrees to which these three components decompose are different and depend on the pyrolysis conditions applied. For example, decomposition temperatures range from 200-260 °C for hemicellulose, from 240-350 °C for cellulose, and from 280-500 °C for lignin.¹³ Therefore, materials with different lignocellulosic compositions, even belonging to the same type of lignocellulosic biomass (e.g. wood), may present different chemical and physical properties.²⁷

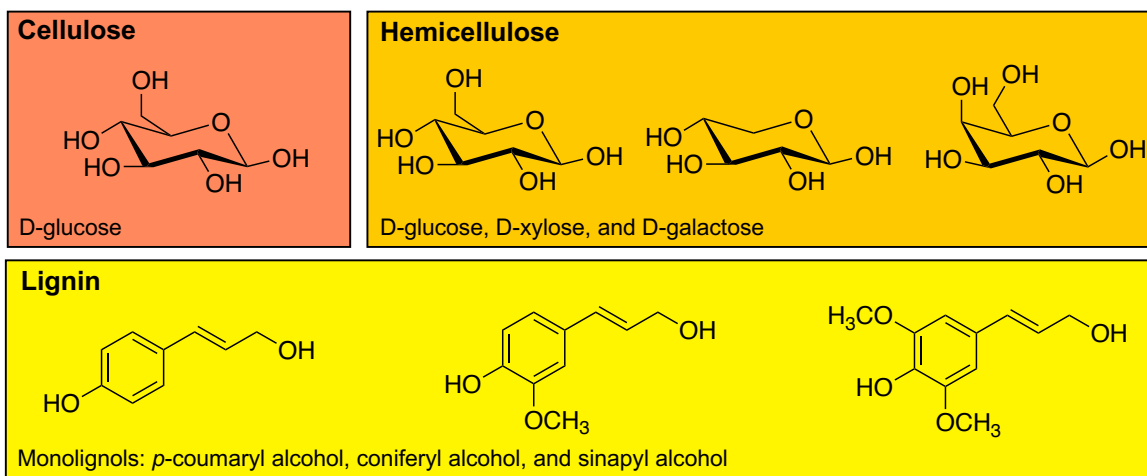


Figure 1.6. Most important monomers of cellulose, hemicellulose, and lignin.

To better understand the effects of biomass feedstock in the new biochar applications discussed and developed in this thesis, biochars obtained from waste of the two main groups of forestry feedstocks (i.e. hardwood and softwood) are studied herein. Hardwoods are angiosperms and present broad leaves. Most of those trees are deciduous and lose their leaves annually. They also present a characteristic type of cell wall known as vessel element (i.e. pore), which is used for the transport of nutrients and water. In contrast, softwoods are gymnosperms which present cones with needles that are evergreen, and therefore, persist throughout the entire year.³¹ A comparison between hardwood and softwood characteristics and typical inherent compositions is shown in **Figure 1.7**.

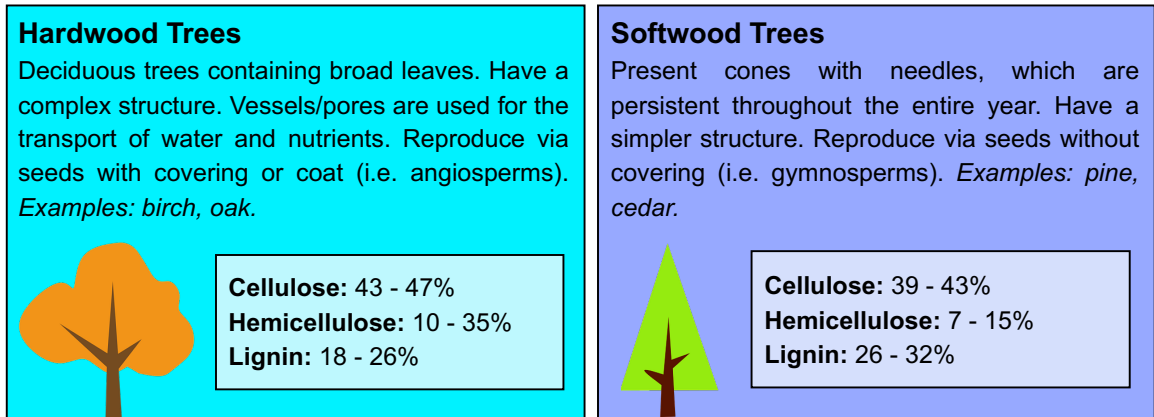


Figure 1.7. Characteristics and typical cellulose, hemicellulose, and lignin compositions of the two main groups of forestry biomass feedstocks: Hardwood and softwood trees.

As mentioned previously, pyrolysis parameters including heating rate, temperature, pressure, gas flow rate, reactor type, and residence time also significantly influence the chemical and physical properties of the material obtained.^{13,20} For example, an increase in

pyrolysis temperatures can decrease biochar yields, but produce bio-based carbon-materials with more crystalline and ordered structures, higher carbon contents, and also increased surface areas and pore volumes.^{13,32} On the other hand, an increase in retention time and gas pressure might be detrimental to the quality of the material synthesized, thus causing deformations in the structure of the biochar produced.²⁰ This complexity and variability related to biomass feedstock nature and operating conditions represent some of the challenges responsible for limiting the large-scale and high value applications of biochar to date. In order to increase the utilization of this inexpensive, sustainable, and renewable material in the design of our future processes and products, the functionalization of biochar represents a fundamental step.

1.3.3 Functionalization of Biochar

As mentioned in **Section 1.3**, biochar presents a rich surface functionality and abundant porosity, which can be easily adjusted through functionalization to enhance its performance and improve its applications in high value-added fields. Generally, functionalization processes can be performed by adding reactants with the waste biomass in the pyrolysis chamber (i.e. direct or in situ modification) or by incorporating the desired functional groups on biochar after it has been produced (i.e. post-synthetic modification).³³ Regardless of the strategy implemented, oxidation is the most common method of biochar functionalization. Using this methodology, a large number of oxygenated groups such as carbonyl (-C=O), hydroxyl (-OH), and carboxyl (-COOH)

groups can be incorporated on the surface of biochar. This introduction of oxygenated functional groups has been achieved using hydrogen peroxide, ozone, potassium permanganate, or nitric acid as reagents.³⁴⁻³⁸ However, functionalization of biochar using nitric acid has been demonstrated to be the most effective method to oxidize this carbon material in regards of reproducibility and amount of oxygenated groups introduced.¹³

The insertion of sulfonic acid groups (-SO₃H) is also an important strategy to amplify the use and implementation of biochar, and it has been achieved through reactions with sulfuric acid or derivatives (e.g. *p*-toluenesulfonic acid and hydroxyethylsulfonic acid).³⁹⁻⁴⁴ In cases where concentrated sulfuric acid is used for sulfonation, oxidation is also performed to some extent, since oxygenated groups are often incorporated in addition to the sulfonic acid moieties.^{43, 44}

Different methods and procedures to promote biochar amination have been also employed. Conventional chemical treatments involve the utilization of ammonia in situ under high temperatures or a combination of nitration and reduction reactions using sulfuric and nitric acids, but more environmentally-friendly alternatives using amino acids have been studied to insert amino (-NH₂) groups onto biochar's surface.⁴⁵⁻⁴⁹ Reactions with 3-aminopropyltriethoxysilane (APTES) are also known to promote amination of biochar's surface alongside with silanization.⁴⁸ Recently, a combination of biochar amination and sulfonation methods has been developed, and highly functionalized biochars containing amino and sulfonic groups have been synthesized using 4-*tert*-butylaniline and 4-aminobenzenesulfonic acid.^{50, 51}

The incorporation of different heteroatoms (e.g. nitrogen, boron, phosphorus, sulfur, and fluorine) into the carbonaceous framework of biochar is also largely applied. The most common doping approaches include the production of nitrogen-rich (*N*-doped) biochars, which have been synthesized using in situ or post-synthetic modification methods using different nitrogen precursors such as urea, macroalgae, and melanin.⁵²⁻⁵⁶ Different doped carbon materials can also be produced from the pyrolysis of inherent heteroatom-rich biomass feedstocks, such as chitin.⁵⁷⁻⁶⁰ Other approaches to produce functionalized biochars include modification with ionic liquids, and pre- or post-pyrolysis loading of metal particles.⁶¹⁻⁶⁶ The latter strategy is very common, and both have been integrated with other biochar functionalization methods to optimize its modification and performance.⁶⁷⁻⁷³

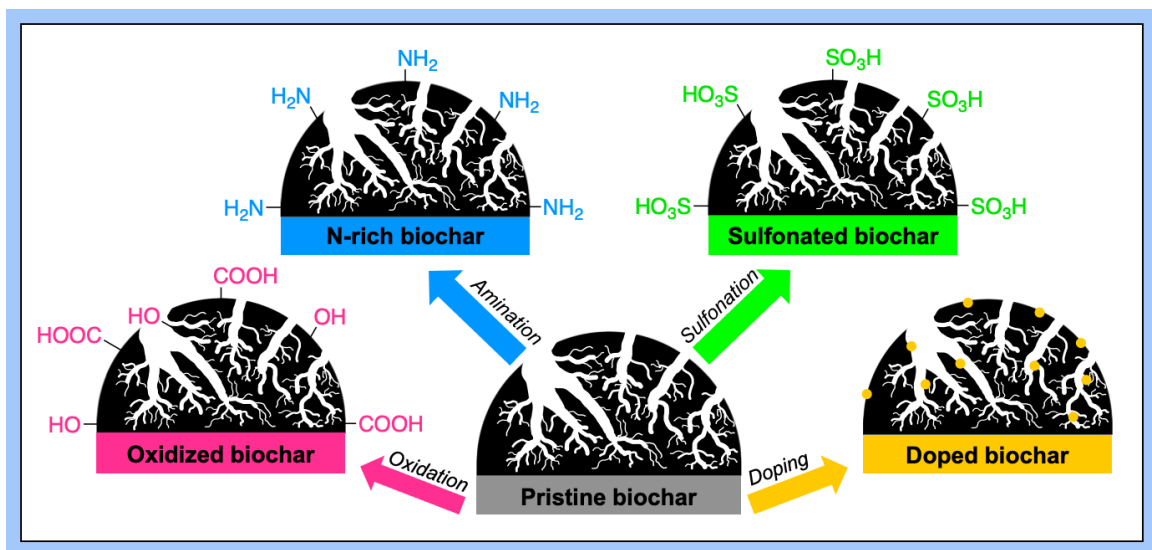


Figure 1.8. General representation of the most common employed methods of biochar surface and carbon framework functionalization: Oxidation, amination, sulfonation, and doping.

As detailed throughout this section, various functionalization approaches have been studied to tune biochar characteristics and properties, with efforts to overcome the drawbacks related to this carbon material variability and complexity. The most commonly used and employed methods of biochar modification are generally represented in **Figure 1.8**. Although the development and design of more cost-effective, sustainable, and benign processes is still needed, the research performed so far already contributed significantly towards the promotion of biochar as an advanced platform material via the adjustment of its structure, enhancement of its performance, and improvement of its applications. Some of those recent refined applications and the contribution of different types of biochar functionalization for their implementation will be discussed thoroughly in **Section 1.3.4** and in **Section 1.3.5**.

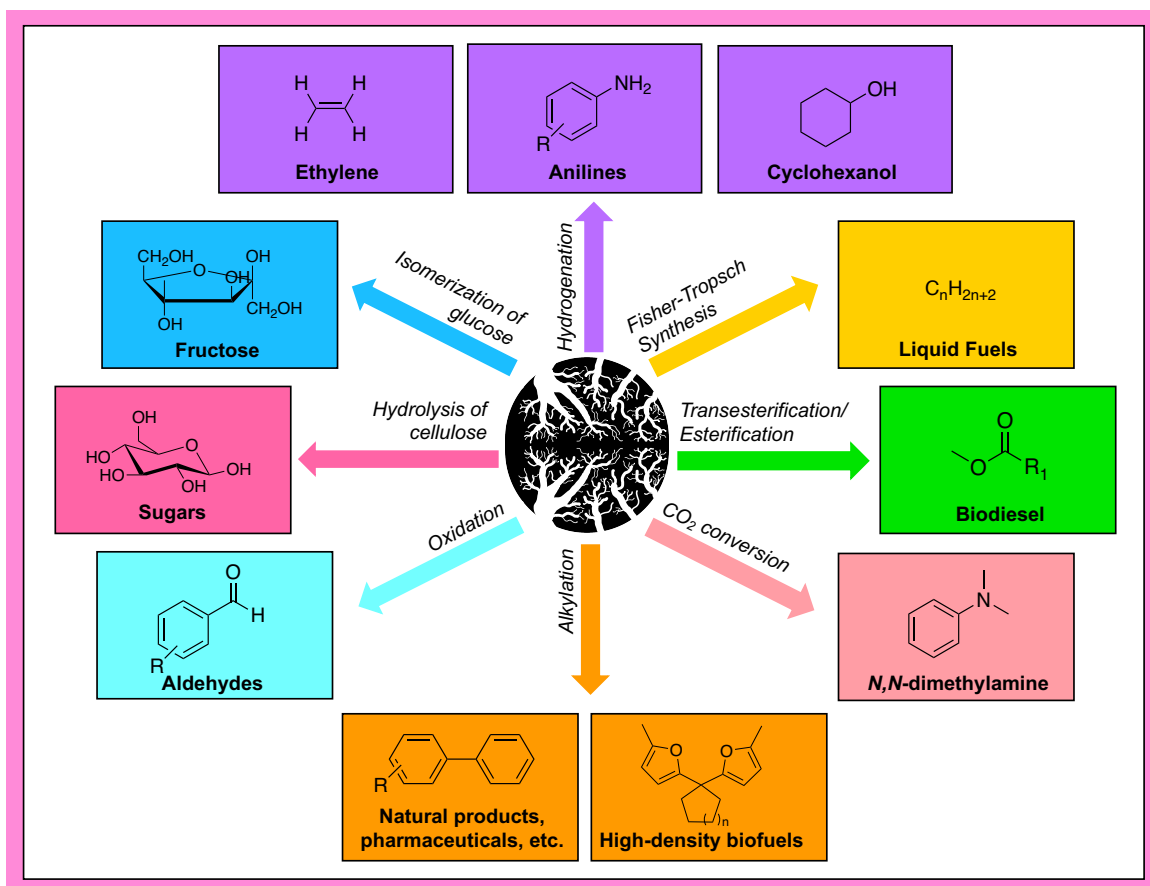
1.3.4 Biochar Applications in Catalysis

The first report involving agricultural civilizations in the Amazon forest dates from 1542.¹⁹ The association between those civilizations with the use of anthropogenic and productive black earth soils (i.e. *Terra Preta de Índio*) has been investigated by anthropologists in the twentieth century.⁷⁴ During the 1990s, scientists discovered large amounts of biochar present in those *Terra Preta de Índio* soils, and in 2006 Lehmann discussed the potential of biochar to be used in climate change mitigation.^{24,75} Due to the history of this bio-based carbon material, it is no surprise that the majority of research involving biochar has been conducted to evaluate its performance and potential as a soil

amendment agent and as a carbon sink.⁷⁶⁻⁸¹ Biochars from different biomass feedstocks have been also largely utilized in other environmental protection applications, including in CO₂ adsorption,^{48, 82} and wastewater organic and inorganic pollutant removal.^{55, 83-89} However, these lower value applications mentioned will not be discussed further in this thesis.

Over the years, the development and design of different modification methods has allowed the production of diverse types of functionalized biochars, thus expanding the implementation of this bio-based material in higher value-added fields as advanced materials for energy storage (i.e. supercapacitors, electrodes) or as catalysts.⁹⁰ One of the most important examples of this application is the production of biodiesel using biochar catalysts.⁹¹ The production of this renewable diesel substitute via esterification or transesterification reactions is conventionally catalyzed by homogeneous acids and bases (e.g. sulfuric acid, sodium hydroxide, and potassium hydroxide), which generates acidic and basic waste harmful to the environment.^{92, 93} Several heterogeneous catalysts have been implemented for this transformation, but they often rely on expensive metal precursors.^{94, 95} To overcome those drawbacks, sulfonated biochar has been applied as an inexpensive heterogeneous catalyst for biodiesel production from vegetable and waste cooking oils under moderate conditions, with high yields, and great recyclability.^{44, 96-99} Although wood waste derived materials have been the most employed, carbon materials obtained from different feedstocks such as municipal sludge and algae could also promote esterification and transesterification reactions.^{100, 101} A comprehensive discussion about

the influence of different biochar types in the process, and a detailed comparison between biochars and the most common catalysts for biodiesel production can be found in the reviews of Cao and collaborators,¹⁰² and Kwon and co-workers,⁹¹ respectively.



Scheme 1.2. Representation of some products produced using biochar catalysts studied to date.

Other types of biomass transformations have also been promoted by sulfonate and ionic liquid-derived biochars, including the hydrolysis of cellulose for the production of sugars,¹⁰²⁻¹⁰⁶ which are considered platform chemicals and can be further used in isomerization reactions, also using biochar catalysts.^{66, 107, 108} Functionalized biochars with

doped iron nanoparticles have been also used as catalysts for the production of hydrocarbons from syngas via Fischer-Tropsch synthesis,⁶³ whereas biochars catalysts derived from corn stover have been successfully employed for the pyrolysis and conversion of waste plastics into liquid fuels and hydrogen gas.¹⁰⁹ A summary of the catalytic reactions using biochar studied to date can be found on **Scheme 1.2**.

Although the majority of studies using biochar catalysts focused on biomass transformation processes, research involving traditional chemical reactions has become more common, thus allowing the implementation of this bio-based material in the synthesis of intermediates and industrially used products. Recently, *N*-doped biochars from different biomass feedstocks have been loaded with metal nanoparticles to catalyze hydrogenation reactions.¹¹⁰⁻¹¹² The hydrogenation of acetylene to ethylene could be performed using biochars from forage crops as catalysts.¹¹⁰ Acetylene is a by-product of the synthesis of ethylene from petroleum cracking processes, and it could be detrimental for the conversion of the respective alkene into other materials.¹¹³ The hydrogenation of acetylene is one the most widely employed methods for ethylene purification, but it is often promoted by metal catalysts with low selectivity and short lifetimes.¹¹⁴ Although energy-intensive conditions are required for the process (i.e. temperatures of 200 °C), biochars could facilitate hydrogenation reactions with excellent conversions whilst maintaining high selectivity for 27 h.¹¹⁰ Inherent *N*-doped biochars from shrimp containing supported metal particles have been utilized as catalysts for the hydrogenation of nitroarenes to produce anilines.¹¹¹ The latter are considered key building blocks and

can be widely used for the fabrication of bulk chemicals, agrochemicals, dyes, and pharmaceuticals.¹¹⁵ With the assistance of biochar, various nitroarenes and nitroarene-based drugs could be converted to the respective aniline analogues with excellent yields (i.e. about 99%), and moderate temperatures and hydrogen pressures (i.e. 110 °C, 40 bar). A decrease in activity is observed after four catalytic cycles, but good yields of anilines are obtained nevertheless.¹¹¹ Another examples of hydrogenation reactions facilitated by biochar are the hydrogenation of quinolines using *N*-doped biochar catalysts also containing supported metal nanoparticles,¹¹² and the production of the industrially applied cyclohexanol using lignin model compounds as substrates.^{116, 117}

Highly functionalized biochars containing metal particles on their surface have been used to promote carbon-carbon (C-C) cross-coupling reactions.¹¹⁸ Those reactions are used for the synthesis of various pharmaceuticals, natural products, polymers, hydrocarbons, and advanced materials, but are conventionally facilitated by expensive, sometimes toxic, and air-sensitive heterogeneous metal catalysts.^{119, 120} Biochars after silanization and metal loading could successfully catalyze C-C coupling of a wide range of substrates, at temperatures ranging from 80-120 °C. The Principles of Green Chemistry were further embraced in this work by extensive solvent screening and selection of a greener alternative (e.g. polyethylene glycol 400) as a solvent in the process described.¹¹⁸ Alkylation reactions could also be performed with the assistance of biochars from coconut shell functionalized with sulfonic and amino groups.⁵⁰ Besides exhibiting great recyclability, those biochar catalysts displayed great performance with conversions higher

than 90% for the alkylation of furans with cyclic ketones and phenols. The resulting products could be used as platform chemicals for the synthesis of jet fuels.⁵⁰

Another application of functionalized biochar catalysts consists of the methylation of amino compounds using CO₂ as a feedstock.¹²¹ This reaction provides an important strategy for the conversion of the respective greenhouse gas in products with relevant industrial importance, such as *N,N*-dimethylamine. The latter can be used to produce medicines, agrochemicals, perfumes, and dyes. *N*-doped biochar could catalyze the transformation of different amines to the desired products with conversions higher than 90% and application of relatively mild conditions (e.g. 75 °C, 1 bar CO₂, 20 h) for the CO₂-based methylation.¹²¹

Heteroatom-doped biochars have been obtained via pyrolysis at different temperatures and applied as catalysts for the aerobic oxidation of alcohols to aldehydes,¹²² which is often performed using toxic and corrosive oxidants, and expensive noble metal-based catalysts.¹²³ By using biochar catalysts doped with phosphorus atoms, the synthesis of aldehydes could be performed using oxygen as the oxidant and water as a solvent. The catalyst could be recycled 8 times without loss in activity, the substrate scope investigated was very broad, and the aldehydes produced, which are considered important intermediates for the fabrication of industrially used chemicals, were obtained as the only product. Moreover, the heteroatom-doped biochars presented similar activities to other heterogeneous catalysts previously used for the oxidation of alcohols such as *N*-doped graphene, graphene oxide, and different noble metal-based catalysts.¹²²

It is worth mentioning that a large variety of carbon materials has been studied for different high value-added applications. For example, carbon solid materials obtained after hydrothermal processing of biomass (i.e. hydrochars) have been studied as catalysts for the production of pharmaceutically important *N*-heterocycles,⁷² industrially applied anilines,⁶¹ or promising liquid fuels.¹²⁴ They have also been used for the oxidative coupling of benzyl alcohols or amines to synthesize aldehydes and imines as valuable end products and building blocks.^{72, 125} Although some authors might refer to those carbon materials as “biochars” and even treat them identically, they differ from biochars with regards to production, characteristics, and chemical and physical properties.¹²⁶ The difference between biochar and other carbon materials derived from biomass is thoroughly discussed in **Section 1.3.6**.

1.3.5 Biochar Applications in Building Materials

Besides being used in the area of catalysis, biochars have been employed as additives in the area of construction science for the reinforcement of cements.¹²⁷⁻¹³⁰ The cement industry is one of the largest in the world, but it is far from being the most environmentally friendly since about 5% of anthropogenic CO₂ emissions are generated by cement manufacturing.⁴⁹ For those reasons, there is an urgency to continue developing strong, long-lasting materials for building purposes using more sustainable and cost-effective designs. Very small additions of biochar (i.e. 1-2 wt%) have shown to be adequate and sufficient to improve cement composites strength, toughness, and durability.¹²⁷⁻¹³⁰

High performance concretes have been also fabricated using biochars. Concretes are building materials displaying great strength and durability, and are produced from the mixture of different agglomerates with cement. As previously mentioned, the fabrication of cement is a powerful driver of greenhouse gas emissions, and comprises 50% of the total environmental and health damages of concrete manufacturing.¹³¹ Different types of biochar have been successfully applied as partial or full cement replacements in the fabrication of concrete, thus representing more sustainable alternatives for the production of construction materials through the reduction of worldwide energy-intensive cement demands.¹³²⁻¹³⁴

1.3.6 Biochar, its Definition, and Other Carbon Materials Derived from Biomass

Researchers often use a range of sometimes interchangeable terms to describe carbons produced from biomass. However, they are not all the same and it is important to define them to avoid confusion (**Table 1.3**). Although the differences between biochar and other amorphous carbon-materials have been discussed by Yu and collaborators,¹³ and Lehmann and Joseph,²⁰ there is still significant overlap in the literature surrounding their definitions, since different terms are often attributed to the same products. In 2018, the International Union of Pure and Applied Chemistry (IUPAC) has created the “Glossary of Terms Used in Biochar Research” project in efforts to standardize and regulate the terminology involved in the work of amorphous carbon-based materials.¹³⁵

In this thesis, the previously and comprehensively adopted literature conventions

will be followed, where biochar is defined and referred to as a solid material produced from the thermochemical conversion of biomass under low concentrations of oxygen and moderate temperatures (i.e. 400-600 °C).^{13, 136} According to this definition, biochar is considered a specific type of carbon material derived from biological sources (i.e. biocarbon). However, other types of biocarbon can be synthesized using thermochemical processes. Hydrochars are biocarbons produced after hydrothermal carbonization (HTC) of biomass or biomass-derived compounds (e.g. lignin, carbohydrates) at relatively low temperatures (i.e. 130-250 °C) and high pressures.^{137, 138} Unlike pyrolysis, hydrothermal carbonization requires the feedstock to be submerged in water, thus being more suitable for the processing of biomass with high moisture contents (> 30%).^{126, 139}

Table 1.3. A comparison between biochar and other amorphous carbon materials.

Carbon material	Carbon material feedstock	Thermochemical conversion	Processing temperatures	Carbon content
Biochar	Biomass	Pyrolysis	400-700 °C	40-90%
Hydrochar	Biomass/biomass-derived compounds	HTC	130-250 °C	50-60%
Activated Carbon	Biomass, asphalt, coal, and others	Carbonization with activation	700-1000 °C	80-95%
Carbon Black	Petroleum, coal, asphalt, and others	Combustion in air-poor conditions	-	> 95%

^aTable constructed with the data from Yu and collaborators,¹³ and Lehmann and Joseph.²⁰

Regarding chemical and physical properties, biochars are composed of aromatic layers arranged randomly, whereas hydrochars are mostly dominated by alkyl moieties

and present spherically shaped carbonaceous nanoparticles on their surface.¹⁴⁰ Hydrochars present higher surface functionality, but have lower surface areas and decreased porosity, when compared to the carbon materials obtained from pyrolysis.^{141, 142} Those different types of biocarbon also behave differently in respect to the variation of parameters during thermochemical conversion, approach which is comprehensively reviewed in the comparative work performed by Kambo and Dutta.¹²⁶ Perhaps the most important difference between biochars and hydrochars relies on the potential for carbon sequestration. Results obtained so far show a much lower stability of hydrochars (i.e. half-lives of 100 days) in contrast to biochars (i.e. half-lives of thousands of years), thus showing that biocarbons produced from HTC processes do not possess the same capacity for climate change mitigation as observed for the materials obtained from the pyrolysis of biomass.¹⁴³⁻¹⁴⁵

Activated carbons are other types of carbon-based materials, which are chemically or physically activated under even higher temperature regimes (i.e. 700-1000 °C), have a high carbon content (i.e. 80-95%), and can be derived from any finite or renewable carbon source, such as biomass, coal, or asphalt.¹³ In the case where activated carbons are produced from biomass feedstocks, they are often considered activated biochars. On the opposite side, the term “carbon black” is often used to refer to carbon-materials mainly synthesized from fossil feedstocks (e.g. petroleum, coal) which present a carbon content higher than 95%.¹³

1.4 Implementation of a Circular and Bio-Based Economy

For us to truly achieve a sustainable future and tackle our current environmental challenges, a massive change in the way our current chemical industry operates is needed. Nearly 140,000 industrial chemicals are marketed worldwide, and the majority is currently manufactured through a linear path, using finite substances, fossil precursors, and highly reactive and persistent reagents, thus generating high quantities of toxic waste.^{146, 147} A more sustainable and environmentally friendly approach for the future chemical sector can be achieved by employing more circular processes, where renewably sourced precursors are used to synthesize benign materials using intrinsic greener reagents. Moreover, the waste generated should be further treated as a feedstock for the design of other products and processes. This concept is also known as circular economy, a holistic system addressed to eliminating waste, recycling products, saving resources, and promoting a sustainable development.¹⁴⁶

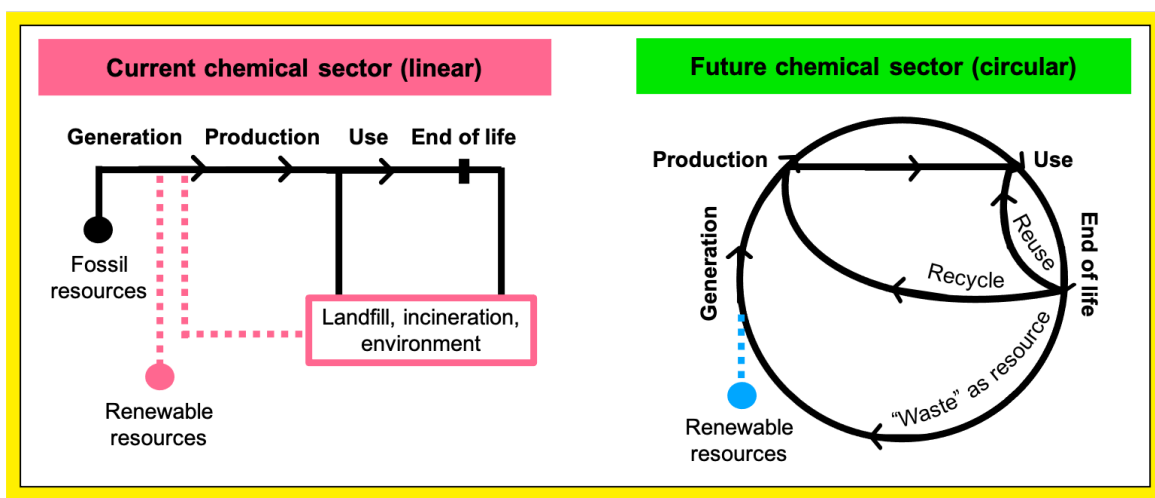


Figure 1.9. Comparison between the linear and circular chemical sectors.

Nexus solutions are considered important strategies in the implementation of a circular economy. These solutions consider the entire system and can synergistically tackle multiple sustainability challenges, thus magnifying benefits and avoiding accidental consequences.^{147, 148} An increase in the large-scale applications of biochar represents an important nexus solution for the achievement of a bio-based and circular economy, since a carbon sink material obtained from waste could be employed as a feedstock for the production of cleaner energy, fabrication of advanced materials, and synthesis of industrially used chemicals. This is a key hypothesis in this thesis.

From here in, different approaches that have been pursued through this thesis for the improvement and enhancement of biochar applications as a nexus solution will be highlighted. Strategies in the areas of CO₂ transformation (**Section 1.5**), layered materials exfoliation (**Section 1.6**), polymer composites reinforcement (**Section 1.7**), and their respective applications in biochar research are discussed and reviewed.

1.5 The Good and the Bad of CO₂

The use of CO₂ as a feedstock in the manufacture of chemicals integrates the 12 Principles of Green Chemistry and the concept of a Circular Economy. CO₂ is known for being a greenhouse gas, thus absorbing a part of the radiation emitted by our planet and re-emitting it towards the Earth. Although the natural greenhouse effect is responsible for keeping our planet habitable, anthropogenic activities are amplifying its intensity and causing devastating consequences to our climate and to our world. It all started with the

Industrial Revolution (1760) onwards, when the burning of fossil fuels has become our main process of energy production.²⁹

Fossil fuels (e.g. coal, oil, and natural gas) are ancient forms of carbon-rich materials formed by the decomposition of buried animals and plants aging over millions of years. By burning these non-renewable fuels to produce energy, huge amounts of CO₂ (i.e. about 7 billion tonnes per year) are rapidly released into our atmosphere, which now has concentrations of 412 ppm of this greenhouse gas, compared to 280 ppm in the pre-industrial era.^{29, 149} If our current CO₂ generation tendency continues, concentrations are estimated to reach 570 ppm by 2100, thus causing a rise of about 1.9 °C in our mean global temperature, increasing the sea levels by up to 1 m, intensifying desert formation, and resulting in the extinction of several species.²⁵

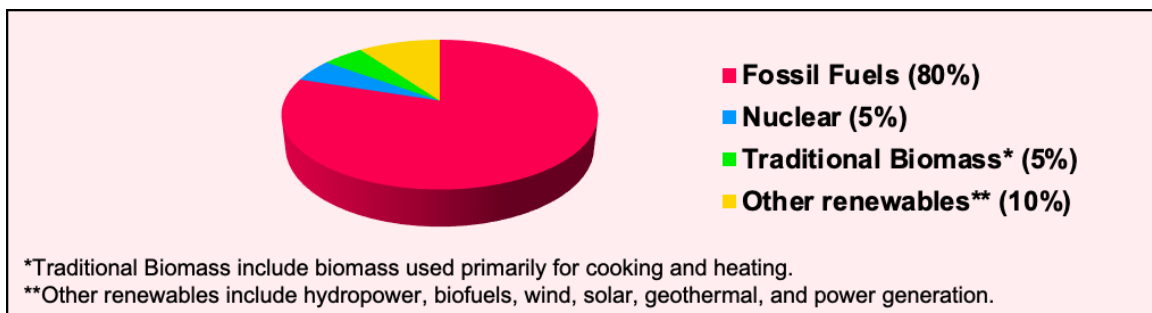


Figure 1.10. Share of total energy demand by fuel in 2019. Constructed with the data from the International Energy Agency (IEA) Global Energy Review for 2019.¹⁵⁰

Although cleaner energy sources can reduce our reliance on fossil fuels, the latter and traditional option comprised 80% of the total worldwide energy demand in 2019 (Figure 1.10). To assist in the offset of anthropogenic CO₂ emissions, one area of focus should be education in Green Chemistry and sustainable development, which could help

our society to develop more knowledgeable citizens, with a more conscious thinking and attitude towards our environment and the impact of energy utilization in it.¹⁵¹ Another focus, attractive in terms of a circular economy is the use of CO₂ as a feedstock.

Of the total abundance of CO₂ in our planet, only 0.1% is currently consumed by the chemical industry.¹⁵² The main reason for this very small proportion is related to the stability and inertia of CO₂ towards chemical transformations, which can be overcome by the utilization of reactive co-reagents, high-energy inputs, or the employment of an appropriate catalyst. However, it should be noted that other characteristics of CO₂ such as non-toxicity, availability, and recyclability, are suitable for its implementation as an important chemical building block.¹⁵³ Some important industrial conversions that use CO₂ as a feedstock include the synthesis of carboxylic acids, urea, and methanol.¹⁵⁴ Another important example of CO₂ transformation into fine chemicals is in the synthesis of cyclic carbonates.

1.5.1 Cycloaddition Reaction Between CO₂ and Epoxides

The production of cyclic carbonates through the cycloaddition reaction between CO₂ and epoxides (**Figure 1.11**) is one important transformation of this greenhouse gas and has been previously studied in the Kerton research group at Memorial University of Newfoundland. In terms of Green Chemistry, this conversion is a great example of an atom economic reaction (Green Chemistry Principle number 2), in which 100% of the atoms in the reactants are incorporated in the products without generating any waste.¹⁵⁵

Moreover, the cyclic carbonates produced through this transformation can be used as green solvents due to their low toxicity and moderate polarity. Therefore, the reaction of CO₂ and epoxides is often performed under neat conditions, thus eliminating the use of solvents that can be harmful to human health and the environment.¹⁵⁶

Cyclic carbonates also find applications as greener reactants in chemical synthesis, as intermediates in the synthesis of fine chemicals, as building blocks for polymer production, in the dissolution of electrolytes in batteries, and as constituents of oils and paints.¹⁵⁷ As mentioned previously in **Section 1.5**, CO₂ conversion processes generally require severe reaction conditions to activate this stable form of oxidized carbon. However, to transform CO₂ in an important tool for sustainable development, more efficient, benign, and cost-effective methods using mild conditions that avoid the further release of this greenhouse gas to our atmosphere need to be developed.

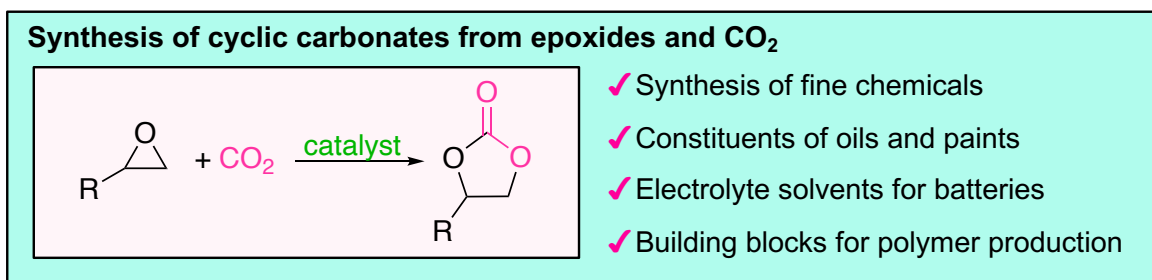


Figure 1.11. Cycloaddition reaction between CO₂ and epoxides to synthesize cyclic carbonates, with their respective applications.

Industrially, the synthesis of cyclic carbonates is typically catalyzed by halide salts, but a wide variety of homogeneous and heterogeneous metal-based and organocatalysts have been investigated.¹⁵⁷⁻¹⁵⁹ Although the metal-based alternatives are usually more

efficient, metal-free catalysts represent a non-toxic, air and moisture stable, and low-cost option to facilitate the cycloaddition reaction between CO₂ and epoxides.¹⁵⁸ Different carbon-based materials have been employed as catalysts for the production of cyclic carbonates, but some of them presented poor recyclability or were investigated under a very narrow substrate scope.¹⁶⁰⁻¹⁶³ Although great results and conversions of cyclic carbonates higher than 95% can be obtained using relatively mild conditions and even very low amounts of graphene oxide as a catalyst (e.g. 2.5 mg),¹⁶¹ challenges associated with use of solvents and further production complexity limit the further applications of this carbon material. Graphene, a precursor for the production of graphene oxide was first produced using a Nobel-prize winning process known as exfoliation.

1.6 Exfoliation of Layered Materials

In 2004, Andre Geim and Konstantin Novoselov synthesized the first ever two-dimensional (2D) material from graphite using a sticky tape to peel single layers of graphene.¹⁶⁴ Six years later, they were awarded the 2010 Nobel Prize in Physics for their “groundbreaking experiments regarding the two-dimensional material graphene” through a type of mechanical exfoliation, also known as Scotch-tape technique, handcraft, or micromechanical cleavage.¹⁶⁵ Since the investigation performed by Geim and Novoselov, exfoliation has become a powerful methodology for the production of unique materials with outstanding properties.

Layered materials are solids that present strong in-plane chemical bonds and weak

interlayer interactions, such as van der Waals forces. Through exfoliation, an external force is introduced to weaken or break the attractive van der Waals interactions between layers, thus producing a single or a small number (< 10) of stacked monolayers.¹⁶⁶ By revealing the inherent nanostructure of the layers, exfoliation can greatly increase their accessible surface area, enhance their chemical and physical activities, and further improve their applications. In fact, exfoliated materials have been employed in the areas of electronics, catalysis, composites and energy storage.^{167, 168}

Although the highest-quality samples of exfoliated materials have been obtained using micromechanical cleavage, it is a very time consuming and low yield process. For those reasons, different and more scalable exfoliation techniques have been developed throughout the years.^{168, 169} One environmentally friendly alternative investigated for the production of remarkable 2D materials uses ultrasound.

1.6.1 Ultrasound

Ultrasound consists of sound waves with frequencies higher than those detectable by human hearing (i.e. 20 kHz to 15 MHz). These waves are usually propagated through a medium by alternating expansion and compression cycles. In expansion cycles, molecules are pulled apart, whereas in the compression cycles they are pushed together. During an expansion cycle, ideal conditions can overcome the attractive forces of the molecule to create bubbles (i.e. cavities), which continually grow throughout the cycles. Eventually, the cavity cannot absorb energy from the ultrasound anymore and implodes,

generating very high local temperatures (i.e. about 5000 K) and pressures (i.e. over than 1000 atm).¹⁷⁰ Although temperatures similar to the surface of the sun and pressures equivalent to the deepest point in the ocean are created during sonication, the ambient conditions remain essentially unaffected. This happens because the imploding bubbles are very small compared to the volume of the liquid and therefore, lose most of the energy generated rapidly to their surroundings.¹⁷¹ An illustration of the formation, growth, and collapse of the bubbles created through ultrasound is shown in **Figure 1.12**.

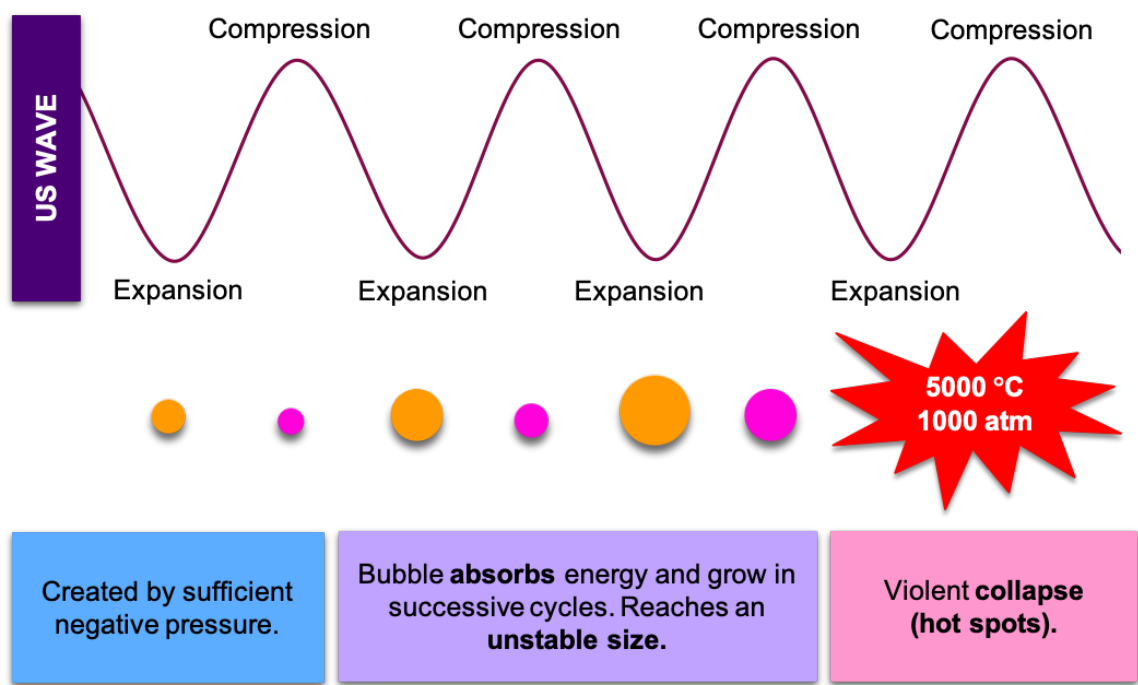


Figure 1.12. Illustrative representation of the formation, growth, and implosion of bubbles created during the cavitation phenomenon.

Sonication can be achieved via direct or indirect processes, which require the use of different apparatus. During direct sonication, a high-energy ultrasonic device such as a horn or probe is directly immersed into the sample, whereas indirect sonication is

generally performed using an ultrasound bath, and occurs when the sound waves need to propagate through a medium before reaching the vessel containing the sample.¹⁷¹ Indirect sonication is generally not as powerful as the direct alternative, but it eliminates the risk of contamination coming from the potential detachment of metals from the probe.¹⁷²

In the context of applications, the distinct environment created by the collapse of the cavities can promote the study of chemical reactions powered by ultrasound, which is known as sonochemistry. Sonochemistry is often seen as a greener alternative to reactions performed under classical circumstances, since less waste is generated, less hazardous reagents are used, milder conditions are employed, and improved yields are obtained.¹⁷³ Moreover, ultrasound can be applied to rapidly disperse solids, synthesize nanostructures, and exfoliate layered materials.¹⁷⁰⁻¹⁷³

1.6.2 Liquid-Phase Exfoliation

The exfoliation of layered materials promoted by ultrasound is known as mechanical liquid, ultrasonic, or liquid-phase exfoliation (LPE). In this process, the solid multilayered material is immersed in a solvent and exposed to ultrasound waves. Those waves and the resulting cavitation phenomenon can overcome and break the interlayer van der Waals attractions of the material, thus producing mono- or few-layer nanosheets (**Figure 1.13**).¹⁶⁶

The first exfoliation assisted by indirect sonication was performed four years after the discovery of the Scotch-tape technique, and also involved the production of graphene.

During this work performed by Coleman and collaborators,¹⁷⁴ it was found that properties of the solvent could play a significant role in facilitating the process. In fact, the energy cost of LPE is minimized if solvents present similar surface tensions to the surface energy of the layered materials, thus stabilizing the exfoliated material against reaggregation.

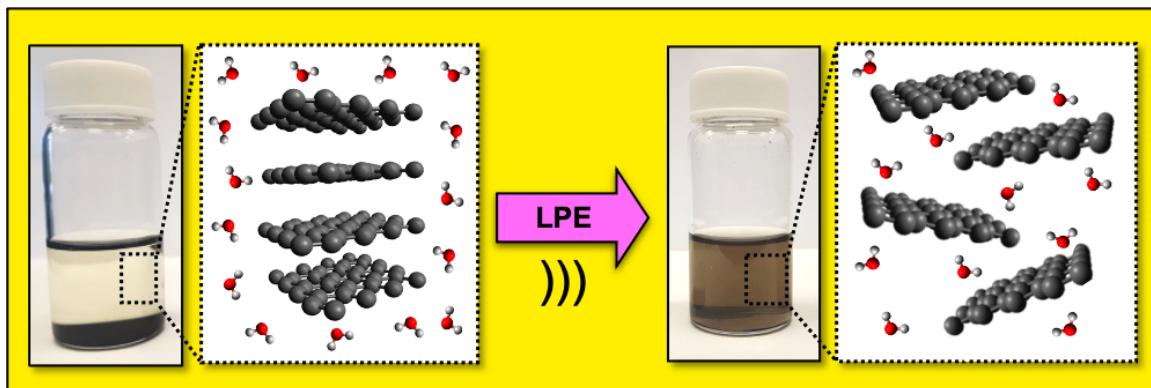


Figure 1.13. Illustrative representation of the LPE of layered materials. Ultrasound waves and further cavitation phenomenon overcome interactions between layers of the bulk material to produce single or a small number (< 10) of stacked nanosheets with superior applications.

Biochar samples have been previously exfoliated using LPE and other exfoliation methods.¹⁷⁵⁻¹⁷⁹ In one of the works involving the liquid-phase processing, nanostructures of rice-husk biochar have been obtained in *N*-methyl-pyrrolidone (NMP) with the objective of promoting a better characterization and comprehension of this carbon material complex structure.⁸⁹ In the investigation by Xing and collaborators,¹⁷⁷ biochar samples from peanut shell and cotton straw have been exfoliated in a more benign solvent (i.e. deionized water). After sonication for 15 min, settling for 24 h, and centrifugation for 30 min, low-yields (i.e. 0.47-2.36%) of the so-called “nanobiochar” structures from

different pyrolysis temperatures were obtained as dispersions, with potential to enhance the efficiency of biochar as a soil amendment. Using the same methodology, exfoliated biochars from elephant grass and wheat straw have been produced, and presented larger surface area, higher stability, and smaller pore sizes when compared to the bulk counterparts.¹⁷⁹

Unfortunately, the exfoliation of layered materials using sonication presents some disadvantages. For example, NMP is the best solvent reported for the exfoliation of graphite and other layered materials using ultrasound.¹⁶⁸ Besides having a high boiling point (e.g. 202 °C) which limits its processing potential, NMP is also an expensive reprotoxic solvent, meaning it can adversely affect sexual function and fertility in adults.¹⁸⁰ Moreover, solvents with similar surface tensions have shown drastically different exfoliation abilities for the same material. Several approaches have been used to explain the mechanisms and solvent selection needed for LPE, but these also present inherent limitations.¹⁸¹ Therefore, another drawback comprises the complex nature of ultrasonic exfoliation, which still remains unclear.

It is important to highlight the obstacles involved in the large-scale implementation of LPE. However, if some of those challenges are tackled, this exfoliation method displays great potential to be applied as a scalable and environmentally friendly methodology for the production of advanced materials. The nanostructures produced using this process show promising applications as electrodes for batteries and supercapacitors, as catalysts for the production of fuels, and also as fillers for polymer composites.¹⁸²

1.7 Ocean Plastics Pollution

One of the biggest environmental challenges currently faced by our society is the ocean pollution with plastics. Although plastics are light, cheap, and versatile materials which have promoted great economic and social development, the numbers resulting from their use are alarming.¹⁸³ From the 300 million tonnes of plastic produced every year, only 14% is collected for recycling, whereas the rest eventually ends up in landfill sites or leaks to our environment.^{3,184} Furthermore, if current plastic management and production trends continue, it is estimated that there will be more plastics than fish in our oceans by 2050.¹⁸⁴ The production of various chemical building blocks from a bio-based material that could mitigate climate change effects and plastics pollution problems simultaneously represents a gigantic step towards a more sustainable economy. An important strategy to tackle ocean plastic pollution consists in the enhancement of physical properties (i.e. reinforcement) of plastics with increased biodegradability via the production of polymer composites.

1.7.1 Polymer Composites

Composites are defined as materials containing two or more chemically and physically distinct phases. When combined, these phases work synergically to produce a material with superior properties.¹⁸⁵ The continuous phase (i.e. matrix phase) fills the volume, holds the dispersed phase, and shares loads with it. The dispersed phase (i.e. reinforcing phase) is discontinuously embedded in the matrix, it is usually stronger and

therefore, it is responsible for enhancing the composite properties. In the case of polymer composites, the continuous phase is comprised of the polymer, whereas the dispersed phase is made up by the filler.¹⁸⁶ When those fillers or additives are in their nanosized state, these specific composite materials can be referred to as polymer nanocomposites.

The history of composite materials dates from the early 1900s during the mass-production of a reinforced resin known as Bakelite. However, only 100 years later, with the growing availability of different fillers, the interest in polymer composites research has increased.¹⁸⁷ In fact, the improvement in the properties of composites such as stiffness, strength, durability, chemical reactivity, biodegradability, and thermal conductivity are completely dependent on the nature of the fillers employed and their contents, dispersions, orientations, and dimensions.¹⁸⁶ Microfiller contents in the order of a dozen wt% are usually required to enhance the properties of polymer composites, whereas the maximum effect of nanofillers on nanocomposites is often shown at concentrations in the range of from 3-5 wt%.¹⁸⁸

Due to their remarkable mechanical properties and relatively low-cost, light-weight, and durability, polymer composites have been widely employed in aerospace, automotive, civil engineering, commercial, and biomedical applications.¹⁸⁵⁻¹⁸⁸ However, drawbacks associated with the end-of-life recycling and fossil fuel consumption during their synthesis limits the implementation of some of those composites.¹⁸⁹ To solve this issue, research efforts concerning the development of more environmentally friendly and sustainable alternatives are growing. Green or bio-based polymer composites can be

produced by the utilization of a renewable dispersed phase and a synthetic or natural biodegradable matrix.¹⁸⁵ With this approach, lighter, stronger, biodegradable, and high-performance materials obtained from renewable resources can be synthesized and applied in different fields.¹⁸⁹⁻¹⁹¹ In this context, the utilization of biochar as a reinforcing phase for the production of green polymer composites is important.

The majority of studies utilizing of biochar as a polymeric filler involves the most common plastics currently used by our society, polyethylene (PE) and polypropylene (PP). PE is primarily used to produce plastic bags and other types of packaging, whereas the higher stiffness, chemical and heat resistance of PP allow its implementation in the automotive, fabrics, healthcare, and also packaging fields.¹⁹² The incorporation of biochars from different biomass feedstocks (e.g. rice husk, bamboo, poplar) in the PE matrix has greatly improved the thermal and mechanical properties of the composites produced.¹⁹³⁻¹⁹⁶ Pyrolysis temperatures for the fabrication of PE composites with the best properties have been also investigated, and found to be between 500 and 600 °C.^{195, 196} PP composites containing biochar from date palm waste with contents up to 15 wt% also have shown enhanced mechanical properties, but reduced crystallinity due to poor interactions between the polymer and the dispersed phase.¹⁹⁷ In order to overcome these drawbacks and synthesize composites with superior characteristics and applications, biochars have been employed as fillers for polymer blends or as a co-additives in the fabrication of wood composites with fire retardant abilities.¹⁹⁸⁻²⁰⁰ Composites comprising other matrixes such as polyvinyl alcohol, polyamide, and polytrimethylene terephthalate

(PTT) have also been synthesized using biochar.²⁰¹⁻²⁰³ The repeating units of the various matrixes used for the fabrication of different biochar composites is shown in **Figure 1.14**.

Poly(lactic acid) (PLA) is a biodegradable polymer derived from renewable resources (e.g. corn starch, tapioca, sugarcane) and therefore, has great potential to substitute traditional fossil fuel-based alternatives. In fact, PLA production processes achieve yields higher than 95%, require 30-50% fewer petroleum-based sources and can cause a reduction of 30-60% in greenhouse gas emissions.³ Although this biopolymer is employed in biomedical, textiles, and food packaging applications, its industrial relevance is restricted due to its fragile nature (i.e. low toughness and heat resistance).²⁰⁴ Waste coffee powder, bamboo, and sewage sludge, and even functionalized biochars with investigated compositions ranging from 2.5-30 wt% have been successfully used as polymer reinforcements to produce PLA biocomposites with improved mechanical and thermal properties or even better water resistance.²⁰⁵⁻²¹⁰ Another important dispersed phase for the production of biodegradable green composites is poly(ϵ -caprolactone).

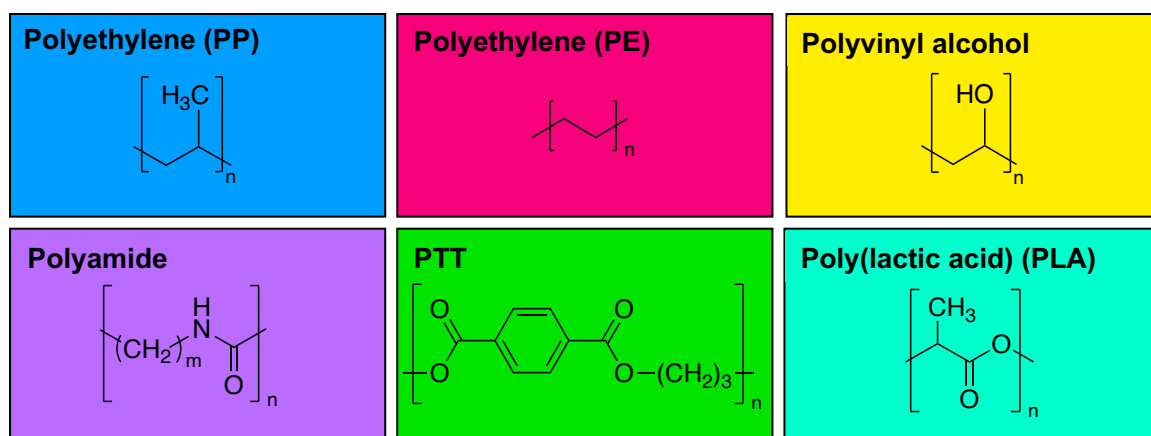


Figure 1.14. Repeating unit of different polymer composites produced using biochar.

1.7.2 Poly(ϵ -caprolactone)

Poly(ϵ -caprolactone) (PCL) is an aliphatic and hydrophobic polyester comprised of hexanoate repeating units. It was first synthesized in the early 1930s and soon became commercially available due to its hydrophobicity, high solubility at room temperature, easy processability due to low melting temperature (e.g. about 60 °C), relative low cost, compatibility with the living issue (i.e. biocompatibility), and biodegradability.²¹¹ The two latter characteristics are the reason why PCL is largely employed in the biomedical fields. This polymer has been also applied with some success in non-medical fields such as in microelectronics, adhesives, and packaging.²¹² However, unlike polycaprolactam (i.e. Nylon 6), further industrial applications of PCL are limited due to its poor mechanical properties (e.g. flexibility, weakness).²¹²

Although PCL can be produced from sugars,²¹³ it is a polymer typically derived from fossil fuels instead. However, it has been largely studied in the area of Green Chemistry as a possible solution for our current ocean plastics issue due to its biodegradability. Many different microorganisms present in nature are able to completely degrade PCL, process which can take up to several years depending on properties such as degradation conditions, polymer molecular weight, and degree of crystallinity.²¹⁴ Moreover, PCL is more degradable than PLA under a broad range of conditions,²¹⁵ and its sustainability can be further increased by the utilization of renewable fillers for the production of bio-based polymer composites with enhanced properties.

Materials sourced from different renewable feedstocks including chitosan, cellulose,

lignin, and wood have been used as fillers for PCL.²¹⁶⁻²²¹ Those polymer composites were prepared via ring-opening polymerization (ROP) of the monomer ϵ -caprolactone (ϵ -CL) initiated by the hydroxyl or carboxyl groups present onto the filler's surface. The ROP of ϵ -CL (**Figure 1.15**) is a process catalyzed by metal-based, enzymatic, or organic systems.²¹² Although there are ingestion, inhalation, and skin absorption toxicity issues associated with its utilization, $\text{Sn}(\text{oct})_2$ (i.e. tin octoate) is the most used catalyst for the production of PCL composites. Regarding the utilization of carbon materials as additives for the ROP of ϵ -CL, the majority of studies performed so far involve the use of graphene oxide and carbon nanotubes.²²²⁻²²⁶ Rolled-up nanosheets of graphene or its oxidized form have been successfully employed for the synthesis of PCL with superior thermal and mechanical properties, but biocarbon alternatives have not been applied to this end yet.

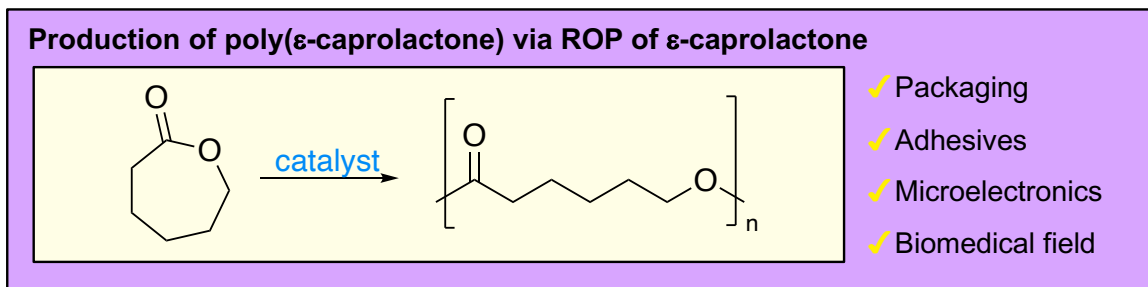


Figure 1.15. ROP of ϵ -CL to synthesize PCL and its current applications.

1.8 Objectives

The main objective of this work is to demonstrate the application of a bio-based material obtained from waste (i.e. biochar) as a feedstock for the design of more sustainable processes and products. A secondary objective is to gain an improved

understanding on its structure. Biochar is a biomass-derived material with remarkable properties, and an important tool for carbon sequestration and climate change mitigation. An increase in biochar applications could play a significant role in the transition of our society to a bio-based and circular economy. Through utilization of the Green Chemistry Principles, biochar could be an important platform in moving towards a sustainable future.

In **Chapter 2: Oxidized Biochar as a Renewable, Sustainable Catalyst for the Production of Cyclic Carbonates from Carbon Dioxide and Epoxides**, one type of functionalized biochar (i.e. oxidized biochar) is used as a catalyst for the cycloaddition reaction between CO₂ and epoxides. This research applies a material that sequesters CO₂ during its production for the further transformation of CO₂ into useful compounds. It was demonstrated that oxidized biochars from different types of waste biomass (i.e. hard- and softwood trees) could produce cyclic carbonates under relatively mild conditions. The success of the catalytic system relies on the presence of hydroxyl and carboxyl groups on the surface of oxidized biochar, which are capable of interacting via hydrogen-bonding with the oxygen atom of the epoxide, activating it for further ring-opening. This theory was confirmed by the lower conversions of cyclic carbonates obtained using the non-functionalized (i.e. pristine) biochar analogues. The functionalized biochar catalyst could also be recycled at least 5 times without loss in activity.

In **Chapter 3: Green Solvents for the Liquid-Phase Exfoliation of Biochar**, a comprehensive study on the LPE of biochar is performed. In this Chapter, functionalized

and non-functionalized biochar samples from hard- and softwood waste biomasses were exfoliated in a variety of solvents to produce nanostructures of the respective bio-based materials. Despite the complex nature of LPE, a correlation between solvent densities, surface tensions, and Kamlet-Taft solvatochromic parameters with exfoliation efficiency was discovered. This relationship then allowed the investigation of more benign alternative solvents for the LPE of different types of biochar, which had similar performances and gave comparable results to the toxic and most common solvent used in exfoliation, NMP.

In **Chapter 4: Biochar as a Sustainable and Renewable Additive for the Production of Poly(caprolactone) Composites**, the nanostructures of oxidized biochar produced via LPE were applied as PCL reinforcements. Hydroxyl and carboxyl groups on the surface of oxidized biochar nanostructures can work as initiators to promote the ring-opening polymerization of the ϵ -caprolactone monomer. During degradation studies, Scanning Electron Microscope images showed the presence of cracks on the surface of the PCL/exfoliated biochar composites, which have also presented increased storage and loss moduli in the melt and solid states when compared to pure PCL.

In the remaining chapters, additional experiments and the conclusion of this thesis are shown. Other applications of functionalized biochar as a catalyst for important chemical reactions have been discussed in **Chapter 5: Green Ring-Closing Metathesis of Aliphatic Ethers and Esterification of Terpene Alcohols Catalyzed by Biochar Catalysts**. In **Chapter 6: Future Work and Conclusions**, suggestions for future work

involving biochar as a catalyst and as advanced material, in conjunction with the conclusions obtained during our investigation are presented.

1.9 References

1. Allen, B., *Green Chem.* **2000**, *2*, 56-58.
2. Diebel, L. Vale targets pristine lake for tailings. https://www.thestar.com/news/canada/2010/09/10/vale_targets_pristine_lake_for_tailings.html (accessed Oct. 1, 2021).
3. Lancaster, M., *Green Chemistry: An Introductory Text*. 3rd ed.; Royal Society of Chemistry: 2016.
4. Anastas, P. T.; Warner, J. C., *Green Chemistry: Theory and Practice*. Oxford University Press: 1998.
5. TechNavio. *Global Green Chemicals Market 2019-2023*; 2019.
6. Sanderson, K., *Nature* **2011**, *469*, 18-20.
7. Transforming our world: The 2030 Agenda for Sustainable Development, United Nations. <https://sdgs.un.org/2030agenda> (accessed July 15, 2020).
8. Chemistry & Sustainable Development Goals, American Chemical Society. <https://www.acs.org/content/acs/en/sustainability/chemistry-sustainable-development-goals.html> (accessed July 15, 2020).
9. Anastas, P. T.; Zimmerman, J. B., *Curr. Opin. Green Sustain. Chem.* **2018**, *13*, 150-153.
10. Matlin, S. A.; Mehta, G.; Hopf, H.; Krief, A., *Nat. Chem.* **2015**, *7*, 941-943.
11. Chen, T.-L.; Kim, H.; Pan, S.-Y.; Tseng, P.-C.; Lin, Y.-P.; Chiang, P.-C., *Sci. Total Environ.* **2020**, *716*, 136998-137014.

12. United Nations, Sustainable Development Goals. <https://sdgs.un.org/> (accessed July 12, 2021).
13. Liu, W. J.; Jiang, H.; Yu, H. Q., *Chem. Rev.* **2015**, *115*, 12251-12285.
14. Lehmann, J.; da Silva, J. P.; Steiner, C.; Nehls, T.; Zech, W.; Glaser, B., *Plant Soil* **2003**, *249*, 343-357.
15. Titirici, M.-M.; White, R. J.; Brun, N.; Budarin, V. L.; Su, D. S.; del Monte, F.; Clark, J. H.; MacLachlan, M. J., *Chem. Soc. Rev.* **2015**, *44*, 250-290.
16. Graphene-info: The Graphene Experts. <https://www.graphene-info.com/nanorexplre-plans-10000-ton-graphene-powder-facility> (accessed January 30, 2021).
17. Butler, L.; Altdorff, D.; Young, E.; Galagedara, L.; Hawboldt, K.; Helleur, R.; Unc, A. *Organic Waste in NL: A Review of Available Agriculture, Fishery, Forestry and Municipal Waste Literature*; The Harris Centre, Memorial Univeristy: 2017.
18. Woolf, D.; Amonette, J. E.; Street-Perrott, F. A.; Lehmann, J.; Joseph, S., *Nat. Commun.* **2010**, *1*, 56-65.
19. Laird, D. A.; Brown, R. C.; Amonette, J. E.; Lehmann, J., *Biofuel. Bioprod. Bior.* **2009**, *3*, 547-562.
20. Lehmann, J.; Joseph, S., *Biochar for environmental management: Science and Technology*. Earthscan: Sterling, VA, 2009.
21. Zacher, A. H.; Olarte, M. V.; Santosa, D. M.; Elliott, D. C.; Jones, S. B., *Green Chem.* **2014**, *16*, 491-515.
22. Wang, H.; Male, J.; Wang, Y., *ACS Catal.* **2013**, *3*, 1047-1070.

23. Wang, L.; O'Connor, D.; Rinklebe, J.; Ok, Y. S.; Tsang, D. C. W.; Shen, Z.; Hou, D., *Environ. Sci. Technol.* **2020**, *54*, 14797-14814.
24. Lehmann, J., *Nature* **2007**, *447*, 143-144.
25. *IPCC Fifth Assessment Report: Climate Change 2014 (AR5)*.
26. Brown, R. C.; Wang, K., *Fast Pyrolysis of Biomass - Advances in Science and Technology*. Royal Society of Chemistry: 2017; p 1-11.
27. Basu, P., *Biomass Gasification, Pyrolysis and Torrefaction*. 2nd ed.; Academic Press: Boston, 2013.
28. Huber, G. W.; Iborra, S.; Corma, A., *Chem. Rev.* **2006**, *106*, 4044-4098.
29. Wertz, J.-L.; Bédue, O., *Lignocellulosic Biorefineries*. 1st ed.; EPFL Press: New York, 2013.
30. Mohan, D.; Pittman, C. U.; Steele, P. H., *Energy Fuels* **2006**, *20*, 848-889.
31. Wiedenhoeff, A. C., Structure and Function of Wood. In *Handbook of Wood Chemistry and Wood Composites*, 2nd ed.; Rowell, R. M., Ed. CRC Press: Boca Raton, 2013.
32. Chen, B.; Zhou, D.; Zhu, L., *Environ. Sci. Technol.* **2008**, *42*, 5137-5143.
33. De, S.; Balu, A. M.; van der Waal, J. C.; Luque, R., *ChemCatChem* **2015**, *7*, 1608-1629.
34. Li, Y.; Shao, J.; Wang, X.; Deng, Y.; Yang, H.; Chen, H., *Energy Fuels* **2014**, *28*, 5119-5127.
35. Kharel, G.; Sacko, O.; Feng, X.; Morris, J. R.; Phillips, C. L.; Trippe, K.; Kumar, S.; Lee, J. W., *ACS Sustain. Chem. Eng.* **2019**, *7*, 16410-16418.
36. Huff, M. D.; Lee, J. W., *J. Environ. Manage.* **2016**, *165*, 17-21.

37. Ternero-Hidalgo, J. J.; Rosas, J. M.; Palomo, J.; Valero-Romero, M. J.; Rodríguez-Mirasol, J.; Cordero, T., *Carbon* **2016**, *101*, 409-419.
38. Gokce, Y.; Aktas, Z., *Appl. Surf. Sci.* **2014**, *313*, 352-359.
39. Wang, J.; Xu, W.; Ren, J.; Liu, X.; Lu, G.; Wang, Y., *Green Chem.* **2011**, *13*, 2678-2681.
40. Nakajima, K.; Hara, M., *ACS Catal.* **2012**, *2*, 1296-1304.
41. Liang, X.; Zeng, M.; Qi, C., *Carbon* **2010**, *48*, 1844-1848.
42. Corrêa, A. P. C.; Bastos, R. R. C.; Rocha Filho, G. N. d.; Zamian, J. R.; Conceição, L. R. V. d., *RSC Adv.* **2020**, *10*, 20245-20256.
43. Wu, Y.; Fu, Z.; Yin, D.; Xu, Q.; Liu, F.; Lu, C.; Mao, L., *Green Chem.* **2010**, *12*, 696-700.
44. Toda, M.; Takagaki, A.; Okamura, M.; Kondo, J. N.; Hayashi, S.; Domen, K.; Hara, M., *Nature* **2005**, *438*, 178-178.
45. Yang, G.-X.; Jiang, H., *Water Res.* **2014**, *48*, 396-405.
46. Jansen, R. J. J.; van Bekkum, H., *Carbon* **1994**, *32*, 1507-1516.
47. Zhang, X.; Wu, J.; Yang, H.; Shao, J.; Wang, X.; Chen, Y.; Zhang, S.; Chen, H., *RSC Adv.* **2016**, *6*, 98157-98166.
48. Bamdad, H.; Hawboldt, K.; MacQuarrie, S., *Energy Fuels* **2018**, *32*, 11742-11748.
49. Mahasenan, N.; Smith, S.; Humphreys, K., The Cement Industry and Global Climate Change. In *Greenhouse Gas Control Technologies - 6th International Conference*, Gale, J.; Kaya, Y., Eds. Pergamon: Oxford, 2003; pp 995-1000.

50. Zhong, Y.; Zhang, P.; Zhu, X.; Li, H.; Deng, Q.; Wang, J.; Zeng, Z.; Zou, J.-J.; Deng, S., *ACS Sustain. Chem. Eng.* **2019**, *7*, 14973-14981.
51. Zhong, Y.; Deng, Q.; Yao, Q.; Lu, C.; Zhang, P.; Li, H.; Wang, J.; Zeng, Z.; Zou, J.-J.; Deng, S., *ACS Sustain. Chem. Eng.* **2020**, *8*, 7785-7794.
52. Li, Q.; Hou, Y.; Wang, J.; Liu, Y.; Xiang, N.; Huang, Z., *ACS Sustain. Chem. Eng.* **2020**, *8*, 11308-11316.
53. Ding, D.; Yang, S.; Qian, X.; Chen, L.; Cai, T., *Appl. Catal. B.* **2020**, *263*, 118348-118363.
54. Leng, L.; Xu, S.; Liu, R.; Yu, T.; Zhuo, X.; Leng, S.; Xiong, Q.; Huang, H., *Bioresour. Technol.* **2020**, *298*, 122286-122299.
55. Zhu, S.; Huang, X.; Yang, X.; Peng, P.; Li, Z.; Jin, C., *Environ. Sci. Technol.* **2020**, *54*, 8123-8132.
56. Li, Y.; Xing, B.; Wang, X.; Wang, K.; Zhu, L.; Wang, S., *Energy Fuels* **2019**, *33*, 12459-12468.
57. Chaudhari, N. K.; Song, M. Y.; Yu, J.-S., *Sci. Rep.* **2014**, *4*, 5221-5231.
58. Zhao, L.; Baccile, N.; Gross, S.; Zhang, Y.; Wei, W.; Sun, Y.; Antonietti, M.; Titirici, M.-M., *Carbon* **2010**, *48*, 3778-3787.
59. Nguyen, T.-D.; Shopsowitz, K. E.; MacLachlan, M. J., *J. Mater. Chem. A* **2014**, *2*, 5915-5921.
60. Li, P.; Feng, T.; Song, Z.; Tan, Y.; Luo, W., *RSC Adv.* **2020**, *10*, 30077-30086.

61. Sadjadi, S.; Akbari, M.; Léger, B.; Monflier, E.; Heravi, M. M., *ACS Sustain. Chem. Eng.* **2019**, *7*, 6720-6731.
62. Santos, J. L.; Mäki-Arvela, P.; Monzón, A.; Murzin, D. Y.; Centeno, M. Á., *Appl. Catal. B.* **2020**, *268*, 118423-118435.
63. Yan, Q.; Wan, C.; Liu, J.; Gao, J.; Yu, F.; Zhang, J.; Cai, Z., *Green Chem.* **2013**, *15*, 1631-1640.
64. Zhao, R.; Jia, L.; Yao, Y.-x.; Huo, R.-p.; Qiao, X.-l.; Fan, B.-g., *Energy Fuels* **2019**, *33*, 11408-11419.
65. Diacon, A.; Mocanu, A.; Răducanu, C. E.; Busuioc, C.; Şomoghi, R.; Trică, B.; Dinescu, A.; Rusen, E., *Sci. Rep.* **2019**, *9*, 16840-16854.
66. Yang, X.; Yu, I. K. M.; Cho, D.-W.; Chen, S. S.; Tsang, D. C. W.; Shang, J.; Yip, A. C. K.; Wang, L.; Ok, Y. S., *ACS Sustain. Chem. Eng.* **2019**, *7*, 4851-4860.
67. Yan, J.; Qian, L.; Gao, W.; Chen, Y.; Ouyang, D.; Chen, M., *Sci. Rep.* **2017**, *7*, 43051-43060.
68. Pi, L.; Jiang, R.; Cai, W.; Wang, L.; Wang, Y.; Cai, J.; Mao, X., *ACS Appl. Mater. Interfaces* **2020**, *12*, 3642-3653.
69. Zhang, C.; Fu, Z.; Liu, Y. C.; Dai, B.; Zou, Y.; Gong, X.; Wang, Y.; Deng, X.; Wu, H.; Xu, Q.; Steven, K. R.; Yin, D., *Green Chem.* **2012**, *14*, 1928-1934.
70. Zhang, C.; Fu, Z.; Dai, B.; Zen, S.; Liu, Y.; Xu, Q.; Kirk, S. R.; Yin, D., *Ind. Eng. Chem. Res.* **2013**, *52*, 11537-11543.
71. Liu, W.-J.; Tian, K.; Jiang, H.; Yu, H.-Q., *Sci. Rep.* **2013**, *3*, 2419-2426.

72. Song, T.; Ren, P.; Ma, Z.; Xiao, J.; Yang, Y., *ACS Sustain. Chem. Eng.* **2020**, *8*, 267-277.
73. Ye, Y.-Y.; Qian, T.-T.; Jiang, H., *Ind. Eng. Chem. Res.* **2020**, *59*, 15614-15623.
74. Smith, N. J. H., *Ann. Am. Assoc. Geogr.* **1980**, *70*, 553-566.
75. Lehmann, J.; Gaunt, J.; Rondon, M., *Mitig. Adapt. Strateg. Glob. Chang.* **2006**, *11*, 403-427.
76. Campos, P.; Miller, A. Z.; Knicker, H.; Costa-Pereira, M. F.; Merino, A.; De la Rosa, J. M., *Waste Manage.* **2020**, *105*, 256-267.
77. Ulusal, A.; Apaydın Varol, E.; Bruckman, V. J.; Uzun, B. B., *Biomass Convers. Biorefin.* **2020**.
78. Hernandez-Soriano, M. C.; Kerré, B.; Kopittke, P. M.; Horemans, B.; Smolders, E., *Sci. Rep.* **2016**, *6*, 25127-25140.
79. Joseph, S.; Pow, D.; Dawson, K.; Rust, J.; Munroe, P.; Taherymoosavi, S.; Mitchell, D. R. G.; Robb, S.; Solaiman, Z. M., *Sci. Total Environ.* **2020**, *724*, 138153-138164.
80. Breunig, H. M.; Amirebrahimi, J.; Smith, S.; Scown, C. D., *Environ. Sci. Technol.* **2019**, *53*, 12989-12998.
81. Buss, W.; Jansson, S.; Wurzer, C.; Mašek, O., *ACS Sustain. Chem. Eng.* **2019**, *7*, 4204-4209.
82. Liu, S.-H.; Huang, Y.-Y., *J. Clean. Prod.* **2018**, *175*, 354-360.
83. Alam, M. S.; Gorman-Lewis, D.; Chen, N.; Flynn, S. L.; Ok, Y. S.; Konhauser, K. O.; Alessi, D. S., *Environ. Sci. Technol.* **2018**, *52*, 6246-6255.

84. Chen, Z.; Chen, B.; Zhou, D.; Chen, W., *Environ. Sci. Technol.* **2012**, *46*, 12476-12483.
85. Li, R.; Wang, J. J.; Gaston, L. A.; Zhou, B.; Li, M.; Xiao, R.; Wang, Q.; Zhang, Z.; Huang, H.; Liang, W.; Huang, H.; Zhang, X., *Carbon* **2018**, *129*, 674-687.
86. López, J. E.; Builes, S.; Heredia Salgado, M. A.; Tarelho, L. A. C.; Arroyave, C.; Aristizábal, A.; Chavez, E., *J. Phys. Chem. C* **2020**, *124*, 14592-14602.
87. Wan, Z.; Sun, Y.; Tsang, D. C. W.; Yu, I. K. M.; Fan, J.; Clark, J. H.; Zhou, Y.; Cao, X.; Gao, B.; Ok, Y. S., *Green Chem.* **2019**, *21*, 4800-4814.
88. Wang, L.; Wang, Y.; Ma, F.; Tankpa, V.; Bai, S.; Guo, X.; Wang, X., *Sci. Total Environ.* **2019**, *668*, 1298-1309.
89. Xiao, X.; Chen, B.; Chen, Z.; Zhu, L.; Schnoor, J. L., *Environ. Sci. Technol.* **2018**, *52*, 5027-5047.
90. Liu, W.-J.; Jiang, H.; Yu, H.-Q., *Energy Environ. Sci.* **2019**, *12*, 1751-1779.
91. Lee, J.; Kim, K.-H.; Kwon, E. E., *Renew. Sust. Energ. Rev.* **2017**, *77*, 70-79.
92. Changmai, B.; Vanlalveni, C.; Ingle, A. P.; Bhagat, R.; Rokhum, L., *RSC Adv.* **2020**, *10*, 41625-41679.
93. Di Serio, M.; Cozzolino, M.; Giordano, M.; Tesser, R.; Patrono, P.; Santacesaria, E., *Ind. Eng. Chem. Res.* **2007**, *46*, 6379-6384.
94. Ruhul, A. M.; Kalam, M. A.; Masjuki, H. H.; Fattah, I. M. R.; Reham, S. S.; Rashed, M. M., *RSC Adv.* **2015**, *5*, 101023-101044.
95. Sahu, G.; Gupta, N. K.; Kotha, A.; Saha, S.; Datta, S.; Chavan, P.; Kumari, N.; Dutta, P., *ChemBioEng Rev.* **2018**, *5*, 231-252.

96. Dehkhoda, A. M.; West, A. H.; Ellis, N., *Appl. Catal. A Gen.* **2010**, 382, 197-204.
97. Kastner, J. R.; Miller, J.; Geller, D. P.; Locklin, J.; Keith, L. H.; Johnson, T., *Catal. Today* **2012**, 190, 122-132.
98. Yu, J. T.; Dehkhoda, A. M.; Ellis, N., *Energy Fuels* **2011**, 25, 337-344.
99. Zong, M.-H.; Duan, Z.-Q.; Lou, W.-Y.; Smith, T. J.; Wu, H., *Green Chem.* **2007**, 9, 434-437.
100. Chi, N. T. L.; Anto, S.; Ahamed, T. S.; Kumar, S. S.; Shanmugam, S.; Samuel, M. S.; Mathimani, T.; Brindhadevi, K.; Pugazhendhi, A., *Fuel* **2020**, 119411-119420.
101. Wang, Y.; Li, D.; Zhao, D.; Fan, Y.; Bi, J.; Shan, R.; Yang, J.; Luo, B.; Yuan, H.; Ling, X.; Huhe, T.; Chen, Y., *ACS Omega* **2020**, 5, 17471-17478.
102. Cao, X.; Sun, S.; Sun, R., *RSC Adv.* **2017**, 7, 48793-48805.
103. Li, S.; Gu, Z.; Bjornson, B. E.; Muthukumarappan, A., *J. Environ. Chem. Eng.* **2013**, 1, 1174-1181.
104. Wei, Y.; Shen, C.; Xie, J.; Bu, Q., *Sci. Total Environ.* **2020**, 712, 136435-136443.
105. Zhang, C.; Fu, Z.; Liu, Y. C.; Dai, B.; Zou, Y.; Gong, X.; Wang, Y.; Deng, X.; Wu, H.; Xu, Q.; Steven, K. R.; Yin, D., *Green Chem.* **2012**, 14, 1928-1934.
106. Huang, Y.-B.; Fu, Y., *Green Chem.* **2013**, 15, 1095-1111.
107. Chen, S. S.; Yu, I. K. M.; Cho, D.-W.; Song, H.; Tsang, D. C. W.; Tessonnier, J.-P.; Ok, Y. S.; Poon, C. S., *ACS Sustain. Chem. Eng.* **2018**, 6, 16113-16120.
108. Yang, X.; Yu, I. K. M.; Tsang, D. C. W.; Budarin, V. L.; Clark, J. H.; Wu, K. C. W.; Yip, A. C. K.; Gao, B.; Lam, S. S.; Ok, Y. S., *J. Clean. Prod.* **2020**, 268, 122300-122310.

109. Wang, C.; Lei, H.; Qian, M.; Huo, E.; Zhao, Y.; Zhang, Q.; Mateo, W.; Lin, X.; Kong, X.; Zou, R.; Ruan, R., *Sustain. Energy Fuels* **2020**, *4*, 4614-4624.
110. Chen, Y.; Ning, P.; Miao, R.; Shi, Y.; He, L.; Guan, Q., *New J. Chem.* **2020**, 20812-20822.
111. Sahoo, B.; Formenti, D.; Topf, C.; Bachmann, S.; Scalone, M.; Junge, K.; Beller, M., *ChemSusChem* **2017**, *10*, 3035-3039.
112. Cao, Y.; Ding, L.; Qiu, Z.; Zhang, H., *Catal. Commun.* **2020**, *143*, 106048-106053.
113. Aeowjaroenlap, H.; Chotiwiriyakun, K.; Tiensai, N.; Tanthapanichakoon, W.; Spatenka, S.; Cano, A., *Ind. Eng. Chem. Res.* **2018**, *57*, 9943-9951.
114. Yang, B.; Burch, R.; Hardacre, C.; Headdock, G.; Hu, P., *ACS Catal.* **2012**, *2*, 1027-1032.
115. Blaser, H.-U.; Steiner, H.; Studer, M., *ChemCatChem* **2009**, *1*, 210-221.
116. Kumar, A.; Kumar, J.; Bhaskar, T., *Environ. Res.* **2020**, *186*, 109533-109542.
117. Liu, X.; Xu, L.; Xu, G.; Jia, W.; Ma, Y.; Zhang, Y., *ACS Catal.* **2016**, *6*, 7611-7620.
118. Moradi, P.; Hajjami, M.; Valizadeh-Kakhki, F., *Appl. Organomet. Chem.* **2019**, *33*, 5205-5218.
119. He, Z.; Song, F.; Sun, H.; Huang, Y., *J. Am. Chem. Soc.* **2018**, *140*, 2693-2699.
120. Yin; Liebscher, J., *Chem. Rev.* **2007**, *107*, 133-173.
121. Tang, F.; Wang, L.; Liu, Y.-N., *Green Chem.* **2019**, *21*, 6252-6257.
122. Hu, X.; Fan, M.; Zhu, Y.; Zhu, Q.; Song, Q.; Dong, Z., *Green Chem.* **2019**, *21*, 5274-5283.

123. Parmeggiani, C.; Matassini, C.; Cardona, F., *Green Chem.* **2017**, *19*, 2030-2050.
124. Zhu, C.; Wang, H.; Li, H.; Cai, B.; Lv, W.; Cai, C.; Wang, C.; Yan, L.; Liu, Q.; Ma, L., *ACS Sustain. Chem. Eng.* **2019**, *7*, 19556-19569.
125. Liu, C.; Li, N.; Peng, L.; Zhong, W.; Mao, L.; Yin, D., *ACS Sustain. Chem. Eng.* **2020**, *8*, 11404-11412.
126. Kambo, H. S.; Dutta, A., *Renew. Sust. Energ. Rev.* **2015**, *45*, 359-378.
127. Wang, L.; Chen, L.; Tsang, D. C. W.; Guo, B.; Yang, J.; Shen, Z.; Hou, D.; Ok, Y. S.; Poon, C. S., *J. Clean. Prod.* **2020**, *258*, 120678-120686.
128. Gupta, S.; Kua, H. W.; Low, C. Y., *Cement Concrete Comp.* **2018**, *87*, 110-129.
129. Cosentino, I.; Restuccia, L.; Ferro, G. A.; Tulliani, J.-M., *Theor. Appl. Fract. Mech.* **2019**, *103*, 102261-102271.
130. Gupta, S.; Kua, H. W., *Sci. Total Environ.* **2019**, *662*, 952-962.
131. Miller, S. A.; Moore, F. C., *Nat. Clim. Change* **2020**, *10*, 439-443.
132. Dixit, A.; Gupta, S.; Pang, S. D.; Kua, H. W., *J. Clean. Prod.* **2019**, *238*, 117876-117890.
133. Cuthbertson, D.; Berardi, U.; Briens, C.; Berruti, F., *Biomass Bioenergy* **2019**, *120*, 77-83.
134. Akhtar, A.; Sarmah, A. K., *Sci. Total Environ.* **2018**, *616-617*, 408-416.
135. International Union of Pure and Applied Chemistry (IUPAC): Glossary of Terms Used in Biochar Research. https://iupac.org/projects/project-details/?project_nr=2015-056-3-600 (accessed December 6, 2020).

136. International Biochar Initiative. <https://biochar-international.org/> (accessed December 6, 2020).
137. Calcio Gaudino, E.; Cravotto, G.; Manzoli, M.; Tabasso, S., *Green Chem.* **2019**, *21*, 1202-1235.
138. Zhang, X.; Wang, Y.; Cai, J.; Wilson, K.; Lee, A. F., *Energy Environ. Mater.* **2020**, 453-468.
139. Zhang, Z.; Zhu, Z.; Shen, B.; Liu, L., *Energy* **2019**, *171*, 581-598.
140. Cao, X.; Ro, K. S.; Chappell, M.; Li, Y.; Mao, J., *Energy Fuels* **2011**, *25*, 388-397.
141. Fuertes, A. B.; Arbestain, M. C.; M.Sevilla; Maciá-Agulló, J. A.; S.Fiol; R.López; Smernik, R. J.; Aitkenhead, W. P.; Arce, F.; Macias, F., *Soil Res.* **2010**, *48*, 618-626.
142. Liu, Z.; Zhang, F.-S.; Wu, J., *Fuel* **2010**, *89*, 510-514.
143. Owsianiak, M.; Brooks, J.; Renz, M.; Laurent, A., *GCB Bioenergy* **2018**, *10*, 230-245.
144. Eibisch, N.; Helfrich, M.; Don, A.; Mikutta, R.; Kruse, A.; Ellerbrock, R.; Flessa, H., *J. Environ. Qual.* **2013**, *42*, 1565-1573.
145. Malghani, S.; Gleixner, G.; Trumbore, S. E., *Soil Biol. Biochem.* **2013**, *62*, 137-146.
146. Kümmerer, K.; Clark, J. H.; Zuin, V. G., *Science* **2020**, *367*, 369-370.
147. Zimmerman, J. B.; Anastas, P. T.; Erythropel, H. C.; Leitner, W., *Science* **2020**, *367*, 397-400.
148. Liu, J.; Mooney, H.; Hull, V.; Davis, S. J.; Gaskell, J.; Hertel, T.; Lubchenco, J.; Seto, K. C.; Gleick, P.; Kremen, C.; Li, S., *Science* **2015**, *347*, 1258832-1258841.

149. National Oceanic and Atmospheric Administration (NOAA), Climate Change: Atmospheric Carbon Dioxide. <https://www.climate.gov/news-features/understanding-climate/climate-change-atmospheric-carbon-dioxide> (accessed December 8, 2020).
150. *International Energy Agency (IEA) Global Energy Review (2019)*.
151. Aresta, M.; Dibenedetto, A.; Angelini, A., *Chem. Rev.* **2014**, *114*, 1709-1742.
152. Mikkelsen, M.; Jørgensen, M.; Krebs, F. C., *Energy Environ. Sci.* **2010**, *3*, 43-81.
153. Liu, Q.; Wu, L.; Jackstell, R.; Beller, M., *Nat. Commun.* **2015**, *6*, 5933-5948.
154. Artz, J.; Müller, T. E.; Thenert, K.; Kleinekorte, J.; Meys, R.; Sternberg, A.; Bardow, A.; Leitner, W., *Chem. Rev.* **2018**, *118*, 434-504.
155. Kamphuis, A. J.; Picchioni, F.; Pescarmona, P. P., *Green Chem.* **2019**, *21*, 406-448.
156. North, M.; Pasquale, R.; Young, C., *Green Chem.* **2010**, *12*, 1514-1539.
157. Sakakura, T.; Kohno, K., *Chem. Commun.* **2009**, 1312-1330.
158. Fiorani, G.; Guo, W.; Kleij, A. W., *Green Chem.* **2015**, *17*, 1375-1389.
159. Song, Q.-W.; Zhou, Z.-H.; He, L.-N., *Green Chem.* **2017**, *19*, 3707-3728.
160. Samikannu, A.; Konwar, L. J.; Mäki-Arvela, P.; Mikkola, J.-P., *Appl. Catal. B.* **2019**, *241*, 41-51.
161. Zhang, S.; Zhang, H.; Cao, F.; Ma, Y.; Qu, Y., *ACS Sustain. Chem. Eng.* **2018**, *6*, 4204-4211.
162. Lan, D.-H.; Yang, F.-M.; Luo, S.-L.; Au, C.-T.; Yin, S.-F., *Carbon* **2014**, *73*, 351-360.
163. Saptal, V. B.; Sasaki, T.; Harada, K.; Nishio-Hamane, D.; Bhanage, B. M., *ChemSusChem* **2016**, *9*, 644-650.

164. Novoselov, K. S.; Geim, A. K.; Morozov, S. V.; Jiang, D.; Zhang, Y.; Dubonos, S. V.; Grigorieva, I. V.; Firsov, A. A., *Science* **2004**, 306, 666-669.
165. Geim, A. K., *Science* **2009**, 324, 1530-1534.
166. Nicolosi, V.; Chhowalla, M.; Kanatzidis, M. G.; Strano, M. S.; Coleman, J. N., *Science* **2013**, 340, 1420-1438.
167. Tao, P.; Yao, S.; Liu, F.; Wang, B.; Huang, F.; Wang, M., *J. Mater. Chem. A* **2019**, 7, 23512-23536.
168. Tao, H.; Zhang, Y.; Gao, Y.; Sun, Z.; Yan, C.; Texter, J., *Phys. Chem. Chem. Phys.* **2017**, 19, 921-960.
169. Cai, M.; Thorpe, D.; Adamson, D. H.; Schniepp, H. C., *J. Mater. Chem.* **2012**, 22, 24992-25002.
170. Xu, H.; Zeiger, B. W.; Suslick, K. S., *Chem. Soc. Rev.* **2013**, 42, 2555-2567.
171. Thompson, L. H.; Doraiswamy, L. K., *Ind. Eng. Chem. Res.* **1999**, 38, 1215-1249.
172. Bang, J. H.; Suslick, K. S., *Adv. Mater.* **2010**, 22, 1039-1059.
173. Cintas, P.; Luche, J.-L., *Green Chem.* **1999**, 1, 115-125.
174. Hernandez, Y.; Nicolosi, V.; Lotya, M.; Blighe, F. M.; Sun, Z.; De, S.; McGovern, I. T.; Holland, B.; Byrne, M.; Gun'Ko, Y. K.; Boland, J. J.; Niraj, P.; Duesberg, G.; Krishnamurthy, S.; Goodhue, R.; Hutchison, J.; Scardaci, V.; Ferrari, A. C.; Coleman, J. N., *Nat. Nanotechnol.* **2008**, 3, 563-568.
175. Roy, S.; Kumar, U.; Bhattacharyya, P., *Environ. Sci. Pollut. Res. Int.* **2019**, 26, 7272-7276.

176. Genovese, M.; Jiang, J.; Lian, K.; Holm, N., *J. Mater. Chem. A* **2015**, *3*, 2903-2913.
177. Liu, G.; Zheng, H.; Jiang, Z.; Zhao, J.; Wang, Z.; Pan, B.; Xing, B., *Environ. Sci. Technol.* **2018**, *52*, 10369-10379.
178. Xiao, X.; Chen, B., *Environ. Sci. Technol.* **2017**, *51*, 5473-5482.
179. Oleszczuk, P.; Ćwikła-Bundyra, W.; Bogusz, A.; Skwarek, E.; Ok, Y. S., *J. Anal. Appl. Pyrol.* **2016**, *121*, 165-172.
180. Jönsson, B. A.; Akesson, B., *Int. Arch. Occup. Environ. Health* **2003**, *76*, 267-74.
181. Bergin, S. D.; Sun, Z.; Rickard, D.; Streich, P. V.; Hamilton, J. P.; Coleman, J. N., *ACS Nano* **2009**, *3*, 2340-2350.
182. Backes, C.; Higgins, T. M.; Kelly, A.; Boland, C.; Harvey, A.; Hanlon, D.; Coleman, J. N., *Chem. Mater.* **2017**, *29*, 243-255.
183. Sheldon, R. A.; Norton, M., *Green Chem.* **2020**, *22*, 6310-6322.
184. MacArthur, E., *Science* **2017**, *358*, 843-843.
185. Thomas, S.; Joseph, K.; Malhotra, S. K.; Goda, K.; Sreekala, M. S., *Polymer Composites*. Wiley-VCH: 2013; Vol. 3, p 1-16.
186. Subramanian, M. N., *Polymer Blends and Composites : Chemistry and Technology*. John Wiley & Sons, Inc.: Beverly, MA, 2017.
187. Balazs, A. C.; Emrick, T.; Russell, T. P., *Science* **2006**, *314*, 1107-1110.
188. Shchipunov, Y., *Pure Appl. Chem.* **2012**, *84*, 2579-2607.
189. Singh, A. A.; Afrin, S.; Karim, Z., *Green Biocomposites: Design and Applications*. Springer International Publishing: Cham, 2017; p 29-44.

190. Dicker, M. P. M.; Duckworth, P. F.; Baker, A. B.; Francois, G.; Hazzard, M. K.; Weaver, P. M., *Compos. Part A Appl. Sci. Manuf.* **2014**, *56*, 280-289.
191. Zini, E.; Scandola, M., *Polym. Compos.* **2011**, *32*, 1905-1915.
192. Stürzel, M.; Mihan, S.; Mülhaupt, R., *Chem. Rev.* **2016**, *116*, 1398-1433.
193. Arrigo, R.; Jagdale, P.; Bartoli, M.; Tagliaferro, A.; Malucelli, G., *Polymers* **2019**, *11*, 1336-1351.
194. Li, S.; Huang, A.; Chen, Y.-J.; Li, D.; Turng, L.-S., *Compos. B. Eng.* **2018**, *153*, 277-284.
195. Zhang, Q.; Khan, M. U.; Lin, X.; Cai, H.; Lei, H., *Compos. B. Eng.* **2019**, *175*, 107151-107158.
196. Zhang, Q.; Zhang, D.; Lu, W.; Khan, M. U.; Xu, H.; Yi, W.; Lei, H.; Huo, E.; Qian, M.; Zhao, Y.; Zou, R., *Sci. Total Environ.* **2020**, *738*, 139910-139919.
197. Poulouse, A. M.; Elnour, A. Y.; Anis, A.; Shaikh, H.; Al-Zahrani, S. M.; George, J.; Al-Wabel, M. I.; Usman, A. R.; Ok, Y. S.; Tsang, D. C. W.; Sarmah, A. K., *Sci. Total Environ.* **2018**, *619-620*, 311-318.
198. Behazin, E.; Misra, M.; Mohanty, A. K., *Compos. B. Eng.* **2017**, *118*, 116-124.
199. Das, O.; Kim, N. K.; Hedenqvist, M. S.; Lin, R. J. T.; Sarmah, A. K.; Bhattacharyya, D., *Environ. Manage.* **2018**, *62*, 403-413.
200. Das, O.; Sarmah, A. K.; Bhattacharyya, D., *Sci. Total Environ.* **2015**, *512-513*, 326-336.
201. Nan, N.; DeVallance, D. B., *J. Mater. Sci.* **2017**, *52*, 8247-8257.

202. Ogunsona, E. O.; Codou, A.; Misra, M.; Mohanty, A. K., *J. Polym. Environ.* **2018**, *26*, 3574-3589.
203. Picard, M.; Thakur, S.; Misra, M.; Mielewski, D. F.; Mohanty, A. K., *Sci. Rep.* **2020**, *10*, 3310-3324.
204. Nagarajan, V.; Mohanty, A. K.; Misra, M., *ACS Sustain. Chem. Eng.* **2016**, *4*, 2899-2916.
205. Arrigo, R.; Bartoli, M.; Malucelli, G., *Polymers* **2020**, *12*, 892-905.
206. Ho, M.-P.; Lau, K.-T.; Wang, H.; Hui, D., *Compos. B. Eng.* **2015**, *81*, 14-25.
207. Pudełko, A.; Postawa, P.; Stachowiak, T.; Malińska, K.; Drózdź, D., *J. Clean. Prod.* **2021**, *278*, 123850-12856.
208. Qian, S.; Sheng, K.; Yao, W.; Yu, H., *J. Appl. Polym. Sci.* **2016**, *133*, 43425-43434.
209. Qian, S.; Tao, Y.; Ruan, Y.; Fontanillo Lopez, C. A.; Xu, L., *J. Mater. Res.* **2018**, *33*, 3870-3879.
210. Qian, S.; Yan, W.; Zhu, S.; Fontanillo Lopez, C. A.; Sheng, K., *Polym. Compos.* **2018**, *39*, 633-639.
211. Woodruff, M. A.; Hutmacher, D. W., *Prog. Polym. Sci.* **2010**, *35*, 1217-1256.
212. Labet, M.; Thielemans, W., *Chem. Soc. Rev.* **2009**, *38*, 3484-3504.
213. Gregory, G. L.; López-Vidal, E. M.; Buchard, A., *Chem. Commun.* **2017**, *53*, 2198-2217.
214. Lambert, S.; Wagner, M., *Chem. Soc. Rev.* **2017**, *46*, 6855-6871.

215. Guo, W.; Tao, J.; Yang, C.; Song, C.; Geng, W.; Li, Q.; Wang, Y.; Kong, M.; Wang, S., *PLOS ONE* **2012**, *7*, 38341-38347.
216. Ermeydan, M. A.; Cabane, E.; Hass, P.; Koetz, J.; Burgert, I., *Green Chem.* **2014**, *16*, 3313-3321.
217. Papadimitriou, L.; Kaliva, M.; Vamvakaki, M.; Chatzinikolaidou, M., *ACS Biomater. Sci. Eng.* **2017**, *3*, 1341-1349.
218. Habibi, Y.; Goffin, A.-L.; Schiltz, N.; Duquesne, E.; Dubois, P.; Dufresne, A., *J. Mater. Chem.* **2008**, *18*, 5002-5010.
219. Bellani, C. F.; Pollet, E.; Hebraud, A.; Pereira, F. V.; Schlatter, G.; Avérous, L.; Bretas, R. E. S.; Branciforti, M. C., *J. Appl. Polym. Sci.* **2016**, *133*, 43445-43453.
220. Park, I.-K.; Sun, H.; Kim, S.-H.; Kim, Y.; Kim, G. E.; Lee, Y.; Kim, T.; Choi, H. R.; Suhr, J.; Nam, J.-D., *Sci. Rep.* **2019**, *9*, 7033-7044.
221. Najarro, M. C.; Nikolic, M.; Iruthayaraj, J.; Johannsen, I., *ACS Appl. Polym. Mater.* **2020**, *2*, 5767-5778.
222. Wan, C.; Chen, B., *J. Mater. Chem.* **2012**, *22*, 3637-3646.
223. Wang, Y.; Li, T.; Ma, P.; Zhang, S.; Du, M.; Dong, W.; Xie, Y.; Chen, M., *New J. Chem.* **2018**, *42*, 10348-10356.
224. Zeng, H. L.; Gao, C.; Yan, D. Y., *Adv. Funct. Mater.* **2006**, *16*, 812-818.
225. Saeed, K.; Park, S.-Y., *J. Appl. Polym. Sci.* **2007**, *104*, 1957-1963.
226. Murray, E.; Sayyar, S.; Thompson, B. C.; Gorkin Iii, R.; Officer, D. L.; Wallace, G. G., *RSC Adv.* **2015**, *5*, 45284-45290.

CO-AUTHORSHIP STATEMENT

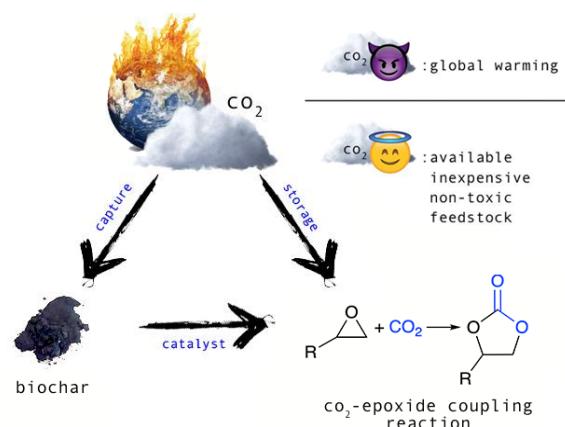
Chapter 2: Oxidized Biochar as a Renewable, Sustainable Catalyst for the Production of Cyclic Carbonates from Carbon Dioxide and Epoxides.¹ Juliana L. Vidal, Vincent P. Andrea, Stephanie L. MacQuarrie, and Francesca M. Kerton. This chapter has been published. Modifications to the paper in preparing this Chapter include: Number of records per publication year on methods for CO₂ capture, storage and transformation; TGA analysis of **APTES-bc_{hw}**; comparison between **oxbc_{hw}** and **oxbc_{sw}** FT-IR spectra; and a model of oxidized biochar as a catalyst for the cycloaddition reaction.

The first author (Juliana L. Vidal) contributed 90% of the content of the article as the main researcher, including performing experiments, collecting the data obtained, and writing the manuscript.

The co-author (Vincent P. Andrea) was responsible for functionalizing hardwood biochar samples (**oxbc_{hw}**, **APTES-bc_{hw}**), collecting data for BET surface area analysis of biochar samples, and acquiring the TGA spectrum of **bc_{hw}**.

The co-author (Stephanie L. MacQuarrie), my co-supervisor, was responsible for suggesting experiments, assisting with data interpretation, and revising the manuscript.

The corresponding author (Francesca M. Kerton), my supervisor, was the principal investigator of this work. She came up with the initial concept, suggested initial experiments, assisted with data interpretation, revised and submitted the manuscript.



References for **Chapter 2** can be found on **Pages 97-100**.

CHAPTER 2: OXIDIZED BIOCHAR AS A RENEWABLE, SUSTAINABLE CATALYST FOR THE PRODUCTION OF CYCLIC CARBONATES FROM CARBON DIOXIDE AND EPOXIDES

2.1 Introduction

Petroleum, coal, and natural gas are our society's main sources of energy, being responsible for 80% of the global energy consumption.² Great economic, social, and technological development has been obtained by burning these ancient forms of carbon to produce energy. However, this process has also increased the concentration of carbon dioxide (CO₂) in our atmosphere, leading to devastating and irreversible consequences such as climate change. With global energy-related CO₂ emissions reaching 30 gigatons per year and atmospheric CO₂ concentrations reaching 412 ppm,³ methods for capture, storage, and transformation of this greenhouse gas have grown in importance over the years, as shown by the increasing number of publications on this subject year by year (**Figure 2.1**).⁴⁻⁹ In particular, an important strategy consists of the production of cyclic carbonates through the cycloaddition between epoxides and CO₂.¹⁰⁻¹²

Cyclic carbonates are materials that present important industrial applications and can be used as precursors for pharmaceutical products, as aprotic polar solvents, as intermediates for polymeric syntheses, and to dissolve electrolytes for batteries.^{10, 13} However, the transformation of CO₂ into cyclic carbonates usually requires high-energy inputs, and catalysts are employed to ensure the use of mild conditions and avoid the further generation and release of this greenhouse gas to our atmosphere.¹³

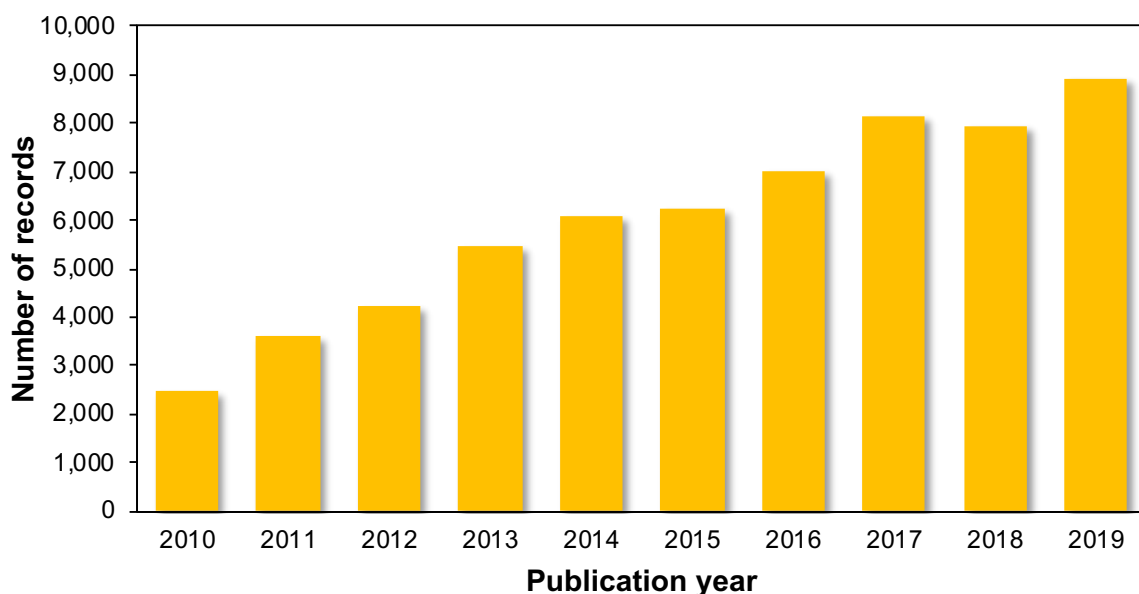


Figure 2.1. Number of records per publication year on methods for CO₂ capture, storage and transformation. Source: Web of Science (May 22nd, 2020). Topic = CO₂ AND fixation OR CO₂ AND modification OR CO₂ AND capture OR CO₂ AND storage or CO₂ AND transformation.

Different catalysts have been studied and applied to produce cyclic carbonates from epoxides and CO₂, including metal-based and organocatalysts.¹³⁻¹⁹ However, some of these catalysts present some disadvantages including low activity, low stability, high costs, or even the generation of non-biodegradable waste. To overcome some drawbacks of the previously studied systems, heterogeneous catalysts might be a good option, since they present a long service life, and can be easily separated, regenerated, and recovered. Carbon-based catalysts such as graphene oxide have been used,^{19,20} but due to the high-cost and toxicity associated with the production of graphene, the application of biochar as a catalyst for the cycloaddition reaction between epoxides and CO₂ represents an

inexpensive and more sustainable alternative.

As mentioned in **Chapter 1: Introduction**, biochar has been mainly used as a pollutant removal and soil amendment,²¹⁻²³ but there is significant scope for its implementation in higher value-added fields, such as in catalysis and in materials science. In terms of its chemical structure, biochar consists of a porous material with high surface area and some surface functionality.^{21, 24} However, in order to further increase its applications, the functionalization of biochar is fundamental. A commonly used type of biochar functionalization consists of its oxidation with nitric acid, which is known to greatly increase the content of oxygenated groups (e.g. carbonyl, carboxyl, and hydroxyl groups) on this carbon material's surface.²⁵⁻²⁸

Previously in the literature, materials containing hydroxyl or carboxyl groups have shown good performances as catalysts for the cycloaddition reaction of CO₂ with epoxides.^{17, 29, 30} They were able to interact via hydrogen-bonding with the epoxide oxygen and facilitate the ring opening of this compound promoted by the co-catalyst. Due to the presence of carboxyl and hydroxyl groups on the surface of oxidized biochar (**oxbc**) that could form a hydrogen-bond with the epoxide, the investigation of the catalytic activity of **oxbc** in the production of cyclic carbonates using epoxides and CO₂ was proposed. Moreover, by using a material that sequesters CO₂ during its production as a catalyst for a process that transforms CO₂ into cyclic carbonates, the objective was to design a process that could play an important role in the mitigation of climate change effects while synthesizing useful compounds (**Figure 2.2**).

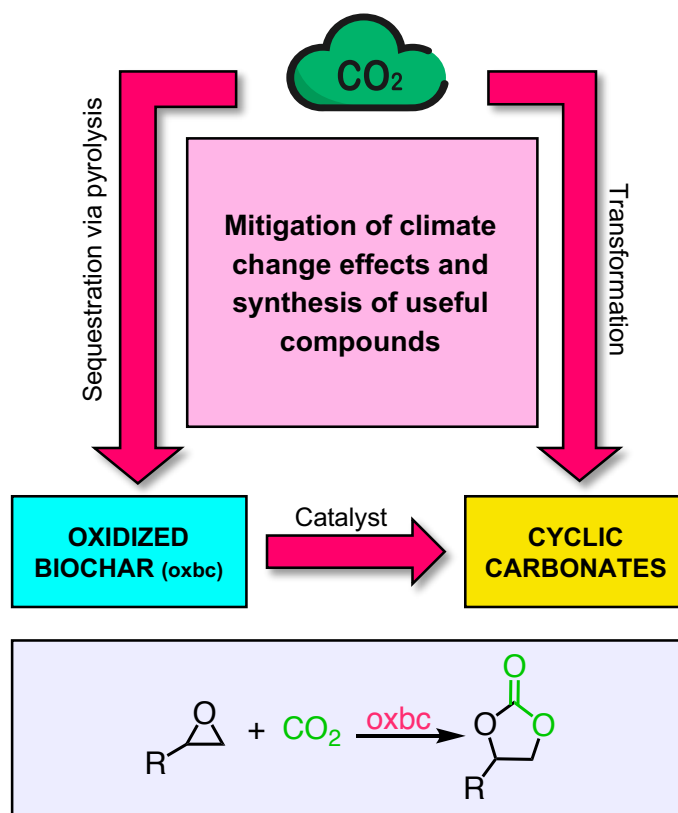
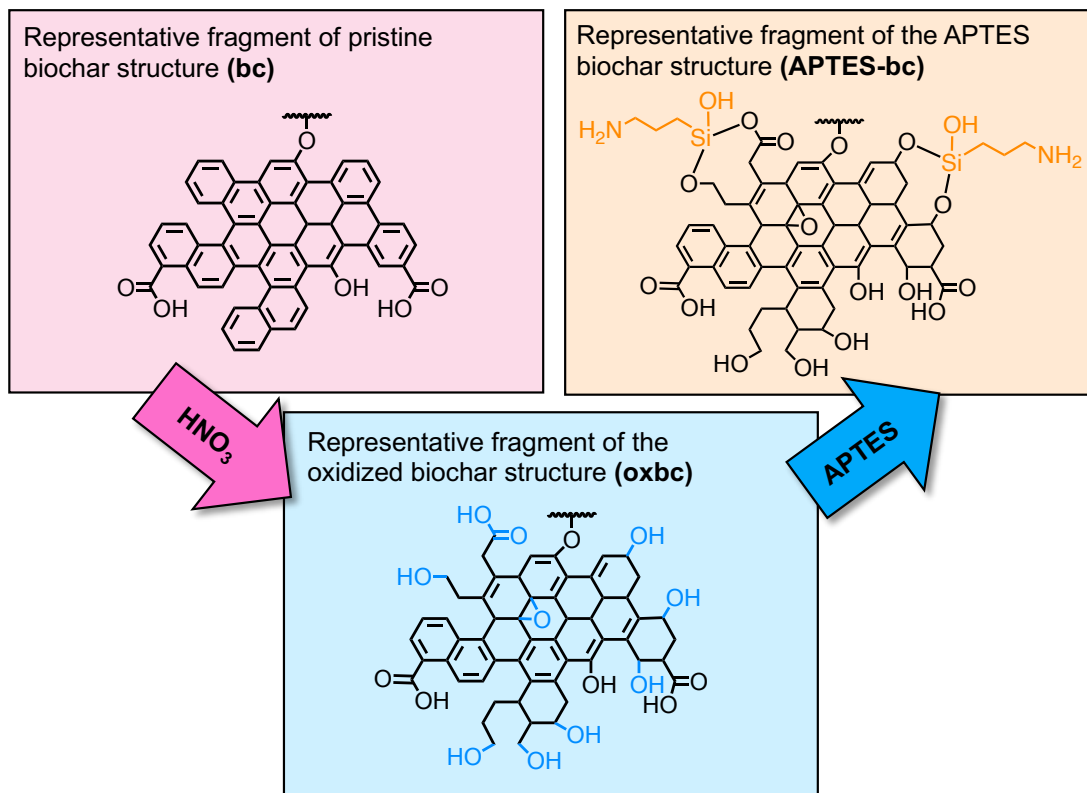


Figure 2.2. Schematic representation of the advantages in using **oxbc** as a catalyst for the production of cyclic carbonates using CO₂ and epoxides.

In this Chapter, the use of **oxbc** as a catalyst for the cycloaddition reaction of CO₂ and epoxides to produce cyclic carbonates is described. The influence of different co-catalysts, biomass feedstocks, substrates, temperatures, reaction times, and pressures were assessed to ensure the use of mild conditions while maintaining process efficiency. A mechanism for the reaction was proposed, and recyclability studies were performed to evaluate the stability of this system. Moreover, a comparison between **oxbc** and other carbon materials previously used as catalysts for the production of cyclic carbonates was performed to assess the efficiency and feasibility of the process described.

2.2 Results and Discussion

2.2.1 Preparation of Functionalized Biochars



Scheme 2.1. Preparation of functionalized biochar catalysts (**oxbc**, **APTES-bc**). Materials are represented as simplified fragments of the extended structures of biochar.

Oxbc samples were prepared after treatment of as-received pristine biochars (**bc**) with nitric acid (HNO_3) at $90\text{ }^\circ\text{C}$ for 3 h. After filtration and washing with deionized water until neutral pH in the filtrate, the black solid obtained was dried and identified as oxidized hardwood biochar (**oxbc_{hw}**) or oxidized softwood biochar (**oxbc_{sw}**), depending on the biomass feedstock used. To analyze the effect of different hydrogen-bonding interactions in the cycloaddition reaction between CO_2 and epoxides, an amino

functionalized biochar was prepared using 3-aminopropyltriethoxysilane (APTES). This reaction was performed by V. P. Andrea (Cape Breton University), and gave a material identified as **APTES-b_{chw}**. An illustration of the chemical modifications used to produce functionalized biochar catalysts is shown in **Scheme 2.1**. More details about preparation of the pristine and functionalized biochars can be found in **Sections 2.4.3, 2.4.4, and 2.4.5**.

2.2.2 Characterization of Functionalized Biochar

The effective functionalization of biochars was first confirmed by Fourier Transform Infrared (FT-IR) analysis. FT-IR spectra of biochars before (**b_{chw}**) and after functionalization (**oxb_{chw}**, **APTES-b_{chw}**) are shown in **Figure 2.3**. In **oxb_{chw}**, the oxidation is confirmed due to an increase in intensity of the OH stretch at 2700 cm⁻¹ and the appearance of a C=O stretch at 1716 cm⁻¹. Bands corresponding to asymmetric and symmetric stretches of NO₂ at 1534 and 1338 cm⁻¹ are also observed, indicating the insertion of nitro groups into the carbonaceous material. Previous studies show that the presence of an acid catalyst such as sulfuric acid is often needed for the nitrogen addition to occur; therefore, the NO₂ groups are inserted in very small quantities.²⁶ The bands at 1540 and 1165 cm⁻¹, which are also present in **b_{chw}** before its oxidation, are attributed to the C=C and C-O stretches, respectively. In **APTES-b_{chw}**, new bands can be observed. The bands present at 3746, 2924 and 1338 cm⁻¹ are related to the N-H, C-H, and C-N stretches, respectively. NH₂ scissoring and wagging are observed at 1567 and 698 cm⁻¹.

The insertion of siloxy groups is supported by the bands at 1090, 1032, and 744 cm^{-1} .

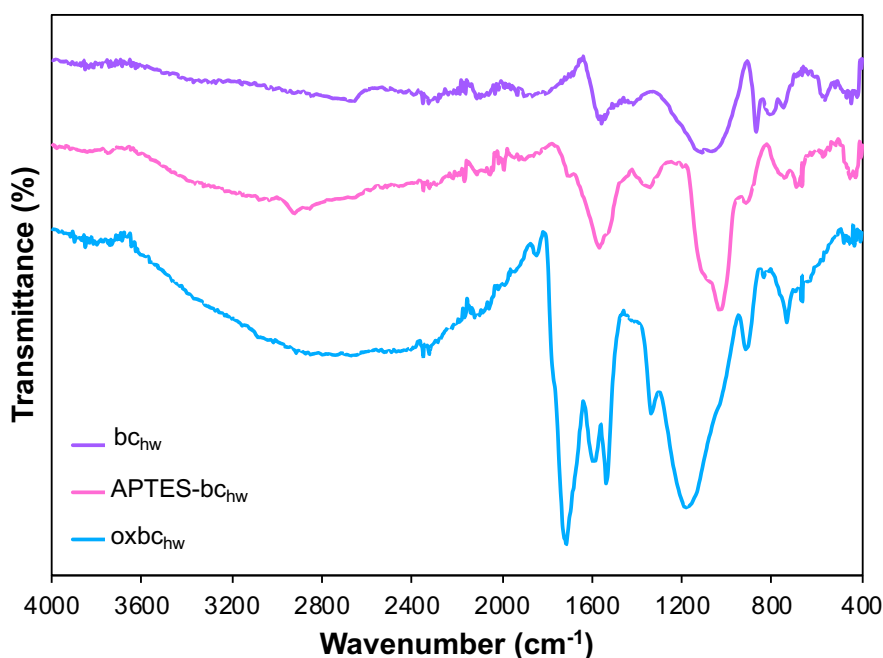


Figure 2.3. FT-IR spectra of bc_{hw} (top, purple), $\text{APTES-bc}_{\text{hw}}$ (pink, middle), and oxbc_{hw} (blue, bottom).

Thermogravimetric analysis (TGA) of pristine and functionalized biochar samples can be found in **Figure 2.4**. The thermogram of bc_{hw} showed a slight decomposition due to the functional groups already present on the surface of pristine biochar. However, rapid decomposition is observed above 250 $^{\circ}\text{C}$ for oxbc_{hw} and $\text{APTES-bc}_{\text{hw}}$. The weight losses observed in TGA analysis are associated with the surface functional groups such as $-\text{C}=\text{O}$, $-\text{OH}$, $-\text{COOH}$, and $-\text{NH}_2$ after biochar functionalization with HNO_3 or APTES. Moreover, the significant amount of residue present may be attributed to the existence of minerals in the structure of biochar and residual carbon since the experiments were performed under a N_2 atmosphere in which graphene and graphene-like portions persist.

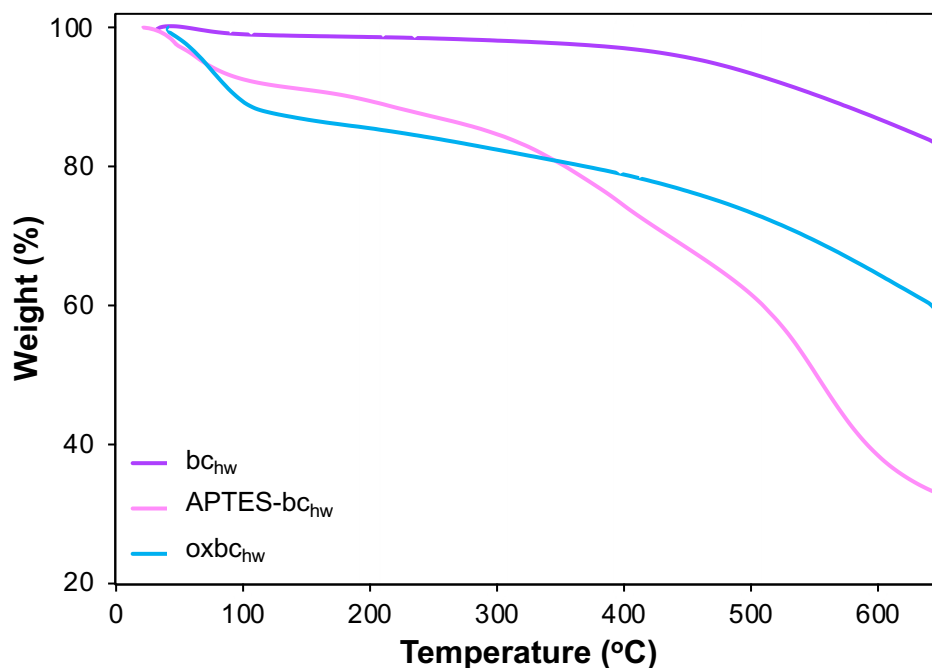
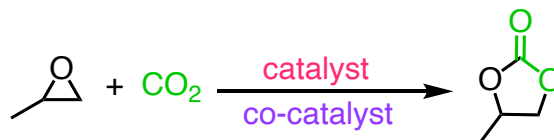


Figure 2.4. TGA plots of **bc_{hw}** (purple), **APTES-bc_{hw}** (pink), and **oxbc_{hw}** (blue).

2.2.3 Cycloaddition of CO₂ and Propylene Oxide

The catalytic performance of pristine and functionalized biochars was assessed using the formation of propylene carbonate (PC) from propylene oxide (PO) and CO₂ as our model reaction system. The results are presented in **Table 2.1**. Reproducibility of the system was evaluated performing experiments in triplicate (SD ≤ 3.3%). Furthermore, all reactions were performed in neat epoxide, without the presence of any additional solvent, which is a very important aspect in terms of Green Chemistry and process feasibility. The absence of organic solvents avoids potential issues related to toxicity, flammability, or smog formation, and also eliminates costs related to energy requirement to remove the used solvents from the reaction medium.^{31, 32}

Table 2.1. Optimization of the cycloaddition reaction between epoxides and CO₂ using PO as a model substrate and different types of biochar as catalysts.^a



Entry	Catalyst	Co-catalyst	Time (h)	Conversion (%) ^f
1	-	TBAB	4	34.2
2	oxbc _{hw}	-	4	0.0
3	oxbc _{hw}	TBAB	4	75.7
4	oxbc _{sw}	TBAB	4	75.1
5	bc _{hw}	TBAB	4	38.3
6	bc _{sw}	TBAB	4	40.0
7	oxbc _{hw}	TBAI	4	76.5
8	oxbc _{hw}	TBAC	4	55.8
9	oxbc _{hw}	ChCl	4	7.4
10 ^b	oxbc _{hw}	TBAB	4	69.6
11 ^b	oxbc _{hw}	TBAB	6	85.3
12 ^c	oxbc _{hw}	TBAB	6	65.2
13 ^b	oxbc _{hw}	PPNN ₃	6	25.4
14 ^b	oxbc _{hw}	PPNCl	6	76.8
15 ^d	oxbc _{hw}	TBAB	16	90.8
16 ^e	oxbc _{hw}	TBAB	6	78.5
17 ^e	APTES-bc _{hw}	TBAB	6	54.8

^a General reaction conditions unless otherwise stated: PO (68 mmol), co-catalyst (0.68 mmol), catalyst (200 mg), CO₂ (20 bar), 110 °C. ^b PO (34 mmol), co-catalyst (0.34 mmol), catalyst (100 mg). ^c 0.17 mmol of co-catalyst. ^d 100 °C. ^e CO₂ (10 bar). ^f Determined by ¹H NMR spectroscopy.

Due to presence of hydroxyl and carboxyl groups on the surface of the material that could facilitate the cycloaddition reaction, the catalytic activity of **oxbc_{hw}** was first investigated. As mentioned in **Section 2.1**, most catalytic systems used in CO₂-epoxide cycloadditions are binary and require the presence of nucleophilic co-catalysts to promote the epoxide ring-opening, while catalysts interact with epoxide and facilitate the process initiation. This synergistic effect between catalyst and co-catalyst could be observed very early in these experiments. Control reactions using only tetrabutylammonium bromide (TBAB), a very common co-catalyst for these reactions, gave moderate conversions of PO to PC (**Table 2.1, Entry 1**), whereas no reactivity was observed using only **oxbc_{hw}** as a catalyst (**Table 2.1, Entry 2**). However, using both **oxbc_{hw}** and TBAB (**Table 2.1, Entry 3**), good conversions of 75.7% were obtained, verifying the binary nature of this system and confirming the need for a co-catalyst for the reaction to occur.

The effects of biochar functionalization and biomass feedstock in the cycloaddition reaction were investigated next. Using **oxbc_{hw}** and **oxbc_{sw}**, 75.7% and 75.1% conversions were obtained (**Table 2.1, Entries 3 and 4**), whilst the pristine analogues **bc_{hw}** and **bc_{sw}** gave 38.3% and 40.0% conversions, respectively (**Table 2.1, Entries 5 and 6**). These results confirm that an increase in hydroxyl and carboxyl groups on the biochar structure provides an increased activity in the reactions of epoxides and CO₂. Moreover, both **bc** and **oxbc** from different types of trees (i.e. hardwood and softwood) gave similar conversions of PO to PC, showing that the biomass feedstock does not affect the activity of the catalytic system. Therefore, **oxbc_{hw}** was chosen for continued experiments due to

its slightly higher PO conversion.

Due to the necessity of a co-catalyst in the cycloaddition reaction studied, other onium salts were studied for the production of cyclic carbonates. TBAB and tetrabutylammonium iodide (TBAI) showed similarly good conversions of PO to PC (**Table 2.1, Entries 3 and 7**), but the corresponding chloride (TBAC) gave a lower conversion (**Table 2.1, Entry 8**). Chloride is a poorer leaving group than bromide and iodide, and this may be the reason why TBAC showed poorer results compared to TBAB and TBAI. Using choline chloride (ChCl), a conversion of only 7.4% was obtained (**Table 2.1, Entry 9**). Other excellent and frequently used co-catalysts for the cycloaddition of CO₂ and epoxides are bis(triphenylphosphine)iminium chloride (PPNCl) and azide (PPNN₃).³³⁻³⁵ However, when applied using **oxbc_{hw}** as a catalyst, the performance of these two co-catalysts was not as good as TBAB. Under the same reaction conditions, a PO conversion of 85.3% was achieved using TBAB as a co-catalyst (**Table 2.1, Entry 11**), while 25.4% and 76.8% conversions were obtained using PPNN₃ and PPNCl, respectively (**Table 2.1, Entries 13 and 14**). This decrease in the co-catalyst activity and process efficiency might be attributed to the intercalation of PPNCl and PPNN₃ aromatic groups between the graphene-like layers of biochar. However, there is also a significant anion effect with the azide co-catalyst being far less effective than the halides. The chemical structures of the co-catalysts used during our studies are shown in **Figure 2.5**.

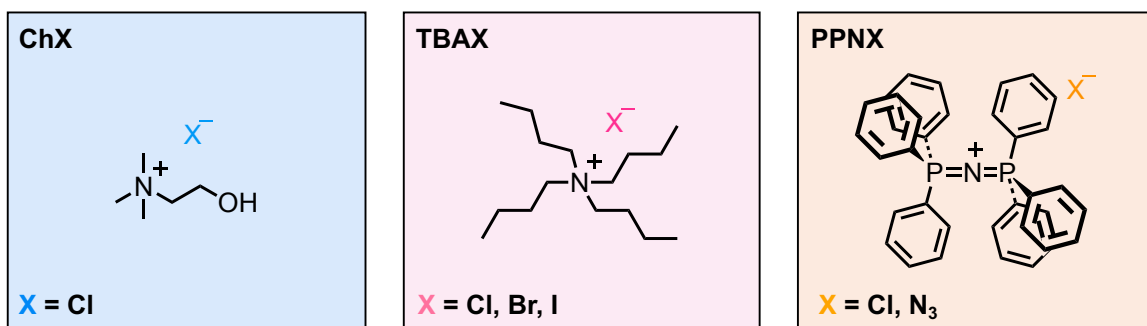


Figure 2.5. Chemical structures of the co-catalysts screened during the investigation of **oxbc** as a catalyst for cycloaddition reaction between CO₂ and epoxides.

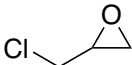
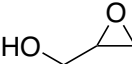
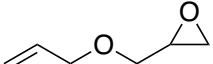
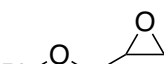
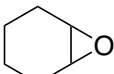
During our optimization studies, over 90% conversions could be obtained using high temperatures (100 °C), pressures (10 bar), and a longer reaction time of 16 h (**Table 2.1, Entry 15**). However, relatively good conversions were obtained using milder and less energy-intensive conditions. Therefore, 100 mg of catalyst, 0.34 mmol of co-catalyst (TBAB), 34 mmol of epoxide, a CO₂ pressure of 10 bar, and a reaction time of 6 h were chosen as optimized conditions (**Table 2.1, Entry 16**).

It is also worth mentioning that lower PO conversions were achieved when APTES functionalized biochar was used instead of its oxidized analogue (**Table 2.1, Entry 17** compared to **Entry 16**). This was somewhat surprising as primary amines are known to be good at activating CO₂.³⁶ However, the activation of the epoxide is clearly more important in these reactions, and hydroxyl and carboxyl groups are better hydrogen-bond donors.³⁶ For that reason, **oxbc_{hw}** was chosen as the standard catalyst for further studies using the optimized parameters.

2.2.4 Cycloaddition of CO₂ and Other Epoxides

The cycloaddition reaction using other epoxides catalyzed by **oxbc_{hw}** was screened under the optimized conditions for PO, and the results are presented in **Table 2.2**. All the epoxides investigated were transformed to their respective cyclic carbonates with conversions higher than 70%, thus showing a broad substrate scope for the catalytic system studied.

Table 2.2. Cycloaddition of CO₂ and different epoxides to yield cyclic carbonates using **oxbc** as a catalyst.^a

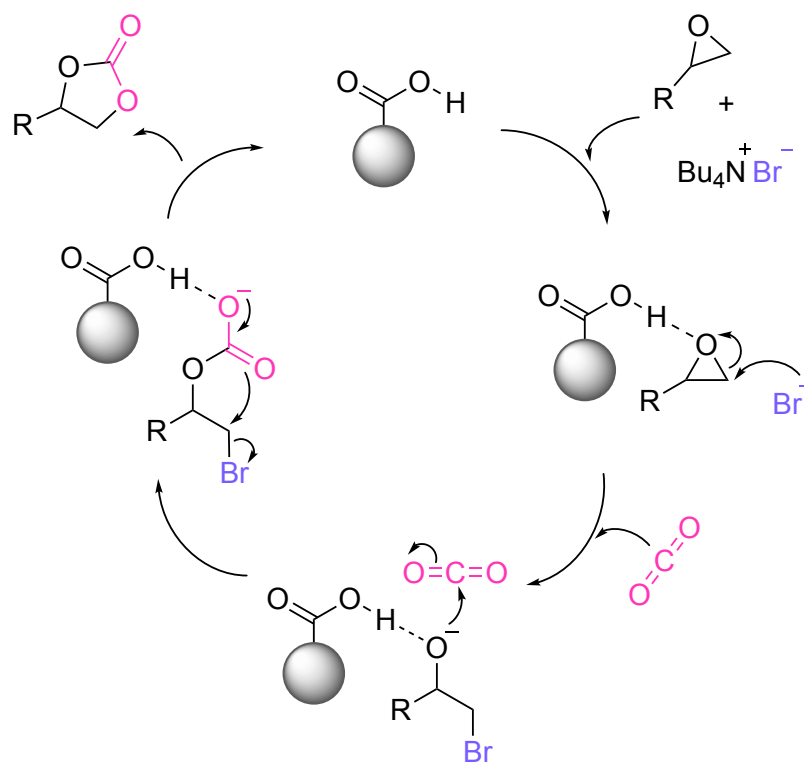
Entry	Epoxide	Conversion (%) ^b
1		78.5
2		97.1
3		> 99.9
4		83.7
5		71.1
6		70.4
7		21.9

^a Reaction conditions: Epoxide (34 mmol), co-catalyst (TBAB, 0.34 mmol), catalyst (**oxbc_{hw}**, 100 mg), CO₂ (10 bar), 110 °C, 6 h. ^b Determined by ¹H NMR spectroscopy.

The trend in the results obtained agrees with previous works in the literature,^{35, 37, 38} and it is related to the electron-withdrawing capacity of the substituents. For example, epoxides containing electron-withdrawing groups are more susceptible to the nucleophilic attack of the co-catalyst anion, and therefore give higher conversions to the cyclic carbonates. When cyclohexene oxide is used as a substrate (**Table 2.2, Entry 7**), poorer results are expected and obtained. Due to the formation of a bicyclic carbonate and steric hindrance effects, the nucleophilic attack promoted by the co-catalyst is obstructed, and low values of conversion to the respective cyclic carbonate are achieved. The ¹H NMR spectra of the cyclic carbonates obtained can be found in **Appendix A: Information for Chapter 2**.

2.2.5 Mechanism of the Cycloaddition Reaction

The mechanism for the cycloaddition reaction between CO₂ and epoxides using **oxbc** as a catalyst was proposed based on the results obtained, and is presented in **Scheme 2.2**. The main role of the co-catalyst, in this case TBAB, is to attack the less hindered carbon of the epoxide to promote ring-opening. The **oxbc** is responsible for interacting via hydrogen-bonding with the epoxide oxygen. This interaction polarizes and activates the C-O bond of the epoxide, leaving it more susceptible for the nucleophilic attack promoted by the co-catalyst. After the epoxide ring-opening, an alkoxide is formed, the CO₂ is inserted, and the cyclic carbonate is formed by intramolecular cyclization and regeneration of the halide anion.



Scheme 2.2. Proposed mechanism for the cycloaddition reaction between CO_2 and epoxides using **oxbc** as a catalyst.

The proposed mechanism agrees with previous works involving hydrogen-bonding catalysts for the cycloaddition of CO_2 and epoxides,^{17, 29, 30} and also explains some of the observations obtained throughout the studies herein. For example, this mechanism explains why the co-catalyst (i.e. TBAB) alone is capable of converting a small amount of epoxide to cyclic carbonate, and also explains why **oxbc** cannot perform the reaction without any additional ring-opening nucleophile. In conclusion, the key to accelerating the epoxide ring-opening performed by the co-catalytic nucleophile is via activation of the C-O bond promoted by the hydroxyl and carboxyl groups on the surface of **oxbc**.

2.2.6 Recycling and Kinetic Studies

The recyclability of the catalytic system using **oxbc_{hw}** was investigated under the optimized conditions using PO as a substrate. After the reaction, the catalyst was separated from the products and re-used. As shown in **Figure 2.6**, no decrease in conversions or catalytic activity was observed even after five reaction cycles.

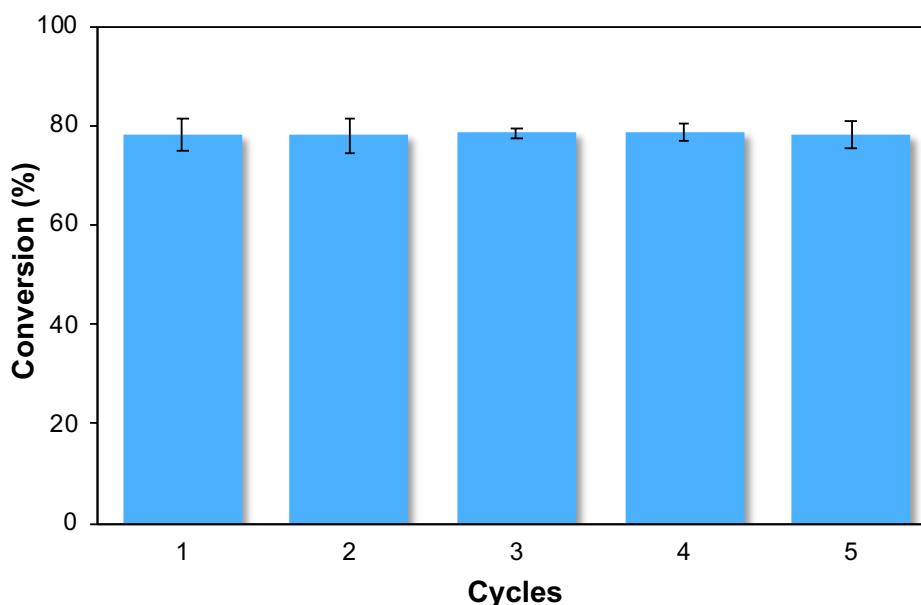


Figure 2.6. Recycling studies for the cycloaddition reaction between CO₂ and epoxides using **oxbc** as a catalyst. Conditions: Epoxide (PO, 34 mmol), co-catalyst (TBAB, 0.34 mmol), catalyst (**oxbc_{hw}**, 100 mg), CO₂ (10 bar), 110 °C, 6 h (bars represent SD).

It is worth mentioning that the separation of the catalyst from the dark mass of the reaction mixture was only possible after several successive cycles of washing, sonication, and centrifugation, as described in more detail in **Section 2.4.7**. Different solvents such as dichloromethane, acetone, and ethanol were tested to assist in the catalyst separation process. However, because of its low ability to disperse **oxbc_{hw}** and its low boiling point,

diethyl ether was chosen as the best solvent to isolate **oxbc** from the products.

The optimized conditions were also applied to briefly study the kinetics of the cycloaddition reaction between CO₂ and epoxides catalyzed by **oxbc_{hw}**. Using PO as a substrate, the reaction was monitored via in situ FT-IR spectroscopy, showing an increase in intensity of the C=O band of PC at 1809 cm⁻¹ as time proceeds (**Figure 2.7**). As shown in **Figure 2.8**, the absence of an induction period shows that no prior transformation is necessary for **oxbc** to promote the reaction.

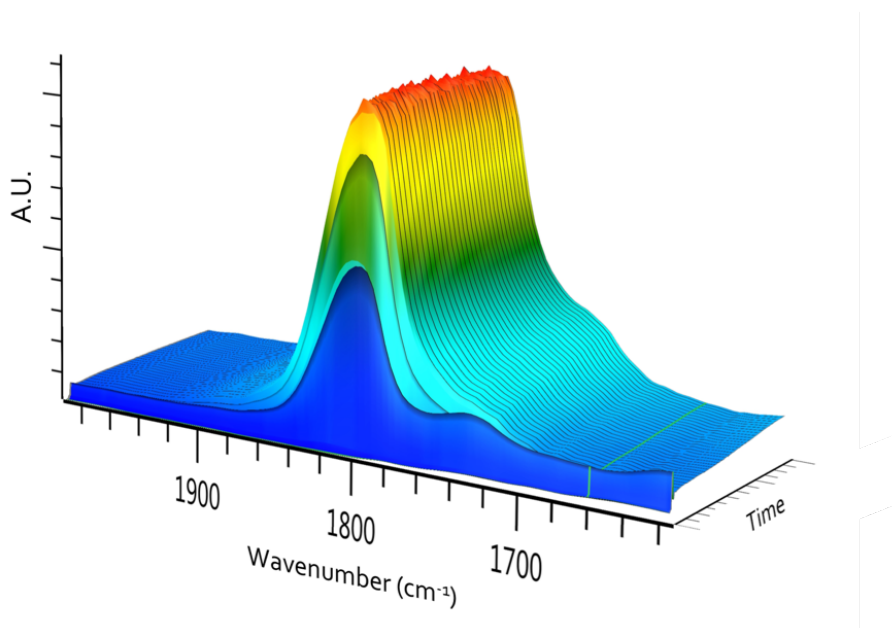


Figure 2.7. 3D stack plot obtained by in situ FT-IR spectroscopy during the cycloaddition reaction between CO₂ and PO using **oxbc** as a catalyst. Conditions: Epoxide (PO, 34 mmol), co-catalyst (TBAB, 0.34 mmol), catalyst (**oxbc_{hw}**, 100 mg), CO₂ (10 bar), 110 °C, 6 h.

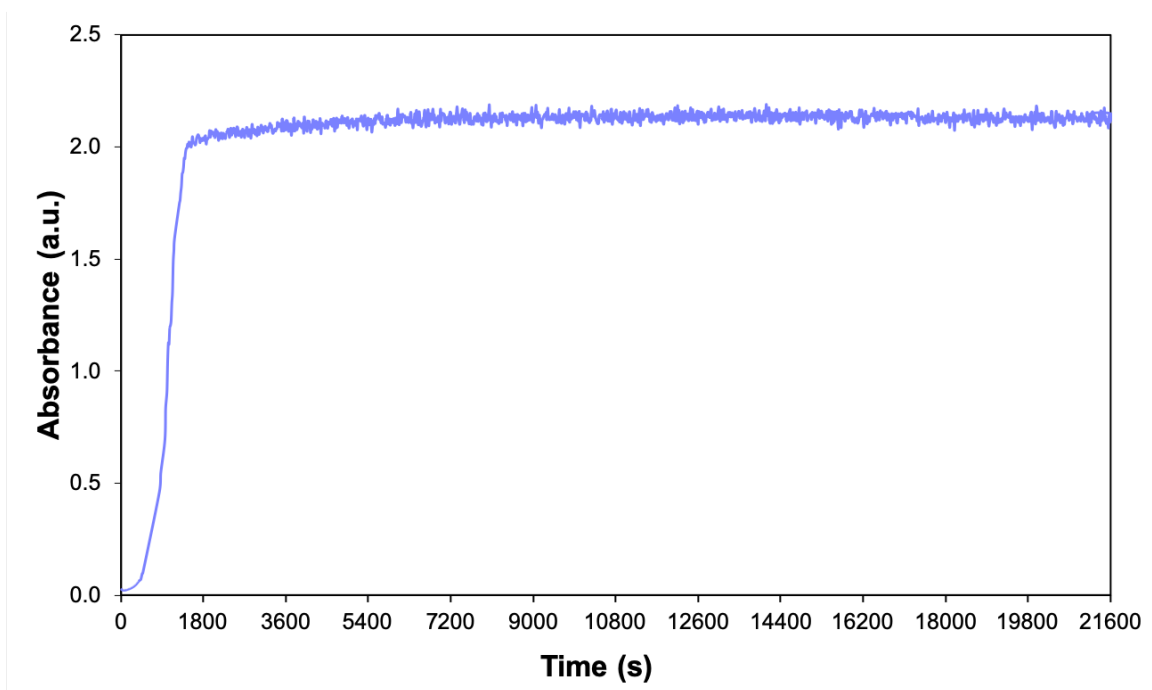


Figure 2.8. Absorbance of the PC C=O peak (1809 cm^{-1}) in function of time for the cycloaddition reaction between CO_2 and epoxides catalyzed by **oxbc**. Conditions: Epoxide (PO, 34 mmol), co-catalyst (TBAB, 0.34 mmol), catalyst (**oxbc_{hw}**, 100 mg), CO_2 (10 bar), $110\text{ }^\circ\text{C}$, 6 h.

2.2.7 Oxidized Biochar as a Catalytic Material

To understand the catalytic system proposed and verify any differences between the **oxbc** from different carbon sources, Scanning Electron Microscopy (SEM) analyses were performed. Through SEM, it was possible to comprehend the surface morphology, particle dimensions, and surface chemistry of **oxbc** and their effects in the cycloaddition reaction. Scanning Electron Microscopy Mineral Liberation Analyses (SEM-MLA) showed similar particle properties between **oxbc_{hw}** and **oxbc_{sw}**. As shown in **Figure 2.9**, the majority of **oxbc_{hw}** and **oxbc_{sw}** particles are in the size range of $125\text{ to }132\text{ }\mu\text{m}^2$.

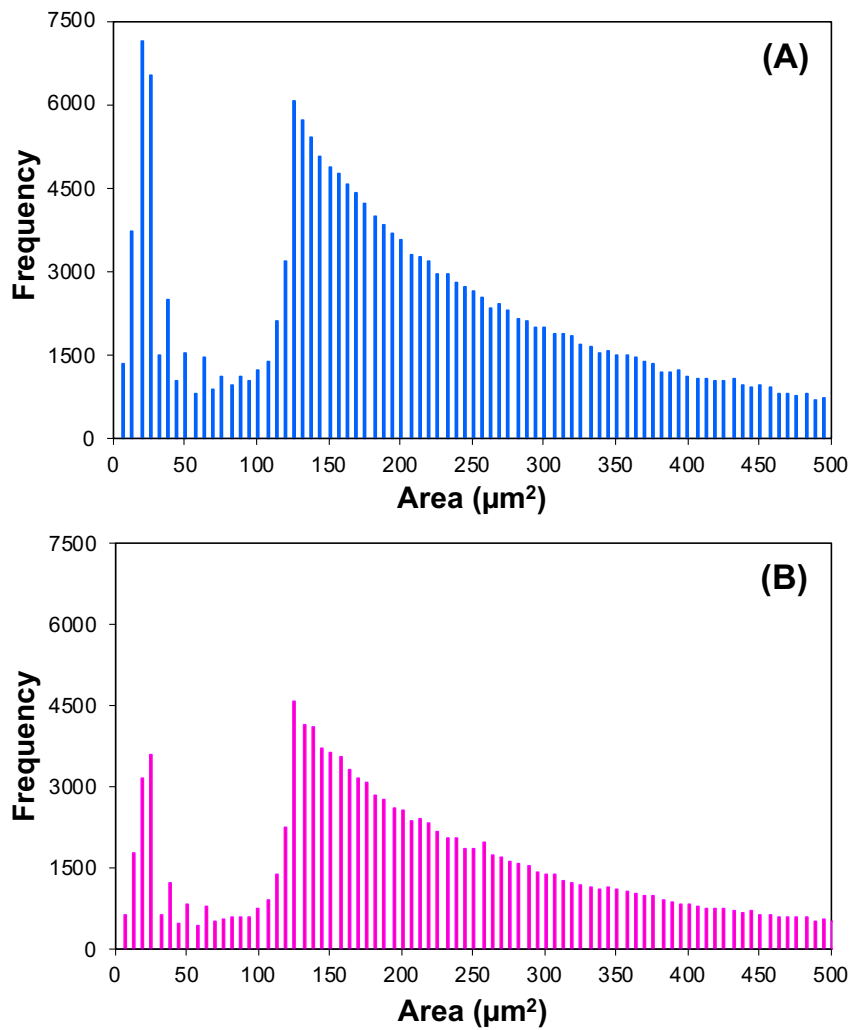


Figure 2.9. Particle distribution and size analyses of (A) **oxbc_{hw}** and (B) **oxbc_{sw}**.

SEM images of **oxbc_{hw}** and **oxbc_{sw}** are shown in **Figure 2.10**, and there are similarities in the morphologies between the two types of **oxbc**. On the surface of both **oxbc** samples, it was possible to observe the presence of pores. However, the presence of small and rounded particles was only seen in **oxbc_{hw}**.

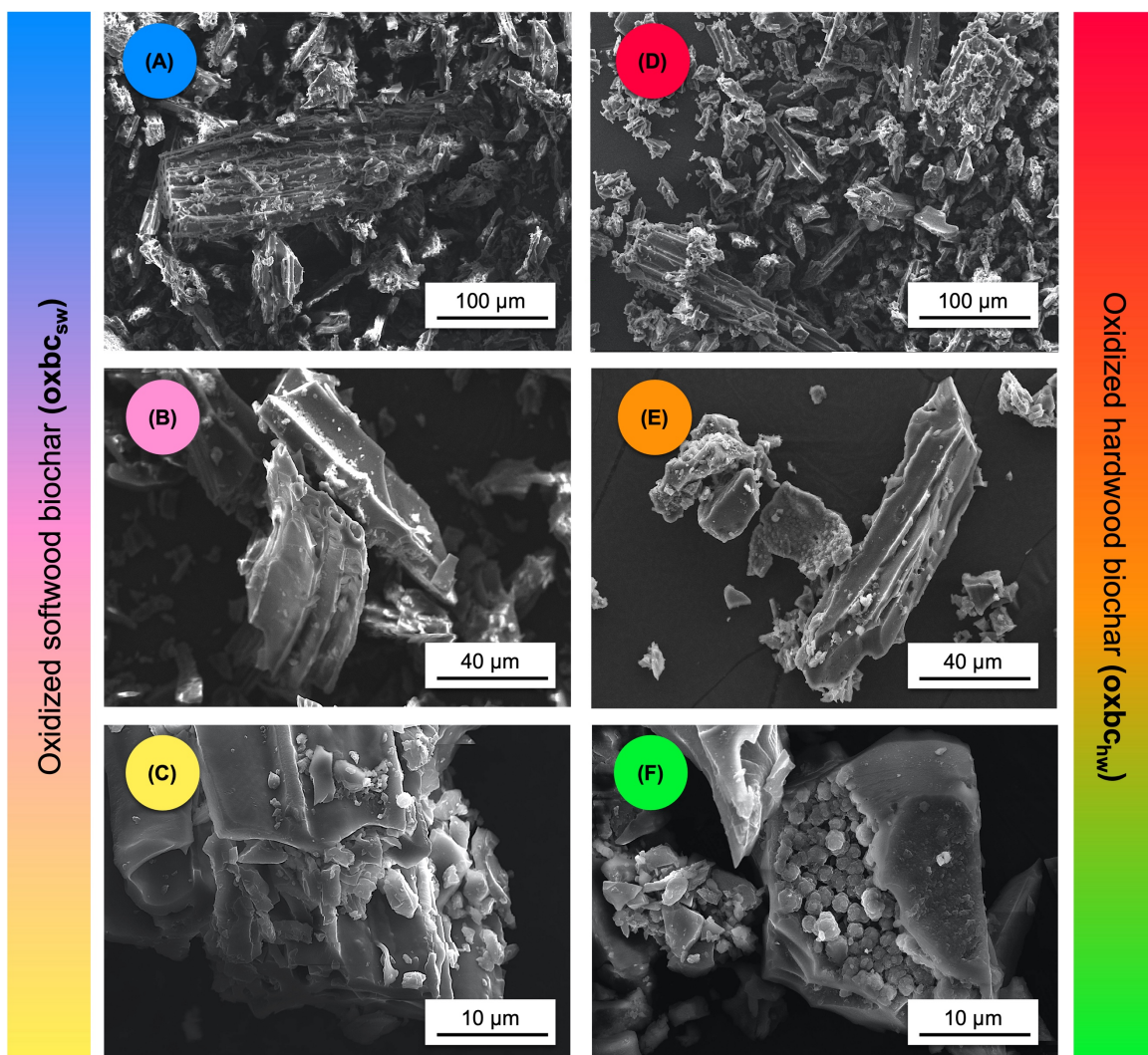


Figure 2.10. SEM images of biochars after oxidation. (A), (B), and (C) images show the presence of pores on the surface of oxbc_{sw} . The presence of pores on the surface of oxbc_{hw} is seen in (D) and (E), whilst the presence of round particles on the surface of oxbc_{hw} is observed in image (F).

To understand and identify the composition of the small and rounded particles found in oxbc_{hw} samples, Scanning Electron Microscopy with Energy Dispersive X-Ray (SEM-EDX) analysis was performed. The particles analyzed in each type of oxbc sample

are highlighted in **Figure 2.11**. The elemental composition of the rounded particles was revealed to be mainly carbon and oxygen, which is the same as the majority of **oxbc**. Small amounts of other elements were also detected in the **oxbc_{hw}** and **oxbc_{sw}** samples (**Table 2.3**).

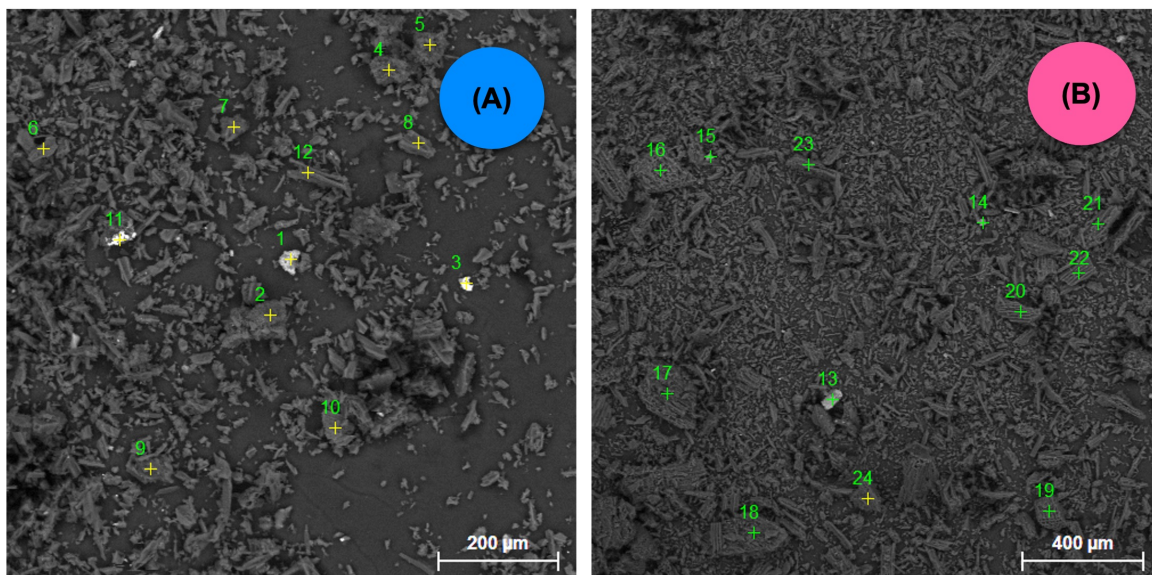


Figure 2.11. Particles of (A) **oxbc_{hw}** and (B) **oxbc_{sw}** analyzed via SEM-EDX.

Table 2.3. Minerals present on the surface of **oxbc** samples.

Biochar	Si	Ti	Mg	Fe	Al	K	Ca	Mn	Cu	Na	Sn
oxbc_{hw}	✓*	✗	✓	✓	✓*	✓	✓	✗	✗	✓	✓
oxbc_{sw}	✓*	✓*	✓*	✓*	✓*	✓	✓	✓	✓	✓	✗

* Relatively high amounts of the respective element present in the analyzed particles of **oxbc**.

The similarities between the **oxbc** samples from different biomass precursors were also observed via FT-IR spectroscopy (**Figure 2.12**). The comparable conversions obtained, and the similarities observed via SEM and FT-IR analyses suggest similar

surface properties for the two **oxbc** samples and therefore, similar catalytic activities in the cycloaddition reactions studied.

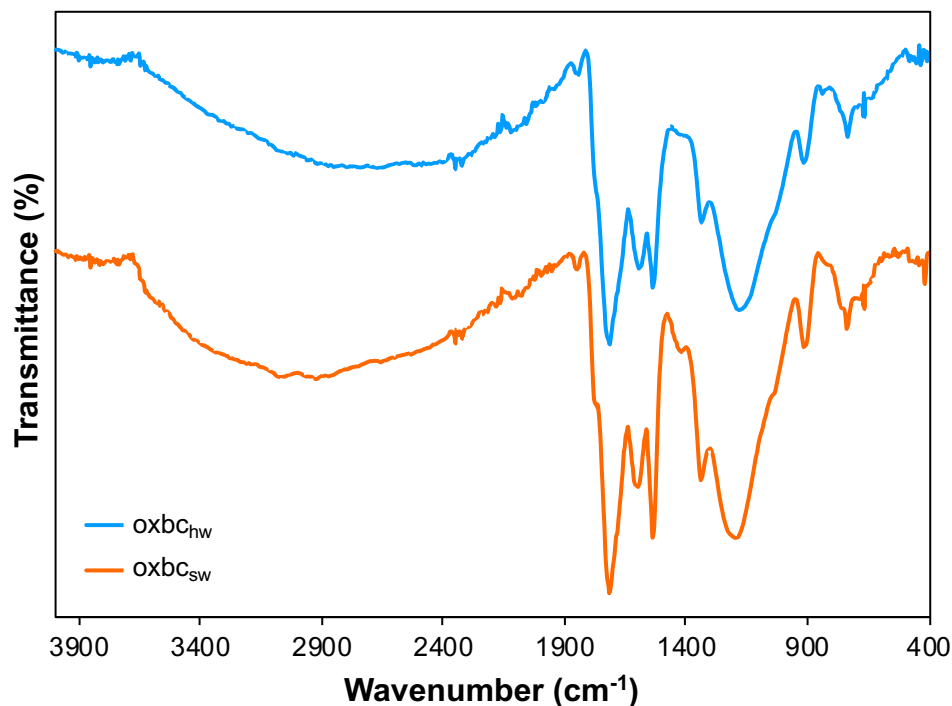


Figure 2.12. Comparison between the FT-IR spectra of **oxbc_{hw}** (top, blue) and **oxbc_{sw}** (bottom, orange).

Regarding the surface area, Brunauer-Emmet-Teller (BET) analysis showed different values for the two types of **oxbc** obtained from different types of biomass feedstocks. As shown in **Table 2.4**, biochar obtained from hardwood waste has close to three times the surface area of its softwood analogue. Although the surface area values are different, macro, meso, and micro porosities are observed in both samples.

Table 2.4. Surface area and average pore size of **oxbc_{hw}** and **oxbc_{sw}** samples, obtained via BET analysis.

Biochar	Surface area (m ² /g)	Pore diameter (Å)
oxbc _{hw}	231.0	29.0
oxbc _{sw}	80.4	42.9

From the conversions and results obtained after FT-IR, SEM, and BET analyses, it is suggested that the catalytic reaction occurs in the pores as well as on the surface of the material (**Figure 2.13**).

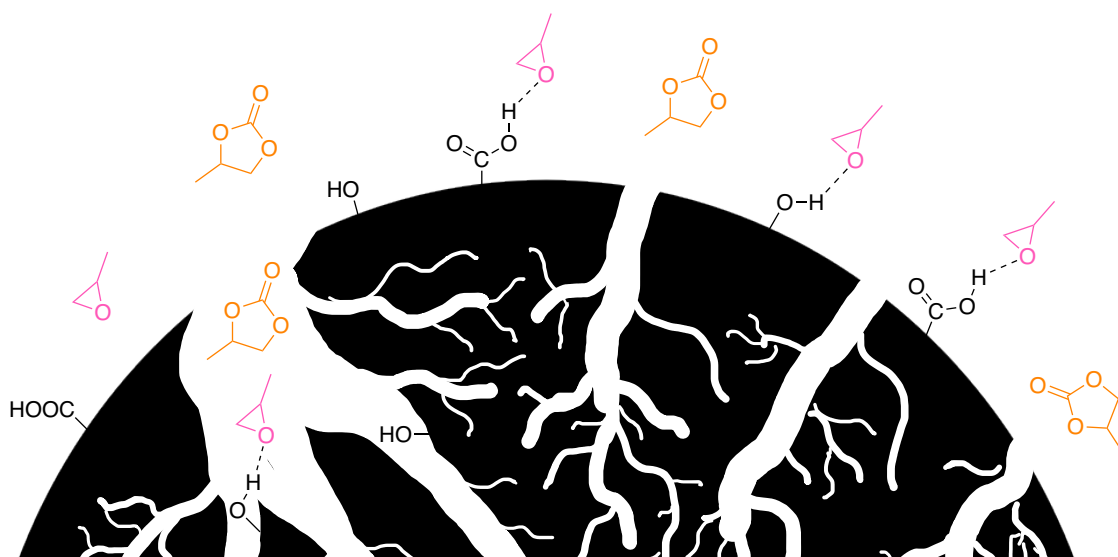


Figure 2.13. A model of porous **oxbc** as a catalyst for the cycloaddition reaction between CO₂ and PO.

2.2.8 Biochar and Other Carbon-Based Catalysts

To evaluate the efficiency of **oxbc**, a comparison between this work and similar studies involving other carbon-based materials as catalysts for the cycloaddition reaction

between CO₂ and epoxides is shown in **Table 2.5**. During the course of this research, *N*-doped active carbon catalysts prepared using a different method from other biomass sources (i.e. de-oiled seed cakes) were reported for the production of cyclic carbonates.¹⁶ In contrast to the work herein, the catalyst was recycled three times, biomass-dependent differences in reactivity were observed, and conversions higher than 30% were achieved using relatively mild conditions only in the presence of epoxides containing electron-withdrawing groups such as epichlorohydrin and glycidol. To obtain good conversions of PO, harsh reaction parameters such as 150 °C, 50 bar of CO₂, and 24 h of reaction time were necessary.

Functionalized and non-functionalized graphene oxide (GO) have shown good catalytic activity for the production of cyclic carbonates, requiring small amounts of GO (e.g. 2.5 mg), short reaction times (e.g. 1 h), or even occurring under atmospheric pressures. Although great results are obtained in the cycloaddition reaction using mild conditions under a broad substrate scope with GO, the production of high-quality graphene generally possesses drawbacks associated with apparatus complexity, use of toxic reagents, and poor cost-efficiency.³⁹ Therefore, the use of **oxbc** from waste hard- and softwood biomasses represents an environmentally and economically sustainable alternative for the production of cyclic carbonates. A co-catalyst is needed for the cycloaddition to occur, but good recyclability and conversions can be obtained under mild conditions.

Table 2.5. Comparison of several carbon-based catalysts used for the production of cyclic carbonates from CO₂ and epoxides.

Carbon-based catalyst	Reaction Parameters ^a	Conv. (%) / Yield (%) ^b	Number of epoxides	Cycles	Ref.
Oxidized biochar from waste hard/softwood biomass	100 mg catalyst, 34 mmol PO, 1 mol % TBAB, 10 bar CO ₂ , 6 h, 110 °C	78.5 (conv.)	7	5	-
<i>N</i> -doped carbons from de-oiled seed cakes	100 mg catalyst, 20 mmol PO, 15 bar CO ₂ , 15 h, 150 °C	30.0 (conv.)	3	3	16
GO	2.5 mg catalyst, 5 mmol PO, 4 mL DMF, 1 bar CO ₂ , 12 h, 140 °C	96.6 (conv.)	5	4	20
GO	50 mg catalyst, 28.6 mmol PO, 2.5 mol % TBAB, 22.5 bar CO ₂ , 1 h, 100 °C	78.0 (yield)	4	2	19
APTMS-GO	30 mg catalyst, 10 mmol PO, 1 mol % TBAI, 1 bar CO ₂ , 12 h, 70 °C	65.0 (yield)	9	7	18

^a Co-catalyst amounts relative to propylene oxide (PO). ^b Conversions or yields determined by ¹H NMR spectroscopy, gas chromatography (GC), or gas chromatography mass spectrometry (GC-MS).

2.3 Conclusions

Strategies that consider the total environment impact of process, thus minimizing or even avoiding any possible hazards associated are the basis of Green Chemistry and are critical for catalyst development and advancements. In this Chapter, a sustainable approach for the catalytic production of cyclic carbonates using **oxbc** is reported. The implementation of a material that reduces overall CO₂ in the environment as a catalyst for a reaction that transforms CO₂ into industrial products is an important step towards holistic considerations for greener catalytic cycles.

The catalytic system herein proposed achieves good conversions to the desired products using mild conditions, possesses a broad substrate scope, shows great recyclability, and utilizes an easily produced, environmentally friendly, and inexpensive feedstock. This work is, therefore, proof-of-concept that **oxbc** prepared from hardwood or softwood waste biomasses can work as an efficient catalyst via hydrogen-bonding activation, representing a greener alternative to existing heterogeneous catalysts for the production of cyclic carbonates via cycloaddition reaction between CO₂ and epoxides.

2.4 Experimental

2.4.1 General Materials

Unless otherwise stated, chemicals were purchased from Sigma Aldrich or Fisher Scientific and used as received. Pristine biochar samples were used without additional treatment from Cape Breton University (Sydney, Nova Scotia) and Sexton Lumber Co.

(Bloomfield, Newfoundland and Labrador). Commercially available solvents were used without any further purification.

2.4.2 Instrumentation

FT-IR spectra were obtained on a Bruker Alpha FT-IR spectrometer fitted with a single-bounce diamond Attenuated Total Reflection (ATR) accessory, from 400 to 4000 cm^{-1} wavelength, 32 scans per sample, and a resolution of 4 cm^{-1} . All measurements were collected ten times to investigate samples homogeneity, averaged, and further plotted for analysis.

^1H NMR spectra were acquired on a Bruker AVANCE™ 300 or 500 MHz spectrometer at 298 K in CDCl_3 or acetone- d_6 . Deuterated solvents were purchased from Cambridge Isotope Laboratories and used without purification. Residual protio-solvent peaks were used as internal standards, and chemical shifts are reported as δ (ppm) values.

For SEM images, biochar samples were coated with carbon and further analyzed on a FEI 650 MLA FEG SEM using an ETD detector, a high voltage of 15.00 kV, and approximate working distance of 10 mm. Images were taken under high vacuum (10^{-6} Torr).

Nitrogen adsorption surface measurements were performed on a Micrometrics ASAP 2020 Surface Area and Porosity Analyzer at 77 K after degassing (350 °C, 340 min). The apparent nitrogen surface area was calculated via BET method.

TGA of **bc_{hw}** was performed on a Perkin Elmer Simultaneous Thermal Analyzer

STA 8000 (20 mL/min N₂, 25 to 650 °C), whereas TGA analyses of **oxbc_{hw}** and **APTES-bc_{hw}** samples were obtained using a TA Instruments Q500 under high resolution dynamic mode (50 mL/min N₂, 25 to 650 °C). Total C, H, and N analysis was performed on a Perkin Elmer 2400 Series II CHNS Analyzer.

Cycloaddition reactions were performed in a 100 mL stainless steel Parr® 5500 reactor equipped with a Parr® 4848 controller and an overhead stirrer. In situ FT-IR monitoring of the cycloaddition reaction was performed using a modified 100 mL stainless steel Parr® 4560 reactor. The vessel was attached to a SiComp Sentinel ATR silicon sensor connected to a Mettler-Toledo ReactIR 15™ base unit through a DS silver-halide Fiber-to-Sentinel conduit. Both of reactors were cleaned and heated under vacuum at 100 °C before experiments to avoid risk of contamination.

2.4.3 Preparation of Pristine Biochars (bc)

Pristine hardwood biochar (**bc_{hw}**) was provided by Cape Breton University (Sydney, Nova Scotia) and prepared by the anaerobic pyrolysis of debarked birch wood at 400 °C,⁴⁰ whilst pristine softwood biochar from pine (**bc_{sw}**) was obtained after pyrolysis at 500 °C of softwood sawmill sawdust feedstock supplied by Sexton Lumber Co. (Bloomfield, Newfoundland and Labrador).⁴¹

2.4.4 Preparation of Oxidized Biochars (oxbc)

In a round bottom flask containing 150 mL of a 7 M HNO₃ solution, 3.0 g of biochar from hardwood (**bc_{hw}**) or softwood (**bc_{sw}**) waste biomass feedstocks were added slowly.

The mixture was stirred and heated to 90 °C under reflux for 3 h. After the reaction, the flask was left aside to cool down for about 10 min. The black solid was separated from the reaction mixture by filtration and washed using deionized water (700 mL) until washings achieved neutral pH. The product was then dried in an oven at 110 °C overnight and further identified as **oxbc_{hw}** or **oxbc_{sw}**, depending on the biochar used as a carbon source.

2.4.5 Preparation of APTES modified biochar (APTES-bc_{hw})

A suspension containing 40 mL of deionized water and 200 mg of **oxbc_{hw}** was sonicated in an ultrasound bath for 60 min. After sonication, 5 mL of a 0.2 M solution of 3-aminopropyltriethoxysilane (APTES) in toluene was added to the dispersion, which was heated to 70 °C for 24 h. The reaction mixture was filtered using ethanol and deionized water for the washes. The black product was dried in a vacuum oven at 50 °C overnight and further identified as **APTES-bc_{hw}**. This procedure was performed by V. P. Andrea (Cape Breton University).

2.4.6 Synthesis of Cyclic Carbonates

In a typical reaction, epoxide (34 mmol), co-catalyst (0.34 mmol), and catalyst (100 mg) were transferred into a reactor vessel, which was charged with the appropriate pressure of CO₂ (usually 10 bar) and heated to 110 °C for 6 h. After the required time, the reactor was cooled to 7 °C in an ice bath and the excess of CO₂ was vented slowly in the fume hood. An aliquot of the reaction mixture was immediately taken, filtered to remove the biochar, and analyzed via ¹H NMR spectroscopy to calculate conversions.

2.4.7 Recycling Studies

Using PO as the epoxide, a cycloaddition reaction was performed as described in **Section 2.4.6**. The mixture removed from the pressure vessel was centrifuged at 7500 rpm for 10 min to decant off liquid components and allow the catalyst (oxbc_{hw}) to be isolated. After isolation, the wet catalyst was washed with 15 mL of diethyl ether, sonicated for 20 min in an ultrasound bath, and then centrifuged again (7500 rpm, 10 min). The supernatant was decanted, and the procedure was repeated until the wet dark mass became powdery, which could involve up to five cycles of washing, sonication, and centrifugation.

The visual difference between the wet dark mass of catalyst and the powder obtained after the washing, sonication, and centrifugation cycles is shown in **Figure 2.14**. Following this successive treatment, the catalyst was dried in a vacuum oven at 60 °C overnight to eliminate residual solvent and used again in another cycloaddition reaction.

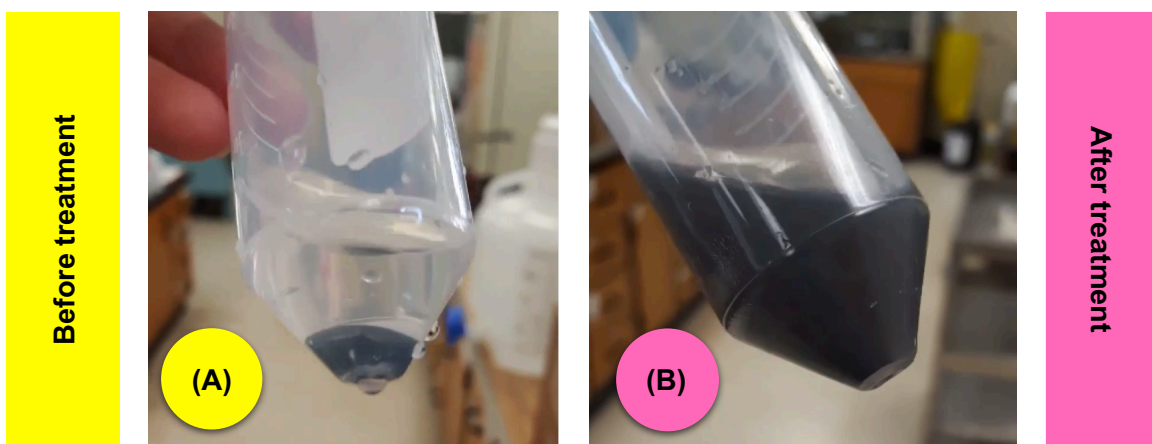


Figure 2.14. Visual difference between oxbc_{hw} catalyst in diethyl ether (A) before and (B) after five cycles of the required treatment for its reutilization in another cycloaddition.

2.5 References

1. Vidal, J. L.; Andrea, V. P.; MacQuarrie, S. L.; Kerton, F. M., *ChemCatChem* **2019**, *11*, 4089-4095.
2. *International Energy Agency (IEA) Global Energy Review (2019)*.
3. National Oceanic and Atmospheric Administration (NOAA), Climate Change: Atmospheric Carbon Dioxide. <https://www.climate.gov/news-features/understanding-climate/climate-change-atmospheric-carbon-dioxide> (accessed December 8, 2020).
4. Aresta, M.; Dibenedetto, A.; Angelini, A., *Chem. Rev.* **2014**, *114*, 1709-1742.
5. Tappe, N. A.; Reich, R. M.; D'Elia, V.; Kühn, F. E., *Dalton Trans.* **2018**, *47*, 13281-13313.
6. Artz, J.; Müller, T. E.; Thenert, K.; Kleinekorte, J.; Meys, R.; Sternberg, A.; Bardow, A.; Leitner, W., *Chem. Rev.* **2018**, *118*, 434-504.
7. Mikkelsen, M.; Jørgensen, M.; Krebs, F. C., *Energy Environ. Sci.* **2010**, *3*, 43-81.
8. Sakakura, T.; Choi, J.-C.; Yasuda, H., *Chem. Rev.* **2007**, *107*, 2365-2387.
9. Liu, Q.; Wu, L.; Jackstell, R.; Beller, M., *Nat. Commun.* **2015**, *6*, 5933-5948.
10. North, M.; Pasquale, R.; Young, C., *Green Chem.* **2010**, *12*, 1514-1539.
11. Kamphuis, A. J.; Picchioni, F.; Pescarmona, P. P., *Green Chem.* **2019**, *21*, 406-448.
12. Sakakura, T.; Kohno, K., *Chem. Commun.* **2009**, 1312-1330.
13. Cokoja, M.; Wilhelm, M. E.; Anthofer, M. H.; Herrmann, W. A.; Kuhn, F. E., *ChemSusChem* **2015**, *8*, 2436-2454.
14. Fiorani, G.; Guo, W.; Kleij, A. W., *Green Chem.* **2015**, *17*, 1375-1389.

15. Song, Q.-W.; Zhou, Z.-H.; He, L.-N., *Green Chem.* **2017**, *19*, 3707-3728.
16. Samikannu, A.; Konwar, L. J.; Mäki-Arvela, P.; Mikkola, J.-P., *Appl. Catal. B.* **2019**, *241*, 41-51.
17. Zhang, S.; Zhang, H.; Cao, F.; Ma, Y.; Qu, Y., *ACS Sustain. Chem. Eng.* **2018**, *6*, 4204-4211.
18. Saptal, V. B.; Sasaki, T.; Harada, K.; Nishio-Hamane, D.; Bhanage, B. M., *ChemSusChem* **2016**, *9*, 644-650.
19. Lan, D.-H.; Yang, F.-M.; Luo, S.-L.; Au, C.-T.; Yin, S.-F., *Carbon* **2014**, *73*, 351-360.
20. Zhang, S.; Zhang, H.; Cao, F.; Ma, Y.; Qu, Y., *ACS Sustain. Chem. Eng.* **2018**, *6*, 4204-4211.
21. Liu, W. J.; Jiang, H.; Yu, H. Q., *Chem. Rev.* **2015**, *115*, 12251-12285.
22. Bamdad, H.; Hawboldt, K.; MacQuarrie, S., *Renew. Sust. Energ. Rev.* **2018**, *81*, 1705-1720.
23. Lehmann, J.; Joseph, S., *Biochar for environmental management: Science and Technology*. Earthscan: Sterling, VA, 2009.
24. Lehmann, J., *Nature* **2007**, *447*, 143-144.
25. Gokce, Y.; Aktas, Z., *Appl. Surf. Sci.* **2014**, *313*, 352-359.
26. Ternero-Hidalgo, J. J.; Rosas, J. M.; Palomo, J.; Valero-Romero, M. J.; Rodríguez-Mirasol, J.; Cordero, T., *Carbon* **2016**, *101*, 409-419.
27. Anstey, A.; Vivekanandhan, S.; Rodriguez-Urbe, A.; Misra, M.; Mohanty, A. K., *Sci. Total Environ.* **2016**, *550*, 241-247.

28. Güzel, F.; Saygılı, H.; Akkaya Saygılı, G.; Koyuncu, F.; Yılmaz, C., *Journal of Cleaner Production* **2017**, *144*, 260-265.
29. Han, L.; Choi, H.-J.; Choi, S.-J.; Liu, B.; Park, D.-W., *Green Chem.* **2011**, *13*, 1023-1028.
30. Zhang, W.; Wang, Q.; Wu, H.; Wu, P.; He, M., *Green Chem.* **2014**, *16*, 4767-4774.
31. Lancaster, M., *Green Chemistry: An Introductory Text*. 3rd ed.; RSC Publishing: Cambridge, UK, 2016.
32. Kerton, F. M.; Marriott, R., *Alternative Solvents for Green Chemistry*. 2nd ed.; RSC Publishing: Cambridge, UK 2013.
33. Kim, S. H.; Han, S. Y.; Kim, J. H.; Kang, Y. Y.; Lee, J.; Kim, Y., *Eur. J. Inorg. Chem.* **2015**, *2015*, 2323-2329.
34. Qin, Y.; Guo, H.; Sheng, X.; Wang, X.; Wang, F., *Green Chem.* **2015**, *17*, 2853-2858.
35. Alhashmialameer, D.; Collins, J.; Hattenhauer, K.; Kerton, F. M., *Catal. Sci. Technol.* **2016**, *6*, 5364-5373.
36. Guo, L.; Lamb, K. J.; North, M., *Green Chem.* **2021**, *23*, 77-118.
37. Yue, S.; Hao, X.-J.; Wang, P.-P.; Li, J., *Mol. Catal.* **2017**, *433*, 420-429.
38. Saptal, V. B.; Bhanage, B. M., *ChemSusChem* **2017**, *10*, 1145-1151.
39. Titirici, M.-M.; White, R. J.; Brun, N.; Budarin, V. L.; Su, D. S.; del Monte, F.; Clark, J. H.; MacLachlan, M. J., *Chem. Soc. Rev.* **2015**, *44*, 250-290.
40. Carrier, A. J.; Abdullahi, I.; Hawboldt, K. A.; Fiolek, B.; MacQuarrie, S. L., *J. Phys. Chem. C* **2017**, *121*, 26300-26307.

41. Bamdad, H.; Hawboldt, K.; MacQuarrie, S., *Energy Fuels* **2018**, 32, 11742-11748.

CO-AUTHORSHIP STATEMENT

Chapter 3: Green Solvents for the Liquid-Phase Exfoliation of Biochar. Juliana L. Vidal, Stephanie M. V. Gallant, Evan P. Connors, Douglas D. Richards, Stephanie L. MacQuarrie, and Francesca M. Kerton. This chapter has been published.¹

The first author (Juliana L. Vidal) contributed 70% of the content of the article as the main researcher, including performing the experiments, collecting and analyzing data, and writing the manuscript.

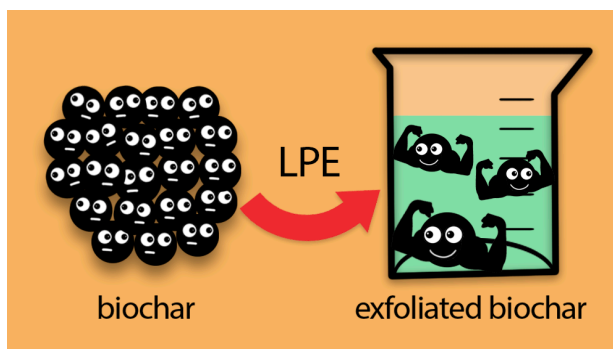
The co-author (Stephanie M. Gallant) was responsible for performing Raman analyses of pristine and exfoliated biochars and computing statistics for the bands observed.

The co-author (Evan P. Connors) was responsible for performing AFM on exfoliated **oxbc_{hw}** samples and calculating the thickness of the structures observed via AFM images.

The co-author (Douglas D. Richards) was responsible for performing Boehm Titrations on the sample of **oxbc_{hw}**.

The co-author (Stephanie L. MacQuarrie), my co-supervisor, was responsible for suggesting experiments, assisting with data interpretation, and revising the manuscript.

The corresponding author (Francesca M. Kerton), my supervisor, was the principal investigator of this work. She came up with the original concept, suggested initial experiments, assisted with data interpretation, revised and submitted the manuscript.



References for **Chapter 3** can be found on **Pages 144-151**.

CHAPTER 3: GREEN SOLVENTS FOR THE LIQUID-PHASE EXFOLIATION OF BIOCHAR

3.1 Introduction

Layered materials are solids that present strong in-plane chemical bonds, and weak interactions between layers, such as van der Waals interactions. Exfoliation is a process through which an external force is introduced to weaken or even break those interlayer attractions to produce a single or a small number (< 10) of stacked monolayers of the respective precursors.²⁻⁴ These small sheets present enhanced chemical and physical properties, thus showing diverse and promising applications as electrodes for batteries and supercapacitors, in photovoltaic or thermoelectric devices, and as reinforcing polymer composites.⁵⁻¹¹ The exfoliation of materials can be achieved using various techniques including chemical vapor deposition, intercalation, and micromechanical cleavage. However, the application of these processes is limited due to drawbacks associated with scalability, high-cost, complexity, or even sensitivity to ambient conditions.^{12, 13}

To overcome some of the limitations and drawbacks of the previously mentioned methods, a technique known as liquid-phase exfoliation (LPE) was first applied to produce graphene from graphite.¹⁴ During LPE, the bulk material is immersed in an appropriate solvent, and then directly or indirectly sonicated using an ultrasound probe or bath, respectively.¹⁵ In the initial LPE work promoted by Coleman and collaborators using graphite,¹⁴ the efficiency of the process has shown to be directly related to some of

the parameters of the solvents used. This and other investigations proposed that ideal values of densities (ρ) and surface tensions (γ) could minimize the interfacial tensions between the material and the solvent used, which would decrease the energy required to separate the sheets and stabilize them against reaggregation.^{12-14, 16} However, this surface-matching aspect could not explain the exfoliation of other layered materials. Therefore, aspects related to the interactions between material and solvent were investigated and used to aid in the explanation of LPE of other materials in later studies.^{17, 18}

Hildebrand solubility parameters have been previously used to describe the process and study the efficiency of LPE, but the information obtained was somewhat limited since this set of parameters can be only applied to nonpolar systems.¹⁹ Hansen solubility parameters (HSP) also could not fully describe or predict the best solvents for LPE, although they have been widely applied to study the solubility of different materials in various solvents.^{18, 20, 21} Kamlet-Taft solvatochromic parameters, which are considered the most extensive and useful parameters for the investigation and understanding of solvation effects, have never been implemented to describe the interaction between solvents and materials during LPE.^{22, 23}

Besides the fact that the full comprehension of LPE remains unclear, the preferred solvents for the process usually possess several health risks. While the ideal solvents for LPE are generally toxic, deionized water has been employed with some success to yield small sheets from layered materials, only with the use of stabilizers, strict control of the ultrasound bath temperature, or very long processing times.^{15, 17} To address this challenge,

Clark and co-workers investigated and identified greener environments for the LPE of graphite.²⁴ Using only 15 min of sonication, dispersions containing up to 0.24 mg/mL of graphene nanosheets could be obtained in benign solvents such as Cyrene[®], triacetin, and butyl lactate.²⁴ Unfortunately, this type of work correlating LPE and Principles of Green Chemistry still remains an exception. To date, comprehensive studies to identify green solvents for LPE of layered materials are not a priority, and therefore this process continues to be implemented using toxic and hazardous alternatives to human health and the environment.

Similarly to graphite, biochar presents a carbon-rich framework containing highly conjugated aromatic sheets of sp^2 carbons.²⁵ The production of small sheets of biochar, which served as inspiration for this project, has been performed previously using flash heat treatment, mechanochemical techniques, and also ultrasound (i.e. LPE).²⁶⁻³² Although LPE may be the cheapest and most scalable biochar exfoliation technique due to the use of mild conditions, it cannot be considered the most benign to human health and the environment. In prior research, biochar samples have been exfoliated in a reproductive toxic solvent known as *N*-methyl-2-pyrrolidone (NMP) or with very low yields in water.³⁰⁻³² Xiao and Chen were able to successfully exfoliate biochar from rice-husk biomass in NMP with the goal of obtaining more information about its molecular structure.³⁰ Although this work is an important step for enhancing the potential applications of biochar in high value-added fields, an investigation of more benign environments for the exfoliation of this carbon material has not been executed by this or

later works involving LPE.³⁰⁻³² Moreover, a comprehensive study to understand the exfoliation mechanism and identify high-performance solvents for the LPE of biochar has not been performed yet. An increased knowledge regarding solvent properties, biomass feedstock, and biochar functionality related to exfoliation efficiency can further improve the understanding of biochar's structure, promote the study of new sustainable and effective alternative solvents, and improve biochar applications as an environmentally benign advanced material.

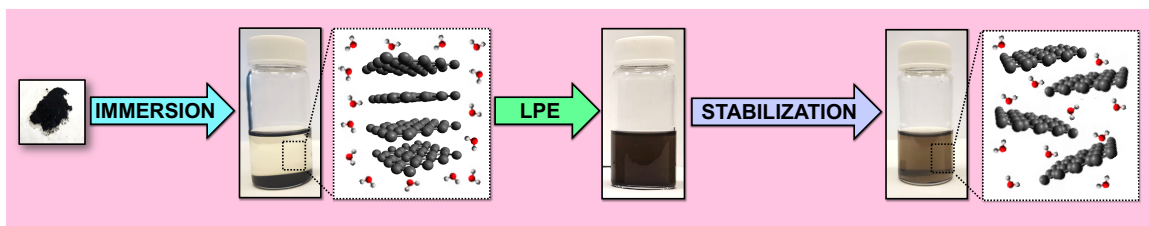


Figure 3.1. Schematic diagram describing the LPE process for biochar. Efficient and preferred solvents minimize the energy requirement of the process and stabilize the produced nanosheets.

The initial objective of this thesis focused on studying the characteristics and high value-added applications of biochar nanosheets in materials science. However, encountering the challenges mentioned above which included the lack of process understanding and use of toxic environments, a different approach was implemented. In this Chapter, the first work pursuing an in-depth investigation of biochar LPE (**Figure 3.1**) is described. Besides an understanding of solvent and solvent-matching effects that can greatly influence the process, the identification of more benign solvents for the production of nanosheets of this carbon material has been realized. These nanosheets

have large potential to be applied in high value fields, and the green solvents herein identified have been classified as safer alternatives by different solvent guides (i.e. Pfizer, CHEM21, and GSK).³³⁻³⁵

3.2 Results and Discussion

3.2.1 Preparation of Exfoliated Biochars

To exfoliate biochar samples, 10 mL of the chosen solvent were added to a vial containing 10 mg of pristine (**bc**) or oxidized biochar (**oxbc**) from different biomass feedstocks. The light gray dispersions produced were sonicated directly for 15 min using an ultrasound probe, thus producing black dispersions of biochar for the most systems studied. Samples were allowed to settle for 3 days at ambient conditions, and the supernatant was carefully removed and further characterized. The biochar dispersions in mg/mL were determined via UV-Vis analyses and were stable for at least 3 weeks. More details about the preparation of exfoliated biochars can be found in **Section 3.4.3**.

3.2.2 Effects of Solvent Parameters in Biochar Exfoliation

To begin our studies, pristine and oxidized biochars from hardwood (**bc_{hw}**, **oxbc_{hw}**) and softwood waste biomass feedstocks (**bc_{sw}**, **oxbc_{sw}**) were exfoliated in a wide range with different solvents. A list of all the solvents applied in this study is shown in **Section 3.4.3**. After settling, the concentration of biochar dispersed in the solvent was measured using UV-Vis spectroscopy at 660 nm, which is shown in the **Appendix B: Information for Chapter 3**. The molar absorptivity coefficient (α) was calculated using the Beer-Lambert

law. As shown in **Figure 3.2**, the slope of the graph of absorbance divided by cell length (A/l) as a function of amount of biochar dispersed gives $\alpha_{660} = 422 \text{ L/m.g}$, which is lower when compared to other works involving the exfoliation of carbon-based materials.^{14, 36} However, it is comparable to an investigation involving graphite exfoliation using the same sonication time applied herein (i.e. 15 min).²⁴ A low number of α at 660 nm has been previously attributed to a higher content of small flakes ($\leq 600 \text{ nm}$) and a lower mean number of layers per flake in a previous work involving the exfoliation of graphene oxide.³⁷

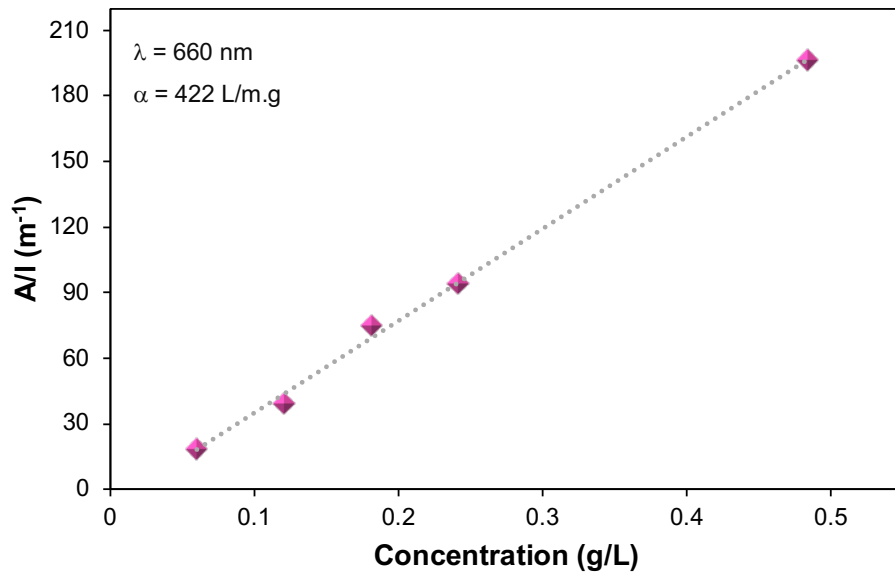


Figure 3.2. Absorbance at 660 nm divided by cell length (A/l) as a function of biochar dispersion with an absorption coefficient of $\alpha_{660} = 422 \text{ L/m.g}$.

To identify some of the most effective solvents for LPE of biochar, the surface-matching aspect was first investigated. This aspect, which has been shown to be critical for the production of nanosheets of other layered materials,^{12-14, 16} can be evaluated by the

assessment of ρ and γ of the chosen solvents. The best solvents for dispersing **bc_{hw}** and **bc_{sw}** presented $\rho \sim 1.0$ g/mL and $\gamma \sim 20$ mN/m. Some examples of the solvents used in the preliminary studies include chloroform (CHCl₃), dichloromethane (CH₂Cl₂), and 1,2-dichlorobenzene (1,2-DCB). Although values of $\rho \sim 1.0$ g/mL were shown to lead to an effective exfoliation of the material, extremely high values of this parameter were found to be detrimental to the process. When hexafluorobenzene (C₆F₆), the solvent with the highest density studied (i.e. 1.62 g/mL) was investigated, **bc** tended to stay on the surface forming a thin film, instead of being dispersed in the medium. This also happened when CHCl₃ was used to disperse **bc_{hw}** samples, and this data suggest that **bc_{hw}** and **bc_{sw}** must possess different properties, including different surface functionalities.

For **oxbc** samples, the amount of solid dispersed in the best solvents for **bc** exfoliation (e.g. CHCl₃, CH₂Cl₂, and 1,2-DCB) was negligible (< 0.05 mg/mL). The highest levels of exfoliated **oxbc** samples were obtained in solvents with $\rho \sim 1.0$ g/mL and $\gamma \sim 40$ mN/m, such as NMP and dimethyl sulfoxide (DMSO). These results demonstrated that different functional groups play a critical role in aiding dispersion of these functional biochars compared with the pristine analogues. It is worth mentioning that the solvents screened initially focused on those employed in previous literature LPE studies and did not consider environmental toxicity and related factors, as most of these solvents are not environmentally benign in nature.

3.2.3 Biomass Feedstock Interference in Liquid-Phase Exfoliation

Providing further evidence that biomass feedstock impacts the process, lower levels of dispersion were observed during the exfoliation of hardwood samples when compared to the softwood ones. The visual difference between the dispersions of bc_{hw} and oxbc_{hw} with bc_{sw} and oxbc_{sw} is shown in **Figure 3.3** and can also be observed from our UV-Vis analyses data described in **Section 3.2.5**. This particular difference was surprising, because the same biochars, even though obtained from different waste biomass feedstocks, gave very similar results when applied as catalysts for the production of cyclic carbonates,³⁸ as previously observed in **Section 2.2.3**.

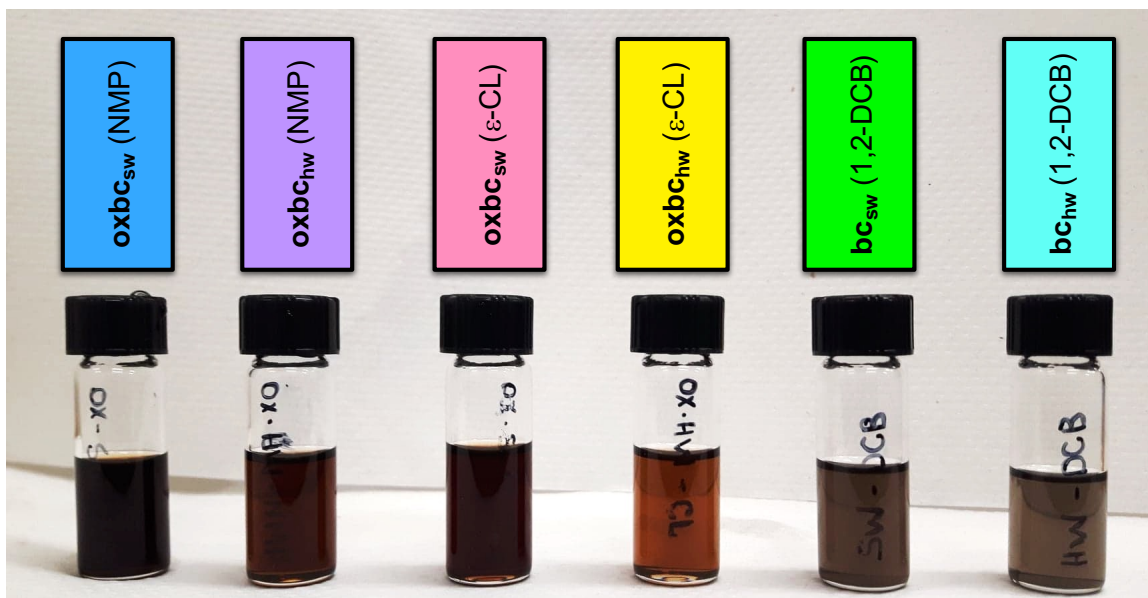


Figure 3.3. Visual comparison of biochar dispersions from different feedstocks, in a range of solvents.

To explain the unpredicted differences observed herein, densities of bc_{hw} and bc_{sw} were calculated using a pycnometer. The density of bc_{hw} was found to be 1.02 g/mL, lower

than the value of 1.19 g/mL obtained for bc_{sw} . The higher and more comparable densities between softwood biochars and the solvents studied could help to explain why hardwood biochars were less dispersible. Besides their density, the molecular structure of biochars and parameters such as the relative amount of sp^2 and sp^3 carbons, and amount of residual oxygen from the original lignocellulosic biomass could also have an impact in the dispersion levels achieved, and was therefore investigated.

3.2.4 Characterization of Exfoliated Biochars

Raman spectroscopy is the most common characterization technique used to comprehend the molecular structure of carbon materials and the effects of LPE on them. To understand more about the molecular structure of biochars from different biomass feedstocks, Raman experiments were performed on biochars before and after exfoliation. For Raman analysis, CHCl_3 was chosen as a solvent due to its high exfoliation efficiency and low boiling point, thus providing fast evaporation on the silicon wafer used as a support.

As shown in **Figure 3.4**, the Raman spectra of as-prepared and exfoliated **bc** contain two bands, known as G and D bands. The G band (observed at 1600 cm^{-1}) is produced from the stretching vibrations of sp^2 carbons and indicates crystallinity or presence of graphitic arrangements. The D band (observed at 1320 cm^{-1}) originates from the breathing mode of hexagonal rings, it is related to defects or disorders of the material, and therefore it is only Raman active if the ring is close to a defect.^{39, 40} The ratio between the

intensity of these two bands (I_G/I_D) is known to estimate the molecular order within the carbon network.⁴¹

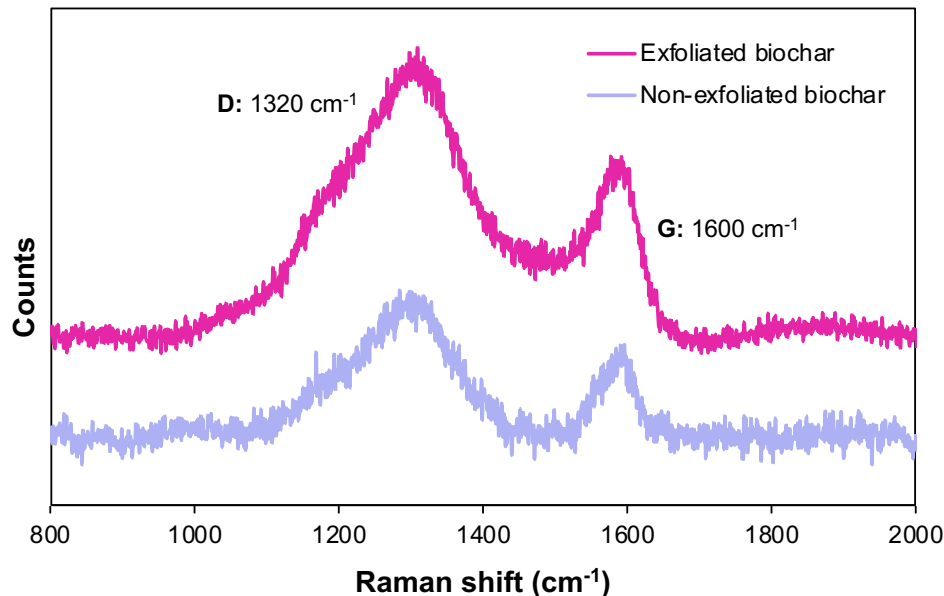


Figure 3.4. Raman spectra of bc_{hw} before and after exfoliation. The G and D bands are related to the crystallinity and deformities of the material produced, and can be used to estimate the effect of exfoliation on its chemical structure.

In the current study, as-prepared and exfoliated bc_{hw} samples present a higher I_G/I_D ratio when compared to the softwood analogues, suggesting an increased sp^2 carbon content and higher level of crystallinity (Table 3.1). Due to their increased order, density, and rigidity, graphitic structures are less susceptible to exfoliation, when compared to the amorphous phase. This explains the higher dispersions of exfoliated bc_{sw} and $oxbc_{sw}$ obtained via LPE in all the solvents studied, and also describes the difficulty in finding high-performance solvents for the processing of the more crystalline materials. Although density filters were used during Raman analysis to decrease laser power and avoid

potential thermal degradation of samples, spectra of **oxbc** before and after exfoliation could not be obtained. It is presumed that, due to the existence of local functional differences and greater molecular asymmetry, bonding vibrations and rotations in **oxbc** might not be intense enough to provide signals or may lead to Raman inactive vibrations.

Table 3.1. Exfoliation effects in the molecular structure of biochars from different biomass sources, determined by Raman spectroscopy.

Biochar	I_G/I_D non-exfoliated	I_G/I_D exfoliated
bc _{hw}	0.45 ± 0.01	0.55 ± 0.05
bc _{sw}	0.18 ± 0.06	0.19 ± 0.01

Raman spectroscopy has also been previously used to estimate crystallite size (L_a), distance between defects (L_D), and number of defects (n_D) of graphene systems using equations that correlate the I_G/I_D ratios of the materials with Raman laser energy.^{41, 42} These can be found in the **Appendix B: Information for Chapter 3**. Applying the strategy to biochar (**Table 3.2**), an increased L_a , longer L_D , and smaller n_D was observed in the exfoliated samples when compared to the non-exfoliated ones. L_a values obtained herein are higher than the ones obtained for multi-heteroatom functionalized biochars (i.e. 5 nm),³² but lower than values obtained during LPE of graphite in NMP (i.e. 136 nm) in a previous work using the same estimation method herein.²⁴ Graphene samples also present higher values of L_D (i.e. 31.6 nm) and lower values of n_D (i.e. $3.6 \times 10^{10} \text{ cm}^{-2}$) when compared with exfoliated biochar due to the presence of a more ordered, crystalline, and organized chemical structure.²⁴

Table 3.2. Exfoliation effects in the estimation of crystallite size (L_a), distance between defects (L_D), and number of defects (n_D) of biochars from different biomass sources, determined by Raman spectroscopy.

Type	Biochar	L_a (nm)	L_D (nm)	n_D (cm ⁻²)
Non-exfoliated	bc _{hw}	51.2	19.6	8.43 x 10 ¹⁰
	bc _{sw}	20.5	12.4	2.11 x 10 ¹¹
Exfoliated	bc _{hw}	62.6	21.7	6.90 x 10 ¹⁰
	bc _{sw}	21.6	12.7	2.00 x 10 ¹¹

Atomic Force Microscopy (AFM) can be applied to give more insights regarding the effect of exfoliation upon the structure of biochar (**Figure 3.5**). For this analysis, biochar samples after exfoliation in CHCl₃ were drop-casted on a glass slide pre-heated at 100 °C before analysis. This procedure provides a uniform dispersion and avoids the reaggregation of nanosheets as described in a previous work.¹² Herein, 100 nanostructures of exfoliated bc_{hw} observed in different AFM images (examples in **Figure 3.5A-D**) were randomly selected and their thicknesses measured to yield a distribution (**Figure 3.5E**). The lowest height value measured was found to be 15 nm, which can be attributed to the thickness of an individual biochar nanosheet. This value can be divided by the distance between defects obtained via Raman (L_D) to give 1 as the approximate number of exfoliated biochar layers (N). From **Figure 3.5E**, the majority of nanostructures (about 60%) are 15-120 nm thick, thus confirming the predominance of a single to a few-multilayered (i.e. N values in the range of 2-8) biochar sheets obtained after exfoliation.

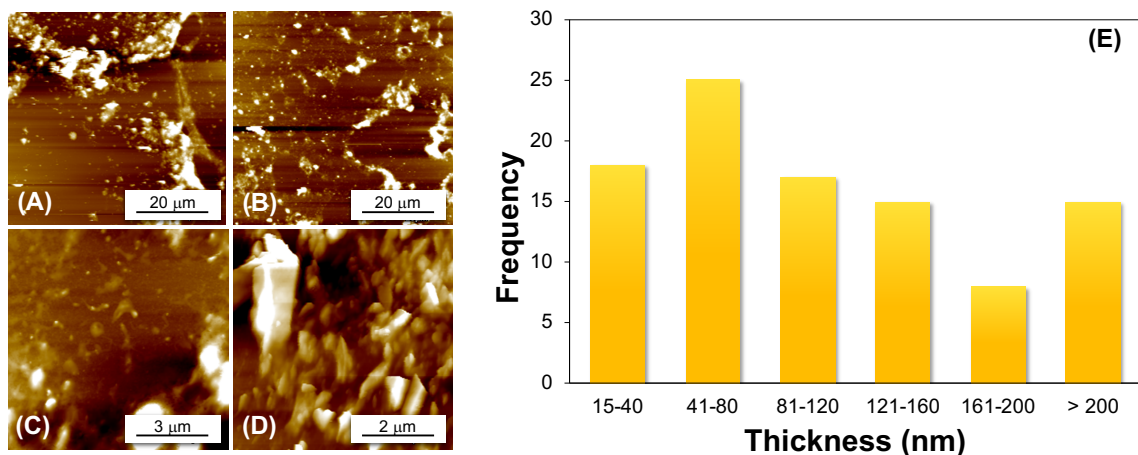


Figure 3.5. AFM characterization of exfoliated biochar samples. Figures (A-D) show the AFM images of exfoliated bc_{hw} samples used to calculate the number of nanostructures containing different heights. The correlation between frequency and exfoliated material thickness can be observed in Figure (E).

Transmission Electron Microscopy (TEM) micrographs of bc_{hw} samples before and after exfoliation in NMP are presented in **Figure 3.6**. A multilayered structure is seen in samples of bc_{hw} before exfoliation (**Figure 3.6A**), whereas the presence of diverse nanostructures is observed in the exfoliated biochar (**Figure 3.6B** and **Figure 3.6C**). Micrographs of the processed material show the presence of aromatic clusters black dots with average length of 18 ± 4 nm (**Figure 3.6B**). Similar structures have been previously assigned to multilayered graphene-like nanosheets randomly ordered.³⁰ Nanocrystalline stripes could also be observed in the structure of exfoliated biochar, as well as the presence of atomic arrangements at the edges of the dispersed material (**Figure 3.6C**). The presence of aromatic clusters, nanocrystalline stripes, and atomic arrangements in the structure of exfoliated biochar observed via TEM demonstrate the value of LPE in gaining access to

the diverse nanostructures of this bio-renewable material.

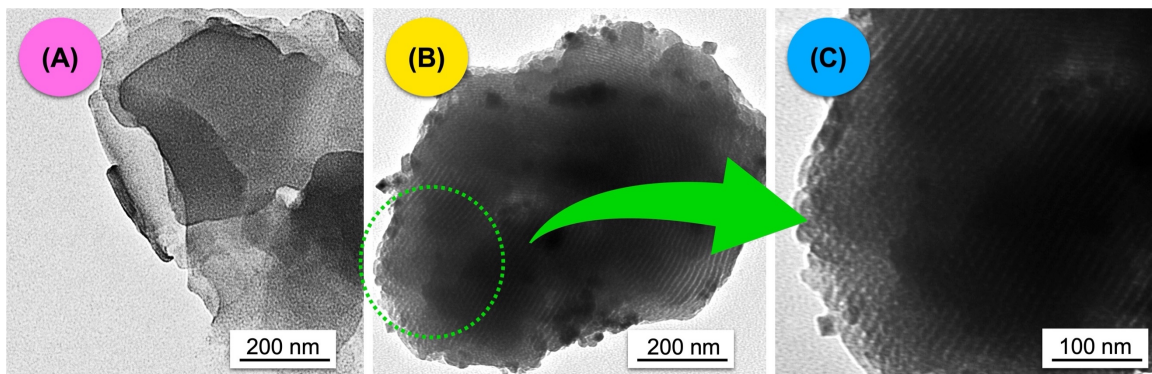


Figure 3.6. TEM micrographs of bc_{hw} samples. Figure (A) show the layered structure of bc_{hw} before exfoliation, whereas aromatic clusters (i.e. black dots), nanocrystalline stripes, and atomic arrangements are observed after LPE in Figure (B). Atomic arrangements observed at the edges of the exfoliated material are further highlighted in Figure (C).

The presence of distinct monolayers is not visible via TEM of exfoliated biochar probably due to reaggregation of nanosheets, which is a reoccurring problem during the characterization of exfoliated materials obtained via LPE. However, the morphology and structures observed herein by TEM for bc samples after ultrasound treatment are similar to those seen previously for rice straw biochar.³⁰ TEM micrographs of the remaining biochars studied (i.e. $oxbc_{hw}$, $oxbc_{sw}$, and bc_{sw}) before and after LPE are shown in **Figure 3.7**. Exfoliated bc_{sw} samples show smaller aromatic clusters (i.e. average length of 10 ± 3 nm) when compared to bc_{hw} samples. This may be related to the lower intrinsic crystallinity of softwood samples previously indicated by Raman spectroscopy. Regarding $oxbc$ biochar, it is known that the oxidation itself can weaken interlayer interactions within the sample due to the insertion of a large number of oxygen-containing groups.⁴³

This might be the reason why oxbc_{hw} and oxbc_{sw} present a larger number of dispersed species after exfoliation. Nevertheless, the sizes of those species are very similar to the bc exfoliated samples (i.e. average length of 17 ± 4 nm for oxbc_{hw} and 12 ± 3 nm for oxbc_{sw}).

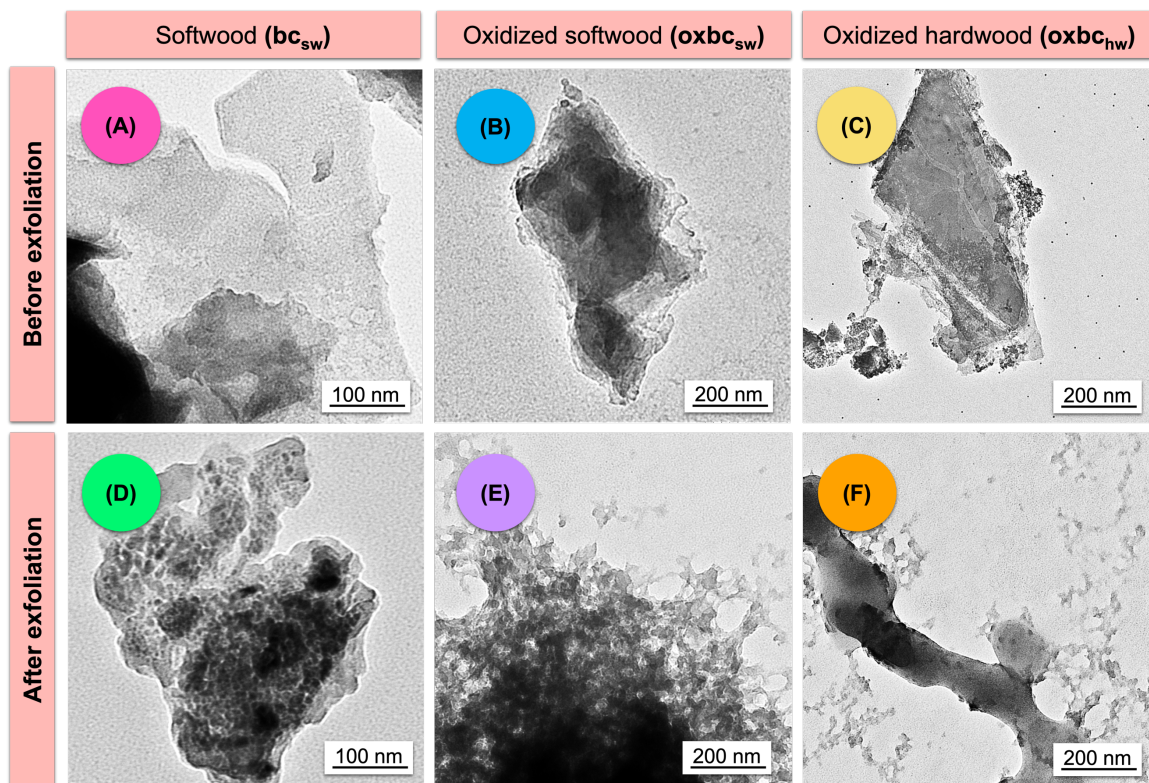


Figure 3.7. Typical TEM micrographs of oxbc_{hw} , oxbc_{sw} and bc_{sw} samples before and after LPE.

Mass spectrometry (MS) analyses were performed on bc_{hw} and oxbc_{hw} samples to provide a better comprehension of the molecular structure of the materials observed in the TEM micrographs. As shown in **Figure 3.8A**, a signal with m/z 854.50 Da is observed for exfoliated bc_{hw} , and hardly any low intensity signals are seen at masses higher than this. For exfoliated oxbc_{hw} (**Figure 3.8**), a signal at m/z 870.49 Da and several signals at higher masses up to 1182.01 Da are observed. This difference can be associated to the

range of high molecular weight oxygen-containing species in the functionalized biochar samples, which have a greater tendency to interact with the organic acid matrix used in the analysis (i.e. 2,5-dihydroxybenzoic acid, DHB).

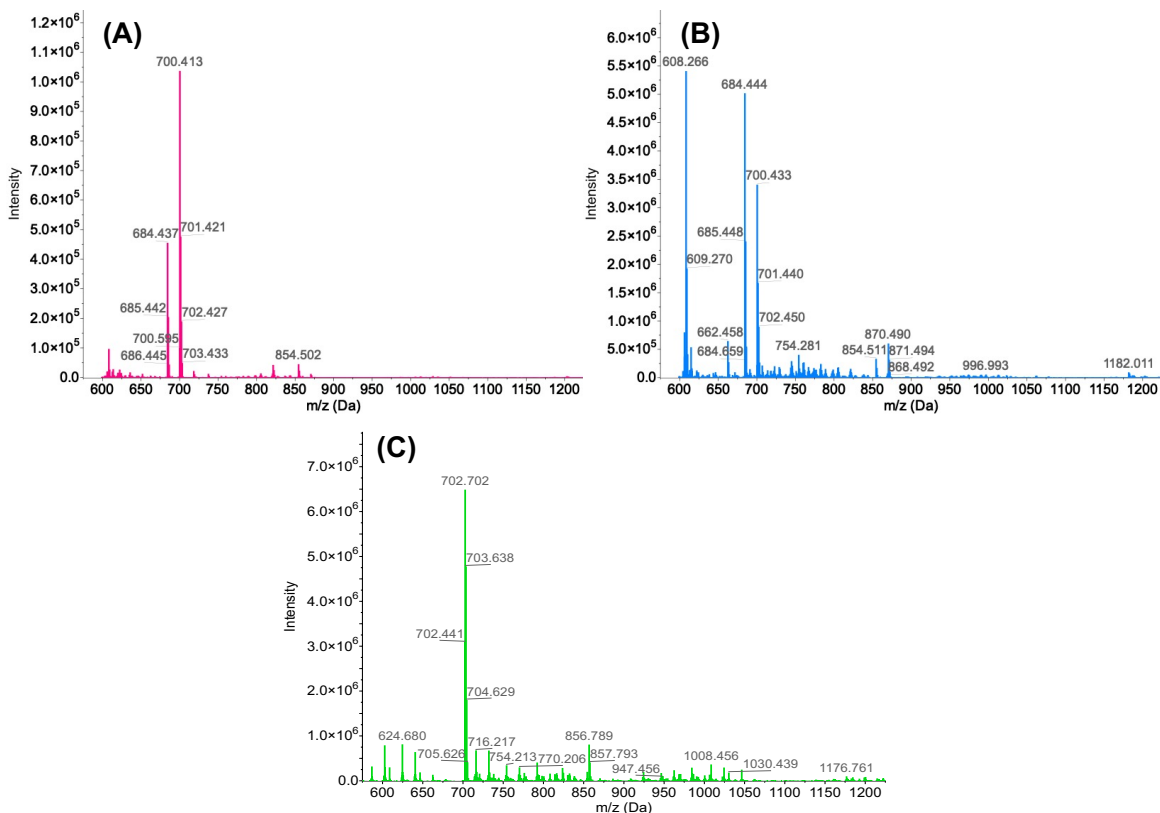


Figure 3.8. MALDI-TOF mass spectra of (A) exfoliated bc_{hw} , (B) exfoliated $oxbc_{hw}$, and (C) non-exfoliated $oxbc_{hw}$ samples in positive-ion mode using DBH as a matrix.

As expected, the spectra do not represent a single molecular structure, and the exfoliated biochar samples seem to display a wide range of structures with primarily 16 and 72 Da weight differences between peaks. These masses can be assigned to an oxygen atom and six carbons from the aromatic motifs, respectively. In comparison with the unexfoliated analogue (**Figure 3.8C**), the MALDI-TOF mass spectrum of exfoliated

oxbc_{hw} presents reduced complexity and fewer peaks, which may be a result from a fractionation of the carbon materials upon exfoliation, with only lower mass species becoming volatilized in the instrument. Further experiments would be needed to gain improved insight into the mass data obtained. Nevertheless, it is possible to observe via MALDI-TOF MS the incorporation of small molecules in biochar samples after LPE.

3.2.5 Greener Solvents for Biochar Exfoliation

Based on the preliminary studies that assessed the surface-matching aspect of biochar LPE and identified ideal values of γ and ρ for the processing of **bc** and **oxbc**, an attempt to explore the nature of LPE and an investigation regarding greener solvents for exfoliation was realized. A correlation between some solvent parameters and the amount of biochar dispersed in the samples during LPE is seen in **Table 3.3** and **Table 3.4**. Further details of this investigation including the HSP and viscosity values for the all the solvents studied herein is shown in **Section 3.4.3**.

Table 3.3. Achieved dispersions and solvent parameters (i.e. density, surface tension, and Kamlet-Taft solvatochromic parameters) for the LPE of **bc** samples.

Entry	Solvent	Biochar type and dispersion (mg/mL)	ρ (g/mL) ^a	γ (mN/m) ^a	Kamlet-Taft parameters		
					α	β	π^*
1	C ₆ F ₆	bc_{hw} , 0.11 bc_{sw} , 0.26	1.62 ⁴⁴	26.5 ⁴⁴	0.00 ⁴⁵	0.02 ⁴⁵	0.33 ⁴⁵
2	CHCl ₃	bc_{hw} , 0.17 bc_{sw} , 0.51	1.48 ⁴⁶	26.6 ⁴⁷	0.44 ²²	0.00 ²²	0.58 ²²
3	CH ₂ Cl ₂	bc_{hw} , 0.21 bc_{sw} , 0.39	1.33 ⁴⁶	27.2 ⁴⁷	0.30 ²²	0.00 ²²	0.82 ²²
4	1,2-DCB	bc_{hw} , 0.21 bc_{sw} , 0.28	1.31 ⁴⁶	37.0 ⁴⁴	0.00 ²²	0.03 ²²	0.80 ²²
5	PhCN	bc_{hw} , 0.15 bc_{sw} , 0.22	1.25 ⁴⁴	39.0 ⁴⁴	0.00 ²²	0.41 ²²	0.90 ²²
6	DMC	bc_{hw} , 0.11 bc_{sw} , 0.20	1.08 ⁴⁸	28.8 ⁴⁸	0.00 ²²	0.38 ²²	0.47 ⁴⁹
7	Solketal	bc_{hw} , 0.15 bc_{sw} , 0.17	1.07 ⁴⁸	32.1 ²⁴	0.81 ⁵⁰	0.62 ⁵⁰	0.64 ⁵⁰
8	NMP	bc_{hw} , 0.09 bc_{sw} , 0.16	1.03 ⁴⁴	40.7 ⁴⁴	0.00 ²²	0.77 ²²	0.92 ²²
9	H ₂ O	bc_{hw} , 0.11 bc_{sw} , 0.13	1.00 ⁴⁷	72.1 ⁴⁷	1.23 ⁵¹	0.49 ⁵¹	1.14 ⁵¹
10	EtOAc	bc_{hw} , 0.12 bc_{sw} , 0.13	0.89 ⁴⁶	23.8 ⁴⁴	0.00 ²²	0.45 ²²	0.55 ²²
11	Acetone	bc_{hw} , 0.09 bc_{sw} , 0.10	0.79 ⁴⁶	22.7 ⁴⁴	0.08 ²²	0.48 ²²	0.71 ²²

^a Values obtained at 20 or 25 °C.

Table 3.4. Achieved dispersions and solvent parameters (i.e. density, surface tension, and Kamlet-Taft solvatochromic parameters) for the LPE of **oxbc** samples.

Entry	Solvent	Biochar type and dispersion (mg/mL)	ρ (g/mL) ^a	γ (mN/m) ^a	Kamlet-Taft parameters		
					α	β	π^*
1	GF	oxbc_{hw} , 0.14 oxbc_{sw} , 0.33	1.22 ⁴⁸	44.5 ⁴⁸	0.59 ²³	0.59 ²³	0.87 ²³
2	PEG 400	oxbc_{hw} , 0.48 oxbc_{sw} , 0.76	1.13 ⁵²	44.7 ⁵³	0.31 ⁵⁴	0.75 ²³	0.91 ²³
3	PEG 200	oxbc_{hw} , 0.48 oxbc_{sw} , 0.69	1.12 ⁵⁵	43.5 ⁵⁶	0.46 ⁵⁴	0.63 ⁵⁴	0.98 ⁵⁴
4	EG	oxbc_{hw} , 0.46 oxbc_{sw} , 0.56	1.11 ⁴⁴	48.5 ⁴⁸	0.90 ²²	0.52 ²²	0.92 ²²
5	DMSO	oxbc_{hw} , 0.41 oxbc_{sw} , 0.45	1.10 ⁴⁶	43.0 ⁴⁴	0.00 ²²	0.76 ²²	1.00 ²²
6	ϵ -CL ^b	oxbc_{hw} , 0.21 oxbc_{sw} , 0.38	1.07 ⁵⁷	32.2 ⁵⁷	-	-	-
7	Solketal	oxbc_{hw} , 0.27 oxbc_{sw} , 0.35	1.07 ⁴⁸	32.1 ²⁴	0.81 ⁵⁰	0.62 ⁵⁰	0.64 ⁵⁰
8	NMP	oxbc_{hw} , 0.23 oxbc_{sw} , 0.42	1.03 ⁴⁴	40.7 ⁴⁴	0.00 ²²	0.77 ²²	0.92 ²²
9	H ₂ O	oxbc_{hw} , 0.14 oxbc_{sw} , 0.27	1.00 ⁴⁷	72.1 ⁴⁷	1.23 ⁵¹	0.49 ⁵¹	1.14 ⁵¹
10	EtOAc	oxbc_{hw} , 0.16 oxbc_{sw} , 0.18	0.89 ⁴⁶	23.8 ⁴⁴	0.00 ²²	0.45 ²²	0.55 ²²
11	Acetone	oxbc_{hw} , 0.17 oxbc_{sw} , 0.24	0.79 ⁴⁶	22.7 ⁴⁴	0.08 ²²	0.48 ²²	0.71 ²²

^a Values obtained at 20 or 25 °C. ^b Kamlet-Taft parameters have not been reported. γ -valerolactone, similar to ϵ -CL, shows values of 0.00, 0.60, and 0.83 for α , β and π^* , respectively.

Reproducibility of the process was assessed by performing procedures in triplicate ($SD \leq 0.05$ mg/mL). As expected, only the evaluation of the surface-matching aspect of exfoliation described by γ and ρ was superficial, and contributions from biochar-solvent interactions were also needed to fully explain the process. Aware of the well-known limitations of the Hildebrand's solubility parameters and their exclusive applicability to nonpolar systems,¹⁹ a correlation between biochar exfoliation and HSP was assessed.

HSP are a set of solvent parameters that has been extensively used in the selection of solvents in coating industries, to predict solvent-polymer compatibility, and also to describe LPE of other layered materials.^{18, 24} Each substance can be described using three HSP, which are related to the energy from dispersion forces (δ_D), dipolar intermolecular forces (δ_P), and hydrogen bonds (δ_H) between molecules.⁴⁶ When HSP of the material and the solvent are similar, they show a high affinity for each other and are likely to easily form a solution. Therefore, similarities between the surface functionality of materials and solvents are expected to aid in dispersion processes.

Some of the solvents able to disperse **bc** and **oxbc** samples had HSP in similar ranges. For example, $\delta_D \sim 17$ MPa^{1/2}, $\delta_H \sim 7$ MPa^{1/2}, and $\delta_P \sim 6$ MPa^{1/2} are average values for CH₂Cl₂ and ethyl acetate (EtOAc), which are good solvents for the LPE of **bc**. On the other hand, $\delta_D \sim 17$ MPa^{1/2}, $\delta_H \sim 20$ MPa^{1/2}, and $\delta_P \sim 11$ MPa^{1/2} are average values of glycerol formal (GF) and ethylene glycol (EG), solvents able to disperse **oxbc** samples. Although this similarity was found, solvents with HSP values out of the ideal ranges delimited by CH₂Cl₂ and EtOAc for **bc**, and GF and EG for **oxbc** were also able to exfoliate

the respective samples. C_6F_6 was an effective solvent for **bc** exfoliation, even though it possesses $\delta_H = 0 \text{ MPa}^{1/2}$ and $\delta_P = 0 \text{ MPa}^{1/2}$. Other examples of effective solvents for LPE with HSP outside the two typical ranges include benzonitrile (PhCN), dimethyl carbonate (DMC), solketal, polyethylene glycols 200 and 400 (PEG 200 and 400), and ϵ -caprolactone (ϵ -CL). Therefore, even though HSP were previously used by others to understand the exfoliation of other materials,^{18, 24} they could not effectively describe the LPE of biochar because a regular, direct, and predictable relationship between the preferred solvents for biochar exfoliation and δ_D , δ_P , and δ_H values could not be obtained.

Kamlet-Taft solvatochromic parameters (i.e. α , β , π^*) are the most used quantitative measure of solvent characteristics and solvent-solute interactions. The parameter α quantifies the ability of the solvent to donate a hydrogen-bond, β is a scale of its ability to accept a hydrogen-bond, whilst π^* represents its polarizability.²² Most solvents present values of α , β , and π^* between 0 and 1. These parameters have been widely applied in the investigation of diverse solvent-solute systems,^{23, 49, 51, 58} but they have not been applied to explore the LPE of materials and provide a better comprehension of the solvents used to stabilize the resulting nanostructures. For those reasons, it was decided to analyze the possible correlation between the amount of biochar dispersed in the exfoliated samples, and the α , β , and π^* values of each of the solvents used.

As observed from preliminary studies, good dispersions of **bc** nanostructures could be observed in solvents with ρ and γ around 1.0 g/mL and 20 mN/m, respectively. However, solvents such as PhCN, 1,2-DCB, NMP, and solketal, which present γ values

higher than 20 mN/m and out of the ideal range, could also successfully exfoliate biochar samples. If the Kamlet-Taft solvatochromic parameters of the solvents are analyzed, these results could be better understood. Effective solvents for pristine biochar exfoliation with values of γ and ρ out of the ideal range presented $\pi^* \geq 0.50$. This observation indicated that solvatochromic parameters could actually help in the comprehension of the nature of biochar exfoliation, since solvents with high polarizability values described by π^* could interact more effectively with the electron cloud generated by the graphene-like sheets within the biochar structure. The proposed interaction is shown pictorially in **Figure 3.9**.

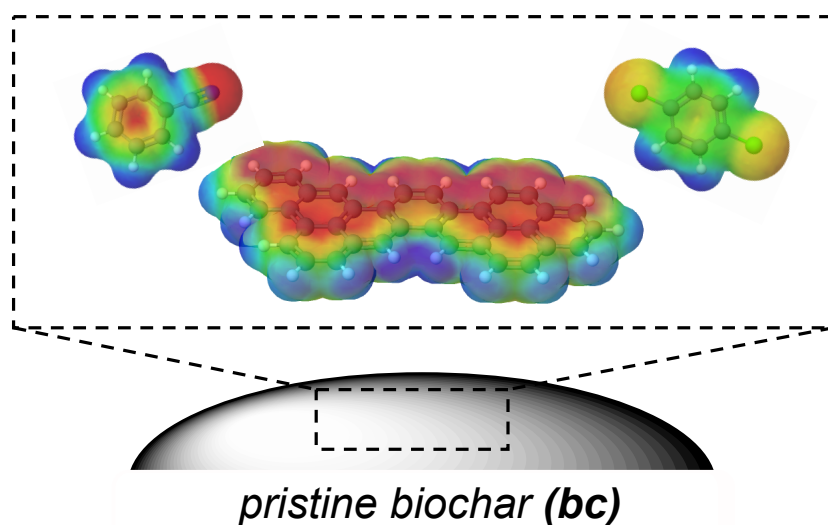


Figure 3.9. Proposed interactions between **bc** and solvents with high polarizability, described by the Kamlet-Taft parameter π^* .

As mentioned previously, LPE of oxidized biochar was not effective in the same solvents that allowed the exfoliation of pristine samples, and was therefore found to be dependent on different solvent parameters. As shown in **Table 3.4**, solvents that could produce **oxbc** nanosheets via LPE presented ρ and γ around 1.0 g/mL and 40 mN/m,

respectively. However, if the values of γ and ρ were different and out of the ideal range, solvents with $\beta \geq 0.50$ could also promote the LPE of **oxbc**. In this case, it is proposed that solvents with good hydrogen-bonding acceptance ability described by high values of β are able to interact more effectively with the hydroxyl and carboxyl groups on the surface of functionalized biochar. This interaction is represented pictorially in **Figure 3.10**, and correlates with the increased acidity of the surface of **oxbc** samples, as characterized via Boehm titrations.

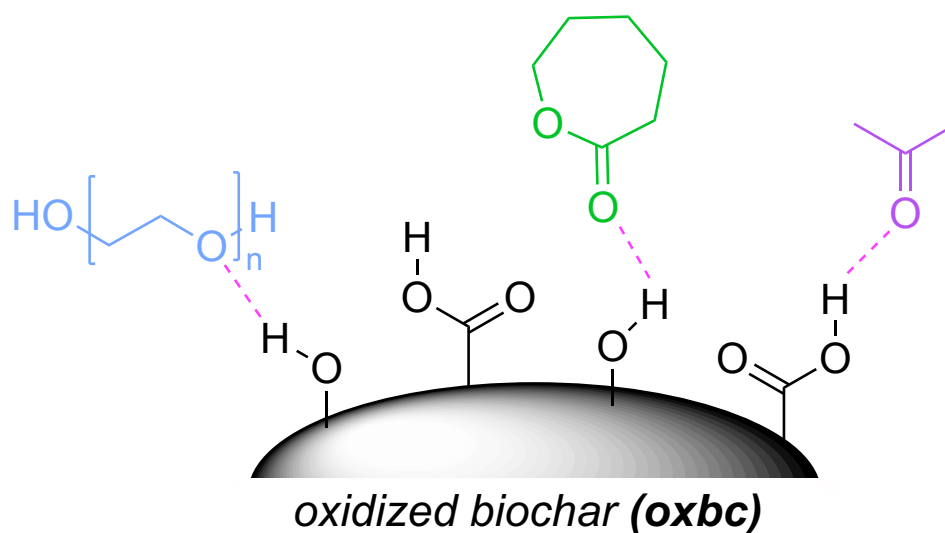


Figure 3.10. Proposed interactions between **oxbc** and solvents with high hydrogen-bonding acceptance ability, described by the Kamlet-Taft parameter β .

The influence of Kamlet-Taft solvatochromic parameters in the exfoliation of **bc** and **oxbc** samples is summarized in plots and shown in **Figure 3.11**. To construct this correlation, deionized water (H_2O) and C_6F_6 were excluded due to their exceptional γ and ρ values, respectively. For pristine biochar samples (**Figure 3.11A**), a synergic effect

between surface tension and polarizability of the solvents is observed, and the highest levels of bc_{sw} dispersion (i.e. orange region in graph) are obtained with solvents presenting low values of γ and high values of π^* . For the oxidized analogues (**Figure 3.11B**), an intensification in exfoliation efficiency is seen with increasing values of surface tension or hydrogen-bonding acceptance ability. Therefore, the dispersion of oxbc_{sw} after LPE is greatly and synergistically increased when the solvents used possess high values of γ and also β (i.e. orange region in graph).

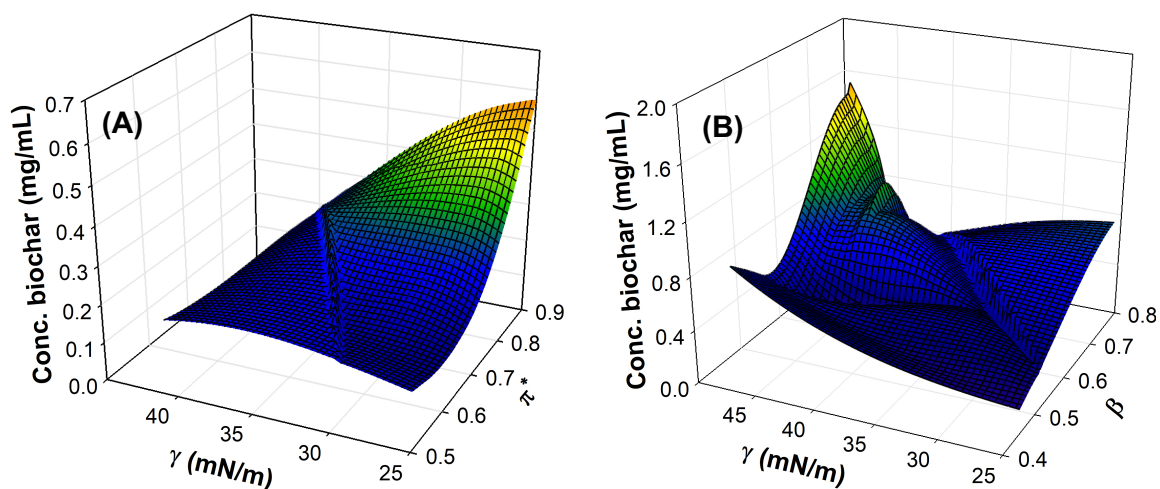


Figure 3.11. Influence of surface tension and Kamlet-Taft solvatochromic parameters in the exfoliation of (A) bc_{sw} and (B) oxbc_{sw} samples. To build this correlation, H_2O and C_6F_6 have not been included in data analysis due to their exceptional values of γ and ρ , respectively.

Although some of the high-performance solvents for the production of biochar nanostructures presented desirable characteristics for processing (e.g. high yields of biochar nanostructures and low-boiling points), the applications of the exfoliated material would be limited due to the high toxicity of the solvents employed.⁵⁹⁻⁶¹ Important health,

safety, and environmental impacts of some of the solvents investigated in biochar LPE, alongside their green credentials obtained from the CHEM21,³³ GSK,³⁴ and Pfizer³⁵ solvent selection guides are shown in **Table 3.5**. Further details on the other solvents studied herein are collated in **Section 3.4.3**.

CHCl_3 , CH_2Cl_2 , and 1,2-DCB are able to disperse more than 0.20 mg/mL of **bc**, but are toxic and suspected carcinogens according to the International Agency for Research on Cancer.⁵⁹⁻⁶¹ For those reasons, CHCl_3 and CH_2Cl_2 are considered hazardous, undesirable, and of major concern by all the solvent guides used herein.³³⁻³⁵ Solvents such as acetone, EtOAc, DMC, solketal, and even H_2O can disperse about 0.10 mg/mL of **bc** using only 15 min sonication, and are considered greener alternatives. Acetone and EtOAc are volatile and flammable, but are also biodegradable and possess low toxicity.⁶² They disperse amounts of biochar comparable to NMP, which is the most commonly used solvent for biochar exfoliation despite its toxicity.^{30, 32} DMC, solketal and H_2O are non-toxic, non-volatile, biodegradable, and obtained from renewable sources.^{24, 33, 62} Solketal can be produced renewably from glycerol, has been widely used as a green solvent for various large-scale applications,^{50, 63} and is recognized by the United States Environmental Protection Agency's Safer Choice Program as a benign compound, with verified low toxicity based on experimental and modeled data.⁶⁴ Moreover, DMC can be derived from CO_2 , contributing to the storage, usage, and transformation of this greenhouse gas.³³

Table 3.5. Selected environmental, health, and safety information on some of the solvents investigated herein and their green credentials obtained from different solvent selection guides.^a

Entry	Solvent	Flash Point (FP), Health, Safety, and Environmental Impacts	Green Credentials from Solvent Guides ^b
1	Acetone	FP = -20 °C. Flammable, volatile, biodegradable, low toxicity. ³³	CHEM21: Recommended Pfizer: Preferred GSK: Some issues
2	CHCl ₃	FP = None. Volatile, toxic, carcinogen. ⁶²	CHEM21: Highly hazardous Pfizer: Undesirable GSK: Major issues
3	CH ₂ Cl ₂	FP = None. Volatile, toxic, carcinogen. ⁶²	CHEM21: Hazardous Pfizer: Undesirable GSK: Major issues
4	DMC	FP = 19 °C. Flammable, non-volatile, renewable, biodegradable, non-toxic. ⁶⁵	CHEM21: Recommended Pfizer: Not included GSK: Few issues
5	DMSO	FP = 85 °C. Combustible, harmful. ⁶²	CHEM21: Problematic Pfizer: Usable GSK: Some issues
6	EG	FP = 111 °C. Non-volatile, renewable, biodegradable, low toxicity. ⁶²	CHEM21: Recommended Pfizer: Usable GSK: Few issues
7	EtOAc	FP = -2 °C. Flammable, volatile, biodegradable, low toxicity. ⁶²	CHEM21: Recommended Pfizer: Usable GSK: Some issues
8	NMP	FP = 86 °C. Combustible, toxic. ³⁵	CHEM21: Hazardous Pfizer: Undesirable GSK: Major issues

^a Solvents shown were evaluated in published solvent selection guides. Information on an expanded selection is shown in **Section 3.4.3**, including those not identified in solvent selection guides. ^b Solvent selection guides used: CHEM21,³³ GSK,³⁴ Pfizer.³⁵

Samples of **oxbc** could be exfoliated in solvents typically used for the LPE of layered materials, such as NMP and DMSO. As shown in **Table 3.5**, DMSO is a better alternative than NMP, but it is also considered problematic due to its combustibility and absorption through skin.⁶² In the current study, more than 0.40 mg/mL of exfoliated **oxbc** could be obtained in safer solvents such as EG, PEG 200, and PEG 400 due to their ideal γ combined with their exceptional β values. PEGs possess biodegradability, biocompatibility, non-toxicity and low flammability, thus allowing these solvents to provide excellent green environments for exfoliation.⁶² They are also widely used in consumer products, and are approved for internal consumption by the US Food and Drug Agency.⁶² EG can be produced sustainably from lignocellulosic biomass, bacteria, and algae, but is considered a less desired alternative when compared to PEGs for the LPE of **oxbc** samples due to their toxicity for human health and aquatic biota upon ingestion or exposure in higher doses.⁶⁶

Other solvents such as GF, ϵ -CL, and solketal present lower γ values when compared to EG and PEGs, but can exfoliate more than 0.20 mg/mL of **oxbc**. Like solketal, GF can be obtained from glycerol after an acid-catalyzed reaction.⁵⁰ It has a high boiling point, low toxicity, and superior miscibility in ethers and acetone. For those reasons, GF can be applied as a green solvent in diverse areas (e.g. paints, pesticide delivery systems, plasticizers).⁵⁰ ϵ -CL can cause eye irritation and it is not widely used as an ester solvent unlike more volatile esters (e.g. EtOAc). However, it is overall considered a non-toxic, affordable, and important commodity chemical for the production of a biodegradable

polymer known as poly(ϵ -caprolactone).⁶⁷ It is worth mentioning that the dispersions obtained herein are comparable to previous works involving the LPE of graphite using ultrasound (e.g. 0.01 mg/mL in NMP,¹⁴ 0.18 mg/mL in CHCl_3 ,³⁶ 0.24 mg/mL in Cyrene[®],²⁴ and 0.13 mg/mL in H_2O at 60 °C.¹⁷)

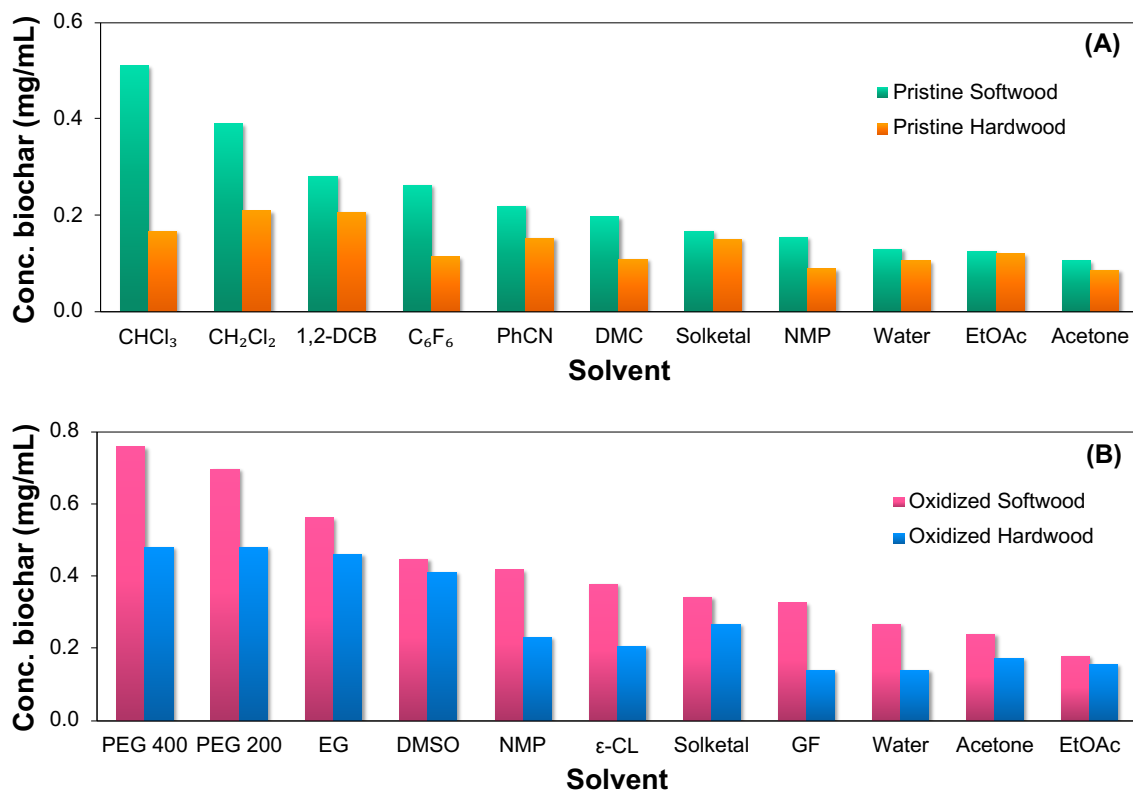


Figure 3.12. Dispersions of exfoliated (A) **bc** and (B) **oxbc** samples in traditional and greener environments investigated for LPE.

A comparison between traditional solvents and their greener alternatives studied herein for the LPE of **bc** and **oxbc** samples is presented in **Figure 3.12**. Based on the diagram and under the conditions explored, **oxbc** generally achieves higher maximum levels of dispersion (i.e. 0.75 mg/mL) when compared to **bc** samples (i.e. 0.51 mg/mL).

This difference is likely due to the hydrogen-bond donating ability of the functional groups on the surface of **oxbc**. The results obtained highlight biochar functionalization as an important strategy for increasing biochar applications in the field of materials science through the discovery of greener environments for its processing and production.

3.2.6 Effect of Sonication Time in Biochar Exfoliation

Processing time has shown to be an important parameter in the LPE of other carbon materials.^{24,36} Although longer LPE periods can increase the yield of nanosheets, they can also diminish the quality of the materials obtained. To avoid and minimize the potential negative effect of time, one alternative is the increase of solvent viscosity. Viscous solvents have shown to stabilize and preserve the integrity of the exfoliated material even after longer sonication times.²⁴

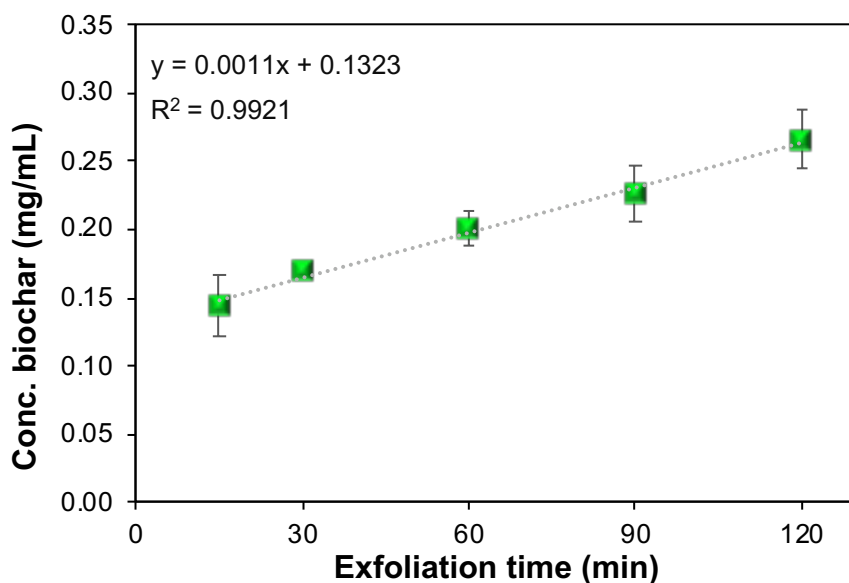


Figure 3.13. Dispersions of exfoliated **bc_{hw}** as a function of exfoliation time, showing a linear behavior following the equation $y = 0.0011 x + 0.1323$ (bars represent SD).

To evaluate the influence of time on the yield and quality of exfoliated biochar, bc_{hw} samples were sonicated for 15, 30, 60, 90, and 120 min in EtOAc, a solvent with low values of viscosity which has shown to be an efficient greener alternative for the LPE of bc . The procedure was performed in triplicate, and the concentration of dispersed bc_{hw} in the samples was found to increase gradually with exfoliation time, as shown in **Figure 3.13**.

The quality of produced biochar nanostructures after different exfoliation times was assessed via Raman spectroscopy, and I_G/I_D ratios of biochar dispersions were calculated after each processing time (**Figure 3.14**). Interestingly, there was no significant decrease in the I_G/I_D ratio values, thus indicating that better yields of biochar nanostructures can be obtained herein using longer sonication times even in solvents with low viscosities.

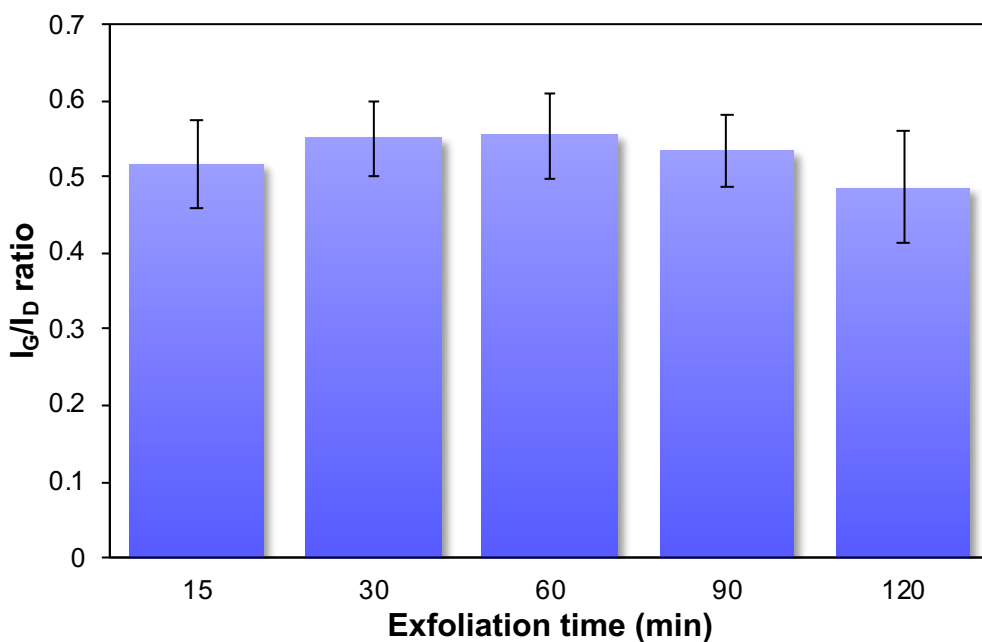


Figure 3.14. I_G/I_D ratios of exfoliated bc_{hw} as a function of processing time in EtOAc (bars represent SD).

3.3 Conclusions

In this work, LPE has been applied to **bc** and **oxbc** from different biomass feedstocks. Besides obtaining biochar nanostructures with potential applications in high value fields, the discovery of more benign chemical systems to human health and the environment for LPE was also achieved. The nanostructures of exfoliated biochar obtained are comprised of a small number (i.e. 2-8) of stacked layers. During this investigation, both surface matching properties such as surface tensions and densities, and biochar-solvent intermolecular interactions have shown to greatly influence the process. Although other solubility parameters were used previously to investigate the LPE of other materials, this is the first time that Kamlet-Taft solvatochromic parameters were applied to aid the understanding of this exfoliation method.

Solvents with density values around 1.0 g/mL, surface tensions of 20 mN/m or good polarizability described by the Kamlet-Taft parameter π^* showed good performance in the exfoliation of **bc**. Solvents with density values around 1.0 g/mL, surface tensions of 40 mN/m or good hydrogen-bond acceptance described by the Kamlet-Taft parameter β could successfully exfoliate **oxbc**. Using only 15 min of sonication, dispersions containing more than 0.10 mg/mL of exfoliated biochar could be obtained in solvents such as acetone, DMC, EtOAc, solketal, H₂O, ϵ -CL, EG, and PEGs. These alternative environments provide similar or better exfoliation results, and are also less harmful than NMP, which is a solvent typically used LPE processes. Moreover, no strict control of temperature was needed, and there was no need to add any types of surfactants to stabilize the dispersions.

These data and reasonings will hopefully allow others to evaluate the solvents applied in LPE of different materials, thus employing greener alternatives to toxic, harmful, and commonly used solvents for this process. The exfoliated material produced in the current study can further help to increase biochar applications in higher value-ended fields. This includes the investigation of exfoliated biochar as an additive and reinforcing agents in polymer composites, which will be presented in **Chapter 4: Biochar as a Sustainable and Renewable Additive for the Production of Poly(caprolactone) Composites.**

3.4 Experimental

3.4.1 General Materials

Unless otherwise stated, chemicals were purchased from Sigma Aldrich or Fisher Scientific and used as received. Pristine biochar samples were used without additional treatment from Cape Breton University (Sydney, Nova Scotia) and Sexton Lumber Co. (Bloomfield, Newfoundland and Labrador).^{68, 69} Commercially available solvents were used without any further purification.

3.4.2 Instrumentation

UV-Vis spectra were acquired using an Ocean Optics USB4000 UV-Vis spectrophotometer using quartz cuvettes. A calibration curve was constructed using oxidized biochar hardwood samples dispersed in ϵ -caprolactone, and the dispersed fractions in the samples were calculated using absorbance values at 660 nm.

Raman spectroscopy analyses were performed by S. M. Gallant (Memorial University of Newfoundland) using a Renishaw confocal Raman microscope containing an 830 nm wavelength laser. Biochar samples before exfoliation were mounted on a quartz wafer and exfoliated samples in CHCl_3 were mounted on a silicon wafer after solvent drying. Scans were performed at 0.5% or 1% laser power for 20 or 25 s, using a 20 \times optical lens. Baseline correction was implemented in Renishaw's WiRE software using a cubic spline interpolation smoothing. Peak areas and heights were calculated using a Gaussian fit in IGOR Pro software.

AFM characterization of exfoliated biochars in CHCl_3 was performed by E. P. Connors (Memorial University of Newfoundland) using an MFP-3D Asylum Research instrument and NSC35/Al BS tips by MikroMasch. Samples were drop-casted onto a glass slide pre-heated at 100 °C to promote a more uniform deposition and avoid reaggregation of the nanostructures. Samples were scanned at 0.1 Hz. The heights of 100 different nanostructures were calculated to obtain a distribution of their thickness.

TEM characterization of **bc** and **oxbc** before and after exfoliation were realized using NMP as a solvent and carried out using a Hitachi HT7700 Transmission Electron Microscope containing a tungsten filament in high contrast (HC) mode at 80 kV in Cape Breton University (Sydney, NS).

MS data were acquired using a Matrix Assisted Laser Desorption/Ionization-Time of Flight (MALDI-TOF) Bruker UltrafleXtreme MS in positive-ion mode. About 1.2 mg of **bc** or **oxbc** samples exfoliated in EtOAc were 50 μL of a 1 mg/mL standard solution of

DHB in THF. After centrifugation, 0.5 μL of the supernatant of the mixture was deposited on the MALDI plate. During analysis, the laser power was carefully increased to 90% to obtain the best results.

3.4.3 Preparation of Exfoliated Biochars

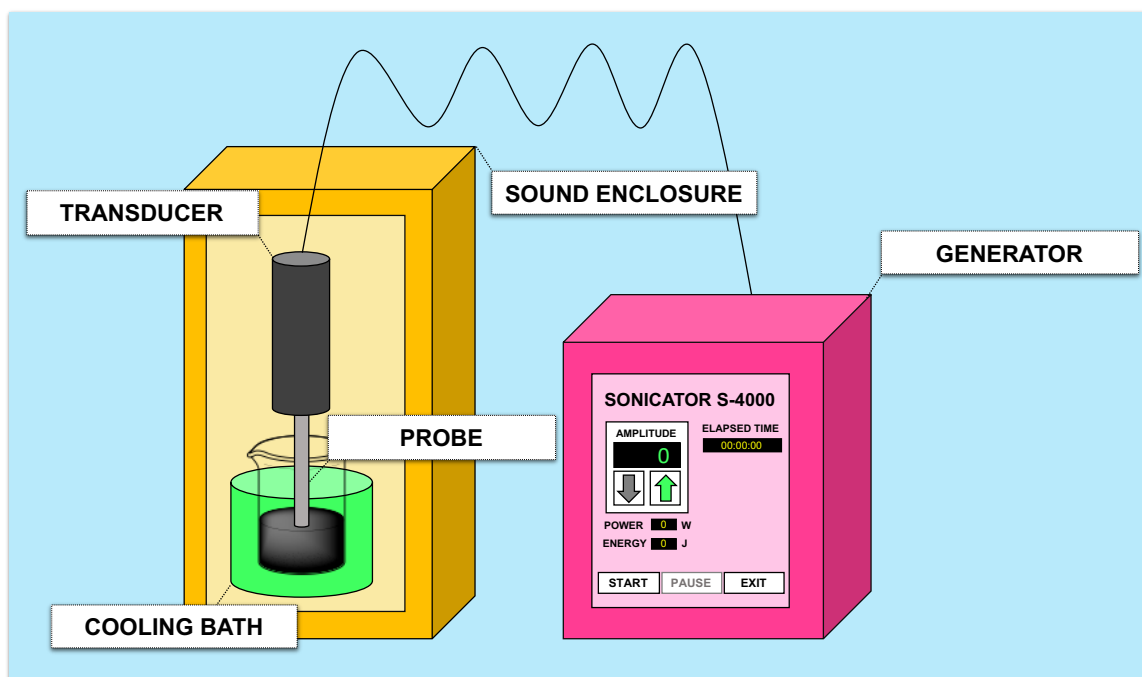


Figure 3.15. Schematic representation of the sonication setup used to exfoliate **bc** and **oxbc** samples. The transducer converts the electrical signal supplied by the generator to mechanical vibrations, which are then transmitted by the probe. The cooling bath is used to avoid heating of samples, and the sound enclosure reduces sound levels.

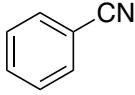
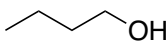
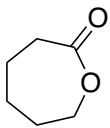
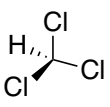
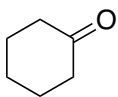
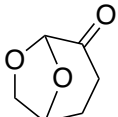
Preparation of **bc** and **oxbc** can be found in **Sections 2.4.3** and **2.4.4**, respectively. Boehm titrations^{70, 71} were performed in biochar samples by D. D. Richards (Cape Breton University), showing an increase in the number of acidic sites (n_{CSF}) in the functionalized biochar, from 3.84 mmol/g in **bc** to 4.88 mmol/g in **oxbc**.

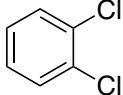
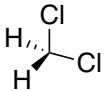
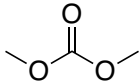
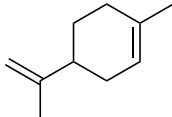
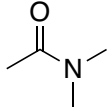
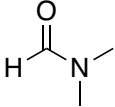
In a scintillation vial containing 10 mg of **bc** or **oxbc** samples from hardwood or softwood biomass feedstocks, 10 mL of the investigated solvent were added. The light gray dispersions produced were then directly sonicated for 15 min using an ultrasound Misonix S-4000 Sonicator setup containing a generator to supply the electrical signal, an aluminum transducer to convert the signal to a mechanical vibration, a titanium alloy probe to transmit the vibration, a sound enclosure to reduce sound levels, and a circulating-cooling bath at 3 °C to avoid heating of the samples. A schematic representation of the sonication setup is shown in **Figure 3.15**.

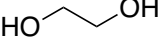
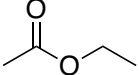
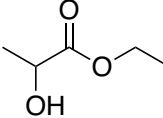
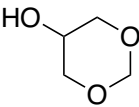
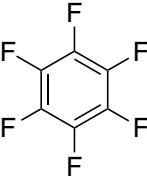
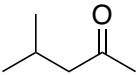
An ultrasonic vibration amplitude of 50% and power of 20 W were chosen to perform exfoliations, providing different sonic energies to the system depending on the solvent used. Solvents used for this procedure included, with abbreviation and energy in parenthesis: Acetone (E = 17.4 kJ); benzonitrile (PhCN, E = 23.8 kJ); 1-butanol (E = 40.5 kJ); ϵ -caprolactone (ϵ -CL, E = 36.8 kJ); chloroform (CHCl₃, E = 18.8 kJ); cyclohexanone (E = 42.1 kJ); Cyrene® (E = 48.2 kJ); 1,2-dichlorobenzene (1,2-DCB, E = 29.5 kJ); dichloromethane (CH₂Cl₂, E = 14.0 kJ); dimethyl carbonate (DMC, E = 25.8 kJ); D-limonene (E = 24.8 kJ); *N,N*-dimethylacetamide (DMA, E = 20.2 kJ); *N,N*-dimethylformamide (DMF, E = 20.6 kJ); dimethyl sulfoxide (DMSO, E = 33.4 kJ); ethanol (E = 25.2 kJ); ethylene glycol (EG = 47.1 kJ); ethyl acetate (EtOAc, E = 20.5 kJ); ethyl lactate (E = 28.8 kJ); glycerol formal (GF, E = 38.3 kJ); hexafluorobenzene (C₆F₆, E = 20.3 kJ); 4-methyl-2-pentanone (E = 19.6 kJ); *N*-methyl-2-pyrrolidone (NMP, E = 31.5 kJ); polyethylene glycol 200 (PEG 200, E = 43.6 kJ); polyethylene glycol 400 (PEG 400, E =

50.2 kJ); solketal (E = 42.7 kJ); toluene (E = 20.9 kJ); and deionized water (H₂O, E = 25.8 kJ). After sonication, black dispersions of biochar were obtained for most of the solvents investigated. The samples were allowed to settle for 3 days at ambient conditions and the supernatant was carefully removed so biochar dispersed fractions could be characterized. The dispersions were stable for at least 3 weeks. A list of all the solvents studied, with their chemical structures and green credentials obtained from different solvent guides is shown in **Table 3.6**, whilst biochar dispersions obtained and their correlations with HSP and viscosities of solvents is seen in **Table 3.7** and **Table 3.8**.

Table 3.6. Chemical structures and health, safety, and environmental impacts for all solvents investigated during the LPE of biochar and green credentials from solvent guides where available.

Entry	Solvent	FP, Health, Safety, and Environmental Impacts	Green Credentials from Solvent Guides ^a
1	Acetone 	FP = -20 °C. Flammable, volatile, biodegradable, low toxicity. ⁶²	CHEM 21: Recommended Pfizer: Preferred GSK: Some issues
2	PhCN 	FP = 71 °C. Combustible, toxic. ⁴⁴	CHEM21: Not included Pfizer: Not included GSK: Not included
3	1-butanol 	FP = 37 °C. Flammable, non-volatile, biodegradable, renewable, low toxicity. ⁴⁷	CHEM 21: Recommended Pfizer: Preferred GSK: Few issues
4	ϵ -CL 	FP = 127 °C. Non-volatile, non-toxic. ⁵⁷	CHEM21: Not included Pfizer: Not included GSK: Not included
5	CHCl ₃ 	FP = None. Volatile, toxic, carcinogen. ⁶²	CHEM21: Highly hazardous Pfizer: Undesirable GSK: Major issues
6	Cyclohexanone 	FP = 44 °C. Flammable, harmful, not sustainable synthesis. ⁴⁷	CHEM21: Problematic Pfizer: Preferred GSK: Some issues
7	Cyrene® 	FP = 108 °C. Non-volatile, renewable, biodegradable, low toxicity. ⁴⁸	CHEM21: Problematic Pfizer: Not included GSK: Not included

Entry	Solvent	FP, Health, Safety, and Environmental Impacts	Green Credentials from Solvent Guides ^a
8	1,2-DCB 	FP = 66 °C. Toxic, carcinogen. ⁴⁴	CHEM21: Not included Pfizer: Not included GSK: Not included
9	CH ₂ Cl ₂ 	FP = None. Volatile, toxic, carcinogen. ⁶²	CHEM21: Hazardous Pfizer: Undesirable GSK: Major issues
10	DMC 	FP = 18 °C. Flammable, non-volatile, renewable, biodegradable, non-toxic. ⁶⁵	CHEM21: Recommended Pfizer: Not included GSK: Few issues
11	<i>D</i> -limonene 	FP = 48 °C. Non-volatile, renewable, biodegradable, toxic. ³³	CHEM21: Problematic Pfizer: Not included GSK: Not included
12	DMA 	FP = 70 °C. Flammable, not sustainable synthesis, toxic. ³⁴	CHEM21: Not included Pfizer: Undesirable GSK: Major issues
13	DMF 	FP = 57 °C. Flammable, toxic. ³⁴	CHEM21: Hazardous Pfizer: Undesirable GSK: Major issues
14	DMSO 	FP = 85 °C. Combustible, harmful. ⁴⁷	CHEM21: Problematic Pfizer: Usable GSK: Some issues

Entry	Solvent	FP, Health, Safety, and Environmental Impacts	Green Credentials from Solvent Guides ^a
15	Ethanol 	FP = 13 °C. Flammable, volatile, renewable, biodegradable, low toxicity. ⁶²	CHEM21: Recommended Pfizer: Preferred GSK: Some issues
16	EG 	FP = 111 °C. Non-volatile, renewable, biodegradable, low toxicity. ⁶²	CHEM21: Recommended Pfizer: Usable GSK: Few issues
17	EtOAc 	FP = -2 °C. Flammable, volatile, biodegradable, low toxicity. ⁶²	CHEM21: Recommended Pfizer: Usable GSK: Some issues
18	Ethyl lactate 	FP = 46 °C. Flammable, non-volatile, renewable, biodegradable, toxic. ⁶²	CHEM21: Problematic Pfizer: Not included GSK: Not included
19	GF 	FP = 93 °C. Non-volatile, renewable, biodegradable, non-toxic. ⁴⁸	CHEM21: Not included Pfizer: Not included GSK: Not included
20	C ₆ F ₆ 	FP = 10 °C. Flammable, harmful. ⁴⁴	CHEM21: Not included Pfizer: Not included GSK: Not included
21	4-methyl-2-pentanone 	FP = 14 °C. Flammable, toxic, carcinogen. ⁷²	CHEM21: Not included Pfizer: Not included GSK: Not included

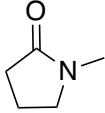
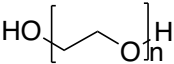
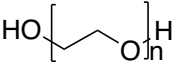
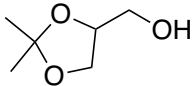
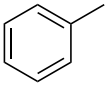
Entry	Solvent	FP, Health, Safety, and Environmental Impacts	Green Credentials from Solvent Guides ^a
22	NMP 	FP = 86 °C. Combustible, toxic. ³⁴	CHEM21: Hazardous Pfizer: Undesirable GSK: Major issues
23	PEG 200 	FP = 139 °C. Non-volatile, biocompatible, biodegradable, non-toxic. ⁶²	CHEM21: Not included Pfizer: Not included GSK: Not included
24	PEG 400 	FP = 238 °C. Non-volatile, biocompatible, biodegradable, non-toxic. ⁶²	CHEM21: Not included Pfizer: Not included GSK: Not included
25	Solketal 	FP = 80 °C. Non-volatile, renewable, biodegradable, non-toxic. ⁷³	CHEM21: Not included Pfizer: Not included GSK: Not included
26	Toluene 	FP = 4 °C. Flammable, teratogen. ⁴⁷	CHEM21: Problematic Pfizer: Usable GSK: Some issues
27	H ₂ O 	FP = None. Non-volatile, non-toxic, renewable. ⁶²	CHEM21: Recommended Pfizer: Preferred GSK: Few issues

Table 3.7. Achieved dispersions and solvent parameters (i.e. HSP and viscosities) for the LPE of **bc** samples.

Entry	Solvent	Biochar type and dispersion (mg/mL)	Hansen Solubility Parameters (MPa ^½)			η (mPa.s) ^a
			δ _D	δ _H	δ _P	
1	C ₆ F ₆	bc_{hw} , 0.11 bc_{sw} , 0.26	16.9 ⁴⁶	0.0 ⁴⁶	0.0 ⁴⁶	0.86 ⁴⁴
2	CHCl ₃	bc_{hw} , 0.17 bc_{sw} , 0.51	17.8 ⁴⁶	5.7 ⁴⁶	3.1 ⁴⁶	0.37 ⁴⁶
3	CH ₂ Cl ₂	bc_{hw} , 0.21 bc_{sw} , 0.39	18.2 ⁴⁶	6.1 ⁴⁶	6.3 ⁴⁶	0.43 ⁴⁶
4	1,2-DCB	bc_{hw} , 0.21 bc_{sw} , 0.28	19.2 ⁴⁶	3.3 ⁴⁶	6.3 ⁴⁶	1.27 ⁴⁶
5	PhCN	bc_{hw} , 0.15 bc_{sw} , 0.22	17.4 ⁴⁶	3.3 ⁴⁶	9.0 ⁴⁶	1.24 ⁴⁴
6	DMC	bc_{hw} , 0.11 bc_{sw} , 0.20	15.5 ⁴⁶	9.7 ⁴⁶	3.9 ⁴⁶	0.59 ⁴⁴
7	Solketal	bc_{hw} , 0.15 bc_{sw} , 0.17	16.6 ²⁴	12.0 ²⁴	7.9 ²⁴	11.0 ²⁴
8	NMP	bc_{hw} , 0.09 bc_{sw} , 0.16	18.0 ⁴⁶	7.2 ⁴⁶	12.3 ⁴⁶	1.67 ⁴⁴
9	H ₂ O	bc_{hw} , 0.11 bc_{sw} , 0.13	15.5 ⁴⁶	42.3 ⁴⁶	16.0 ⁴⁶	1.00 ⁴⁷
10	EtOAc	bc_{hw} , 0.12 bc_{sw} , 0.13	15.8 ⁴⁶	7.2 ⁴⁶	5.3 ⁴⁶	0.44 ⁴⁶
11	Acetone	bc_{hw} , 0.09 bc_{sw} , 0.10	15.5 ⁴⁶	7.0 ⁴⁶	10.4 ⁴⁶	0.35 ⁴⁶

^a Values obtained at 20 or 25 °C.

Table 3.8. Achieved dispersions and solvent parameters (i.e. HSP and viscosities) for the LPE of **oxbc** samples.

Entry	Solvent	Biochar type and dispersion (mg/mL)	Hansen Solubility Parameters (MPa ^½)			η (mPa.s) ^a
			δ _D	δ _H	δ _P	
1	GF	oxbc_{hw} , 0.14 oxbc_{sw} , 0.33	18.4 ²⁴	16.5 ²⁴	10.6 ²⁴	14.2 ²⁴
2	PEG 400	oxbc_{hw} , 0.48 oxbc_{sw} , 0.76	16.6 ⁷⁴	13.3 ⁷⁴	3.7 ⁷⁴	114.5 ⁵²
3	PEG 200	oxbc_{hw} , 0.48 oxbc_{sw} , 0.69	16.7 ⁷⁴	16.7 ⁷⁴	5.6 ⁷⁴	57.3 ⁷⁵
4	EG	oxbc_{hw} , 0.46 oxbc_{sw} , 0.56	17.0 ⁴⁴	26.0 ⁴⁴	11.0 ⁴⁴	20.9 ⁴⁴
5	DMSO	oxbc_{hw} , 0.41 oxbc_{sw} , 0.45	18.4 ⁴⁶	10.2 ⁴⁶	16.4 ⁴⁶	1.98 ⁴⁶
6	ε-CL	oxbc_{hw} , 0.21 oxbc_{sw} , 0.38	19.7 ⁴⁶	7.4 ⁴⁶	15.0 ⁴⁶	4.88
7	Solketal	oxbc_{hw} , 0.27 oxbc_{sw} , 0.35	16.6 ²⁴	12.0 ²⁴	7.9 ²⁴	11.0 ²⁴
8	NMP	oxbc_{hw} , 0.23 oxbc_{sw} , 0.42	18.0 ⁴⁶	7.2 ⁴⁶	12.3 ⁴⁶	1.67 ⁴⁴
9	H ₂ O	oxbc_{hw} , 0.14 oxbc_{sw} , 0.27	15.5 ⁴⁶	42.3 ⁴⁶	16.0 ⁴⁶	1.00 ⁴⁷
10	EtOAc	oxbc_{hw} , 0.16 oxbc_{sw} , 0.18	15.8 ⁴⁶	7.2 ⁴⁶	5.3 ⁴⁶	0.44 ⁴⁶
11	Acetone	oxbc_{hw} , 0.17 oxbc_{sw} , 0.24	15.5 ⁴⁶	7.0 ⁴⁶	10.4 ⁴⁶	0.35 ⁴⁶

^a Values obtained at 20 or 25 °C.

3.5 References

1. Vidal, J. L.; Gallant, S. M. V.; Connors, E. P.; Richards, D. D.; MacQuarrie, S. L.; Kerton, F. M., *ACS Sustain. Chem. Eng.* **2021**, *9*, 9114-9125.
2. Li, Z.; Young, R. J.; Backes, C.; Zhao, W.; Zhang, X.; Zhukov, A. A.; Tillotson, E.; Conlan, A. P.; Ding, F.; Haigh, S. J.; Novoselov, K. S.; Coleman, J. N., *ACS Nano* **2020**, *14*, 10976-10985.
3. Coleman, J. N.; Lotya, M.; O'Neill, A.; Bergin, S. D.; King, P. J.; Khan, U.; Young, K.; Gaucher, A.; De, S.; Smith, R. J.; Shvets, I. V.; Arora, S. K.; Stanton, G.; Kim, H.-Y.; Lee, K.; Kim, G. T.; Duesberg, G. S.; Hallam, T.; Boland, J. J.; Wang, J. J.; Donegan, J. F.; Grunlan, J. C.; Moriarty, G.; Shmeliov, A.; Nicholls, R. J.; Perkins, J. M.; Grievson, E. M.; Theuwissen, K.; McComb, D. W.; Nellist, P. D.; Nicolosi, V., *Science* **2011**, *331*, 568-571.
4. Tao, H.; Zhang, Y.; Gao, Y.; Sun, Z.; Yan, C.; Texter, J., *Phys. Chem. Chem. Phys.* **2017**, *19*, 921-960.
5. Cunningham, G.; Lotya, M.; McEvoy, N.; Duesberg, G. S.; Van der Schoot, P.; Coleman, J. N., *Nanoscale* **2012**, *4*, 6260-6264.
6. Huang, H.-D.; Ren, P.-G.; Chen, J.; Zhang, W.-Q.; Ji, X.; Li, Z.-M., *J. Membr. Sci.* **2012**, *409-410*, 156-163.
7. May, P.; Khan, U.; O'Neill, A.; Coleman, J. N., *J. Mater. Chem.* **2012**, *22*, 1278-1282.
8. Pavlidou, S.; Papaspyrides, C. D., *Prog. Polym. Sci.* **2008**, *33*, 1119-1198.

9. Smith, R. J.; King, P. J.; Lotya, M.; Wirtz, C.; Khan, U.; De, S.; O'Neill, A.; Duesberg, G. S.; Grunlan, J. C.; Moriarty, G.; Chen, J.; Wang, J.; Minett, A. I.; Nicolosi, V.; Coleman, J. N., *Adv. Mater.* **2011**, *23*, 3944-3948.
10. Stankovich, S.; Dikin, D. A.; Dommett, G. H. B.; Kohlhaas, K. M.; Zimney, E. J.; Stach, E. A.; Piner, R. D.; Nguyen, S. T.; Ruoff, R. S., *Nature* **2006**, *442*, 282-286.
11. Zhu, Y.; Murali, S.; Stoller, M. D.; Ganesh, K. J.; Cai, W.; Ferreira, P. J.; Pirkle, A.; Wallace, R. M.; Cychosz, K. A.; Thommes, M.; Su, D.; Stach, E. A.; Ruoff, R. S., *Science* **2011**, *332*, 1537-1541.
12. Backes, C.; Higgins, T. M.; Kelly, A.; Boland, C.; Harvey, A.; Hanlon, D.; Coleman, J. N., *Chem. Mater.* **2016**, *29*, 243-255.
13. Nicolosi, V.; Chhowalla, M.; Kanatzidis, M. G.; Strano, M. S.; Coleman, J. N., *Science* **2013**, *340*, 1226419-1226437.
14. Hernandez, Y.; Nicolosi, V.; Lotya, M.; Blighe, F. M.; Sun, Z.; De, S.; McGovern, I. T.; Holland, B.; Byrne, M.; Gun'Ko, Y. K.; Boland, J. J.; Niraj, P.; Duesberg, G.; Krishnamurthy, S.; Goodhue, R.; Hutchison, J.; Scardaci, V.; Ferrari, A. C.; Coleman, J. N., *Nat. Nanotechnol.* **2008**, *3*, 563-568.
15. Wang, N.; Xu, Q.; Xu, S.; Qi, Y.; Chen, M.; Li, H.; Han, B., *Sci. Rep.* **2015**, *5*, 16764-16772.
16. Ciesielski, A.; Samori, P., *Chem. Soc. Rev.* **2014**, *43*, 381-398.

17. Kim, J.; Kwon, S.; Cho, D. H.; Kang, B.; Kwon, H.; Kim, Y.; Park, S. O.; Jung, G. Y.; Shin, E.; Kim, W. G.; Lee, H.; Ryu, G. H.; Choi, M.; Kim, T. H.; Oh, J.; Park, S.; Kwak, S. K.; Yoon, S. W.; Byun, D.; Lee, Z.; Lee, C., *Nat. Commun.* **2015**, *6*, 8294-8302.
18. Shen, J.; He, Y.; Wu, J.; Gao, C.; Keyshar, K.; Zhang, X.; Yang, Y.; Ye, M.; Vajtai, R.; Lou, J.; Ajayan, P. M., *Nano Lett.* **2015**, *15*, 5449-5454.
19. Reichardt, C., Solute-solvent interactions. In *Solvents and solvent effects in organic chemistry*, 3rd ed.; Wiley-VCH: Weinheim, 2003; pp 5-56.
20. Zhou, K.-G.; Mao, N.-N.; Wang, H.-X.; Peng, Y.; Zhang, H.-L., *Angew. Chem. Int. Ed.* **2011**, *50*, 10839-10842.
21. Bergin, S. D.; Sun, Z.; Rickard, D.; Streich, P. V.; Hamilton, J. P.; Coleman, J. N., *ACS Nano* **2009**, *3*, 2340-2350.
22. Kamlet, M. J.; Abboud, J. L. M.; Abraham, M. H.; Taft, R. W., *J. Org. Chem.* **1983**, *48*, 2877-2887.
23. Jessop, P. G.; Jessop, D. A.; Fu, D.; Phan, L., *Green Chem.* **2012**, *14*, 1245-1259.
24. Salavagione, H. J.; Sherwood, J.; De bruyn, M.; Budarin, V. L.; Ellis, G. J.; Clark, J. H.; Shuttleworth, P. S., *Green Chem.* **2017**, *19*, 2550-2560.
25. Liu, W. J.; Jiang, H.; Yu, H. Q., *Chem. Rev.* **2015**, *115*, 12251-12285.
26. Genovese, M.; Jiang, J.; Lian, K.; Holm, N., *J. Mater. Chem. A* **2015**, *3*, 2903-2913.
27. Oleszczuk, P.; Ćwikła-Bundyra, W.; Bogusz, A.; Skwarek, E.; Ok, Y. S., *J. Anal. Appl. Pyrol.* **2016**, *121*, 165-172.

28. Ramanayaka, S.; Vithanage, M.; Alessi, D. S.; Liu, W.-J.; Jayasundera, A. C. A.; Ok, Y. S., *Environ. Sci. Nano* **2020**, *7*, 3279-3302.
29. Roy, S.; Kumar, U.; Bhattacharyya, P., *Environ. Sci. Pollut. Res. Int.* **2019**, *26*, 7272-7276.
30. Xiao, X.; Chen, B., *Environ. Sci. Technol.* **2017**, *51*, 5473-5482.
31. Liu, G.; Zheng, H.; Jiang, Z.; Zhao, J.; Wang, Z.; Pan, B.; Xing, B., *Environ. Sci. Technol.* **2018**, *52*, 10369-10379.
32. Tian, W.; Gao, Q.; VahidMohammadi, A.; Dang, J.; Li, Z.; Liang, X.; Hamed, M. M.; Zhang, L., *Chem. Eng. J.* **2020**, 127601-127612.
33. Prat, D.; Wells, A.; Hayler, J.; Sneddon, H.; McElroy, C. R.; Abou-Shehata, S.; Dunn, P. J., *Green Chem.* **2016**, *18*, 288-296.
34. Alder, C. M.; Hayler, J. D.; Henderson, R. K.; Redman, A. M.; Shukla, L.; Shuster, L. E.; Sneddon, H. F., *Green Chem.* **2016**, *18*, 3879-3890.
35. Alfonsi, K.; Colberg, J.; Dunn, P. J.; Fevig, T.; Jennings, S.; Johnson, T. A.; Kleine, H. P.; Knight, C.; Nagy, M. A.; Perry, D. A.; Stefaniak, M., *Green Chem.* **2008**, *10*, 31-36.
36. Xu, L.; McGraw, J.-W.; Gao, F.; Grundy, M.; Ye, Z.; Gu, Z.; Shepherd, J. L., *J. Phys. Chem. C* **2013**, *117*, 10730-10742.
37. Su, R.; Lin, S. F.; Chen, D. Q.; Chen, G. H., *J. Phys. Chem. C* **2014**, *118*, 12520-12525.
38. Vidal, J. L.; Andrea, V. P.; MacQuarrie, S. L.; Kerton, F. M., *ChemCatChem* **2019**, *11*, 4089-4095.
39. Ferrari, A. C.; Robertson, J., *Phys. Rev. B* **2000**, *61*, 14095-14107.

40. Guizani, C.; Haddad, K.; Limousy, L.; Jeguirim, M., *Carbon* **2017**, *119*, 519-521.
41. Cançado, L. G.; Jorio, A.; Ferreira, E. H. M.; Stavale, F.; Achete, C. A.; Capaz, R. B.; Moutinho, M. V. O.; Lombardo, A.; Kulmala, T. S.; Ferrari, A. C., *Nano Lett.* **2011**, *11*, 3190-3196.
42. Cançado, L. G.; Takai, K.; Enoki, T.; Endo, M.; Kim, Y. A.; Mizusaki, H.; Jorio, A.; Coelho, L. N.; Magalhães-Paniago, R.; Pimenta, M. A., *Appl. Phys. Lett.* **2006**, *88*, 163106-163109.
43. Nicolosi, V.; Chhowalla, M.; Kanatzidis, M. G.; Strano, M. S.; Coleman, J. N., *Science* **2013**, *340*, 1420-1438.
44. Wypych, A.; Wypych, G., *Databook of solvents* 2nd ed.; ChemTec Publishing: Toronto, 2019.
45. Marcus, Y., *Chem. Soc. Rev.* **1993**, *22*, 409-416.
46. M. Hansen, C., *Hansen Solubility Parameters: A user's handbook*. 2nd ed.; CRC Press: Taylor & Francis: Boca Raton, 2012; p 546.
47. Rumble, J. R., *CRC handbook of chemistry and physics*. 100th (Internet Version) ed.; CRC Press : Taylor & Francis: Boca Raton, 2019.
48. Wypych, A.; Wypych, G., *Databook of green solvents*. 2 ed.; ChemTec Publishing: Toronto, 2014.
49. Laurence, C.; Nicolet, P.; Dalati, M. T.; Abboud, J.-L. M.; Notario, R., *J. Phys. Chem.* **1994**, *98*, 5807-5816.

50. Díaz-Álvarez, A. E.; Francos, J.; Lastra-Barreira, B.; Crochet, P.; Cadierno, V., *Chem. Commun.* **2011**, 47, 6208-6227.
51. Buhvestov, U.; Rived, F.; Ràfols, C.; Bosch, E.; Rosés, M., *J. Phys. Org. Chem.* **1998**, 11, 185-192.
52. Sequeira, M. C. M.; Pereira, M. F. V.; Avelino, H. M. N. T.; Caetano, F. J. P.; Fareleira, J. M. N. A., *Fluid Ph. Equilibria* **2019**, 496, 7-16.
53. Fu, D.; Du, L.; Wang, H., *J. Chem. Thermodyn.* **2014**, 69, 132-136.
54. Kim, I.-W.; Duk Jang, M.; Kyun Ryu, Y.; Hee Cho, E.; Lee, Y.-A.; Hag Park, J., *Anal. Sci.* **2003**, 18, 1357-1360.
55. Millipore Sigma, Polyethylene glycol 200.
http://www.emdmillipore.com/CA/en/product/msds/MDA_CHEM-807483?Origin=PDP
(accessed July 9, 2021).
56. DataPhysics Instruments, Surface tension values of some common test liquids for surface energy analysis. <https://www.dataphysics-instruments.com/Downloads/Surface-Tensions-Energies.pdf> (accessed July 9, 2021).
57. ChemSpider, ϵ -caprolactone. <http://www.chemspider.com/Chemical-Structure.9972.html> (accessed July 6, 2021).
58. Crowhurst, L.; Falcone, R.; Lancaster, N. L.; Llopis-Mestre, V.; Welton, T., *J. Org. Chem.* **2006**, 71, 8847-8853.
59. *IARC monographs on the evaluation of carcinogenic risks to humans: Dichloromethane*. IARC: Lyon, France, 2018; Vol. 110, p 177-255.

60. IARC monographs on the evaluation of carcinogenic risks to humans: Chloroform. IARC: Lyon, France, 1999; Vol. 73, p 131-182.
61. IARC monographs on the evaluation of carcinogenic risks to humans: Dichlorobenzenes. IARC: Lyon, France, 1999; Vol. 73, p 223-276.
62. Kerton, F. M.; Marriott, R., *Alternative Solvents for Green Chemistry*. 2nd ed.; RSC Publishing: Cambridge, UK 2013.
63. Domínguez-Barroso, V.; Herrera, C.; Larrubia, M. Á.; González-Gil, R.; Cortés-Reyes, M.; Alemany, L. J., *Catalysts* **2019**, *9*, 609-623.
64. United States Environmental Protection Agency (EPA).
<https://www.epa.gov/saferchoice/safer-ingredients> (accessed May 22, 2021).
65. Pacheco, M. A.; Marshall, C. L., *Energy Fuels* **1997**, *11*, 2-29.
66. Staples, C. A.; Williams, J. B.; Craig, G. R.; Roberts, K. M., *Chemosphere* **2001**, *43*, 377-383.
67. Labet, M.; Thielemans, W., *Chem. Soc. Rev.* **2009**, *38*, 3484-3504.
68. Bamdad, H.; Hawboldt, K.; MacQuarrie, S., *Energy Fuels* **2018**, *32*, 11742-11748.
69. Carrier, A. J.; Abdullahi, I.; Hawboldt, K. A.; Fiolek, B.; MacQuarrie, S. L., *J. Phys. Chem. C* **2017**, *121*, 26300-26307.
70. Goertzen, S. L.; Thériault, K. D.; Oickle, A. M.; Tarasuk, A. C.; Andreas, H. A., *Carbon* **2010**, *48*, 1252-1261.
71. Oickle, A. M.; Goertzen, S. L.; Hopper, K. R.; Abdalla, Y. O.; Andreas, H. A., *Carbon* **2010**, *48*, 3313-3322.

72. Fisher Scientific, 4-methyl-2-pentanone. <https://www.fishersci.ca/shop/products/4-methyl-2-pentanone-acsc-98-5-3/p-7050022#?keyword=4-methyl-2-pentanone> (accessed July 6, 2021).
73. Clarke, C. J.; Tu, W. C.; Levers, O.; Brohl, A.; Hallett, J. P., *Chem. Rev.* **2018**, *118*, 747-800.
74. Liu, B.; Du, Q.; Yang, Y., *J. Membr. Sci.* **2000**, *180*, 81-92.
75. Cruz, M. S.; Chumpitaz, L. D. A.; Alves, J. G. L. F.; Meirelles, A. J. A., *J. Chem. Eng. Data* **2000**, *45*, 61-63.

CO-AUTHORSHIP STATEMENT

Chapter 4: Biochar as a Sustainable and Renewable Additive the Production of Poly(ϵ -caprolactone) Composites. Juliana L. Vidal, Benjamin M. Yavitt, Mikhailey D. Wheeler, Jennifer L. Kolwich, Lindsay N. Donovan, Clarissa S. Sit, Savvas G. Hatzikiriakos, Nigel K. Jalsa, Stephanie L. MacQuarrie, and Francesca M. Kerton. This chapter has been submitted for publication.¹

The first author (Juliana L. Vidal) contributed 70% of the content of the article as the main researcher, including performing the experiments, collecting and analyzing data, and writing the manuscript.

The co-author (Benjamin M. Yavitt) was responsible for performing measurements and analyzing rheological data in the neat poly(ϵ -caprolactone) and its biochar composites under the supervision of the co-author Savvas G. Hatzikiriakos.

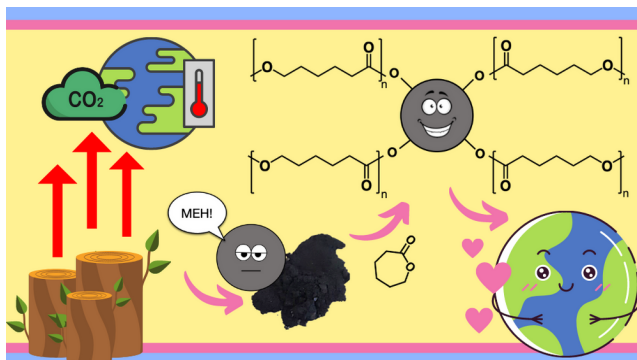
The co-author (Mikhailey D. Wheeler) was responsible for performing degradation studies in different environments for neat poly(ϵ -caprolactone) its composite containing 0.1 wt% of exfoliated oxidized biochar.

The co-authors (Jennifer L. Kolwich, Lindsay N. Donovan and Clarissa S. Sit) were responsible for performing genetic sequence analyses and culturing microbial samples that had grown on neat poly(ϵ -caprolactone) and its composites.

The co-author (Nigel K. Jalsa) was responsible for fruitful discussions and help during the GPC analysis of the composite samples.

The co-author (Stephanie L. MacQuarrie), my co-supervisor, was responsible for suggesting experiments, assisting with data interpretation, and revising the manuscript.

The corresponding author (Francesca M. Kerton), my supervisor, was the principal investigator of this work. She came up with the concept, suggested initial experiments, assisted with interpreting data, revised, and submitted the manuscript.



References for **Chapter 4** can be found on **Pages 184-188**.

CHAPTER 4: BIOCHAR AS A SUSTAINABLE AND RENEWABLE ADDITIVE FOR THE PRODUCTION OF POLY(CAPROLACTONE) COMPOSITES

4.1 Introduction

Poly(ϵ -caprolactone) (PCL) is an aliphatic polyester containing hexanoate repeating units.² Due to its biocompatibility, biodegradability, easy processability, and relative low cost, PCL is used in biomedical fields, microelectronics, adhesives, and packaging.^{2, 3} However, further potential industrial applications of PCL are limited due to its poor mechanical properties, including flexibility and softness.

Although PCL can be produced from sugars,⁴ it is currently derived from fossil fuels on an industrial scale. The environmental sustainability associated with its manufacture and commercialization can be improved by the utilization of biomass-derived fillers.^{5, 6} These fillers act as matrix reinforcements, as polymer composites generally present enhanced mechanical and thermal properties when compared to the pure polymer.⁷ Renewable materials such as wood, chitosan, cellulose, and lignin have been used to produce PCL composites via ring-opening polymerization (ROP) of the monomer ϵ -caprolactone (ϵ -CL). This process can be catalyzed by different catalytic systems, and it is initiated by the hydroxyl and carboxyl groups present on the surface of these bio-based materials, which serve as sites for polymer growth.⁸⁻¹⁴

In terms of its applications as a polymer additive, biochars from different biomass feedstocks have been employed as fillers for the most common plastics used in society, polyethylene and polypropylene.¹⁵⁻²² Investigations regarding the implementation of

biochar in the production of poly(lactic acid) have been performed,²³⁻²⁸ and also in its use as a co-additive for the fabrication of wood composites.^{29, 30} Although biochar has been employed as a filler for these and other polymeric systems,^{31, 32} studies involving the application of this bio-based material as a reinforcement for the production of PCL have not been performed to this date. Research regarding carbon materials as supports or initiators for the ROP of ϵ -CL have mostly been conducted using expensive and non-renewable precursors such as graphene oxide and carbon nanotubes.³³⁻³⁶

Given (i) the similarity in functional groups between graphene oxide and oxidized biochar and (ii) the ability of ϵ -CL to support the formation of dispersed nanostructures of biochar through exfoliation as shown previously in **Chapter 3: Green Solvents for the Liquid-Phase Exfoliation of Biochar**, the use exfoliated oxidized biochar as a bio-based filler for the production of greener PCL composites is investigated in this Chapter. The materials produced herein present higher percent crystallinity and stiffness when compared to pure PCL, and also show promising results in our preliminary degradation studies.

4.2 Results and Discussion

4.2.1 Preparation of PCL/biochar Composites (PCL/Eoxbc)

Biochar samples after oxidation with HNO_3 (**oxbc**) were directly sonicated in ϵ -CL, thus producing exfoliated oxidized biochar (**Eoxbc**). The catalyst was added to the dispersion, which was heated using an aluminum block. The polymer was then dissolved

in CH_2Cl_2 , precipitated in *n*-hexane, dried under vacuum, and identified as **PCL/Eoxbc**. A schematic representation of the production of **PCL/Eoxbc** composites is shown in **Figure 4.1**. Characterization of **Eoxbc** is described previously in **Section 3.2.4**, whereas more details about the preparation of composites can be found in **Section 4.4.3**.

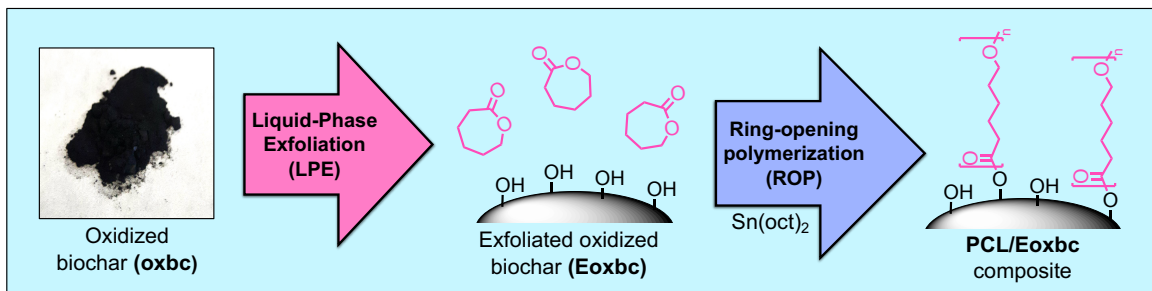


Figure 4.1. Schematic representation of **PCL/Eoxbc** composites production via ROP of ϵ -CL using **Eoxbc** as a support.

4.2.2 Catalytic Screening for the Production of PCL/Eoxbc Composites

Different catalytic systems with various activities have been used for the production of PCL,² and therefore various catalysts were screened before choosing a standard system for use throughout the current study. The reaction conditions applied herein were chosen following previous works in the literature,² and the results obtained are shown in **Table 4.1**. Reactions and analyses were performed in triplicate ($\text{SD} \leq 2.6\%$), and tin octoate (SnOct_2) was chosen in the initial studies, since it is an efficient and commonly used catalyst for the ROP of ϵ -CL. Without any biochar in the medium, $\text{Sn}(\text{oct})_2$ alone can convert 55.2% of ϵ -CL into relatively high molecular weight (M_n) PCL (**Table 4.1, Entry 1**), whilst no PCL is produced in the absence of the catalyst (**Table 4.1, Entry 4**). In the presence of both **Eoxbc** and $\text{Sn}(\text{oct})_2$, the conversion increased to 88.4% and the M_n of

PCL decreased under the same reaction conditions (Table 4.1, Entry 3).

Table 4.1. Catalyst screening for the ROP of ϵ -CL using biochar as a support.^a

Entry	Biochar	Catalyst	Time	T (°C)	Conv. (%) ^e	M _{n, NMR} (g/mol) ^e	M _{n, GPC} (g/mol) ^f	D ^f
1 ^b	-	Sn(oct) ₂	2 h	110	55.2	30,900	31,400	1.2
2 ^b	oxbc	Sn(oct) ₂	2 h	110	65.1	26,800	29,600	1.2
3 ^b	Eoxbc	Sn(oct) ₂	2 h	110	88.4	10,200	13,000	1.3
4	Eoxbc	-	2 h	110	0.0	-	-	-
5 ^c	Eoxboc	DABCO	7 days	110	42.2	2,500	4,400	1.2
6 ^c	Eoxbc	DBU	7 days	60	28.9	3,600	4,600	1.9
7 ^d	Eoxbc	N435	7 days	60	> 99.9	1,400	1,200	1.3
8 ^c	Eoxbc	CALB	7 days	60	> 99.9	1,400	2,500	1.3

^a General reaction conditions unless otherwise stated: ϵ -CL (5.0 g), biochar (0.1 wt%, 5 mg). Loadings of catalyst used: ^b 1 mol%. ^c 1,4-diazabicyclo(2.2.2)octane (DABCO), diazabicycloundecene (DBU), *Candida antartica* lipase B (CALB), 10 mol%. ^d Novozyme[®] 435 (N435), 5 wt%, with respect to ϵ -CL. ^e Determined by ¹H NMR spectroscopy. ^f Determined by gel permeation chromatograph (GPC) using tetrahydrofuran (THF) as a solvent. More information about the GPC analysis is shown in **Section 4.4.2**.

In previous works, the homogeneous dispersion of the nanofiller throughout the polymer matrix has been shown to greatly influence the physical properties of the polymers produced.^{11, 37, 38} In cases where the nanomaterial is dispersed homogeneously, polymer properties could be improved with the addition of small amounts of reinforcements. To assess the necessity of exfoliation in the system, a PCL blended composite was produced by following a similar procedure to that used to make PCL/Eoxbc grafted composites. If **oxbc** is simply added in the reaction medium without

any exfoliation treatment prior to the ROP, the M_n of the polymer produced and the conversion values obtained (**Table 4.1, Entry 2**) are in between those obtained for the neat ϵ -CL ROP and the **PCL/Eoxbc** grafted composites. Due to the higher conversions obtained and visibly better mechanical properties, it was decided to focus future experiments using **Eoxbc** as a nanofiller.

The catalytic activity of organocatalysts and enzymes was investigated during initial screenings. 1,4-diazabicyclo(2.2.2)octane (DABCO) and diazabicycloundecene (DBU) required very long reaction times to produce low M_n materials, with conversion values lower than 50% (**Table 4.1, Entries 5 and 6**). Excellent conversions were obtained using Novozyme® 435 (N435) and *Candida antartica* lipase B (CALB), but unfeasibly long reaction times were required for enzymatic ROP of ϵ -CL (**Table 4.1, Entries 7 and 8**). Previous reports in the literature involving enzymes also required the use of long reaction times (i.e. up to 20 days) to obtain good conversions (i.e. higher than 90%) to PCL, with M_n between 1,000 to 4,000 g/mol.^{2, 39} Although greener, neat reactions were associated with the synthesis of polymers with wide dispersity values (i.e. $\mathcal{D} \sim 3$), these could be narrowed to ~ 1 with the use of solvents such as acetonitrile, CHCl_3 , benzene, dioxane, toluene, or THF.² Herein, all polymers produced showed similar and narrow values of \mathcal{D} , with the exception of the composite produced using DBU as a catalyst.

Although there are known toxicity issues associated with the use of $\text{Sn}(\text{oct})_2$,⁴⁰ it was by far the most effective catalyst studied herein, capable of achieving good conversions in only 2 h of reaction and therefore, using less energy-intensive conditions. For these

reasons, Sn(oct)₂ was chosen as the standard catalyst and used to further study ROP reactions of ε-CL using **Eoxbc** as a support.

Table 4.2. Effect of **Eoxbc** loading in the production of **PCL/Eoxbc** composites using Sn(oct)₂ as a catalyst.^a

Entry	Sample	Conv. (%) ^b	M _{n, NMR} (g/mol) ^b	M _{n, GPC} (g/mol) ^c	<i>D</i> ^c
1	PCL/Eoxbc-0.1	88.4	10,200	13,000	1.3
2	PCL/Eoxbc-0.5	92.4	7,800	8,900	1.3
3	PCL/Eoxbc-1.0	93.5	5,900	7,900	1.3
4	PCL/Eoxbc-5.0	56.7	1,500	1,900	1.2

^aGeneral reaction conditions unless otherwise stated: ε-CL (5.0 g), Sn(oct)₂ (1 mol%, with respect to ε-CL), 110 °C, 2 h. ^bDetermined by ¹H NMR spectroscopy. ^cDetermined by GPC using THF as a solvent. More information about the GPC analysis is shown in **Section 4.4.2**.

After the catalyst screening, the influence of **Eoxbc** loadings was further assessed through the production and analysis of **PCL/Eoxbc** composites containing 0.1, 0.5, 1.0 and 5.0 wt% of **Eoxbc**. As seen in **Table 4.2**, an increase in **Eoxbc** content results in a decrease in the M_n of the composites both by NMR and GPC analyses. Moreover, monomer conversions were excellent in all except the case of **PCL/Eoxbc-5.0** (**Table 4.2, Entry 4**). The behavior observed in the formation of these composites might be indicative that **Eoxbc** is working as a support and as a multifunctional initiation site to promote the growth of PCL chains. It is proposed that, with the increase of **Eoxbc** content, long molecular chains of PCL would undergo chain transfer with the hydroxyl groups on the surface of the **Eoxbc** nanostructures, thus explaining why lower values of M_n and higher

conversions are obtained for the **PCL/Eoxbc** composites containing more biochar. However, a significant increase in the biochar loading (about 5.0 wt%,) led to a decrease in the dispersibility of the nanostructures within the polymeric matrix, thus promoting agglomeration of the **Eoxbc** particles, decreasing the growth ratio of PCL chains, and leading to lower conversions. A visual comparison between the different **PCL/Eoxbc** composites produced is shown in **Figure 4.2**. The ^1H NMR spectrum of the ROP of $\epsilon\text{-CL}$ using 5.0 wt% of **Eoxbc** is seen in **Appendix C: Information for Chapter 4**.



Figure 4.2. Visual comparison between **PCL/Eoxbc** composites containing different **Eoxbc** loadings (0.1, 0.5, 1.0, and 5.0 wt%).

4.2.3 Characterization of PCL/Biochar Composites

The FT-IR spectra of **oxbc**, neat PCL, and the **PCL/Eoxbc-5.0** grafted composite are presented in **Figure 4.3**. In comparison with **oxbc**, the spectrum of **PCL/Eoxbc-5.0** shows an intense peak at 1720 cm^{-1} related to the stretching of the PCL carbonyl group ($\text{C}=\text{O}$), two peaks at 2920 and 2945 cm^{-1} attributed to symmetric and asymmetric CH_2 stretching, and a reduction in the hydroxyl stretching band (O-H) intensity between $3400\text{-}3700\text{ cm}^{-1}$. The subtle differences between the FT-IR spectra of neat PCL and its composite observed herein are quite common, especially in cases where the filler content utilized is considerable low (i.e. $< 10\text{ wt}\%$).¹¹⁻¹⁴

Although the presence of a less intense O-H stretching band in the composite, an increase in the ester C=O peak intensity, as well as the widening of the C-O peak at 1160 cm^{-1} with increasing reinforcement loadings have been previously used to suggest the grafting of PCL onto the surface of various materials,¹¹⁻¹⁴ the confirmation of PCL supported by **Eoxbc** nanostructures was confirmed via calculation of grafting percentage (G%) after Soxhlet extraction.⁴¹⁻⁴³ A value of 96.8% of G% was obtained for **PCL/Eoxbc-0.1**, thus confirming that the PCL chains grow on the surface of **Eoxbc**. The equation to calculate G% and the FT-IR spectra of other composites produced in this work can be found in the **Appendix C: Information for Chapter 4**.

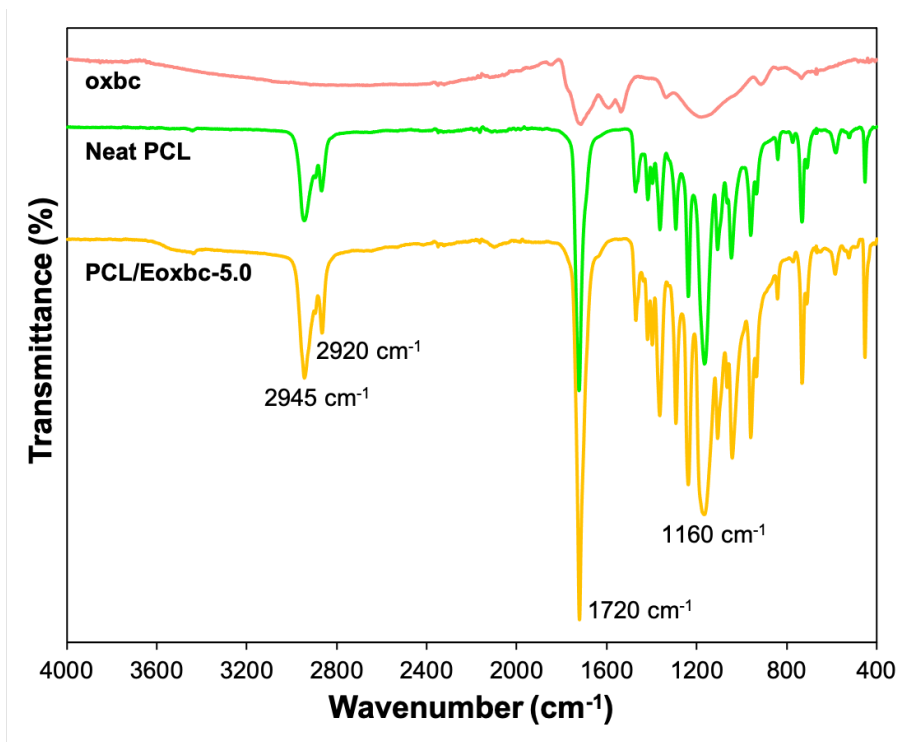


Figure 4.3. FT-IR spectra of **oxbc** (top, pink), neat PCL (middle, green), and the **PCL/Eoxbc-5.0** composite (bottom, yellow).

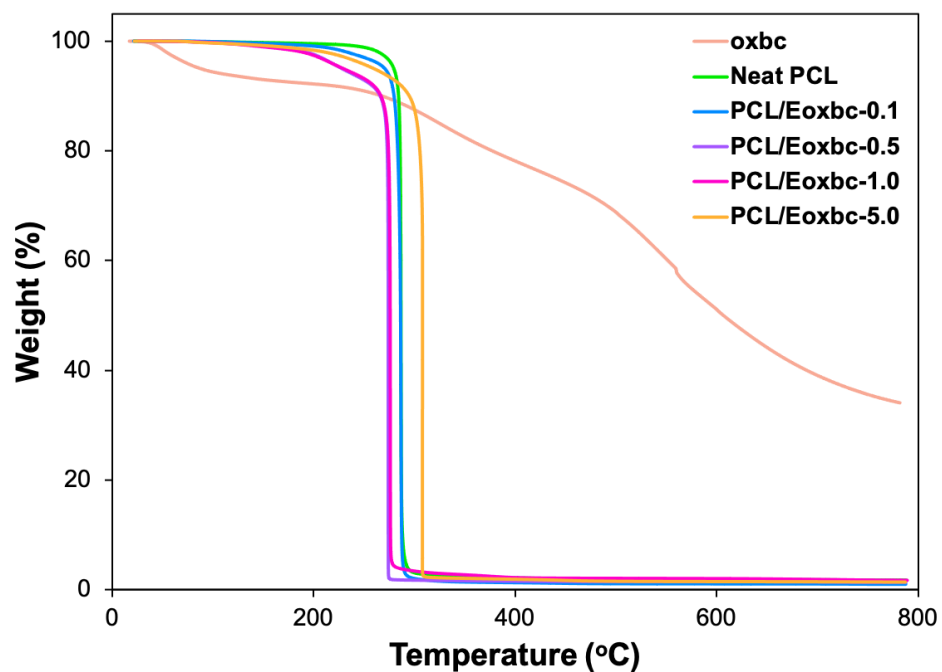


Figure 4.4. TGA analyses of neat PCL and PCL/Eoxbc composites with different Eoxbc loadings at a scanning rate of 10 °C/min under N₂.

TGA was performed to analyze the thermal stability of PCL and its composites. As shown in **Figure 4.4** and **Table 4.3**, neat PCL presents a single main degradation step at a relatively high maximum temperature (T_{\max}) of 288 °C (**Table 4.3, Entry 1**). PCL/Eoxbc composites containing 0.1, 0.5, and 0.1 wt% of Eoxbc present lower T_{\max} and are less thermally stable than the neat polymer. With the increase of Eoxbc loading from 0.1 to 1.0 wt%, there is a decrease in T_{\max} , reaching 276 °C for PCL/Eoxbc-1.0 (**Table 4.3, Entry 4**). The lower T_{\max} of composites are likely observed due to their shorter chains, as previously shown in **Table 4.2**. However, PCL/Eoxbc-5.0 has the lowest M_n of the composites produced ($M_{n, \text{PCL/Eoxbc-5.0}} = 1,900 \text{ g/mol}$) and its T_{\max} (308 °C) is significantly higher than the ones observed for neat PCL and its composites (**Table 4.3, Entry 5**). This

may be attributed to the agglomeration of thermally stable **Eoxbc** particles on the surface of the composite containing 5.0 wt% of **Eoxbc**. Moreover, the difference between mass losses of composites and **oxbc** at 800 °C can infer the amount of polymer grafted onto the support.⁴² The equations used can be found in the **Appendix C: Information for Chapter 4**. In the case of **PCL/Eoxbc-0.1**, considering the mass loss values (34.03% for **oxbc** and 99.01% for the composite), the amount of grafted polymer is 330.4 mg/g. Moreover, the calculated G% obtained via TGA in the temperature range of 200-800 °C was found to be 98.8%, which agrees within experimental error with the value of 96.8% obtained via Soxhlet extraction.

Table 4.3. TGA data from heating thermograms of neat PCL and **PCL/Eoxbc** composites with different **Eoxbc** loadings.

Entry	Sample	T _{onset} (°C)	T _{range} (°C)	T _{max} (°C)	Mass loss (%)
1	Neat PCL	285.6	268.8-297.1	288.0	98.27
2	PCL/Eoxbc-0.1	285.6	269.7-289.8	287.8	99.01
3	PCL/Eoxbc-0.5	275.0	258.4-275.3	274.3	98.64
4	PCL/Eoxbc-1.0	275.9	260.0-276.9	276.4	98.26
5	PCL/Eoxbc-5.0	300.1	289.8-309.2	308.1	98.61

Differential Scanning Calorimetry (DSC) was used to study the effect of exfoliation and biochar loadings on the thermal properties of the polymers. The third heating and cooling scans of the samples at scanning rates of 10 °C/min are shown in **Figure 4.5**. Characteristics such as degree of crystallinity (X_c) melting temperature (T_m), melting

enthalpy (ΔH_m), crystallization temperature (T_c), and crystallization enthalpy (ΔH_c) of samples were obtained and the results are summarized in **Table 4.4**.

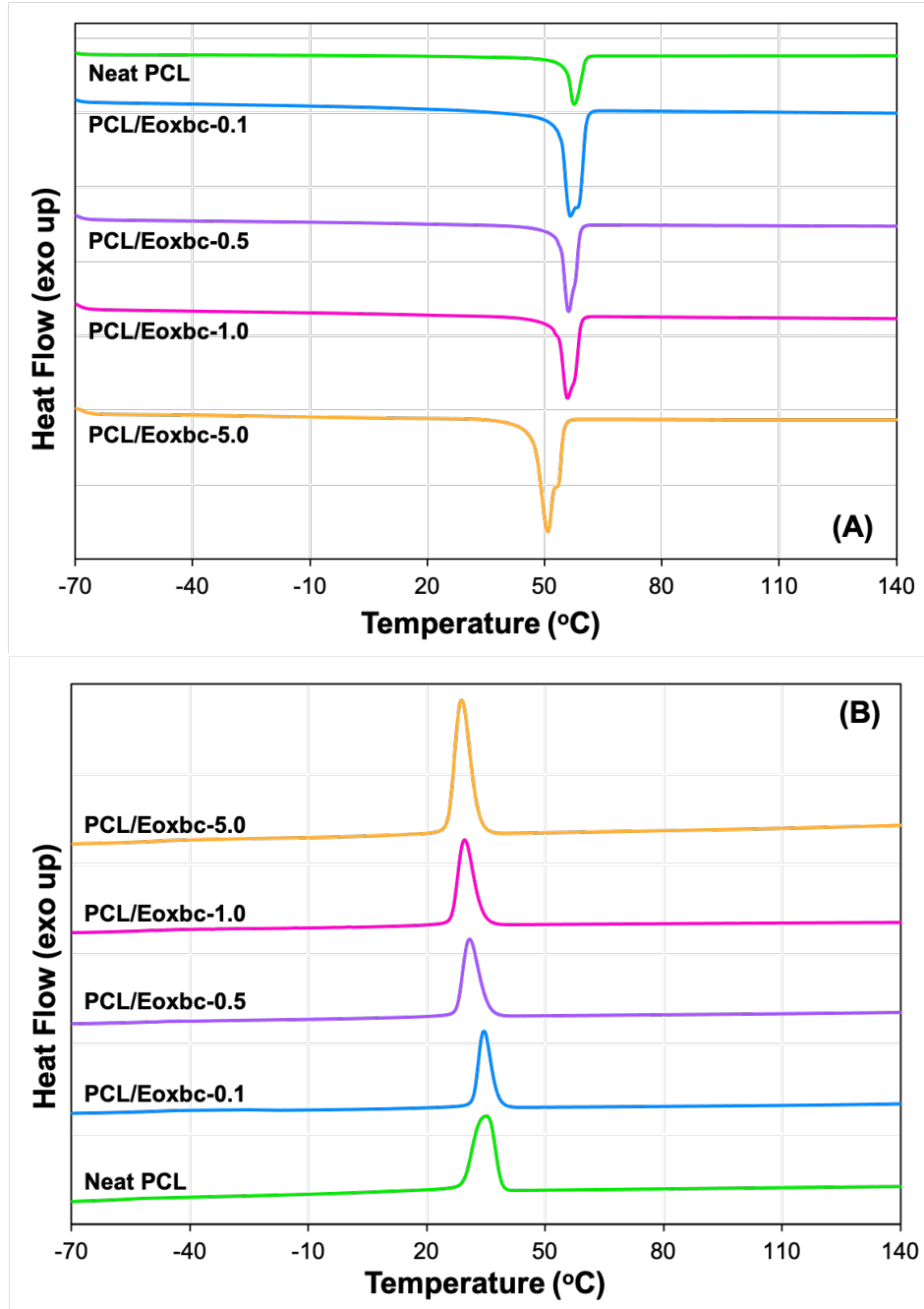


Figure 4.5. DSC third heating (A) and third cooling (B) scans of neat PCL and its composites with different **Eoxbc** loadings at a scanning rate of 10 °C/min.

Neat PCL shows a small and single endothermic melting peak with T_m of 57.3 °C and ΔH_m of 31.3 J/g (**Table 4.4, Entry 1**). With the increase of biochar loading, T_m decreases significantly while ΔH_m increases, reaching values of 50.3 °C and 46.3 J/g for **PCL/Eoxbc-5.0** (**Table 4.4, Entry 5**). Moreover, double melting peaks are present for all the **PCL/Eoxbc** composites studied. They have been observed in previous works involving polymer additives and are associated to an α' - α phase transition of the polymer crystal.^{25, 28} It is suggested that the peak at a lower temperature is associated to the melting of the α' form crystal, which is then recrystallized to a more stable α form. The second melting peak observed is then correlated to the melting of the α form crystal produced. The glass transition of PCL and their composites at about -60 °C was not observed due to limits in the accessible temperature range of the DSC instrument used.

Table 4.4. DSC data from third cooling and heating thermograms of neat PCL and its composites with different **Eoxbc** loadings at a scanning rate of 10 °C/min.

Entry	Sample	X_c (%)	T_m (°C)	ΔH_m (J/g)	T_c (°C)	ΔH_c (J/g)
1	Neat PCL	22.5	57.3	-31.3	35.3	30.7
2	PCL/Eoxbc-0.1	24.8	55.8	-34.7	32.9	33.1
3	PCL/Eoxbc-0.5	26.7	55.8	-37.3	31.1	33.4
4	PCL/Eoxbc-1.0	26.8	55.4	-37.4	30.0	33.2
5	PCL/Eoxbc-5.0	31.3	50.3	-43.6	29.3	38.4

Regarding the crystallization behavior, neat PCL shows a small and wide crystallization exotherm at a T_c of 35.3 °C and ΔH_c of 30.7 J/g (**Table 4.4, Entry 1**). With

the incorporation of **Eoxbc**, the crystallization peak narrowed and shifted to lower temperatures, reaching 29.3 °C for **PCL/Eoxbc-5.0** (Table 4.4, Entry 5). This crystallization behavior has been observed previously and may be attributed to the fact that **Eoxbc** is acting as a nucleating agent in the polymer matrix.^{27, 28} Compared to neat PCL, the ΔH_c were slightly higher, but constant (around 33 J/g) for the composites containing 0.1, 0.5, and 1.0 wt% of **Eoxbc**. A significant increase was observed for the ΔH_c of **PCL/Eoxbc-5.0**, which reached 38.4 J/g (Table 4.4, Entry 5). The crystallinity of PCL also increased with the increase in **Eoxbc** loadings. X_c values increased from 22.5% for neat PCL (Table 4.4, Entry 1) to 31.3% for **PCL/Eoxbc-5.0** (Table 4.4, Entry 5), thus suggesting that **Eoxbc** increases the ability for crystalline regions to form, which could lead to the production of composites with potential increased densities and stiffness.

The effect of **Eoxbc** in the morphology of PCL composites was studied via SEM analysis (Figure 4.6). The surface of neat PCL is homogeneous, smooth, and uniform (Figure 4.6A), whereas some small pores of 50 μm in size are shown on the surface of **PCL/Eoxbc-0.1** (Figure 4.6B). Increasing the **Eoxbc** loading, the presence of tightly packed spherulites could be observed in the composites. These spherulites are 80-110 μm and contain porous regions around peripheries, as observed in the images of **PCL/Eoxbc-0.5** (Figure 4.6C) and **PCL/Eoxbc-1.0** (Figure 4.6D). **PCL/Eoxbc-5.0**, however, shows a different morphology (Figure 4.6E). No spherulites were observed, thin cracks were seen through the surface, and also agglomerates of about 2 μm in size. An expansion of the small agglomerates observed in **PCL/Eoxbc-5.0** is shown in Figure 4.6F.

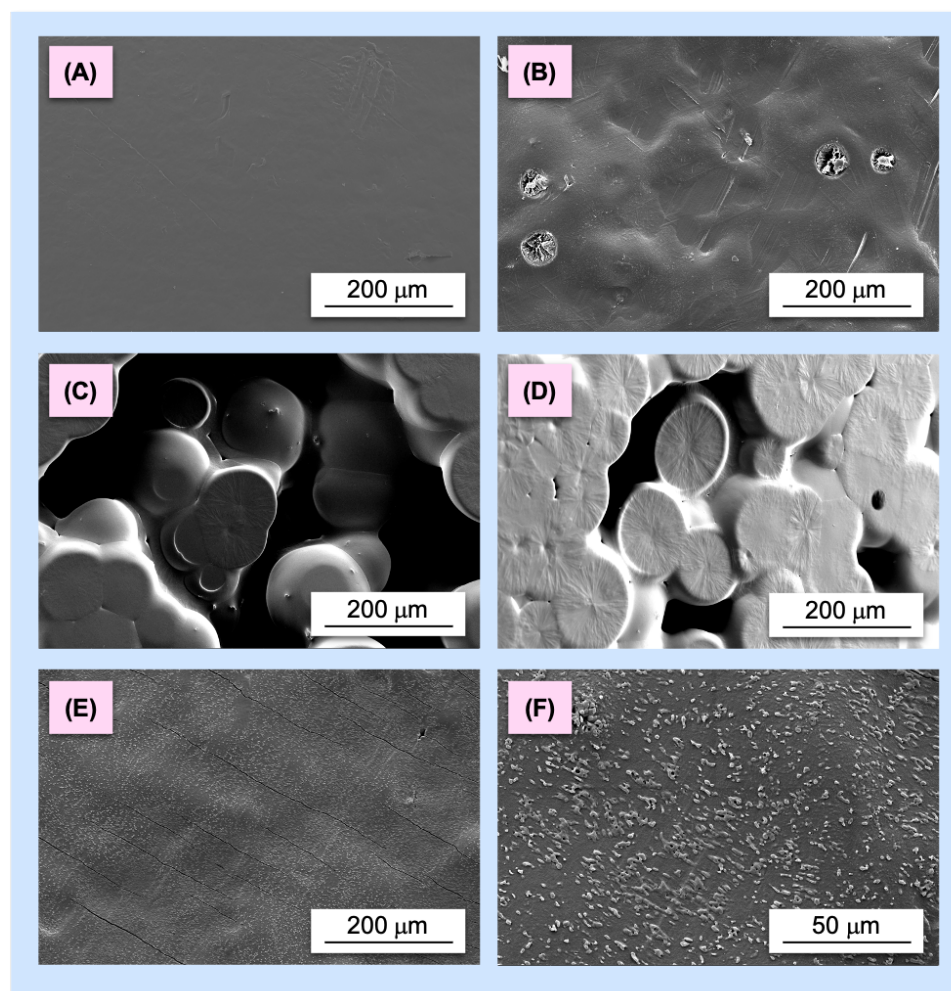


Figure 4.6. SEM images for surfaces of (A) neat PCL, (B) **PCL/Eoxbc-0.1**, (C) **PCL/Eoxbc-0.5**, (D) **PCL/Eoxbc-1.0**, (E) **PCL/Eoxbc-5.0**, and (F) expansion of agglomerates in **PCL/Eoxbc-5.0**.

The results obtained via SEM provide evidence that **Eoxbc** is facilitating the growth of PCL chains through heterogeneous nucleation, because an increase in biochar loadings leads to the formation of larger in number, but smaller spherulites. Moreover, the results obtained also indicate that **Eoxbc** is well dispersed within the polymeric matrix of the composites at lower contents, but starts agglomerating at significantly higher biochar

loadings. This has been observed in previous works involving polymer composites,^{27, 37, 44} and explains the lower conversions of ϵ -CL to PCL obtained during the production of **PCL/Eoxbc-5.0**. TEM analysis (**Figure 4.7**) also confirmed the production of the PCL composites due to the presence of **Eoxbc** dispersed nanostructures embedded within PCL matrix. The calculated average length of these particles was found to be 9 ± 2 nm.

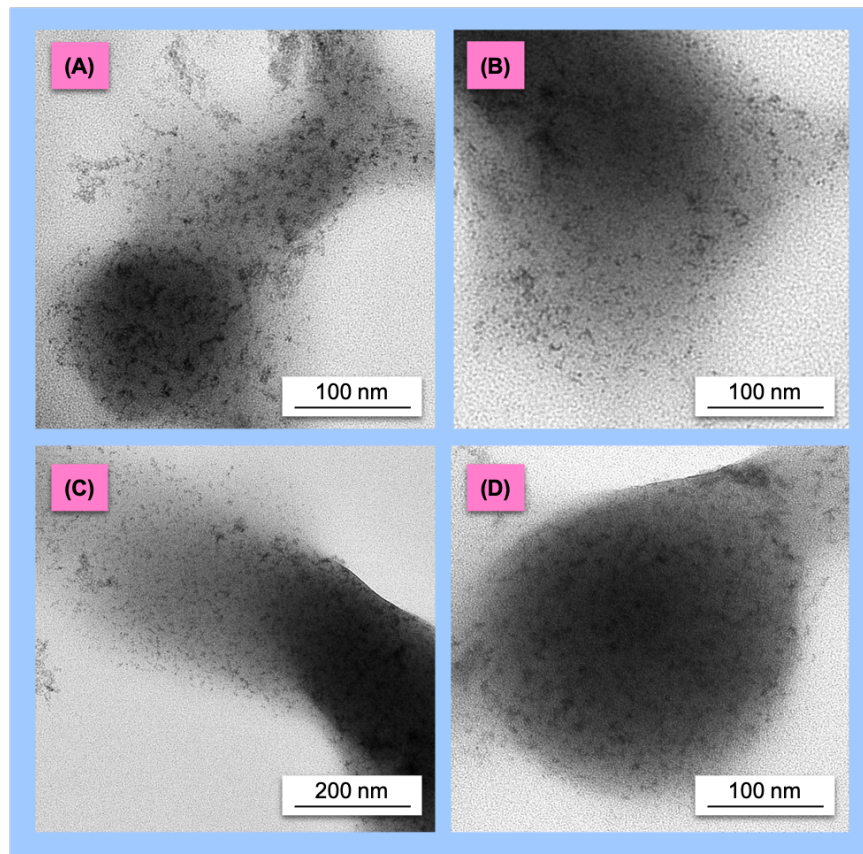


Figure 4.7. TEM micrographs for the **PCL/Eoxbc-0.1** composite, where the presence of **Eoxbc** nanostructures with approximate lengths of 9 nm embedded in the PCL matrix is shown.

4.2.4 Rheological Analysis of PCL/biochar Composites

PCL and the composites produced herein are rather brittle materials and will break

easily during traditional Dynamic Mechanical Analysis (DMA). Therefore, rheological analyses were performed to understand the viscoelastic properties of the materials, and their results are shown in **Figure 4.8**. The mechanical properties are sensitive to molecular weights, and reaction conditions were adapted to compare neat PCL and its composites with $M_n \sim 10,000$ g/mol. Moreover, 0.1 wt% of **oxbc** was mixed and blended with neat PCL to synthesize **Blend PCL/oxbc-0.1**, which would allow the assessment of oxidized biochar's effect as a support in the mechanical properties of the composites. M_n of polymers used in this study are shown in **Table 4.5**.

Table 4.5. Average molecular weights for the neat PCL and PCL/biochar composite samples produced for rheological measurements.

Entry	Sample	$M_{n, \text{NMR}}$ (g/mol) ^a	$M_{n, \text{GPC}}$ (g/mol) ^b
1	Neat PCL	10,300	15,900
2	Blend PCL/oxbc-0.1	9,800	10,100
3	PCL/Eoxbc-0.1	11,300	16,400
4	PCL/Eoxbc-0.5	9,700	11,100

^a Determined by ¹H NMR spectroscopy. ^b Determined by GPC using THF as a solvent. More information about the GPC analysis is shown in **Section 4.4.2**.

Rheological experiments of neat PCL and its composites in the melt state at 65 °C demonstrate the correlation between shear viscosity (η) and shear rate ($\dot{\gamma}$) (**Figure 4.8A**). For neat PCL and its blended composite, it is possible to notice η generally independent of $\dot{\gamma}$, thus showing a Newtonian flow behavior for these samples. However, **PCL/Eoxbc-0.1** and **PCL/Eoxbc-0.5** show decreasing η values at highest $\dot{\gamma}$, indicating the emergence

of shear thinning behavior. In addition, composites show higher η overall in comparison with neat PCL, and **PCL/Eoxbc-0.1** shows a higher η than its corresponding blend with the same biochar content. **PCL/Eoxbc-0.5** possesses lower η than its analogue containing 0.1 wt% of **Eoxbc**, which may be attributed to its lower molecular weight as well as the presence of a less uniform surface morphology, as previously observed via SEM.

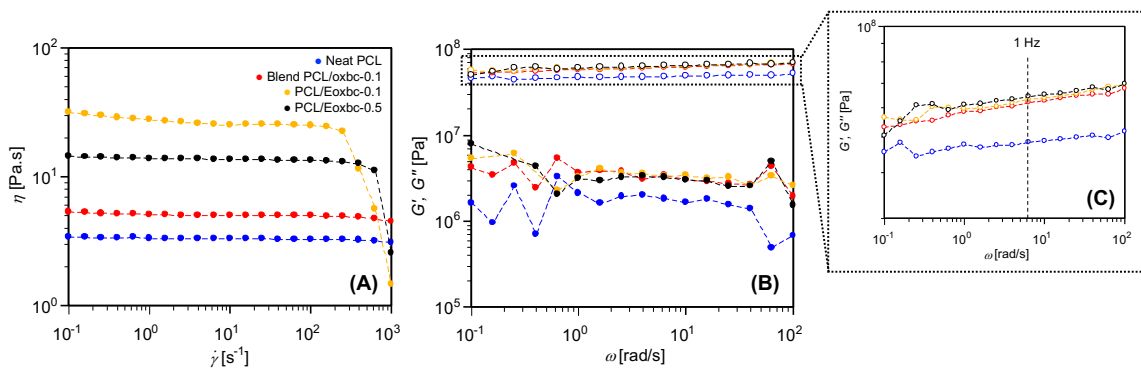


Figure 4.8. (A) Rheological analysis and correlation of the melt state shear viscosity for neat PCL and PCL/biochar composites containing $M_n \sim 10,000$ g/mol and (B) the solid state modulus (G' , open symbols) and loss modulus (G'' , closed symbols) over a range of oscillatory frequencies (ω). (C) Enhanced view of G' at 1 Hz ($\omega = 6.28$ rad/s).

For solid state rheology experiments (**Figure 4.8B** and **Figure 4.8C**), elastically dominated behavior is observed according to the significantly larger values of G' (storage modulus) in comparison with G'' (loss modulus) over the oscillatory frequency regime (ω). To provide a better comprehension of the trend in modulus behavior in the different types of polymers synthesized, a comparison of G' in **Figure 4.8B** is realized at a constant frequency of 1 Hz ($\omega = 6.28$ rad/s), as seen in **Table 4.6**. Although the modulus increase between the synthesized blend and the grafted composite is mild, the incorporation of

Eoxbc as a filler is able to provide an improvement of about 50% in the modulus of PCL (Table 4.6, Entries 1 and 3), thus confirming that biochar composites present better mechanical properties than the pure polymeric matrix. This behavior was expected through the known role of fillers in polymer matrices. Crystalline structures will dominate the solid-state mechanical response of the composites due to the absence of chain entanglements. The increased modulus in **PCL/Eoxbc** composites is also likely enhanced by the increase in X_c provided by the **Eoxbc** support.

Table 4.6. Viscosity (η) and storage modulus values (G') obtained during rheological experiments in melt and solid states for neat PCL and PCL/biochar composites.

Entry	Sample	η (Pa.s)	G' at 1 Hz (Pa)
1	Neat PCL	3.4	4.84×10^7
2	Blend PCL/oxbc-0.1	5.4	6.22×10^7
3	PCL/Eoxbc-0.1	31.2	6.36×10^7
4	PCL/Eoxbc-0.5	14.5	6.45×10^7

Melt state measurements also show a direct independent correlation between complex viscosity (η^*) of samples with oscillatory frequency (ω) (Figure 4.9A and Figure 4.9B). They also demonstrate the presence of a viscously dominating behavior due to the larger loss modulus (G'') in comparison with storage modulus (G') (Figure 4.9C). The grafted composite containing 0.1 wt% of **Eoxbc** has a viscosity almost 6 times higher than the corresponding blend with exactly the same biochar loading (Table 4.6, Entries 2 and 3). Although **PCL/Eoxbc-0.5** contains a larger number of particles embedded in the

polymer matrix, its viscosity is lower than PCL/Eoxbc-0.1 (Table 4.6, Entries 3 and 4), which could be also attributed to the absence of a completely uniform morphology.

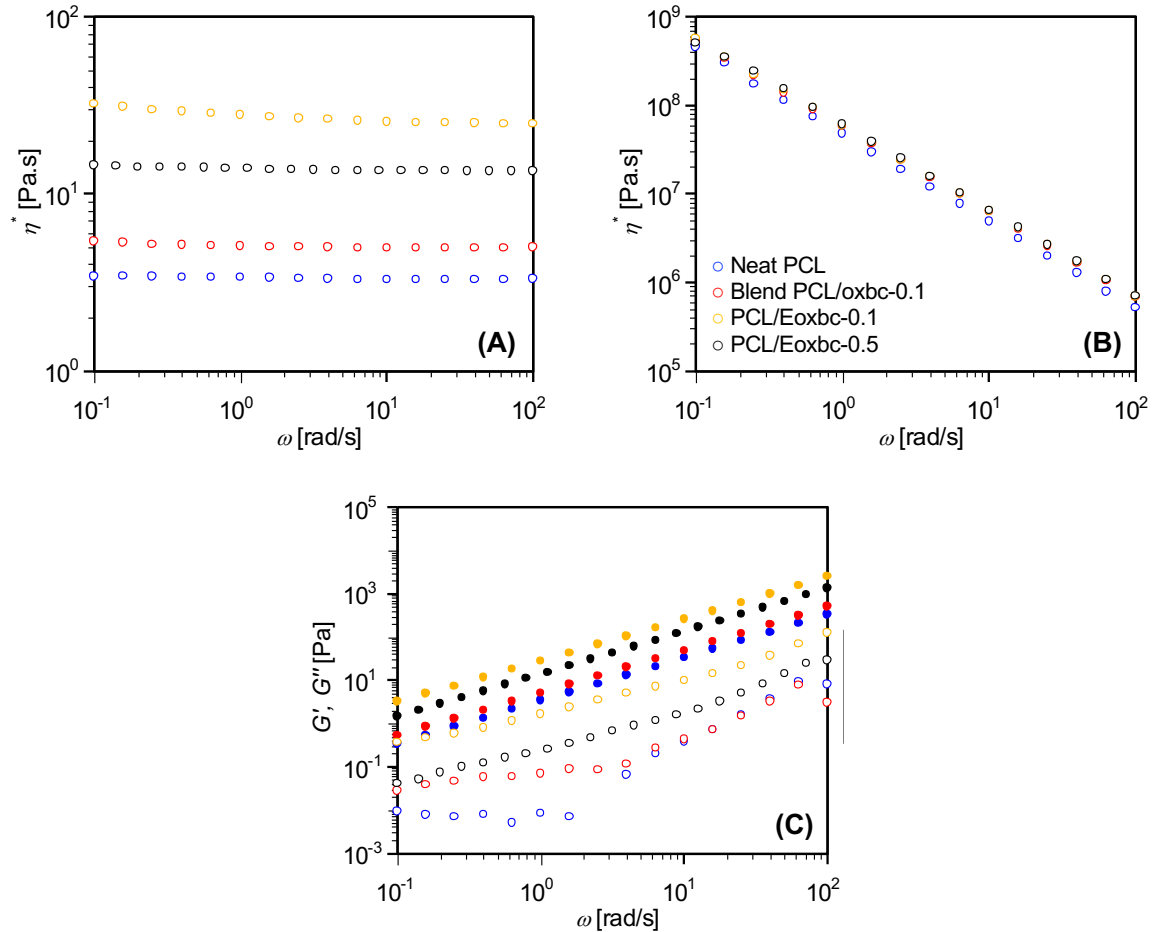


Figure 4.9. Rheological measurements for neat PCL and PCL/biochar composites with $M_n \sim 10,000$ g/mol and correlation between angular frequency (ω) with (A) complex viscosity (η^*) in the melt state, (B) complex viscosity (η^*) in the solid state, and (C) storage modulus (G') and loss modulus (G'') in the melt state.

Due to the shear response shown by PCL grafted composites in the melt state, we can presume that the PCL/biochar composites synthesized are unentangled polymers.

The entanglement molecular weight (M_c) of PCL was determined to be $\sim 20,000$ g/mol in a previous study.⁴⁵ The fact that $M_c < M_{n,\text{neat PCL}}$ and $M_c > M_{n,\text{PCL/Eoxbc-0.1}}$ under the same reaction conditions (i.e. 2 h, 110 °C) observed in **Table 4.2** also suggests that **Eoxbc** is acting as a support for the growth of unentangled PCL. The further decrease in M_n and increase in PCL conversions with the increase of **Eoxbc** up to 1.0 wt% loadings also indicates that the formation of a higher number of shorter unentangled PCL chains can be produced by using this bio-based material as a filler.

4.2.5 Preliminary Degradation Studies

To perform our preliminary degradation studies, neat PCL and **PCL/Eoxbc-0.1** were stirred for 28 days under different aqueous environments to provide a control evaluation without exposure to an enzyme. For samples immersed in deionized water and synthetic seawater, SEM images of **PCL/Eoxbc-0.1** (**Figure 4.10**) and the pure polymer (**Figure 4.11**) under those conditions show some degradations even in the absence of enzyme. As it can be observed from the baseline sample of a film stored in air (**Figure 4.10A** and **Figure 4.10B**), the surface of the PCL composite is mostly uniform and smooth, containing some fractures and pores previously associated with the incorporation of the heterogenous and dispersed phase of **Eoxbc**. Composite samples after shaking in deionized water (**Figure 4.10C** and **Figure 4.10D**) or synthetic seawater (**Figure 4.10E** and **Figure 4.10F**) displayed the presence of cracks on their borders, and fractures throughout and beneath their surface, thus suggesting some degree of

degradation.

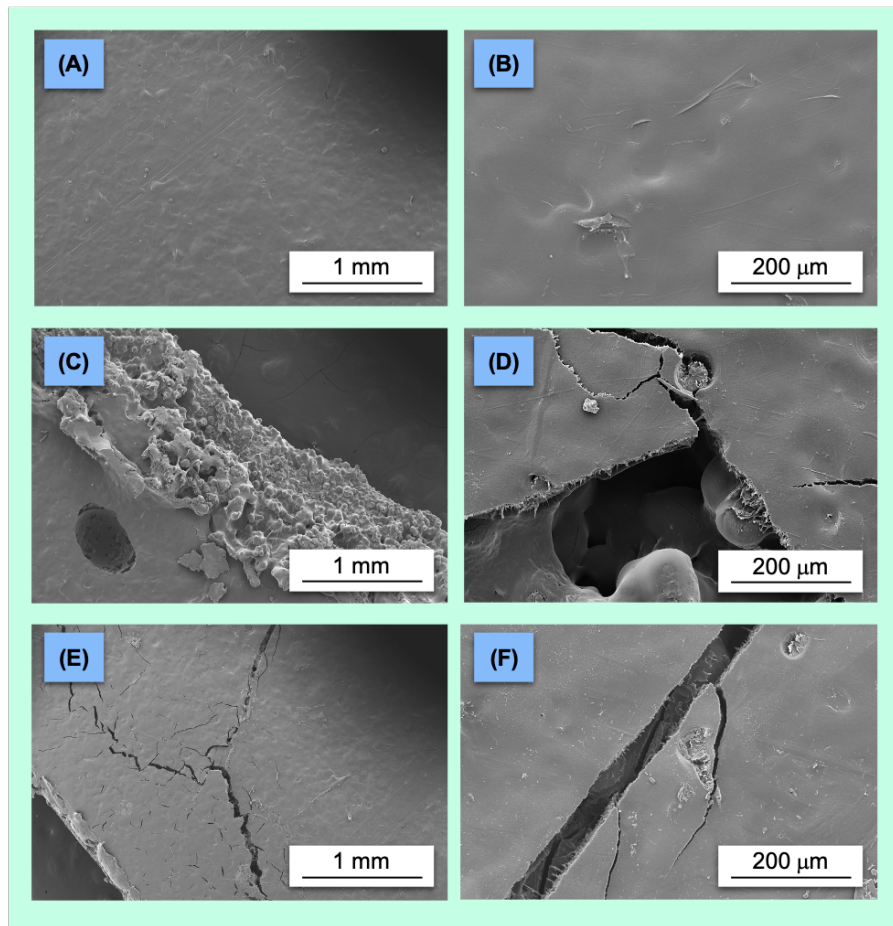


Figure 4.10. Representative SEM images for the surfaces of **PCL/Eoxbc-0.1** (A, B) stored in air, baseline samples, and after degradation studies in (C, D) deionized water, and (E, F) synthetic seawater.

Although both neat PCL and **PCL/Eoxbc-0.1** show some levels of degradation in the conditions studied herein, the respective composite appears to present greater degradation (i.e. more fractures) when compared to the pure polymer, especially in the presence of deionized water. As shown in **Figure 4.11**, PCL seems to simply wrinkle and crump rather than forming cracks and fractures, indicating that the presence of biochar

does affect polymer behavior in water.

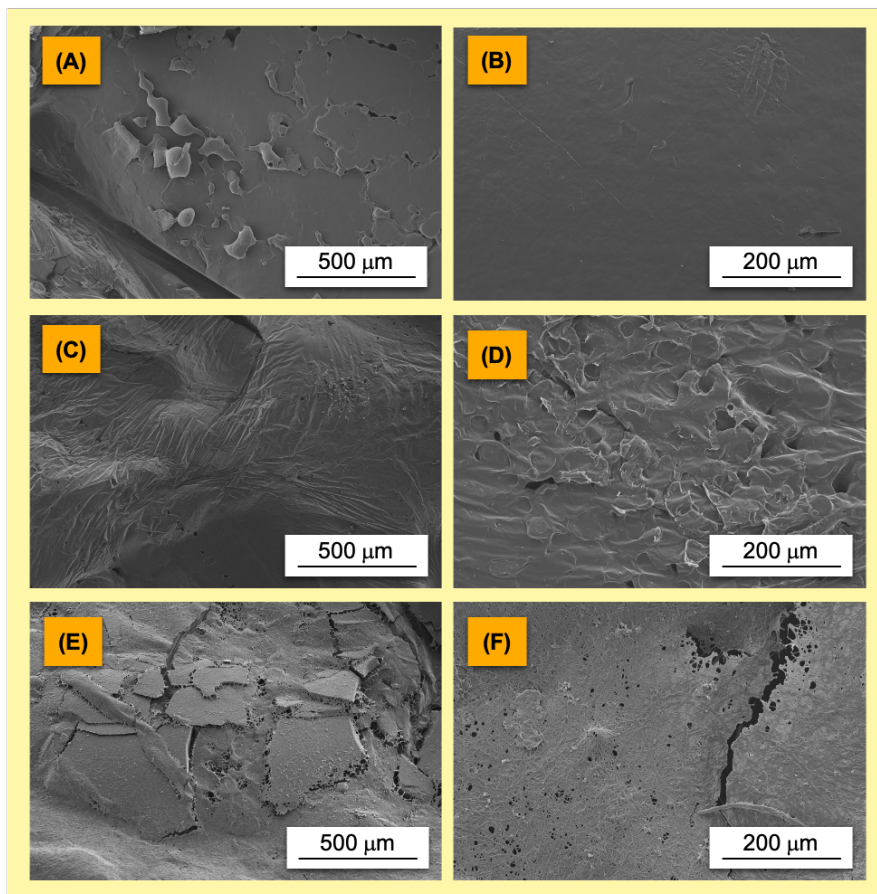


Figure 4.11. Representative SEM images for the surfaces of neat PCL after degradation studies in (A, B) air (control), (C, D) deionized water, and (E, F) synthetic seawater.

Mass loss can be used to estimate the extent of polymer degradation. For those reasons, PCL and **PCL/Eoxbc-0.1** samples were weighed before and after stirring in deionized water and synthetic seawater, and allowed to air dry (**Table 4.7** and **Table 4.8**). The PCL composite shows higher mass reduction in both of the environments studied (**Table 4.8, Entry 4**) when compared to the neat polymer (**Table 4.7, Entry 4**). These results suggest a positive effect of **Eoxbc** upon PCL's degradation, and also strengthen the

hypothesis of higher biodegradation levels achieved for **PCL/Eoxbc-0.1** previously suggested by SEM. It is worth mentioning that the mass difference serves only as an estimation of degradation levels of the samples.

Table 4.7. Analysis of the degradability of neat PCL.

Entry	Parameter	Neat PCL in deionized water	Neat PCL in synthetic seawater
1	Original mass (mg)	37.8	28.5
2	After 28 days of stirring (mg)	41.3	35.4
3	After 2 days of drying (mg)	37.0	28.4
4	Mass loss (%)	2.12	0.35

Table 4.8. Analysis of the degradability of the **PCL/Eoxbc-0.1** composite.

Entry	Parameter	PCL/Eoxbc-0.1 in deionized water	PCL/Eoxbc-0.1 in synthetic seawater
1	Original mass (mg)	58.9	57.4
2	After 28 days of stirring (mg)	60.8	57.1
3	After 2 days of drying (mg)	56.5	56.5
4	Mass loss (%)	4.07	1.57

A slightly different behavior was observed for the biodegradation of neat PCL and its composite under enzymatic conditions. A commercially available lipase enzyme, Novozyme® 51032 (N51032), was chosen for these studies, as it has been used in previous investigations regarding PCL degradation.⁴⁶ After only 3 days of stirring, samples fractured and shattered into smaller pieces, and microbial growth was observed on PCL

and **PCL/Eoxbc-0.1** films after 11 days. After 28 days, the films treated with enzyme had disappeared. Further characterization of the microbes present was achieved through genetic sequencing, and further details about this investigation can be found in **Appendix C: Information for Chapter 4**. Microbes that grew on the neat PCL film were identified as *Debaryomyces* fungi and *Paraburkholderia* bacteria. The hypothesized species of fungi are *D. prosopidis*, which can be isolated from the exudate of mesquite trees,⁴⁷ and *D. udenii*, which can be found in soil.⁴⁸ The two hypothesized species of bacteria are *P. madseniana* or *P. fungorum*.⁴⁹ *P. madseniana* are recently discovered bacteria, with great performance for breaking down organic matter including cancer-causing chemicals, and for mitigating climate change effects.⁵⁰ *P. fungorum* have been used to improve growth, yields, and contents of antioxidants in plants.⁵¹ In addition to *Paraburkholderia* bacteria, two species of fungi grew on the **PCL/Eoxbc-0.1** film. *Exophiala oligosperma* and *Simplicillium Chinese* are usually isolated from environmental sources, such as soil or water.^{52, 53} These preliminary degradation results suggest that the materials described herein can support growth of microbes that are present in the natural environment.

4.3 Conclusions

In this work, the first attempt to improve PCL mechanical properties and increase its degradation using a sustainable approach driven by the incorporation of biochar is reported. Through oxidation and further sonication, stable dispersions of biochar containing significant amounts of hydroxyl groups (**Eoxbc**) in ϵ -CL can initiate the ROP

of the monomer to produce **PCL/Eoxbc** composites. The incorporation of very small loadings of **Eoxbc** (i.e. 0.1 wt%) are sufficient to accelerate the production and increase the crystallinity of the composites by heterogeneous nucleation. Although high filler contents (i.e. 5.0 wt%) seem to promote agglomeration and are detrimental to the yields of polymer produced, they improved the thermal stability of PCL.

Compared to neat PCL, the composites containing biochar are more viscous, present a shear thinning behavior, and also higher storage and loss moduli in the melt and solid states. Preliminary tests also suggest higher levels of degradation of the composites in comparison with the pure polymer. The accurate extent of degradation will be explored in the future using Total Organic Carbon analysis. Nevertheless, the work presented in this Chapter represents a proof-of-concept that **Eoxbc** can work as an important nexus solution for tackling some of our current sustainability challenges. The utilization of a waste-derived material with significant climate change mitigation potential for the further production of bio-based and biodegradable polymers is a process entirely aligned with the Principles of Green Chemistry. Such applications could play a significant role in the implementation of a circular economy.

4.4 Experimental

4.4.1 General Materials

Pristine hardwood biochar samples were provided by Cape Breton University (Sydney, NS) and prepared by the anaerobic pyrolysis of debarked birch wood at 400 °C

for 30 min, followed by rapid quenching in cold water.⁵⁴ Chemicals including solvents were purchased from Sigma Aldrich or Fisher Scientific and used as received. The enzymes used in this study including Novozyme[®] 51032 (N51032), Novozyme[®] 435 (N435), and *Candida antarctica* lipase B (CALB) were purchased from Strem Chemicals. Synthetic seawater was prepared by dissolving sea salts purchased from Sigma Aldrich in deionized water to a concentration of 33 g/L, the global average salinity of seawater.⁵⁵

4.4.2 Instrumentation

DSC data were collected on a Mettler Toledo DSC1 Star^e System under N₂ flow of 50 mL/min and a scanning rate of 10 °C/min. Neat PCL and PCL/biochar composites (5 mg) were sealed in aluminum pans, melted at 140 °C and then cooled to -70 °C. Samples were held for one minute at both the initial and final temperatures. The procedure was repeated more than two times to remove the thermal history of polymers. Both the third and cooling scans were used for analysis. Values of degree of crystallinity (X_c) were obtained from the melting enthalpy (ΔH_m) of samples, using the Star^e software and the melting enthalpy of 100% PCL ($\Delta H_m^{100} = 139.5$ J/g) as a reference.^{56, 57}

FT-IR spectra were obtained using a Bruker Alpha FT-IR spectrometer fitted with as single-bounce diamond attenuated total reflection (ATR) accessory (400 to 4000 cm⁻¹ wavelength, 32 scans per sample, resolution of 4 cm⁻¹). All measurements were collected in triplicates, averaged, and further plotted for analysis.

GPC analyses were performed on a setup consisting of a miniDawn TREOS light-

scattering detector, a Viscostar-II viscometer, and an Optilab T-rEX differential refractive index detector (Wyatt Technology). These were connected to an Agilent Infinity 1260 HPLC system equipped with two Phenogel 10^3 \AA 300 x 4.60 mm column. THF was used as an eluent and also to prepare the samples at a concentration of approximately 4 mg/mL, which were filtered through a 0.2 μm syringe filter and further analyzed at a flow rate of 0.3 mL/min at 25 °C. Refractive index increment (dn/dc) values were calculated online (columns detached) assuming 100% mass recovery using the Astra 6 software package (Wyatt Technologies). Obtained dn/dc values of polymers: Neat PCL = 0.0791 mL/g, **PCL/Eoxbc** (SnOct₂) = 0.0688 mL/g, **PCL/Eoxbc** (DABCO) = 0.0883 mL/g, **PCL/Eoxbc** (DBU) = 0.0515 mL/g, **PCL/Eoxbc** (N435) = 0.1213 mL/g, **PCL/Eoxbc** (CALB) = 0.1706 mL/g, **PCL/Eoxbc-0.5** = 0.0695 mL/g, **PCL/Eoxbc-1.0** = 0.0674 mL/g, **PCL/Eoxbc-5.0** = 0.0666 mL/g.

¹H NMR spectra were obtained on a Bruker AVANCE™ 300 MHz spectrometer at 298 K in CDCl₃. Deuterated solvents were purchased from Cambridge Isotope Laboratories and used without purification. Residual protio-solvent peaks were used as internal standards, and chemical shifts are reported as δ (ppm) values.

For SEM analysis, polymer films with approximate dimensions of 0.5 x 0.5 x 0.1 cm were prepared, coated with gold, and analyzed on a FEI 650 MLA FEG SEM. An ETD detector was used, with a high voltage of 15.00 kV, and approximate working distance of 10 mm. The images were taken under high vacuum (10^{-6} Torr).

TGA was performed using a TA Instruments Q500 TGA under high resolution

dynamic mode. Approximately 20 mg of sample were heated at a rate of 10 °C/min under N₂ gas flow of 50 mL/min from room temperature to 800 °C.

TEM characterization of PCL/biochar composites were carried out at Cape Breton University (Sydney, NS) using a Hitachi HT7700 Transmission Electron Microscope containing a tungsten filament in high contract (HC) mode at 80 kV.

4.4.3 Exfoliation of Biochar and Preparation of PCL/Biochar Grafted Composites

Preparation of pristine biochar, **oxbc**, and **Eoxbc** can be found in Sections 2.4.3, 2.4.4, and 3.4.3, respectively. In a typical experiment, PCL/biochar composites were prepared via ring-opening polymerization of ϵ -CL using Sn(oct)₂ as a catalyst. In a glass vial, 5.0 g of ϵ -CL were added to 5 mg of **oxbc** (0.1 wt%). Samples were directly sonicated for 15 min using a Misonix S-4000 Sonicator using an amplitude of 50% and providing a sonic energy of about 37 MJ, thus producing exfoliated oxidized biochar (**Eoxbc**) in ϵ -CL. Sn(oct)₂ (1 mol%) was added to the black dispersion, which was then heated to 110 °C under vigorous stirring for 2 h in an aluminum heating block. After the required reaction time, the grey reaction mixture was dissolved in CH₂Cl₂ (30 mL), precipitated in *n*-hexane (60 mL), further dried at 60 °C under vacuum overnight, and identified as **PCL/Eoxbc-0.1**. Confirmation of grafting of PCL onto the surface of **Eoxbc** was obtained via Soxhlet extraction. About 1.5 g of **PCL/Eoxbc-0.1** was placed in a 24 x 80 mm cellulose Soxhlet extraction thimble and refluxed at 60 °C using CH₂Cl₂ (200 mL) as a solvent. After 6 h, the system was cooled down, and the thimble and round bottom flask used were dried

under vacuum overnight to calculate grafting percentage (G%).

4.4.4 Rheological Analysis

For rheological measurements, PCL samples with $M_n \sim 10,000$ g/mol were synthesized via ROP of ϵ -CL at 110 °C for 45 min using 1 mol% of $\text{Sn}(\text{oct})_2$ as a catalyst. Half of the polymer obtained after dissolution, precipitation, and drying was stored (neat PCL). The other half was dissolved in CH_2Cl_2 (5 mL) and mixed with 0.1 wt% of **oxbc** using a stirring rod for about 5 min. The sample was then further dried in a vacuum oven at 60 °C overnight to produce **Blend PCL/oxbc-0.1**. For the synthesis of **PCL/Eoxbc-0.5** containing $M_n \sim 10,000$ g/mol, the procedure for preparation of PCL/biochar grafted composites described in **Section 4.4.3** was repeated using 0.5 wt% of **Eoxbc** and a reaction time of 2.5 h. The rheological properties of the composites were analyzed by B. M. Yavitt (University of British Columbia) in a MCR 501 shear rheometer (Anton Paar) equipped with a cone-and-plate geometry (CP) and parallel plate (PP) geometries (25 mm in diameter). Bulk samples were placed into the rheometer at 65 °C for sufficient time to be melted before testing. The shear viscosity (η) in the melt state (65 °C) was measured over a range of shear rates ($\dot{\gamma} = 0.1\text{-}1000$ s⁻¹) using the CP geometry. The storage (G') and loss modulus (G'') were also measured over a range of oscillatory frequencies ($\omega = 0.1\text{-}100$ rad/s) at applied strain amplitude of $\gamma = 10\%$. For solid state characterization, the composites were loaded in the PP fixture, cooled to 25 °C, and equilibrated for 10 min. G' and G'' were measured over a range of oscillatory frequency $\omega = 0.1\text{-}100$ rad/s at an

applied strain amplitude of $\gamma = 0.005\%$, found to be within the linear viscoelastic regime and below the yield strain of the composites.

4.4.5 Degradation Studies

Control degradation studies were performed by M. D. Wheeler (Memorial University of Newfoundland) by adding 30-60 mg of neat PCL or **PCL/Eoxbc-0.1** films in 100 mL of deionized water or synthetic seawater. Samples were stirred for 28 days on a shaker plate, removed from solution, and weighed to determine mass loss (before and after air drying). For enzymatic degradation studies, 750 μL of N51032 was added to 30-60 mg of neat PCL or **PCL/Eoxbc-0.1** films previously shaken in deionized water for 48 h. After 30 days under ambient light and shaking, no polymer was visible. Microbial samples visible during degradation were further cultured by C. S. Sit, J. L. Kolwich and L. N. Donovan (Saint Mary's University) on 100% yeast mold agar plates and further sent to GenomeQuebec for analysis. Genetic sequences obtained were then cross-referenced with BLAST and UNITE databases to find the most probable identity of each microbe.

4.5 References

1. Vidal, J. L.; Yavitt, B. M.; Wheeler, M. D.; Kolwich, J. L.; Donovan, L. N.; Sit, C. S.; Hatzikiriakos, S. V.; Jalsa, N. K.; MacQuarrie, S. L.; Kerton, F. M., *Submitted, ACS Sustain. Chem. Eng. (sc-2021-06375x)* **2021**.
2. Labet, M.; Thielemans, W., *Chem. Soc. Rev.* **2009**, *38*, 3484-3504.
3. Woodruff, M. A.; Hutmacher, D. W., *Prog. Polym. Sci.* **2010**, *35*, 1217-1256.
4. Gregory, G. L.; López-Vidal, E. M.; Buchard, A., *Chem. Commun.* **2017**, *53*, 2198-2217.
5. Zini, E.; Scandola, M., *Polym. Compos.* **2011**, *32*, 1905-1915.
6. Lambert, S.; Wagner, M., *Chem. Soc. Rev.* **2017**, *46*, 6855-6871.
7. Balazs, A. C.; Emrick, T.; Russell, T. P., *Science* **2006**, *314*, 1107-1110.
8. Simão, J. A.; Bellani, C. F.; Branciforti, M. C., *J. Appl. Polym. Sci.* **2017**, *134*, 44493-44502.
9. Papadimitriou, L.; Kaliva, M.; Vamvakaki, M.; Chatzinikolaidou, M., *ACS Biomater. Sci. Eng.* **2017**, *3*, 1341-1349.
10. Ermeydan, M. A.; Cabane, E.; Hass, P.; Koetz, J.; Burgert, I., *Green Chem.* **2014**, *16*, 3313-3321.
11. Bellani, C. F.; Pollet, E.; Hebraud, A.; Pereira, F. V.; Schlatter, G.; Avérous, L.; Bretas, R. E. S.; Branciforti, M. C., *J. Appl. Polym. Sci.* **2016**, *133*, 43445-43453.
12. Najarro, M. C.; Nikolic, M.; Iruthayaraj, J.; Johannsen, I., *ACS Appl. Polym. Mater.* **2020**, *2*, 5767-5778.

13. Park, I.-K.; Sun, H.; Kim, S.-H.; Kim, Y.; Kim, G. E.; Lee, Y.; Kim, T.; Choi, H. R.; Suhr, J.; Nam, J.-D., *Sci. Rep.* **2019**, *9*, 7033-7044.
14. Habibi, Y.; Goffin, A.-L.; Schiltz, N.; Duquesne, E.; Dubois, P.; Dufresne, A., *J. Mater. Chem.* **2008**, *18*, 5002-5010.
15. Zhang, Q.; Khan, M. U.; Lin, X.; Cai, H.; Lei, H., *Compos. B. Eng.* **2019**, *175*, 107151-107158.
16. Behazin, E.; Misra, M.; Mohanty, A. K., *Compos. B. Eng.* **2017**, *118*, 116-124.
17. Arrigo, R.; Jagdale, P.; Bartoli, M.; Tagliaferro, A.; Malucelli, G., *Polymers* **2019**, *11*, 1336-1351.
18. Zhang, Q.; Zhang, D.; Lu, W.; Khan, M. U.; Xu, H.; Yi, W.; Lei, H.; Huo, E.; Qian, M.; Zhao, Y.; Zou, R., *Sci. Total Environ.* **2020**, *738*, 139910-139919.
19. Li, S.; Huang, A.; Chen, Y.-J.; Li, D.; Turng, L.-S., *Compos. B. Eng.* **2018**, *153*, 277-284.
20. Stürzel, M.; Mihan, S.; Mülhaupt, R., *Chem. Rev.* **2016**, *116*, 1398-1433.
21. Poulouse, A. M.; Elnour, A. Y.; Anis, A.; Shaikh, H.; Al-Zahrani, S. M.; George, J.; Al-Wabel, M. I.; Usman, A. R.; Ok, Y. S.; Tsang, D. C. W.; Sarmah, A. K., *Sci. Total Environ.* **2018**, *619-620*, 311-318.
22. Das, O.; Kim, N. K.; Hedenqvist, M. S.; Lin, R. J. T.; Sarmah, A. K.; Bhattacharyya, D., *Environ. Manage.* **2018**, *62*, 403-413.
23. Pudelko, A.; Postawa, P.; Stachowiak, T.; Malińska, K.; Drózdź, D., *J. Clean. Prod.* **2021**, *278*, 123850-12856.

24. Qian, S.; Yan, W.; Zhu, S.; Fontanillo Lopez, C. A.; Sheng, K., *Polym. Compos.* **2018**, *39*, 633-639.
25. Arrigo, R.; Bartoli, M.; Malucelli, G., *Polymers* **2020**, *12*, 892-905.
26. Ho, M.-P.; Lau, K.-T.; Wang, H.; Hui, D., *Compos. B. Eng.* **2015**, *81*, 14-25.
27. Qian, S.; Tao, Y.; Ruan, Y.; Fontanillo Lopez, C. A.; Xu, L., *J. Mater. Res.* **2018**, *33*, 3870-3879.
28. Qian, S.; Sheng, K.; Yao, W.; Yu, H., *J. Appl. Polym. Sci.* **2016**, *133*, 43425-43434.
29. Das, O.; Sarmah, A. K.; Bhattacharyya, D., *Sci. Total Environ.* **2015**, *512-513*, 326-336.
30. Nan, N.; DeVallance, D. B., *J. Mater. Sci.* **2017**, *52*, 8247-8257.
31. Ogunsona, E. O.; Codou, A.; Misra, M.; Mohanty, A. K., *J. Polym. Environ.* **2018**, *26*, 3574-3589.
32. Picard, M.; Thakur, S.; Misra, M.; Mielewski, D. F.; Mohanty, A. K., *Sci. Rep.* **2020**, *10*, 3310-3324.
33. Saeed, K.; Park, S.-Y., *J. Appl. Polym. Sci.* **2007**, *104*, 1957-1963.
34. Zeng, H. L.; Gao, C.; Yan, D. Y., *Adv. Funct. Mater.* **2006**, *16*, 812-818.
35. Wang, Y.; Li, T.; Ma, P.; Zhang, S.; Du, M.; Dong, W.; Xie, Y.; Chen, M., *New J. Chem.* **2018**, *42*, 10348-10356.
36. Murray, E.; Sayyar, S.; Thompson, B. C.; Gorkin Iii, R.; Officer, D. L.; Wallace, G. G., *RSC Adv.* **2015**, *5*, 45284-45290.
37. Wang, M.; Deng, X.-Y.; Du, A.-K.; Zhao, T.-H.; Zeng, J.-B., *RSC Adv.* **2015**, *5*, 73146-73154.

38. Zhang, J.; Qiu, Z., *Ind. Eng. Chem. Res.* **2011**, *50*, 13885–13891.
39. Albertsson, A.-C.; Srivastava, R. K., *Adv. Drug Delivery Rev.* **2008**, *60*, 1077-1093.
40. Hege, C. S.; Schiller, S. M., *Green Chem.* **2014**, *16*, 1410-1416.
41. Mansoori, Y.; Akhtarparast, A.; Reza Zamanloo, M.; Imanzadeh, G.; Masooleh, T. M., *Polym. Compos.* **2011**, *32*, 1225-1234.
42. Mansoori, Y.; Khodayari, A.; Banaei, A.; Mirzaeinejad, M.; Azizian-Kalandaragh, Y.; Pooresmaeil, M., *RSC Adv.* **2016**, *6*, 48676-48683.
43. Comer, C. M.; Jessop, J. L. P., *Starch - Stärke* **2008**, *60*, 335-339.
44. Nizamuddin, S.; Jadhav, A.; Qureshi, S. S.; Baloch, H. A.; Siddiqui, M. T. H.; Mubarak, N. M.; Griffin, G.; Madapusi, S.; Tanksale, A.; Ahamed, M. I., *Sci. Rep.* **2019**, *9*, 5445-5456.
45. Izuka, A.; Winter, H. H.; Hashimoto, T., *Macromolecules* **1992**, *25*, 2422-2428.
46. De Hoe, G. X.; Zumstein, M. T.; Tiegs, B. J.; Brutman, J. P.; McNeill, K.; Sander, M.; Coates, G. W.; Hillmyer, M. A., *J. Am. Chem. Soc.* **2018**, *140*, 963-973.
47. Phaff, H. J.; Vaughan-Martini, A.; Starmer, W. T., *Int. J. Syst. Evol. Microbiol.* **1998**, *48*, 1419-1424.
48. Van Der Walt, J. P.; Smith, M. T.; Yamada, Y., *Antonie van Leeuwenhoek* **1989**, *56*, 233-239.
49. Webster, G.; Mullins, A. J.; Bettridge, A. S.; Jones, C.; Cunningham-Oakes, E.; Connor, T. R.; Parkhill, J.; Mahenthiralingam, E., *Microbiol. Resour. Announc.* **2019**, *8*, 1-4.

50. Wilhelm, R. C.; Murphy, S. J. L.; Feriancek, N. M.; Karasz, D. C.; DeRito, C. M.; Newman, J. D.; Buckley, D. H., *Int. J. Syst. Evol. Microbiol.* **2020**, *70*, 2137-2146.
51. Rahman, M.; Sabir, A. A.; Mukta, J. A.; Khan, M. M. A.; Mohi-Ud-Din, M.; Miah, M. G.; Rahman, M.; Islam, M. T., *Sci. Rep.* **2018**, *8*, 2504-2515.
52. Zhao, D.; Liu, B.; Li, L. Y.; Zhu, X. F.; Wang, Y. Y.; Wang, J. Q.; Duan, Y. X.; Chen, L. J., *Biocontrol Sci. Techn.* **2013**, *23*, 980-986.
53. Estévez, E.; Veiga, M. C.; Kennes, C., *Appl. Microbiol. Biotechnol.* **2005**, *67*, 563-568.
54. Carrier, A. J.; Abdullahi, I.; Hawboldt, K. A.; Fiolek, B.; MacQuarrie, S. L., *J. Phys. Chem. C* **2017**, *121*, 26300-26307.
55. US Dept of Commerce, National Weather Service, National Oceanic and Atmospheric Administration. Sea Water.
<https://www.weather.gov/jetstream/seawater#:~:text=Sea%20water%20salinity%20is%20expressed,33%E2%80%B0%20%2D%2037%E2%80%B0> (accessed May 29, 2021).
56. Brandrup, J.; Immergut, E. H.; Grulke, E. A., *Polymer Handbook*. 4th ed.; Wiley: New York, 1999.
57. Izquierdo, R.; Garcia-Giralt, N.; Rodriguez, M. T.; Cáceres, E.; García, S. J.; Gómez Ribelles, J. L.; Monleón, M.; Monllau, J. C.; Suay, J., *J. Biomed. Mater. Res. A* **2008**, *85A*, 25-35.

CO-AUTHORSHIP STATEMENT

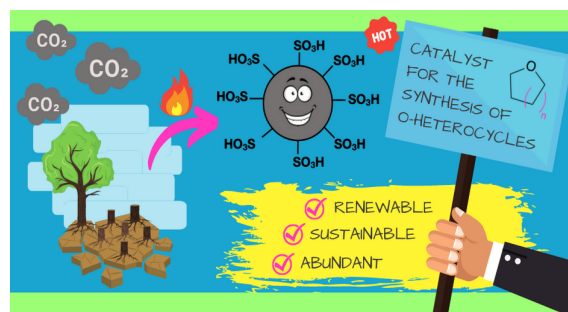
Chapter 5: Green Ring-Closing Metathesis of Aliphatic Ethers and Esterification of Terpene Alcohols Catalyzed by Biochar Catalysts. Juliana L. Vidal, Olivia M. Wyper, Stephanie L. MacQuarrie, and Francesca M. Kerton. This chapter has been submitted for publication.¹

The first author (Juliana L. Vidal) contributed 90% of the content of the article as the main researcher, including performing the experiments, collecting and analyzing data, and writing the manuscript.

The co-author (Olivia M. Wyper) was responsible for performing initial experiments on the esterification reactions in the terpene alcohols.

The co-author (Stephanie L. MacQuarrie), my co-supervisor, was responsible for suggesting experiments, assisting with data interpretation, and revising the manuscript.

The corresponding author (Francesca M. Kerton), my supervisor, was the principal investigator of this work. She came up with the concept, suggested initial experiments, assisted with interpreting data, revised, and submitted the manuscript.



References for **Chapter 5** can be found on **Pages 205-206**.

CHAPTER 5: GREEN RING-CLOSING METATHESIS OF ALIPHATIC ETHERS AND ESTERIFICATION OF TERPENE ALCOHOLS CATALYZED BY BIOCHAR CATALYSTS

5.1 Introduction

The ring-closing C-O/C-O metathesis of aliphatic ethers has emerged as an efficient strategy to prepare cyclic ethers, including tetrahydrofurans, tetrahydropyrans, morpholines, and dioxanes.^{2,3} These *O*-heterocycles are widely used in industry, and are usually obtained by methods with a higher overall number of synthetic steps, use of toxic reagents, or expensive precious metal catalysts.⁴⁻⁷ Morandi and co-workers studied different Lewis acid catalysts for ether ring-closing metathesis reactions, with the optimized system using iron triflate (FeOTf₃) in *n*-hexane.² Although good yields of various cyclic ethers were obtained and detailed mechanistic studies were performed, the metal-based system suffers from separation difficulty, toxicity, and moisture sensitivity.² To address these challenges, Liu and co-workers described the use of ionic liquids (ILs) as heterogeneous catalysts for the same reaction.³ In this catalytic system, the ether is synergically activated by hydrogen-bonding with the cationic and anionic portions of the IL containing sulfonate (-SO₃H) and trifluoromethanesulfate (triflate, -OTf) groups, respectively.³ Although the heterogeneous system proposed in this work is efficient and recyclable, general concerns over toxicity and biodegradability of ILs further limit their applications.^{8,9}

Carbon-based materials can tackle some of the challenges presented by previous catalysts used in the ring-closing metathesis of aliphatic ethers. However, they are often

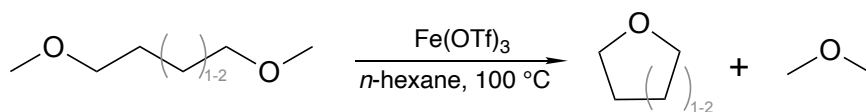
produced from fossil fuel precursors via chemical vapor deposition, electric-arc discharge, and laser ablation techniques, which require harsh synthetic conditions.¹⁰ The overall sustainability of those materials can be further increased using renewable, abundant, and inexpensive feedstocks.^{10, 11} In this context, the diversification of biochar applications represents an important approach. The functionalization of biochar can further improve its applications as a catalyst and advanced material, with its sulfonation being one of the most common processes.^{12, 13}

As previously mentioned in **Section 1.3.3**, sulfonated biochar (**sbc**) has been used to facilitate several chemical reactions, most of them related to the hydrolysis of biomass and the esterification of fatty acids to produce biodiesel.¹³⁻¹⁵ In this regard, the esterification of terpene alcohols catalyzed by biochar is also an important strategy for the synthesis of important compounds that has not been studied to this date. Although the products obtained are widely applied in the food, perfume, cosmetic, and pharmaceutical industries, this reaction is traditionally facilitated by toxic or corrosive catalysts.^{14, 15}

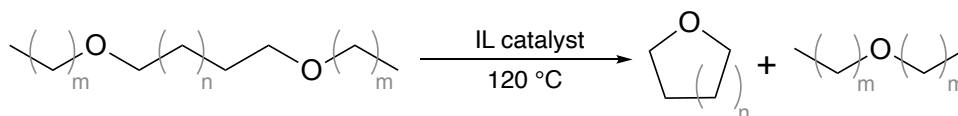
Given (i) the presence of $-\text{SO}_3\text{H}$ groups on the surface of **sbc** that could promote the synthesis of *O*-heterocycles, (ii) the previously demonstrated ability of functionalized biochar to function as an efficient catalyst via a hydrogen-bonding mechanism, and (iii) the lack of studies using **sbc** as an alternative catalyst for the synthesis of terpene esters, the investigation of **sbc** as a heterogeneous catalyst for the ring-closing metathesis of aliphatic ethers and the esterification of terpene alcohols is pursued in this Chapter. The system herein proposed achieves good conversions to *O*-heterocycles and terpene esters

under neat conditions and represents a sustainable approach for the synthesis of valuable chemicals from renewable feedstocks (Figure 5.1).

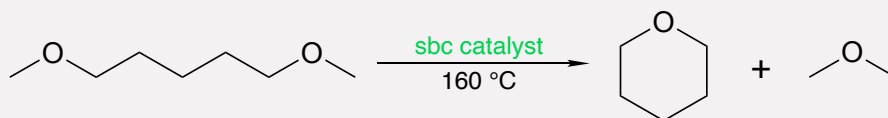
Iron-catalyzed ring-closing metathesis (Ref. 2)



Ionic liquid-catalyzed ring-closing metathesis (Ref. 3)



Sulfonated biochar-catalyzed ring-closing metathesis (This work)



- ✓ First carbon-based material used for the ring-closing C-O/C-O metathesis.
- ✓ Renewable, sustainable, inexpensive catalyst obtained from waste.
- ✓ Performed under neat conditions.

Figure 5.1. A comparison between the previous catalytic systems studied for the ring-closing C-O/C-O metathesis of aliphatic ethers and the catalytic system proposed herein using sbc.

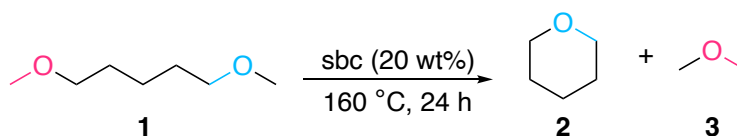
5.2 Results and Discussion

5.2.1 Ring-Closing Metathesis of 1,5-dimethoxypentane

The investigation of sbc as a catalyst for the ring-closing C-O/C-O metathesis of aliphatic ethers was initially performed using the conversion of 1,5-dimethoxypentane **1** to tetrahydropyran **2** as our model reaction system. The reaction conditions were chosen based on previous works in the literature,^{2,3} and the results obtained during our initial

studies are shown in **Table 5.1**. Reactions were carried out under neat conditions, performed in triplicate to assess reproducibility ($SD \leq 4.8\%$), with conversions calculated using 1,3,5-trimethylbenzene (i.e. mesitylene) as an internal standard.

Table 5.1. Optimization of the ring-closing C-O/C-O metathesis of aliphatic ethers using the conversion of 1,5-dimethoxypentane **1** to tetrahydropyran **2** as a model reaction system, and different types of biochar as catalysts.^a



Entry	Catalyst	T (°C)	t (h)	Conversion (%) ^f
1	-	140	24	0.0
2	bc	140	24	0.0
3	oxbc	140	24	2.0
4	sbc	140	24	44.8
5 ^b	sbc	140	24	43.8
6 ^c	sbc	140	24	21.7
7 ^d	sbc	140	24	61.7
8 ^e	sbc	140	24	68.5
9	sbc	140	48	81.3
10	sbc	160	24	75.2

^a General reaction conditions unless otherwise stated: 1,5-dimethoxypentane (**1**, 2 mmol), catalyst (20 wt%).

^b Under N₂ atmosphere. ^c *n*-hexane (1 mL). ^d LiOTf (5 wt%). ^e sbc (30 wt%, 75 mg). ^f Determined by ¹H NMR spectroscopy using mesitylene as an internal standard.

In the absence of the catalyst and in the presence of **bc**, no reaction was seen (**Table**

5.1, Entries 1 and 2), whilst low conversions to **2** were obtained **oxbc** (Table 5.1, Entry 3). Under the same reaction conditions, 44.8% conversion to **2** was obtained employing **sbc** as a catalyst (Table 5.1, Entry 4). Previous ring-closing C-O/C-O metathesis reactions required the use of an inert atmosphere or used *n*-hexane as a solvent.^{2,3} In these previous studies, the ability of the triflate anion [OTf]⁻ to facilitate and promote the reaction via hydrogen-bonding was demonstrated mechanistically.² For these reasons, similar conditions were explored and compared. Conversions of **1** to **2** under N₂ atmosphere (Table 5.1, Entry 5) were similar to those performed under air (Table 5.1, Entry 4) whereas using *n*-hexane as a solvent, conversions were decreased by two-fold (Table 5.1, Entry 6). Employing 5 wt% of lithium triflate (LiOTf) as an additive, a conversion of 61.7% was obtained (Table 5.1, Entry 7), and even better values were obtained by increasing biochar loadings (Table 5.1, Entry 8), reaction times (Table 5.1, Entry 9), and temperatures (Table 5.1, Entry 10). A more detailed study to comprehend the effect of biochar loading and reaction temperatures on the formation of cyclic ethers catalyzed by **sbc** was also undertaken and it is shown in Figure 5.2 and Figure 5.3. With the overall sustainability, efficiency, and feasibility of the process as priorities, the procedure was optimized by using 2 mmol of **1**, 20 wt% of **sbc** and a temperature of 160 °C for 24 h, leading to 75.2% conversion of **1** to **2**. The ¹H NMR spectrum of the ring-closing metathesis of **1** using **sbc** as a catalyst can be found in Appendix D: Information for Chapter 5.

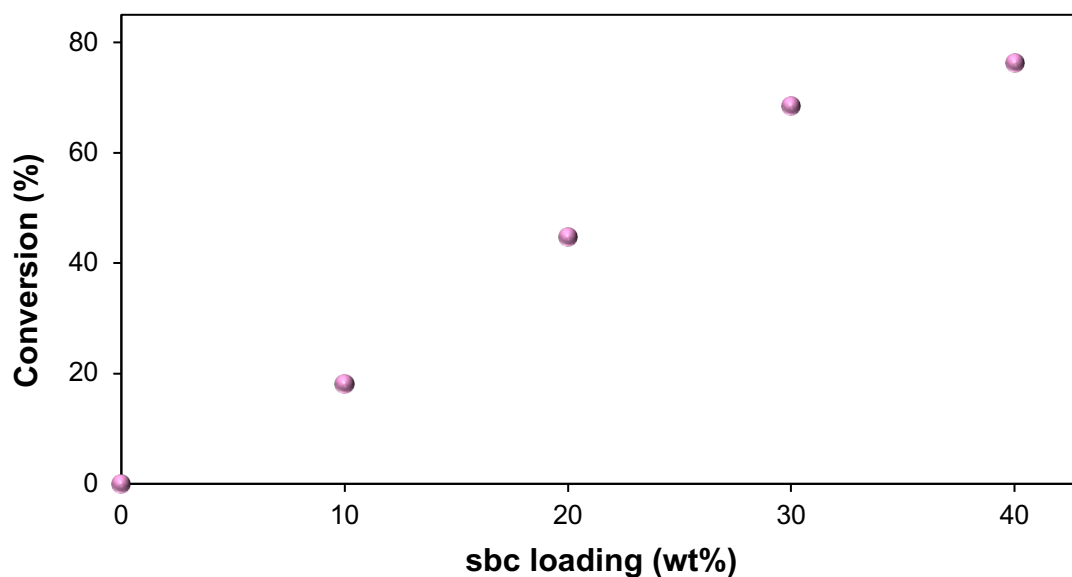


Figure 5.2. Effect of **sbc** loadings in the ring-closing C-O/C-O metathesis of 1,5-dimethoxypentane. Reaction conditions used: 1,5-dimethoxypentane (1, 2 mmol), 140 °C, 24 h.

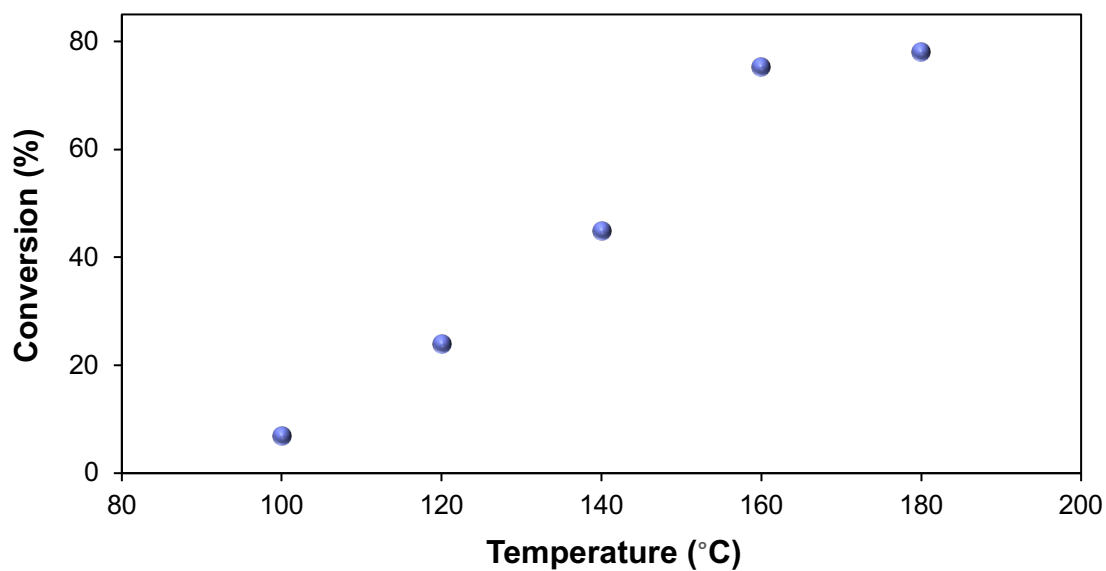


Figure 5.3. Effect of temperature in the ring-closing C-O/C-O metathesis of 1,5-dimethoxypentane. Reaction conditions used: 1,5-dimethoxypentane (1, 2 mmol), **sbc** (20 wt%), 24 h.

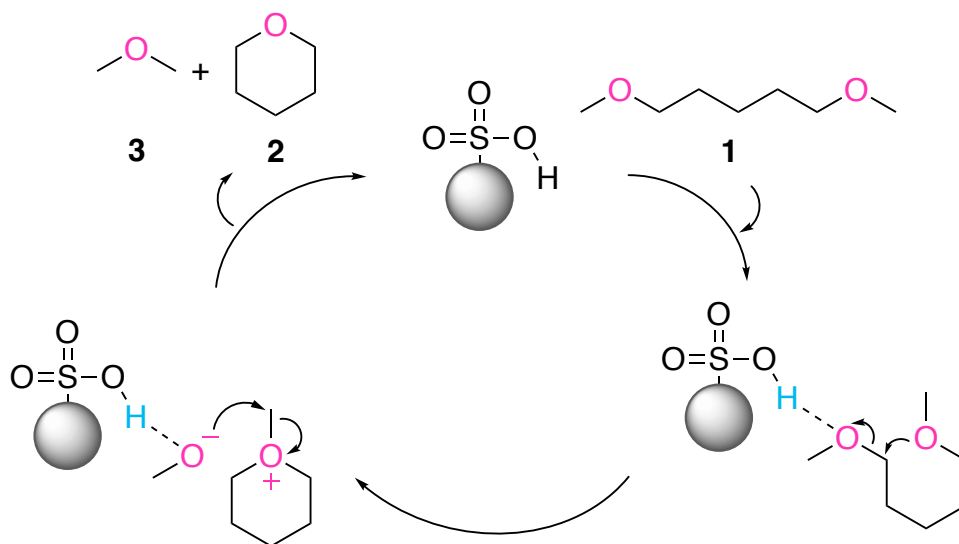
After the reaction, **sbc** can be easily separated from the reaction mixture and recovered through simple filtration followed by washing with ethanol or diethyl ether. In the context of recycling and reuse, our catalyst shows a significant decrease in reactivity after the first reaction cycle (i.e. from 75.2% to 23.3% using the optimized conditions). This effect has been observed in previous works involving heterogeneous catalysts as a result of leaching of the $\text{-SO}_3\text{H}$ surface functional groups.¹⁶⁻¹⁸ Treatment of the recovered catalyst with concentrated H_2SO_4 (0.5 mL) and washes with deionized water (10 mL) until neutral pH are able to reactivate **sbc** for another reaction. Through this process, conversions of **1** to **2** after reuse are similar to the ones obtained under the initial optimized reactions (75.0%). No conversions were observed in control reactions using a 0.1 M solution of H_2SO_4 as a catalyst alone, and low conversions of 3.3% were obtained using H_2SO_4 in combination of **oxbc**, thus demonstrating that the heterogeneous $\text{-SO}_3\text{H}$ groups in **sbc** are responsible for the catalysis.

5.2.2 Ring-Closing Metathesis of Other Aliphatic Ethers

Good results for the ring-closing C-O/C-O metathesis of aliphatic ethers are obtained using **sbc** as a catalyst and 1,5-dimethoxypentane as a substrate, but higher **sbc** loadings and longer reaction times are required to perform the transformation of 1,6-dimethoxyhexane. Using 40 wt% of **sbc** and a reaction time of 96 h, the unfavoured formation of a 7-membered ring is observed, and very low conversions (7.8%) of the respective cyclic ether are obtained. This was not unexpected, since the decrease in

reactivity with the increase of the carbon-chain length has been observed in previous works involving the metathesis of aliphatic ethers.^{2,3} Although the results obtained in this study show the ability of the proposed system to react with another ether, the effect of various substituents and their electronegativity in the production of various cyclic ethers still needs further investigation. Unfortunately, due to delays in delivery of chemicals during the COVID-19 pandemic, these additional reactions could not be performed now.

5.2.3 Mechanism for the Ring-Closing Metathesis



Scheme 5.1. Proposed mechanism for the ring-closing C-O/C-O metathesis of 1,5-dimethoxypentane **1** to tetrahydropyran **2** using **sbc** as a catalyst.

Based on the experimental results obtained herein and on the previous works involving the synthesis of *O*-heterocycles,^{2,3} a mechanism for the ring-closing C-O/C-O metathesis using **sbc** as a catalyst is proposed in **Scheme 5.1**. The purpose of **sbc** is to polarize and activate the C-O bond of the aliphatic ether **1** via hydrogen-bonding. After

intramolecular nucleophilic attack of the non-activated oxygen of the aliphatic ether, the oxonium intermediate is formed. This intermediate is further demethylated by the $\text{-SO}_3\text{H}$ groups on the surface of **sbc**, thus yielding the cyclic ether **2** and also dimethyl ether **3** as a by-product.

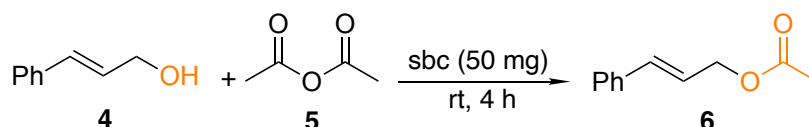
5.3 Esterification of Cinnamyl Alcohol

Regarding the performance of **sbc** as a catalyst for the synthesis of terpene esters, reaction optimization studies were performed using cinnamyl alcohol **4** to produce cinnamyl acetate **6** as our model reaction system. The results obtained during our initial studies for the esterification of terpene alcohols are shown in **Table 5.2**. Experiments were performed neat, at room temperature (rt), with reproducibility assessed by performing analyses in triplicate ($\text{SD} \leq 4.1\%$).

Control reactions in the absence of biochar gave low conversions of **4** to **6** (**Table 5.2, Entry 1**), as well as reactions using both **bc** and **oxbc** (**Table 5.2, Entries 2 and 3**). However, excellent conversions to **6** were obtained using **sbc** as a catalyst (**Table 5.2, Entry 4**), confirming that an increase in the $\text{-SO}_3\text{H}$ groups led to a significant increase in the activity of esterification reactions. A good conversion of 84.3% to the respective ester could still be obtained even with reaction times further reduced to 4 h (**Table 5.2, Entry 5**). Due to the known hazards of acetic anhydride **5**,¹⁹ reactions were performed using half of its amount (**Table 5.2, Entry 6**), in which a very low conversion value of 14.8% was achieved. Therefore, a molar ratio of 1:2 of **4** to **5** was kept constant throughout our

experiments. The ^1H NMR spectrum of the esterification of **4** using **sbc** as a catalyst can be found in **Appendix D: Information for Chapter 5**.

Table 5.2. Optimization of the esterification of terpene alcohols using the conversion of cinnamyl alcohol **4** to cinnamyl acetate **6** as a model reaction system and different types of biochar as catalysts.^a



Entry	Catalyst	t (h)	Conversion (%) ^c
1	-	6	9.2
2	bc	6	12.7
3	oxbc	6	15.2
4	sbc	6	97.8
5	sbc	4	84.3
6 ^b	sbc	4	14.8

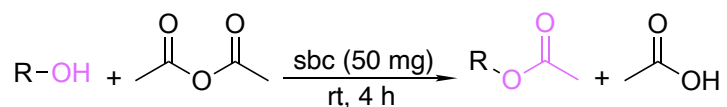
^a General reaction conditions unless otherwise stated: Cinnamyl alcohol (**4**, 10 mmol), acetic anhydride (**5**, 20 mmol), catalyst (50 mg), rt. ^b Acetic anhydride (**5**, 10 mmol). ^c Determined by ^1H NMR spectroscopy using mesitylene as an internal standard.

5.3.4 Esterification of Other Terpene Alcohols

The substrate scope of the catalytic system using **sbc** was further investigated using common terpene alcohols, and it is shown in **Table 5.3**. Cinnamyl alcohol (**Table 5.3, Entry 1**), citronellol (**Table 5.3, Entry 2**), geraniol (**Table 5.3, Entry 3**), and menthol (**Table 5.3, Entry 4**) could be transformed into their respective esters with excellent conversions using **sbc** as a catalyst. The slightly lower conversion of cinnamyl alcohol to

cinnamyl acetate obtained could be related to a possible repulsive interaction between the phenyl groups of the substrate and the aromatic (i.e. graphene-like) groups of **sbc**. This effect has been previously observed in **Section 2.2.4** when using **oxbc** to promote the synthesis of various cyclic carbonates via hydrogen-bonding. The ^1H NMR spectra of all the terpene esters produced herein can be found in **Appendix D: Information for Chapter 5**.

Table 5.3. Esterification of different terpene alcohols using **sbc** as a catalyst.^a



Entry	Terpene Alcohol	Conversion (%) ^b
1		84.3
2		> 99.9
3		> 99.9
4		> 99.9

^a General reaction conditions: Terpene alcohol (10 mmol), acetic anhydride (20 mmol), **sbc** (50 mg), 4 h, rt. ^b Determined by ^1H NMR spectroscopy using mesitylene as an internal standard.

5.4 Conclusions

In this Chapter, a novel and sustainable approach for the synthesis of *O*-heterocycles and terpene esters using **sbc** is reported. Besides being a bio-based, renewable, abundant, and inexpensive material, biochar is also considered a carbon-sink and presents recognizable climate change mitigation potential. The catalytic system developed using **sbc** for the ring-closing C-O/C-O metathesis of aliphatic ethers achieves good conversions under neat conditions, and it is easily separable and re-used after activation of the -SO₃H groups.

Sbc was also very efficient to facilitate the synthesis of terpene esters from terpene alcohols under neat and ambient conditions (rt, 4 h). Some of the most common used terpene alcohols (i.e. cinnamyl alcohol, citronellol, geraniol, and menthol) could be transformed into their respective esters with excellent conversions (i.e. > 84.3%) using small amounts of **sbc** (50 mg). Both of the systems proposed represent good alternatives to traditional processes requiring toxic, moisture sensitive, or difficult to separate catalysts, since good and reproducible conversions can be obtained using a benign, sustainable, and environmentally friendly carbon-based material.

5.5 Experimental

5.5.1 General Materials

Unless otherwise stated, chemicals were purchased from Sigma Aldrich or Fisher Scientific and used as received. Pristine biochar samples were used without additional

treatment from Cape Breton University (Sydney, Nova Scotia) and Sexton Lumber Co. (Bloomfield, Newfoundland and Labrador).²⁰ Commercially available solvents were used without any further purification.

5.5.2 Instrumentation

¹H NMR spectra were obtained on a Bruker AVANCE™ 300 MHz spectrometer at 298 K in CDCl₃. Deuterated solvents were purchased from Cambridge Isotope Laboratories and used without purification. Residual protio-solvent peaks were used as internal standards, and chemical shifts are reported as δ (ppm) values.

5.5.3 Preparation of Sulfonated Biochars (sbc)

Preparation of **bc** and **oxbc** can be found in **Sections 2.4.3** and **2.4.4**, respectively. Sulfonation of biochar was performed following the previous optimization procedure by Conceição and collaborators.²¹ 3.0 g of **bc** was slowly added with vigorous stirring to 30 mL of concentrated H₂SO₄. The mixture was heated under reflux at 200 °C for 4 h, then allowed to cool down for about 15 min. The product was separated by filtration and washed with deionized water until neutral pH. The black solid obtained was dried in an oven at 110 °C overnight and identified as **sbc**.

5.5.4 Synthesis of *O*-heterocycles

In a typical experiment, **sbc** (50 mg) and 1,5-dimethoxypentane (**1**, 26.4 mg, 2 mmol) were sequentially added into a vial containing a stir bar, and then sealed under air.

The vial was heated in an aluminum block at the desired temperature (e.g. 160 °C) and stirred for 24 h. After this time, the vial was cooled down for about 15 min. For analysis, mesitylene (200 μL) was added as an internal standard into the reaction mixture and stirred vigorously. An aliquot was collected, dissolved in CDCl₃, filtered to remove **sbc**, and then analyzed by ¹H NMR spectroscopy to determine the conversion to tetrahydropyran, **2**.

5.5.5 Synthesis of Terpene Esters

In a typical experiment, cinnamyl alcohol (**4**, 1.34 g, 10 mmol) and acetic anhydride (**5**, 2.04 g, 20 mmol) were sequentially added into a 2 dram vial containing a stir bar. The reaction mixture was stirred at room temperature (e.g. 20.1 °C) for 15 min to dissolve the terpene alcohol, and **sbc** (50 mg) was then added into the vial. After 4 h, mesitylene (1 mL) was added as an internal standard into the reaction medium and stirred vigorously. An aliquot was collected, dissolved in CDCl₃, filtered to remove **sbc**, and then analyzed by ¹H NMR spectroscopy to determine the conversion to cinnamyl acetate, **6**.

5.5.6 Recycling Studies

Using 1,5-dimethoxypentane as a substrate, a ring-closing C-O/C-O metathesis reaction was performed under the optimized conditions as described in **Section 5.5.4**. The mixture removed from the reaction vial was mixed with 15 mL of ethanol and centrifuged at 7500 rpm for 10 min to decant off liquid components and isolate the catalyst (**sbc**). The supernatant was decanted, the procedure was repeated two more times,

and the catalyst was dried in a vacuum oven at 60 °C overnight to eliminate residual solvent.

Treatment of the recovered catalyst is able to reactive **sbc** for another ring-closing metathesis reaction. After drying, the catalyst was stirred with 0.5 mL of concentrated H₂SO₄ for 5 min and washed with deionized water (10 mL) until neutral pH. To facilitate drying, the wet catalyst was again mixed with 15 mL of ethanol and centrifuged using the parameters above. After further supernatant decantation and catalyst drying, **sbc** is then ready to be used for another reaction.

5.6 References

1. J. L. Vidal; O. M. Wyper; S. L. MacQuarrie; Kerton, F. M., *Submitted, ChemCatChem* (cctc.202101369) **2021**.
2. Biberger, T.; Makai, S.; Lian, Z.; Morandi, B., *Angew. Chem., Int. Ed.* **2018**, *57*, 6940-6944.
3. Wang, H.; Zhao, Y.; Zhang, F.; Wu, Y.; Li, R.; Xiang, J.; Wang, Z.; Han, B.; Liu, Z., *Angew. Chem., Int. Ed.* **2020**, *59*, 11850-11855.
4. Ammann, S. E.; Rice, G. T.; White, M. C., *J. Am. Chem. Soc.* **2014**, *136*, 10834-10837.
5. Azuma, T.; Murata, A.; Kobayashi, Y.; Inokuma, T.; Takemoto, Y., *Org. Lett.* **2014**, *16*, 4256-4259.
6. Asai, S.; Kato, M.; Monguchi, Y.; Sajiki, H.; Sawama, Y., *Chem. Commun.* **2017**, *53*, 4787-4790.
7. Hartwig, J. F., *Nature* **2008**, *455*, 314-322.
8. Thuy Pham, T. P.; Cho, C.-W.; Yun, Y.-S., *Water Res.* **2010**, *44*, 352-372.
9. Kerton, F. M.; Marriott, R., *Alternative Solvents for Green Chemistry*. 2nd ed.; RSC Publishing: Cambridge, UK 2013.
10. Titirici, M.-M.; White, R. J.; Brun, N.; Budarin, V. L.; Su, D. S.; del Monte, F.; Clark, J. H.; MacLachlan, M. J., *Chem. Soc. Rev.* **2015**, *44*, 250-290.
11. De, S.; Balu, A. M.; van der Waal, J. C.; Luque, R., *ChemCatChem* **2015**, *7*, 1608-1629.
12. Liu, W. J.; Jiang, H.; Yu, H. Q., *Chem. Rev.* **2015**, *115*, 12251-12285.
13. Lee, J.; Kim, K.-H.; Kwon, E. E., *Renew. Sust. Energ. Rev.* **2017**, *77*, 70-79.

14. da Silva, M. J.; Ayala, D. A. M., *Catal. Sci. Technol.* **2016**, *6*, 3197-3207.
15. Tao, D.-J.; Dong, Y.; Cao, Z.-J.; Chen, F.-F.; Chen, X.-S.; Huang, K., *J. Ind. Eng. Chem.* **2016**, *41*, 122-129.
16. Macquarrie, D. J.; Mena Durán, C. J., Chapter 4 Heterogeneous Acid Catalysis in Nonasymmetric Synthesis. In *Sustainable Catalysis: Without Metals or Other Endangered Elements, Part 1*, The Royal Society of Chemistry: 2016; pp 65-78.
17. Yu, H.; Niu, S.; Lu, C.; Li, J.; Yang, Y., *Energy Convers. Manag.* **2016**, *126*, 488-496.
18. Scholz, D.; Kröcher, O.; Vogel, F., *ChemSusChem* **2018**, *11*, 2189-2201.
19. Centers for Disease Control and Prevention, Acetic Anhydride. <https://www.cdc.gov/niosh/npg/npgd0003.html> (accessed July 29, 2021).
20. Carrier, A. J.; Abdullahi, I.; Hawboldt, K. A.; Fiolek, B.; MacQuarrie, S. L., *J. Phys. Chem. C* **2017**, *121*, 26300-26307.
21. da Luz Corrêa, A. P.; Bastos, R. R. C.; Rocha Filho, G. N. d.; Zamian, J. R.; Conceição, L. R. V. d., *RSC Adv.* **2020**, *10*, 20245-20256.

CHAPTER 6: FUTURE WORK AND CONCLUSIONS

6.1 Ideas for Future Work

As previously mentioned in **Chapter 1: Introduction**, the diversification of biochar applications is an important strategy for achievement of a circular economy and the United Nations Sustainable Development Goals (SDGs).¹⁻⁴ In this thesis, initial and additional ideas, experiments, and systems for the implementation of biochar as an efficient catalyst, polymer composite, and advanced material have been pursued. However, due to its heterogeneity and the lack of studies involving and correlating its molecular structure, biomass feedstock, and pyrolysis conditions, research efforts are still needed to allow the further use of biochar as a superior alternative to traditional systems.

Future work involving the transformation of biochar as a high value-added material could use a systems thinking approach⁵ through a combination of the works performed in **Chapter 2: Oxidized Biochar as a Renewable, Sustainable Catalyst for the Production of Cyclic Carbonates from Carbon Dioxide and Epoxides** and **Chapter 5: Green Ring-Closing Metathesis of Aliphatic Ethers and Esterification of Terpene Alcohols Catalyzed by Biochar Catalysts**. Through a broader and more extensive substrate scope assessment, sulfonated biochar (**sbc**) can be used to promote the synthesis of different epoxides from aliphatic ethers via ring-closing C-O/C-O metathesis reactions. These *O*-heterocycles can be directly used as intermediates for organic and polymeric syntheses, solvents, pharmaceuticals, natural products, and agrochemicals,⁶⁻⁸ or further applied as building blocks for the production of cyclic carbonates via the cycloaddition

reaction between CO_2 and epoxides catalyzed by oxidized biochar (**oxbc**).⁹ In this regard, the use of **sbc** as a catalyst to facilitate CO_2 -epoxide coupling reactions also deserves further investigation, as the catalyst containing sulfonic acid groups was shown to be more effective than **oxbc** for the synthesis of oxygen-containing heterocycles. A schematic representation of this idea for future work is shown in **Figure 6.1**.

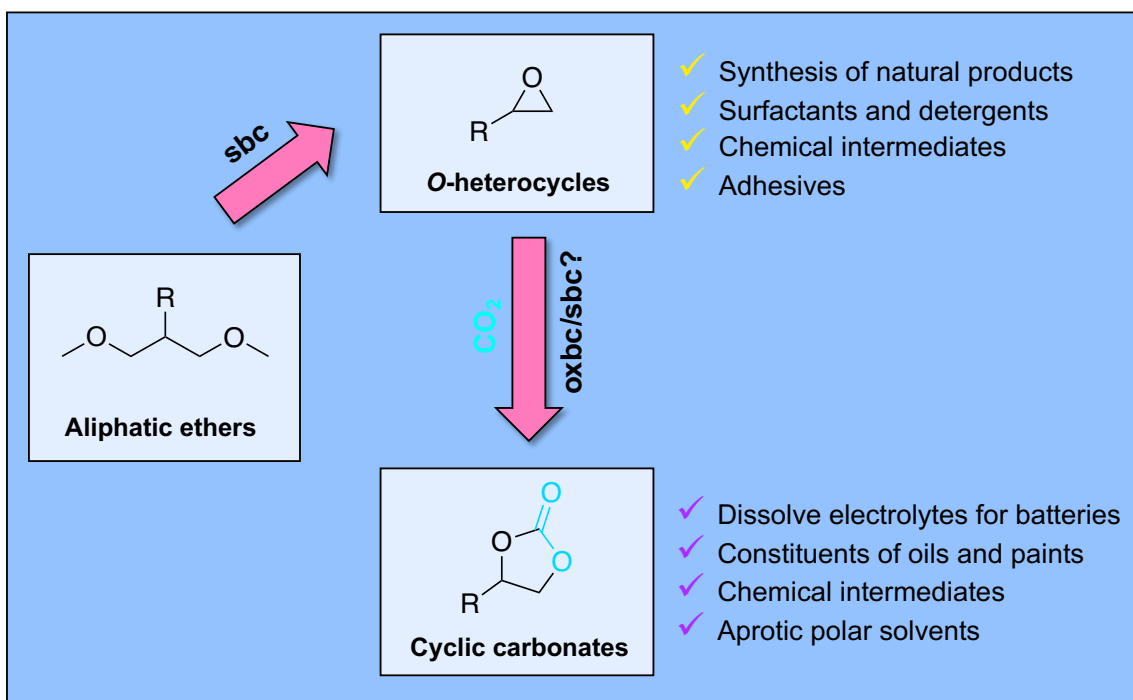


Figure 6.1. Schematic representation of future work idea involving a systems thinking approach for the use of functionalized biochar as a catalyst for the synthesis of both *O*-heterocycles and cyclic carbonates.

Future investigation should include different systems for the production of biochar nanostructures via liquid-phase exfoliation (LPE). Although 27 of the most common solvents have been explored during the work performed in **Chapter 3: Green Solvents for the Liquid-Phase Exfoliation of Biochar**, other alternative environments such as

ionic liquids (ILs) are worth studying. As an example, 1-ethyl-3-methylimidazolium acetate [C₂C₁m][OAc] is a non-hazardous IL that has been used as a common solvent to dissolve both cellulose and lignin to produce fiber blends.¹⁰ The evaluation of different ILs in the LPE of biochar could yield higher amounts of exfoliated material, especially for the exfoliation of pristine samples (i.e. maximum dispersion obtained: 0.51 mg/mL in CHCl₃). Moreover, Kamlet-Taft solvatochromic parameters for different ILs have been calculated or can be predicted to identify promising candidates for biochar exfoliation.¹¹ Further work in biochar LPE involving the effect of all the solvents studied in the size, thickness, and quality of the nanostructures produced is also significant. This analysis could help to build a relationship not only between yield of exfoliated biochar and solvent parameters, but can also provide a correlation between the latter and the characteristics of the materials produced. For instance, the use of different solvents could avoid the reaggregation of exfoliated biochar and allow the clear visualization of its nanostructures during characterization (i.e. AFM and TEM analysis). In this Chapter, preliminary mass spectrometric (MS) studies were performed on pristine and exfoliated biochar. Further studies are now underway using Fourier-Transform Ion Cyclotron Resonance (FT-ICR) MS in collaboration with Dr. Amy McKenna at the National High Magnetic Field Laboratory (Tallahassee, FL).

Besides providing alternative environments for the LPE of biochar, ILs can also be used to prepare bi-functional biochar catalysts for the synthesis of cyclic carbonates and cyclic ethers. Yin and co-workers have previously described the production of an IL-

grafting biochar sulfonic acid (BC-SO₃H-IL) as an efficient catalyst for the hydrolysis of biomass.¹² This system containing -COOH, -OH, -SO₃H, and -Cl⁻ groups grafted onto the surface of biochar presents potential to work synergically for the catalysis of the cycloaddition reaction between CO₂ and epoxides. The hydrogen-bond donating groups of the material (i.e. -COOH, -OH, and -SO₃H) could interact with the oxygen of the epoxide to accelerate its ring-opening, whilst the anionic portion of the functionalized biochar (i.e. Cl⁻ groups) can attack the less-hindered carbon of the epoxide, thus avoiding the further utilization of a co-catalyst to promote the reaction. A similar approach could be applied during the synthesis of *O*-heterocycles, in which the -COOH, -OH, and -SO₃H groups can interact via hydrogen-bonding with one oxygen of the aliphatic ether at the same time that the Cl⁻ groups can interact via the same mechanism with the protons of the CH₃ and CH₂ groups adjacent to the second oxygen atom. A schematic representation of the work involving IL-grafted biochar as a bi-functional catalyst is seen in **Figure 6.2**.

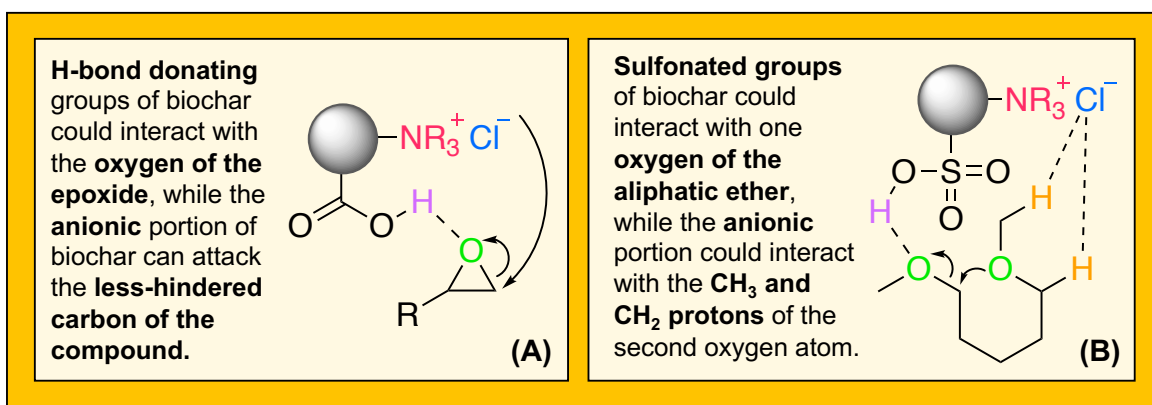


Figure 6.2. Schematic representation of future work idea involving the use of IL-grafted biochar as a bi-functional catalyst for (A) the cycloaddition reaction between CO₂ and epoxides, and (B) the ring-closing C-O/C-O metathesis of aliphatic ethers.

A previous work performed by Loh and collaborators describes the utilization of graphene-oxide as a catalyst for the direct C-C cross-coupling of xanthenes with arenes under aerobic and neat conditions.¹³ During this study, it has been shown that the C=O functionalities and the zigzag edges around defective sites present in the catalyst are the most likely active sites to promote these reactions. Due to the higher presence of zigzag edges and defective sites on the molecular structure of biochar and the increased number of C=O species after its oxidation, another idea for future work is the utilization of **oxbc** as a catalyst for C-C coupling reactions. As previously mentioned in **Chapter 1: Introduction**, biochar is a more environmentally friendly alternative to graphene, which is usually produced from fossil fuel precursors via harsh synthetic conditions.^{14, 15} A schematic representation of the future work idea using **oxbc** to promote C-C coupling reactions is shown in **Figure 6.3**.

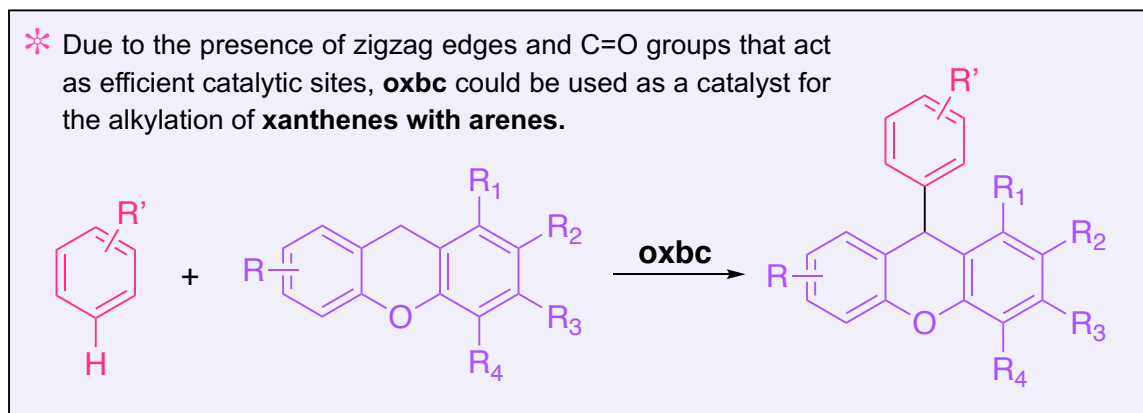


Figure 6.3. Schematic representation of future work idea involving the use of **oxbc** as a catalyst for the direct C-C cross-coupling of xanthenes with arenes.

6.2 Conclusions

Due to its interesting chemical and physical properties and characteristics, the study of biochar and its applications presents great potential as a nexus solution for the achievement of a more sustainable future. Biochar is a carrier for long-term carbon storage obtained from waste, and contains surface-area, porosity, and abundant surface functionality.^{1, 3, 4} Although it has been mainly applied in low value-added fields (i.e. removal of pollutants from aqueous solutions and soil amendment), this thesis shows the use of functionalized biochar as an important catalyst and advanced material for the synthesis of industrially used chemicals and polymer composites.

In **Chapter 1: Introduction**, the driving force of the research performed in this thesis is discussed. A literature review on biochar history, climate change mitigation potential and applications, in conjunction with their correlations with the 12 Principles of Green Chemistry and SDGs is conducted. Research relating to different types of pyrolysis conditions, biomass feedstocks, functionalization methods, and their influence on the chemical and physical properties of biochar has been summarized in this Chapter. In the work developed herein, a focus on the applications of biochar as a catalyst and as an advanced material has been pursued. Regarding the field of catalysis, the vast majority of studies using pristine and functionalized biochars involve the promotion of biomass transformations processes, with a few examples including traditional oxidation, hydrogenation, and alkylation reactions.¹⁶⁻²⁵ In this Chapter, the role of biochar as an additive for the production of reinforced materials is also highlighted. Most of these

studies have been performed in the area of construction science, with the objective of using more sustainable and effective designs for the production of building materials.²⁶⁻³⁰

In **Chapter 2: Oxidized Biochar as a Renewable, Sustainable Catalyst for the Production of Cyclic Carbonates from Carbon Dioxide and Epoxides**,⁹ the use of biochar as a catalyst for the cycloaddition reaction between CO₂ and epoxides is described. Biochar after acidic oxidation with HNO₃ is able to transform 78.5% of propylene oxide into the respective cyclic carbonate using optimized conditions of temperature, time, CO₂, and amounts of catalyst, epoxide, and co-catalyst. Even when biochars from different biomass feedstocks were used, the results obtained were similar, the catalytic system presented a wide substrate scope, and the catalyst could be re-used for at least five reaction cycles. This Chapter represents the first attempt of using biochar to facilitate chemical reactions described in this thesis.

The use of biochar as an advanced material is discussed in **Chapter 3: Green Solvents for the Liquid-Phase Exfoliation of Biochar**.³¹ Biochar nanostructures with enhanced chemical and physical properties, and potential applications in high value fields have been previously produced in toxic and harmful environments.³²⁻³⁴ In this Chapter, the respective nanostructures were produced in greener environments via LPE using ultrasound. The exfoliated material is comprised of 2-8 monolayers of biochar with 15 nm thickness stacked together, and exfoliation efficiency showed to be related to the surface tensions, densities, and Kamlet-Taft solvatochromic parameters of solvents used. The exfoliation of pristine biochar was significantly impacted by the polarizability of the

liquid environment in which it was immersed, whereas the hydrogen-bonding acceptance ability of the solvent exhibited significant impact in the production of oxidized biochar nanostructures. Once more, the importance of the functionalization of biochar for increasing its applications was highlighted, since its surface modification demonstrated potential to increase its exfoliation efficiency in more benign solvents to human health and the environment.

Further applications for the exfoliated material were discussed in **Chapter 4: Biochar as a Sustainable and Renewable Additive for the Production of Poly(ϵ -caprolactone) Composites**.³⁵ In this Chapter, exfoliated oxidized biochar (**Eoxbc**) nanostructures produced after LPE in ϵ -caprolactone (ϵ -CL) were used as additives for the production of poly(ϵ -caprolactone) (PCL) composites. Although largely used in the biomedical field, further applications of PCL are limited due to its poor mechanical properties.^{36,37} Very small loadings of **Eoxbc** (i.e. 0.1 wt%) were sufficient to increase the conversions of ϵ -CL into PCL (i.e. from 55.2% without **Eoxbc** to 88.4% with **Eoxbc**) and further increase the crystallinity of the composites produced using different catalysts. PCL composites containing **Eoxbc** as an additive presented higher stiffness, viscosity, better mechanical properties, and potential higher levels of degradation when compared to the pure polymer. Although previously used as a polymer additive,³⁸⁻⁴³ in this Chapter we describe the first investigation of biochar for the production of PCL, a polymer with increased biodegradability when compared to other similar analogues such as poly(lactic acid).⁴⁴

In Chapter 5: Green Ring-Closing Metathesis of Aliphatic Ethers and Esterification of Terpene Alcohols Catalyzed by Biochar Catalysts, additional research of biochar in the field of catalysis is explored.⁴⁵ In this Chapter, biochar after acidic oxidation with H₂SO₄ is applied as a catalyst for (i) the synthesis of cyclic ethers via ring-closing C-O/C-O metathesis of aliphatic ethers and (ii) the production of terpene esters via esterification from terpene alcohols. Cyclic ethers are compounds widely used industrially, and their synthesis from their aliphatic counterparts has been previously performed using moisture sensitive or non-biodegradable catalysts with unknown toxicity.^{6, 7} Using 1,5-dimethoxypentane as a substrate and **sbc** as a catalyst, good conversions to tetrahydropyran (75.2%) were achieved under neat and optimized conditions. Although the conditions applied can be considered harsh (i.e. 160 °C, 24 h), they are comparable to previous works involving the ring-closing metathesis of cyclic ethers,^{6, 7} which can be obtained from other precursors using long and tedious synthetic methods.^{8, 46-48} Moreover, the catalytic system proposed in this Chapter can be readily reused after simple filtration and further reactivation of the -SO₃H groups. This is the first time that a carbon-based catalyst has been applied for the ring-closing metathesis of aliphatic ethers. **Sbc** can be also applied for the synthesis of terpene esters from terpene alcohols and acetic anhydride. Good conversions (84.3%) of esters could be obtained under optimized and mild reaction conditions (i.e. rt, 4 h). The system proposed worked well with the most common used substrates, representing an efficient and non-toxic alternative for the synthesis of compounds applied in industry.^{49, 50}

In summary, this thesis represents the very beginning of a long story with many different characters. The diversification of biochar applications is just one of the countless pieces involved in this giant puzzle. Through improved understanding of the molecular structure of biochar, its reactivity, production, and applications through interdisciplinary research, biochar could be transformed into an indispensable building block for the production of energy and outstanding materials using the 12 Principles of Green Chemistry. Although cultural, political, and educational changes are very much needed, hopefully this thesis highlights the amazing things our society can do if we all work together for the achievement of a greener, happier, and more sustainable future for us and the generations to come.

6.3 References

1. Liu, W. J.; Jiang, H.; Yu, H. Q., *Chem. Rev.* **2015**, *115*, 12251-12285.
2. Lehmann, J.; Joseph, S., *Biochar for environmental management: Science and Technology*. Earthscan: Sterling, VA, 2009.
3. Woolf, D.; Amonette, J. E.; Street-Perrott, F. A.; Lehmann, J.; Joseph, S., *Nat. Commun.* **2010**, *1*, 56-65.
4. Lehmann, J., *Nature* **2007**, *447*, 143-144.
5. Williams, A.; Kennedy, S.; Philipp, F.; Whiteman, G., *J. Clean. Prod.* **2017**, *148*, 866-881.
6. Biberger, T.; Makai, S.; Lian, Z.; Morandi, B., *Angew. Chem., Int. Ed.* **2018**, *57*, 6940-6944.
7. Wang, H.; Zhao, Y.; Zhang, F.; Wu, Y.; Li, R.; Xiang, J.; Wang, Z.; Han, B.; Liu, Z., *Angew. Chem., Int. Ed.* **2020**, *59*, 11850-11855.
8. Asai, S.; Kato, M.; Monguchi, Y.; Sajiki, H.; Sawama, Y., *Chem. Commun.* **2017**, *53*, 4787-4790.
9. Vidal, J. L.; Andrea, V. P.; MacQuarrie, S. L.; Kerton, F. M., *ChemCatChem* **2019**, *11*, 4089-4095.
10. Vincent, S.; Prado, R.; Kuzmina, O.; Potter, K.; Bhardwaj, J.; Wanasekara, N. D.; Harniman, R. L.; Koutsomitopoulou, A.; Eichhorn, S. J.; Welton, T.; Rahatekar, S. S., *ACS Sustain. Chem. Eng.* **2018**, *6*, 5903-5910.
11. Venkatraman, V.; Lethesh, K. C., *Frontiers in Chemistry* **2019**, *7*, 605-612.

12. Zhang, C.; Fu, Z.; Liu, Y. C.; Dai, B.; Zou, Y.; Gong, X.; Wang, Y.; Deng, X.; Wu, H.; Xu, Q.; Steven, K. R.; Yin, D., *Green Chem.* **2012**, *14*, 1928-1934.
13. Wu, H.; Su, C.; Tandiana, R.; Liu, C.; Qiu, C.; Bao, Y.; Wu, J. e.; Xu, Y.; Lu, J.; Fan, D.; Loh, K. P., *Angew. Chem., Int. Ed.* **2018**, *57*, 10848-10853.
14. Titirici, M.-M.; White, R. J.; Brun, N.; Budarin, V. L.; Su, D. S.; del Monte, F.; Clark, J. H.; MacLachlan, M. J., *Chem. Soc. Rev.* **2015**, *44*, 250-290.
15. De, S.; Balu, A. M.; van der Waal, J. C.; Luque, R., *ChemCatChem* **2015**, *7*, 1608-1629.
16. Chen, Y.; Ning, P.; Miao, R.; Shi, Y.; He, L.; Guan, Q., *New J. Chem.* **2020**, 20812-20822.
17. Bartoli, M.; Giorcelli, M.; Jagdale, P.; Rovere, M.; Tagliaferro, A., *Materials* **2020**, *13*, 261.
18. Zhong, Y.; Zhang, P.; Zhu, X.; Li, H.; Deng, Q.; Wang, J.; Zeng, Z.; Zou, J.-J.; Deng, S., *ACS Sustain. Chem. Eng.* **2019**, *7*, 14973-14981.
19. Kumar, A.; Kumar, J.; Bhaskar, T., *Environ. Res.* **2020**, *186*, 109533-109542.
20. Cao, Y.; Ding, L.; Qiu, Z.; Zhang, H., *Catal. Commun.* **2020**, *143*, 106048-106053.
21. Tang, F.; Wang, L.; Liu, Y.-N., *Green Chem.* **2019**, *21*, 6252-6257.
22. Sahoo, B.; Formenti, D.; Topf, C.; Bachmann, S.; Scalone, M.; Junge, K.; Beller, M., *ChemSusChem* **2017**, *10*, 3035-3039.
23. Moradi, P.; Hajjami, M.; Valizadeh-Kakhki, F., *Appl. Organomet. Chem.* **2019**, *33*, 5205-5218.
24. Lee, J.; Kim, K.-H.; Kwon, E. E., *Renew. Sust. Energ. Rev.* **2017**, *77*, 70-79.

25. Cao, X.; Sun, S.; Sun, R., *RSC Adv.* **2017**, *7*, 48793-48805.
26. Gupta, S.; Kua, H. W.; Low, C. Y., *Cement Concrete Comp.* **2018**, *87*, 110-129.
27. Akhtar, A.; Sarmah, A. K., *Sci. Total Environ.* **2018**, *616-617*, 408-416.
28. Gupta, S.; Kua, H. W., *Sci. Total Environ.* **2019**, *662*, 952-962.
29. Cuthbertson, D.; Berardi, U.; Briens, C.; Berruti, F., *Biomass Bioenergy* **2019**, *120*, 77-83.
30. Wang, L.; Chen, L.; Tsang, D. C. W.; Guo, B.; Yang, J.; Shen, Z.; Hou, D.; Ok, Y. S.; Poon, C. S., *J. Clean. Prod.* **2020**, *258*, 120678-120686.
31. Vidal, J. L.; Gallant, S. M. V.; Connors, E. P.; Richards, D. D.; MacQuarrie, S. L.; Kerton, F. M., *ACS Sustain. Chem. Eng.* **2021**, *9*, 9114-9125.
32. Liu, G.; Zheng, H.; Jiang, Z.; Zhao, J.; Wang, Z.; Pan, B.; Xing, B., *Environ. Sci. Technol.* **2018**, *52*, 10369-10379.
33. Xiao, X.; Chen, B., *Environ. Sci. Technol.* **2017**, *51*, 5473-5482.
34. Oleszczuk, P.; Ćwikła-Bundyra, W.; Bogusz, A.; Skwarek, E.; Ok, Y. S., *J. Anal. Appl. Pyrol.* **2016**, *121*, 165-172.
35. Vidal, J. L.; Yavitt, B. M.; Wheeler, M. D.; Kolwich, J. L.; Donovan, L. N.; Sit, C. S.; Hatzikiriakos, S. V.; Jalsa, N. K.; MacQuarrie, S. L.; Kerton, F. M., *Submitted, ACS Sustain. Chem. Eng. (sc-2021-06375x)* **2021**.
36. Labet, M.; Thielemans, W., *Chem. Soc. Rev.* **2009**, *38*, 3484-3504.
37. Woodruff, M. A.; Hutmacher, D. W., *Prog. Polym. Sci.* **2010**, *35*, 1217-1256.

38. Ogunsona, E. O.; Codou, A.; Misra, M.; Mohanty, A. K., *J. Polym. Environ.* **2018**, *26*, 3574-3589.
39. Qian, S.; Yan, W.; Zhu, S.; Fontanillo Lopez, C. A.; Sheng, K., *Polym. Compos.* **2018**, *39*, 633-639.
40. Zhang, Q.; Zhang, D.; Lu, W.; Khan, M. U.; Xu, H.; Yi, W.; Lei, H.; Huo, E.; Qian, M.; Zhao, Y.; Zou, R., *Sci. Total Environ.* **2020**, *738*, 139910-139919.
41. Nan, N.; DeVallance, D. B., *J. Mater. Sci.* **2017**, *52*, 8247-8257.
42. Picard, M.; Thakur, S.; Misra, M.; Mielewski, D. F.; Mohanty, A. K., *Sci. Rep.* **2020**, *10*, 3310-3324.
43. Das, O.; Kim, N. K.; Hedenqvist, M. S.; Lin, R. J. T.; Sarmah, A. K.; Bhattacharyya, D., *Environ. Manage.* **2018**, *62*, 403-413.
44. Guo, W.; Tao, J.; Yang, C.; Song, C.; Geng, W.; Li, Q.; Wang, Y.; Kong, M.; Wang, S., *PLOS ONE* **2012**, *7*, 38341-38347.
45. J. L. Vidal; O. M. Wyper; S. L. MacQuarrie; Kerton, F. M., *Submitted, ChemCatChem (cctc.202101369)* **2021**.
46. Ammann, S. E.; Rice, G. T.; White, M. C., *J. Am. Chem. Soc.* **2014**, *136*, 10834-10837.
47. Azuma, T.; Murata, A.; Kobayashi, Y.; Inokuma, T.; Takemoto, Y., *Org. Lett.* **2014**, *16*, 4256-4259.
48. Hartwig, J. F., *Nature* **2008**, *455*, 314-322.
49. Tao, D.-J.; Dong, Y.; Cao, Z.-J.; Chen, F.-F.; Chen, X.-S.; Huang, K., *J. Ind. Eng. Chem.* **2016**, *41*, 122-129.

50. da Silva, M. J.; Ayala, D. A. M., *Catal. Sci. Technol.* **2016**, 6, 3197-3207.

APPENDIX A: INFORMATION FOR CHAPTER 2

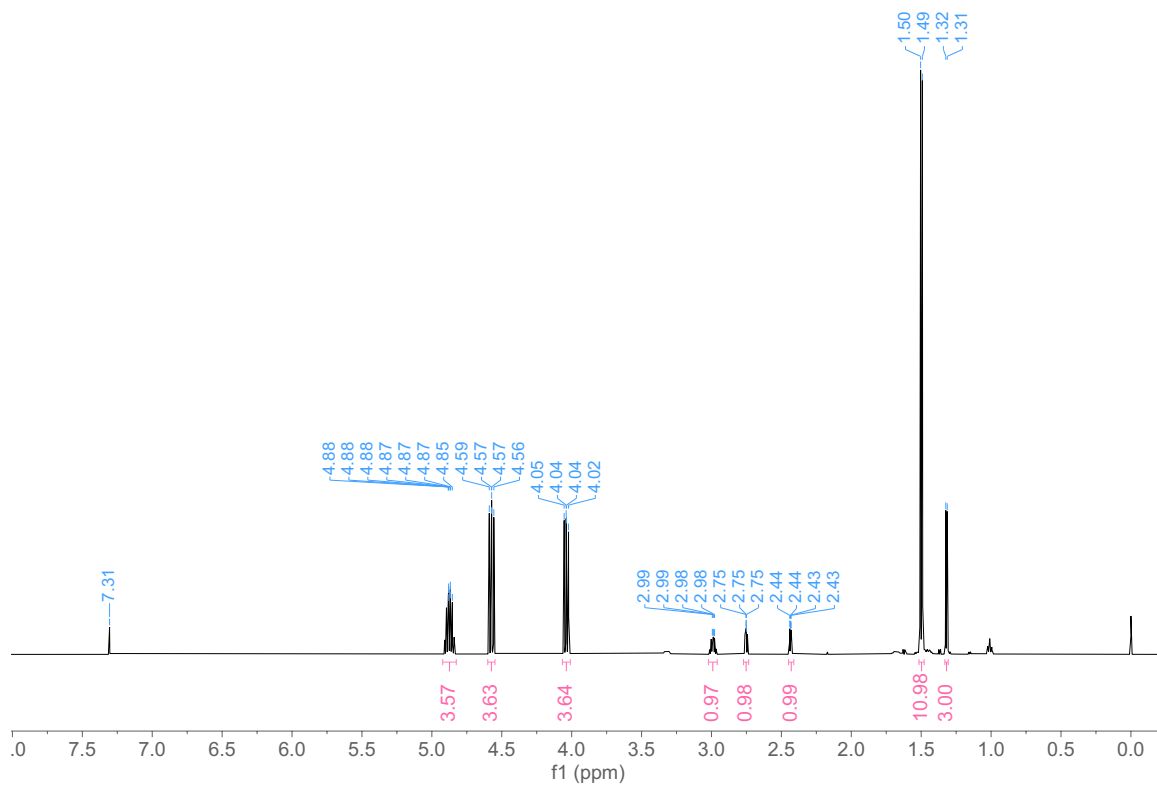


Figure A.1. ^1H NMR spectrum (300 MHz, CDCl_3) of CO_2 and propylene oxide reaction (Table 2.2, Entry 1).

Conversion = integration of cyclic carbonate CH_3 protons (10.98, δ 1.50 ppm) divided by the sum of cyclic carbonate (10.98, δ 1.50 ppm) and epoxide CH_3 protons (3.00, δ 1.32 ppm) multiplied by 100%. Conversion = 78.5%

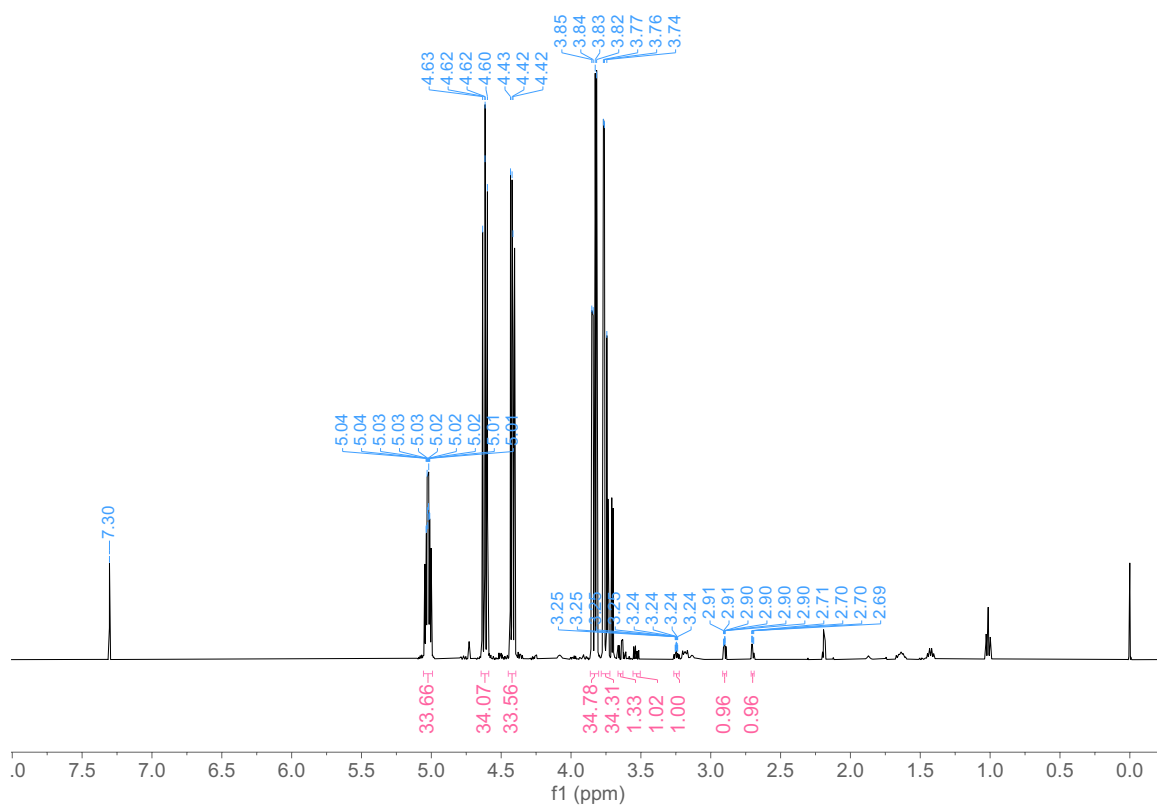


Figure A.2. ^1H NMR spectrum (500 MHz, CDCl_3) of CO_2 and epichlorohydrin reaction (Table 2.2, Entry 2).

Conversion = integration of cyclic carbonate CH proton (33.66, δ 5.02 ppm) divided by the sum of cyclic carbonate (33.66, δ 5.02 ppm) and epoxide CH protons (1.00, δ 3.24 ppm) multiplied by 100%. Conversion = 97.1%

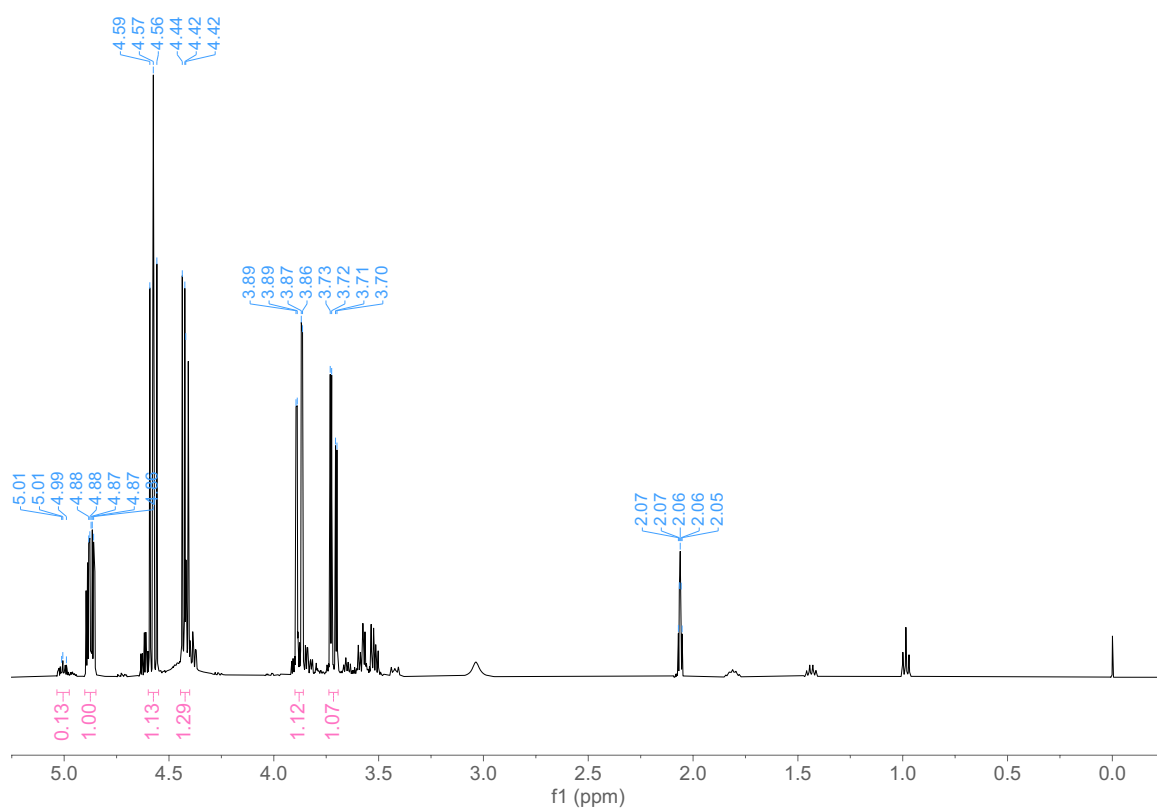


Figure A.3. ¹H NMR spectrum (500 MHz, acetone-d₆) of CO₂ and glycidol reaction (Table 2.2, Entry 3).

Conversion = integration of cyclic carbonate CH proton (1.00, δ 4.87 ppm) divided by the sum of cyclic carbonate (1.00, δ 4.87 ppm) and epoxide CH protons (not visible) multiplied by 100%. Conversion > 99.9%.

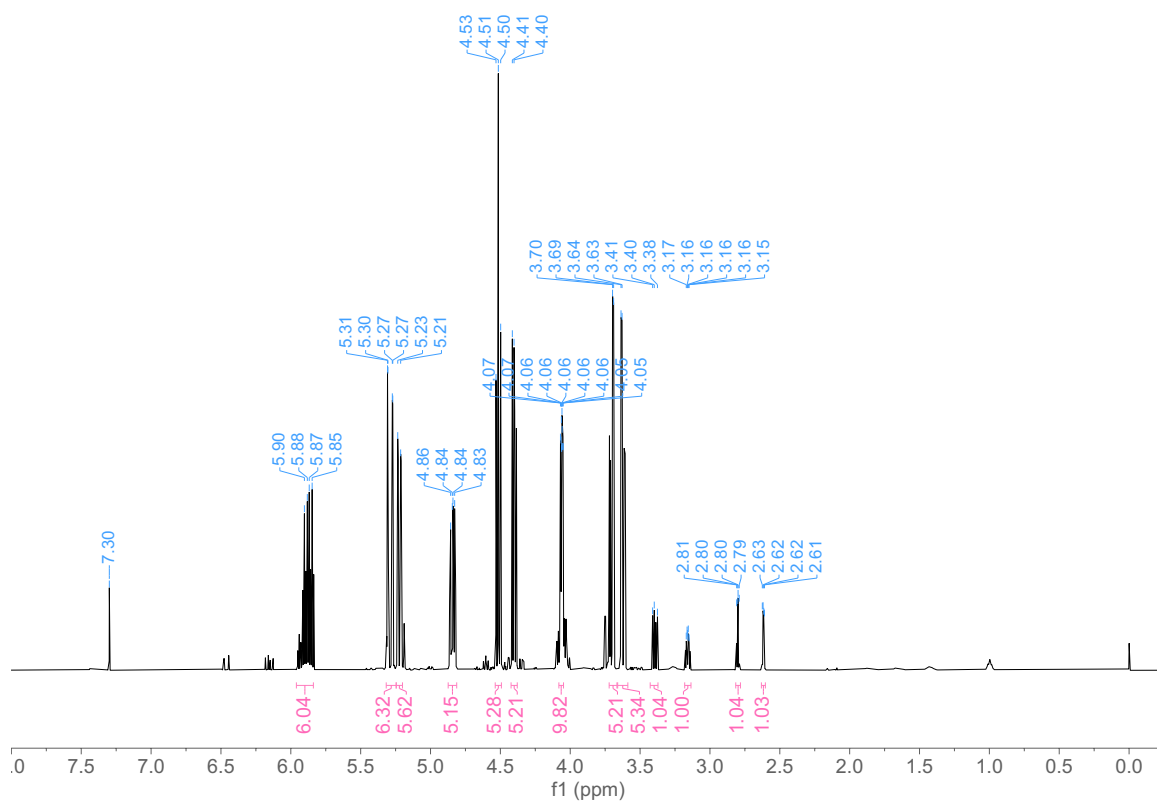


Figure A.4. ^1H NMR spectrum (500 MHz, CDCl_3) of CO_2 and allyl glycidyl ether reaction (Table 2.2, Entry 4).

Conversion = integration of cyclic carbonate CH proton (5.15, δ 4.84 ppm) divided by the sum of cyclic carbonate (5.15, δ 4.84 ppm) and epoxide CH protons (1.00, δ 3.16 ppm) multiplied by 100%. Conversion = 83.7%

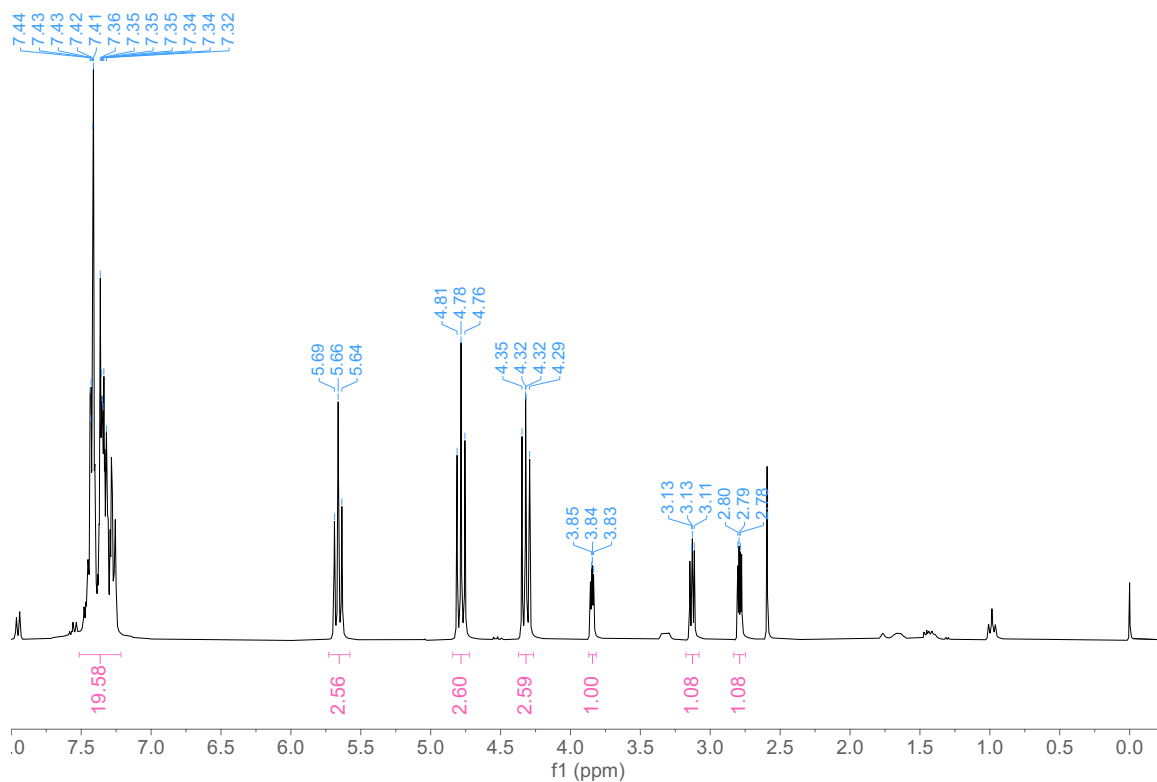


Figure A.5. ¹H NMR spectrum (300 MHz, CDCl₃) of CO₂ and styrene oxide reaction (Table 2.2, Entry 5).

Conversion = integration of cyclic carbonate CH proton (2.56, δ 5.66 ppm) divided by the sum of cyclic carbonate (2.56, δ 5.66 ppm) and epoxide CH protons (1.00, δ 3.84 ppm) multiplied by 100%. Conversion = 71.9%

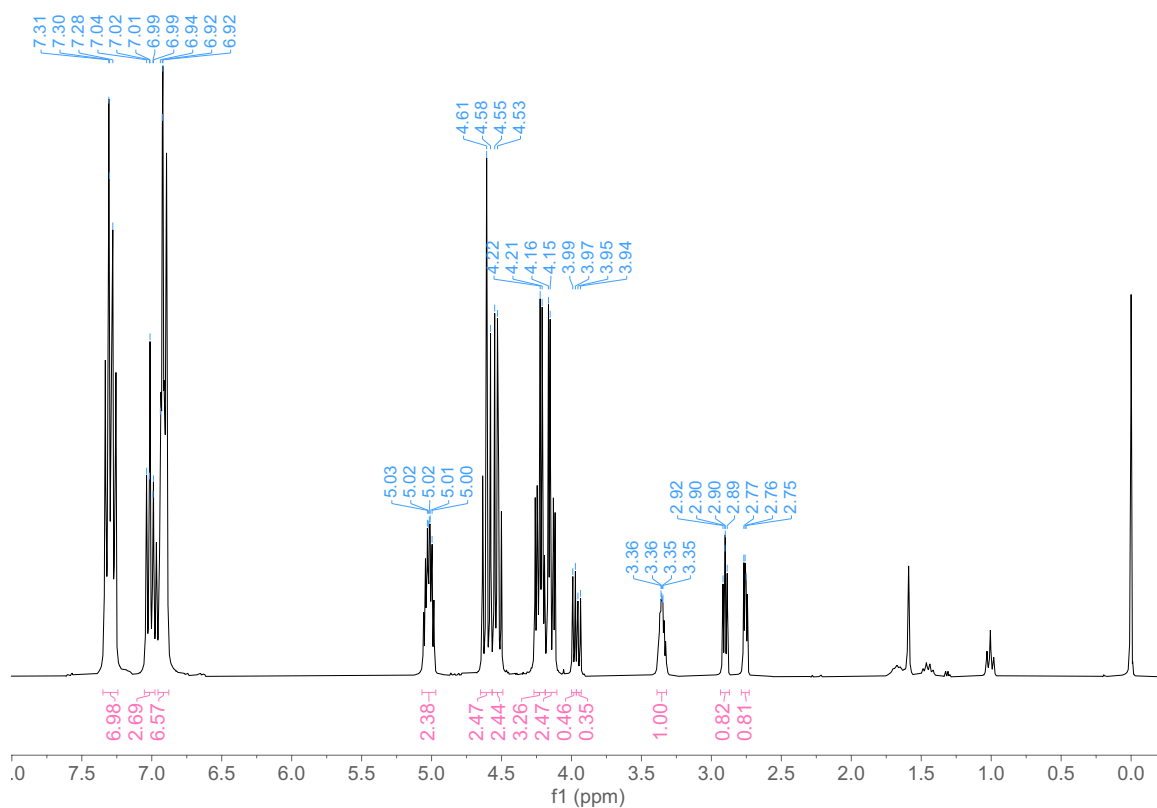


Figure A.6. ¹H NMR spectrum (300 MHz, CDCl₃) of CO₂ and glycidyl phenyl ether reaction (Table 2.2, Entry 6).

Conversion = integration of cyclic carbonate CH proton (2.38, δ 5.02 ppm) divided by the sum of cyclic carbonate (2.38, δ 5.02 ppm) and epoxide CH protons (1.00, δ 3.35 ppm) multiplied by 100%. Conversion = 70.4%

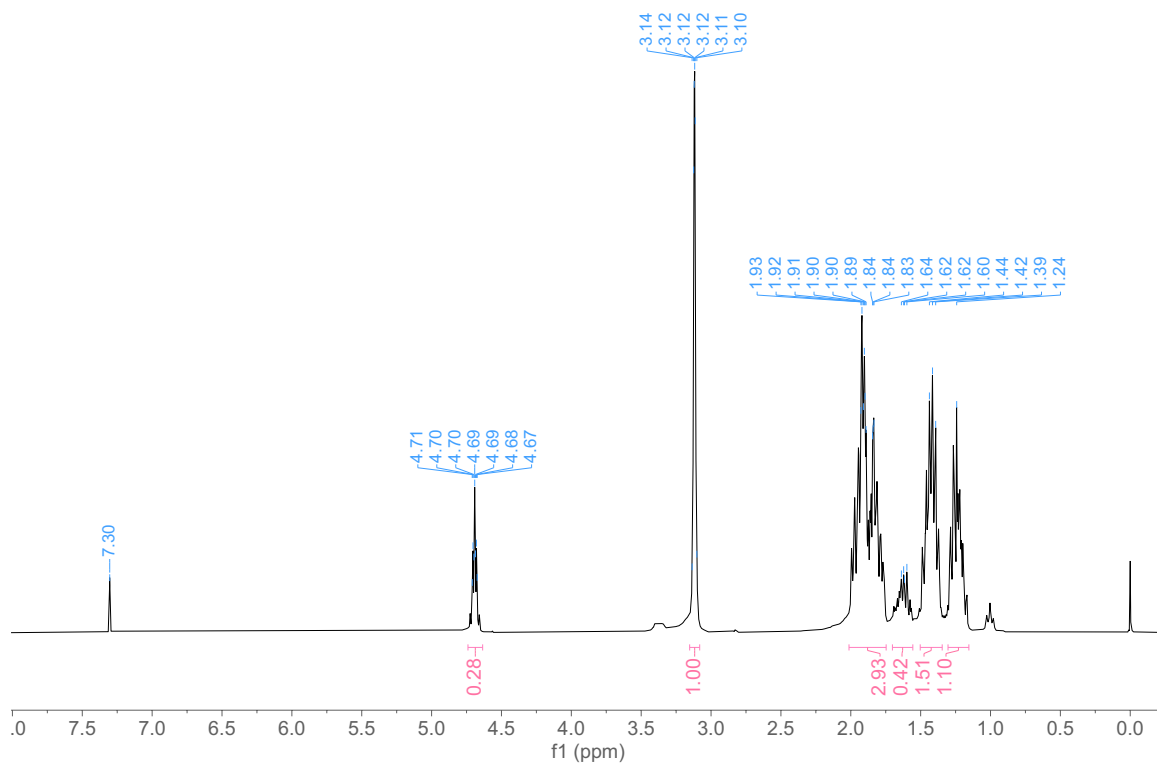


Figure A.7. ^1H NMR spectrum (300 MHz, CDCl_3) of CO_2 and cyclohexene oxide reaction (Table 2.2, Entry 7).

Conversion = integration of cyclic carbonate CH proton (0.28, δ 4.70 ppm) divided by the sum of cyclic carbonate (0.28, δ 4.70 ppm) and epoxide CH protons (1.00, δ 3.12 ppm) multiplied by 100%. Conversion = 21.9%

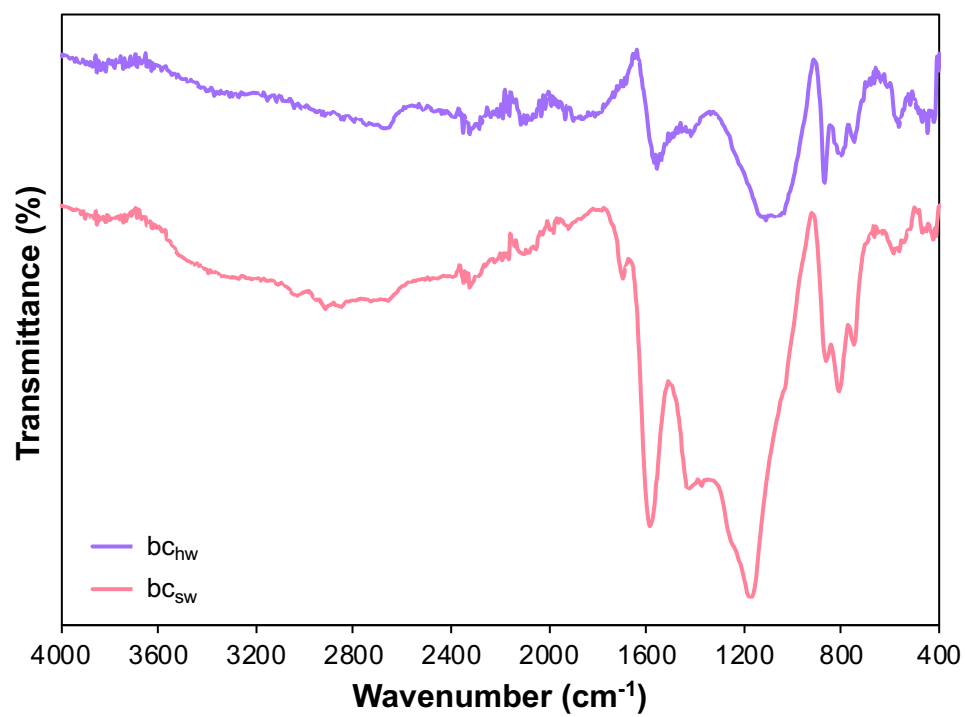


Figure A.8. Comparison between the FT-IR spectra of **bc_{hw}** (top, purple), and **bc_{sw}** (bottom, pink).

APPENDIX B: INFORMATION FOR CHAPTER 3

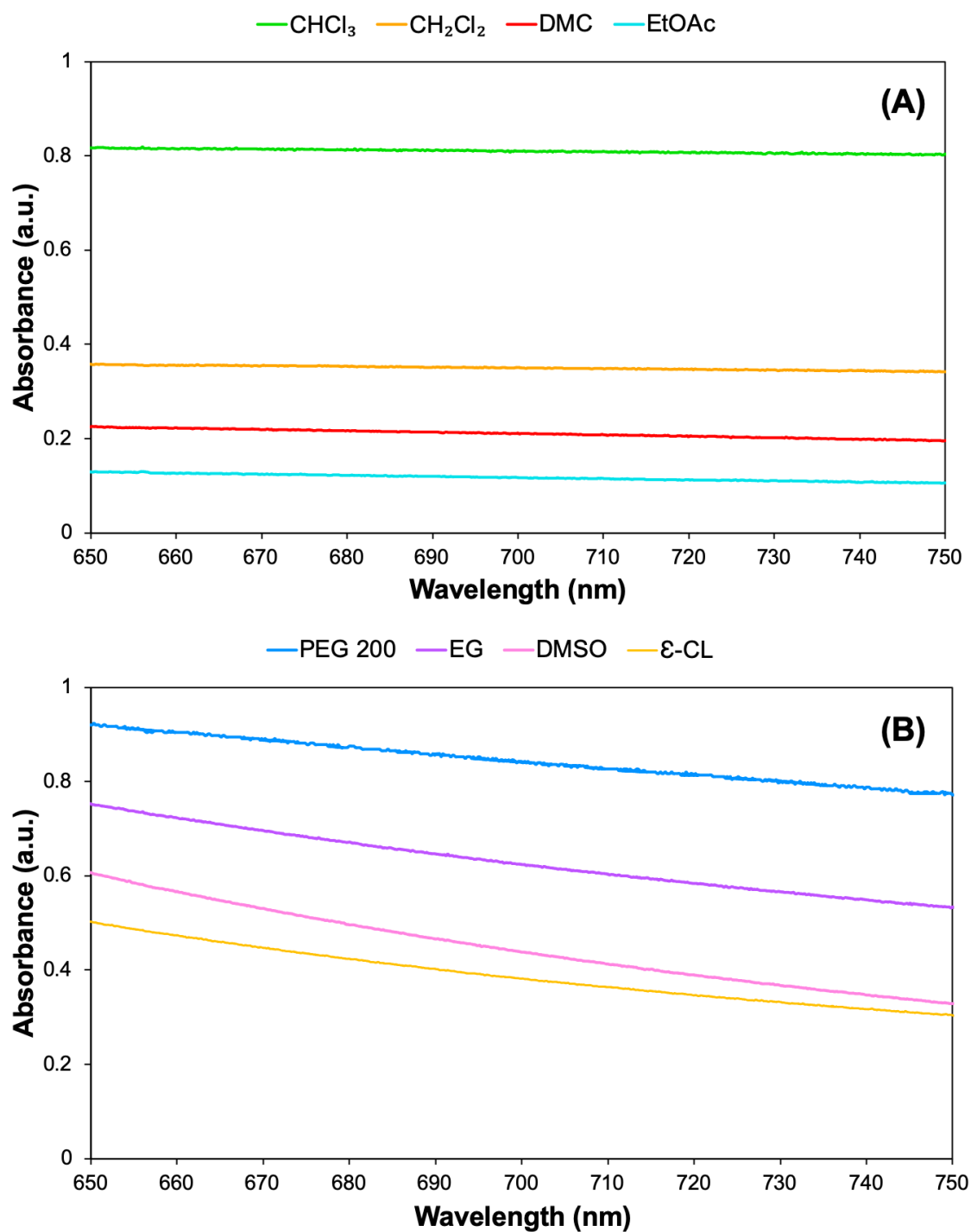


Figure B.1. UV-Vis spectra of (A) bc_{sw} and (B) $oxbc_{sw}$ samples in different solvents.

Equation B.1. General expression for the estimation of the crystallite size of the material (L_a) via Raman spectroscopy using the ratios between the intensity of the G and D bands (I_G/I_D) and the laser wavelength in nm (λ_l).

$$L_a(\text{nm}) = 2.4 \times 10^{-10} \lambda_l^4 \frac{I_G}{I_D} \quad (\text{Equation B.1})$$

Equation B.2. General expression for the estimation of the distance between defects (L_D) via Raman spectroscopy using the ratios between the intensity of the G and D bands (I_G/I_D) and the laser wavelength in nm (λ_l).

$$L_D^2(\text{nm}^2) = (1.8 \pm 0.5) \times 10^{-9} \lambda_l^4 \frac{I_G}{I_D} \quad (\text{Equation B.2})$$

Equation B.3. General expression for the estimation of the defect density (n_D) via Raman spectroscopy using the ratios between the intensity of the G and D bands (I_G/I_D) and the laser wavelength in nm (λ_l).

$$n_D(\text{cm}^{-2}) = \frac{(1.8 \pm 0.5) \times 10^{22}}{\lambda_l^4} \left(\frac{I_D}{I_G} \right) \quad (\text{Equation B.3})$$

APPENDIX C: INFORMATION FOR CHAPTER 4

Equation C.1. Expression for the calculation of polymer composites grafting percentage (G%) after Soxhlet extraction.

$$G\% = \frac{m_{\text{grafted}}}{m_{\text{grafted}} + m_{\text{homopolymer}}} \times 100 \quad (\text{Equation C.1})$$

Equation C.2. Expression for the calculation of grafting percentage (G%) from the TGA curves using the mass loss in the temperature range of 200-800 °C.

$$G\% = \frac{m_{200} - m_{800}}{m_{800}} \times 100 \quad (\text{Equation C.2})$$

Equation C.3. Expression for the calculation of grafted polymer from the TGA curves using the difference between the mass losses of **PCL/Eoxbc** composite and **oxbc** (Δm) at 800 °C.

$$\text{Grafted amount (mg/g)} = \frac{\Delta m}{100} \times 1000 \quad (\text{Equation C.3})$$

Table C.1. Gene sequences for fungi present in neat PCL and PCL/Eoxbc-0.1 samples after enzymatic treatment.

Sample	Fungi gene sequence
Neat PCL	<p>acttgttgtatattgtaaggccgagcctagaataaccgagaaatataaccattaaactattcaacgag ttgataaacctaatacattgaaagtcatatagcactatccagtaccactcatgccaatacatttcaa gcaaacgcctagttcgactaagagtatcactcaatacacaacccgaaggttgagagagaaatgac gctcaaacaggcatgccctctggaataccagagggcgcaatgtgcgttcaaagattcgatgattca cgaaaatctgcaattcatattacttatcgcttctgctgcttctcatcgatgcgagaaccaagagat ccggttgtaagtttgaagattttgaatttaatacaacaattgacaattaaataaataacaattca atataaatattgaagtttagttcagtaaacctctggccaaactatttctagtcagaccaagcaaa agttc</p>
PCL/Eoxbc-0.1 (fungi 1)	<p>tataggtatagaccgggtgccgtcgacccttgagaccggtacgtgctccgtgaagatgctcagtg accgggggttcaacagcccgcgtcattgtcttgggaggggtccagggggttgagggtcccccgg accagaccgtccaacaccaagccgggggcttgaggggtgaaaatgacgctcgaacaggcatgcc cttcggaatacacaagggcgcaatgtgcgttcaaagattcgatgactcacgagaattctgcaattcg cttacttatcgcttctgctgcttctcatcgatgccagaaccaagagatccggttgtaagtttg cttattttaaagacgttactcagacaaagacacggttgggttaagaatttggagttgaggctgctg gtaggcactctccggcggcgctttacggccccggcaggtctataacagatagaccaggccta ccgaagcaactaggtatcataaacaatgggttgggaggtcgggcccgatgaggaccctaactc ggtaatgatccctccgaggtcacctacgaagaccttggttacgacttttacttctct</p>
PCL/Eoxbc-0.1 (fungi 2)	<p>ggcgtggccgctctgagcttccggtgcgagaacaagttactacgcagaggtcgcctcggagggc cgccactagatttcggggcgcgctccccggcgagatgccggggggagtctgccgtcccccaac gccgagccgtcctcaaaagagtcgggctcgagggtgaaatgacgctcgaacaggcatgccgc cagaatgctggggcgcaatgtgcgttcaaagattcgatgattcactgaattctgcaattcacatta cttatcgcttctgctgcttctcatcgatgccagaaccaagagatccggttgtaagtttgattca tttgtattttgccttccggcactcagaaatgctataaaaacaagagttaagtgtcctcggcggc gccgaagcgcgcgccaagcaacaagtggtaagttcacataggggttgggagttgaataactcga taatgatccctccgctggttccaacggagaccttggttacgacttttacttctct</p>

Table C.2. Gene sequences for bacteria present in neat PCL and PCL/Eoxbc-0.1 samples after enzymatic treatment.

Sample	Bacteria gene sequence
Neat PCL	<p>tagccacttctggtaaaaccactcccatggtgtgacgggagggtgtgtacaagaccgggaacgt attcaccgcgcatgctgatccgcgattactagcgattccagcttcacgcactcgagttgcagagtg cgatccggactacgatcggttttctgggattggctccccctcggggttggcgaccctctgtccga ccattgtatgacgtgtgaagccctaccataagggccatgaggacttgacgtcatccccaccttct ccggtttgtaccggcagtctccctagagtgcctttgcgtagcaactagggacaagggttgcgctc gttgcgggacttaaccaacatctcacgacacgagctgacgacagccatgcagcacctgtgttatg gctccctttcgggactcccacctctcagcaggattccatacatgtcaagggtaggttaaggtttctg cgttgcatcgaattaatccacatcatccaccgcttgtgcgggtccccgtcaattcctttgagttta cttgcgaccgtactccccaggcggtcaacttcacgcgtagctacgttaccagcaatgaagacc cgacaactagttgacatcgtttagggcgtggactaccagggtatctaactcctgtttgctccccacgct ttcgtgcatgagcgtcagattggcccagggggctgccttcgcatcggtattcctccacatctctac gcatttactgctacagtggaattctaccccccttgccatacttagcccgNaNtcacaaatg cagttcccagggttaagcccgggatttcacatctgtc</p>
PCL/Eoxbc-0.1	<p>accactcccatggtgtgacgggagggtgtgtacaagaccgggaacgtattcaccgcgcatgct gatccgcgattactagcgattccagcttcacgcactcgagttgcagagtgcgatccggactacgatc ggttttctggggattggctccccctcggggttggcgaccctctgttccgaccattgtatgacgtgtg aagccctaccataagggccatgaggacttgacgtcatccccaccttctccggtttgtaccggc agtctccctagagtgcctttgcgtagcaactagggacaagggttgcgctcgttgcgggacttaacc caacatctcacgacacgagctgacgacagccatgcagcacctgtgttatggctccctttcgggac tcccacctctcagcaggattccatacatgtcaagggtaggttaaggtttttcgcgttgcatcgaatta tccacatcatccaccgcttgtgcgggtccccgtcaattcctttgagtttaactcttgcgaccgtactcc ccaggcggtcaacttcacgcgtagctacgttaccagcaatgaagaccgacaactagttgaca tcgtttagggcgtggactaccagggtatctaactcctgtttgctccccacgcttctgcatgagcgtc agtattggcccagggggctgccttcgcatcggtattcctccacatctctacgcatttactgctaca cgtggaattctaccccccttgccatacttagcccgccagtcacaaatgcagttc</p>

APPENDIX D: INFORMATION FOR CHAPTER 5

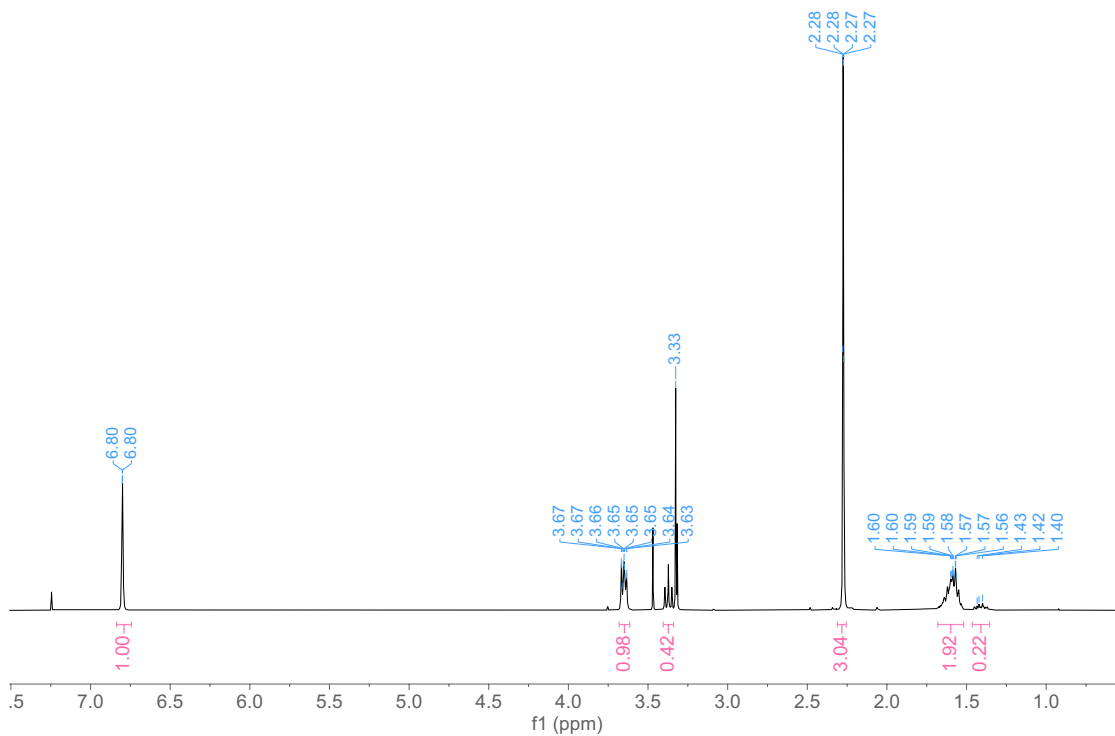


Figure D.1. ¹H NMR spectrum (300 MHz, CDCl₃) of the ring-closing C-O/C-O metathesis of 1,5-dimethoxypentane using **sbc** as a catalyst.

Conversions calculated using 1,5-dimethoxypentane CH₂ protons (0.98, δ 3.63-3.67 ppm) and the internal standard mesitylene aromatic protons (1.00, δ 6.80 ppm).

Conversion = 75.2%.

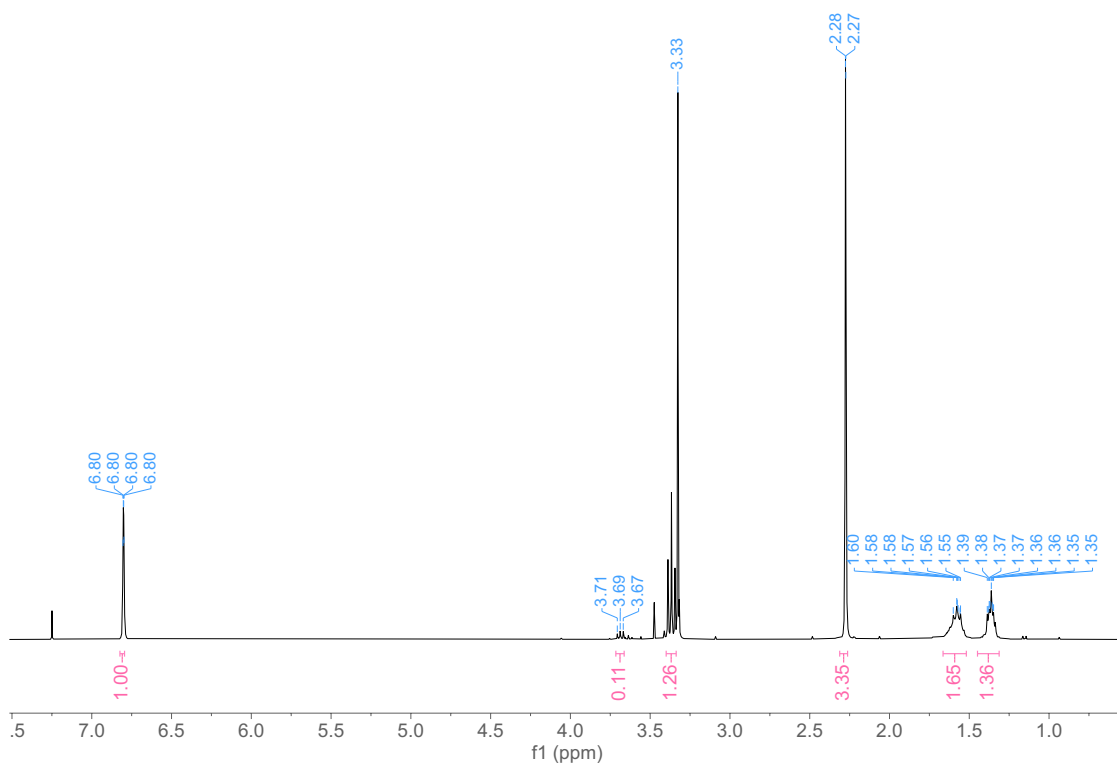


Figure D.2. ¹H NMR spectrum (300 MHz, CDCl₃) of the ring-closing C-O/C-O metathesis of 1,6-dimethoxyhexane using **sbc** as a catalyst.

Conversions calculated using 1,6-dimethoxyhexane CH₂ protons (0.11, δ 3.67-3.71 ppm) and the internal standard mesitylene aromatic protons (1.00, δ 6.80 ppm).

Conversion = 7.8%.

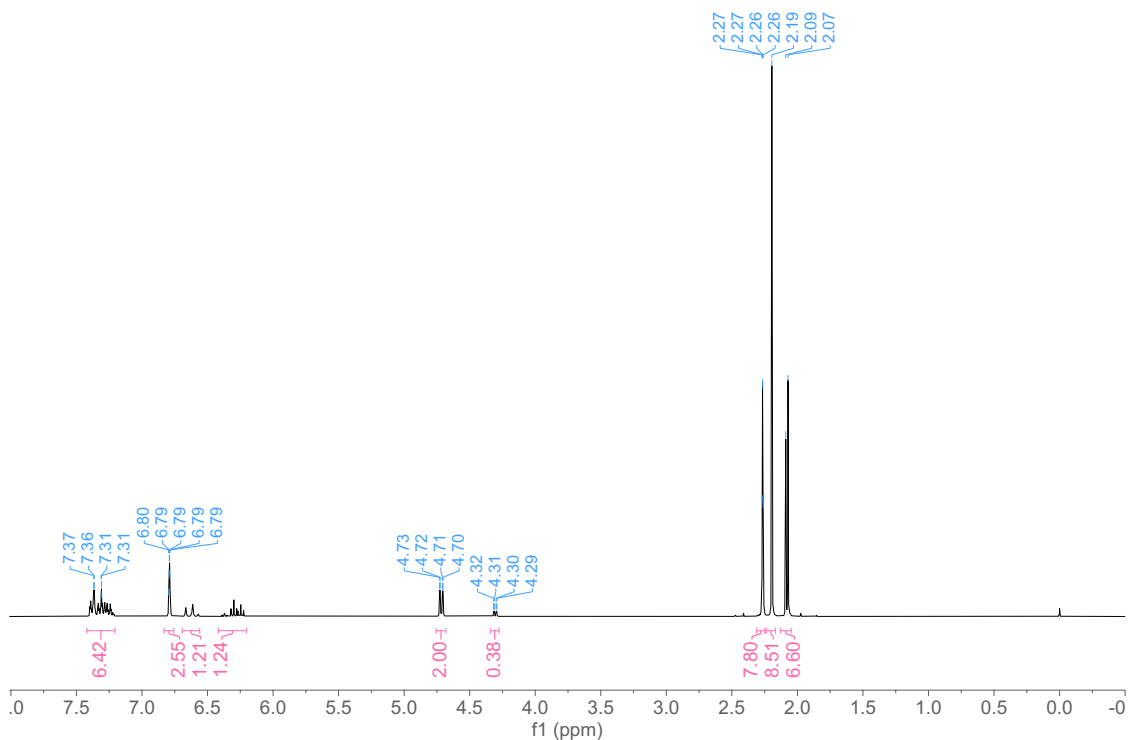


Figure D.3. ¹H NMR spectrum (300 MHz, CDCl₃) of the esterification of cinnamyl alcohol using **sb**c as a catalyst (**Table 5.3, Entry 1**).

Conversions calculated using cinnamyl alcohol CH₂ protons (2.00, δ 4.70-4.73 ppm) and the internal standard mesitylene aromatic protons (2.55, δ 6.80 ppm).

Conversion = 84.3%.

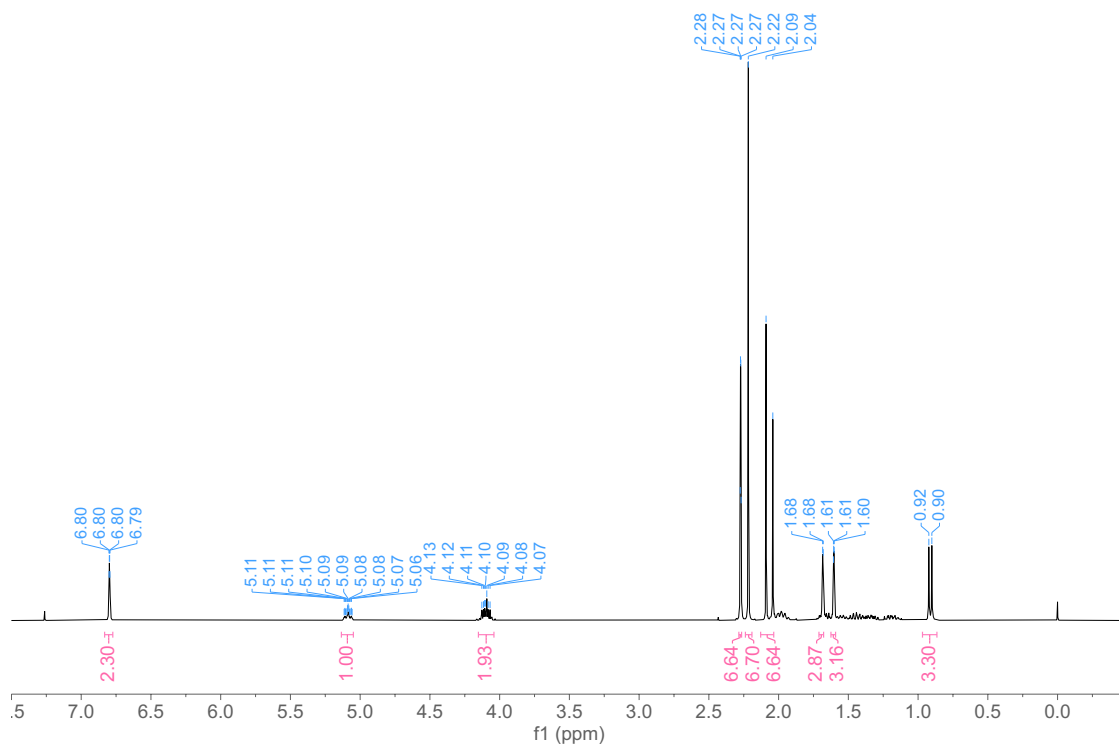


Figure D.4. ^1H NMR spectrum (300 MHz, CDCl_3) of the esterification of citronellol using **sbc** as a catalyst (**Table 5.3, Entry 2**).

Conversions calculated using citronellol CH_2 protons (1.00, δ 5.06-5.11 ppm) and the internal standard mesitylene aromatic protons (2.30, δ 6.80 ppm). Conversion > 99.9%

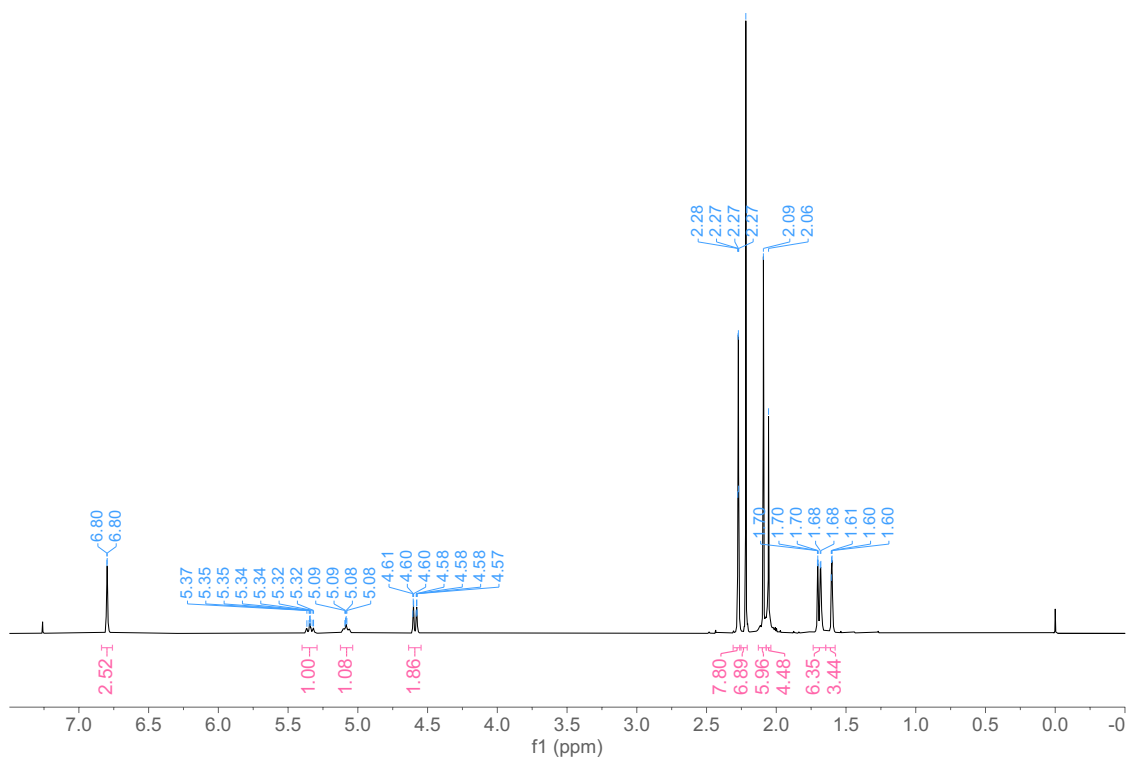


Figure D.5. ^1H NMR spectrum (300 MHz, CDCl_3) of the esterification of geraniol using **sbc** as a catalyst (**Table 5.3, Entry 3**).

Conversions calculated using geraniol CH_2 protons (1.00, δ 5.08-5.37 ppm) and the internal standard mesitylene aromatic protons (2.52, δ 6.80 ppm). Conversion > 99.9%

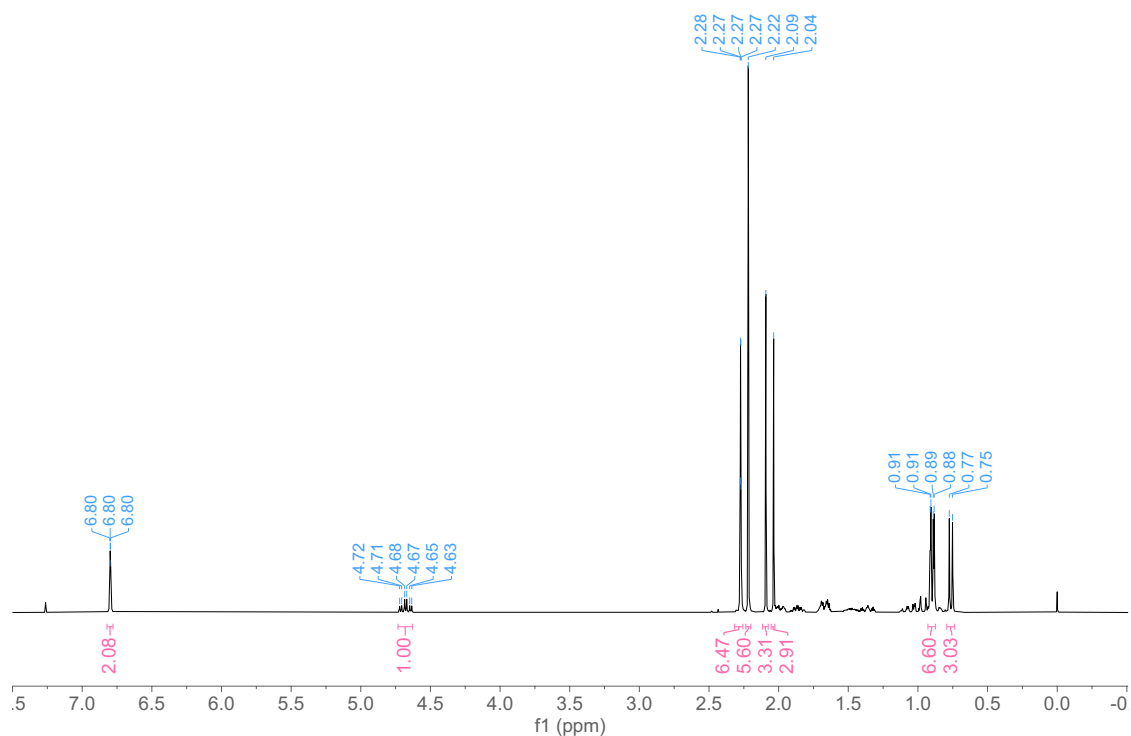


Figure D.6. ¹H NMR spectrum (300 MHz, CDCl₃) of the esterification of menthol using **sbc** as a catalyst (Table 5.3, Entry 4).

Conversions calculated using menthol CH₂ protons (1.00, δ 4.63-4.72 ppm) and the internal standard mesitylene aromatic protons (2.08, δ 6.80 ppm). Conversion > 99.9%